



UNIVERSITAT  
POLITÈCNICA  
DE VALÈNCIA

# **SERVICEABILITY BEHAVIOUR OF REINFORCED UHPFRC TENSILE ELEMENTS**

PhD THESIS

Author:

Majid Khorami

Supervisors:

Prof. Pedro Serna Ros

PhD. Juan Navarro Gregori

València, Spain

January 2023

UNIVERSITAT POLITÈCNICA DE VALÈNCIA  
PROGRAMA DE DOCTORADO EN INGENIERÍA DE LA CONSTRUCCIÓN



# SERVICEABILITY BEHAVIOUR OF REINFORCED UHPFRC TENSILE ELEMENTS

by

Majid Khorami

PhD THESIS

Submitted in fulfilment of the requirements for the degree of Doctor of Philosophy in Building Engineering from the Departamento de Ingeniería de la Construcción y de Proyectos de Ingeniería Civil of the Universitat Politècnica de València

Supervisors:

Prof. Pedro Serna Ros  
PhD. Juan Navarro Gregori



UNIVERSITAT  
POLITÈCNICA  
DE VALÈNCIA

*Universitat Politècnica  
de València*



*Departamento de Ingeniería  
de la Construcción y de  
Proyectos de Ingeniería Civil*



*Instituto de Ciencia y  
Tecnología del Hormigón*

External evaluation committee:

*Prof. Yesid Alexandre Alvarado Vargas, University of Pontifical Javierian University*

*Prof. Héctor Cifuentes Bulte, University of Seville*

*Prof. Alejandro Enfedaque Diaz, Polytechnic University of Madrid*

Thesis committee:

*Prof. Salvador Ivorra Chorro, University of Alicante*

*Prof. José Rocío Martí Vargas, Valencia Polytechnic University*

*Prof. Héctor Cifuentes Bulte, University of Seville*

January 2023, València, Spain



*This thesis is dedicated to my Mother and Father*

## ***Acknowledgements***

First of all, I am extremely grateful to my Thesis Director and co-Director

***Professor Dr. Pedro Serna Ros & Associated Professor Dr. Juan Navarro Gregori***

for devoting your time and giving me the opportunity to work and complete my PhD Thesis at ICITECH (Institute of Science and Technology of Concrete). I very much appreciate this professional support, permanent encouragement, and enthusiasm, which always focus on possibilities and solutions instead of problems and limitations. Thank you for giving me all the advice, experiences, and knowledge during my laboratories campaigns.

I am also grateful to Dr. José Rocio Mart Vargas for his instructions and allowing me to use laboratory equipment, which enabled me to develop a novel test method and apply it to my entire experimental campaign study.

I wish to express my gratitude to the members of the jury and reviewers who generously spent their time to check and improve my work with their insightful and valuable comments:

I am sincerely thankful to all my friends at ICITECH and the Polytechnic University of Valencia: Miguel Ángel Navarro, Hesam, Francisco, Marta caballero, Farid, Eduard, Enrique, MartaRoig-Flores, Nafis, Naeimeh and Paco for their support and interesting discussions. Thank you for sharing your experiences in life research, your laboratory tips, and your loving consideration and confidence in me all these years.

I am extremely grateful to Dayan and Alex, who helped me to run some laboratory experiments during their internship programme.

I wish to dedicate this work to those I love the most, those with whom I sincerely share all the joy and happiness, and who have always been there for me, no matter what the circumstances. I thank my family, my father, brothers, and sister and those who have left us, but still live in my heart. Their love, support and encouragement have been my primary motivation. My deepest gratitude is for Wendy and her unconditional support, encouragement and patience all these years.

To my mother, who has been the biggest inspiration in my life. I thank you for everything you have done for me and also for your last hug.

In addition, I should mention that this thesis is a part of Project “BIA2016-78460-C3-1-R”, supported by the State Research Agency of Spain and carried out in Institutes of ICITECH. This research project aimed to define the design bases of sustainable UHPFRC structures at the pre-standard level, and this thesis is a part of this project, focused on SLS design requirements for R-UHPFRC structural elements. I am also thankful for their support with their grant.

Majid Khorami

January 2023

## ***Abstract***

All structures, particularly reinforcement concrete structures, apart from meeting necessary security against Ultimate Limit States (ULS), must exhibit appropriate behaviour under service conditions. Generally, the fundamental serviceability requirements that concrete structures should meet are functionality, user comfort and appearance. These requirements cannot, however, be directly checked. Therefore, performance criteria, such as deflection control, vibration control and cracking control, are defined to meet these requirements.

Serviceability calculation is complicated because of the cracking phenomenon, the tension stiffening effect, shrinkage, and creep effects. Cracking control in reinforced concrete (RC) structures is generally achieved by limiting stress in steel reinforcement and the concrete matrix. Many concrete code designs specify a maximum steel reinforcement stress after cracking and a maximum crack width for RC or fibre-RC (FRC) structural members, while the design serviceability aspects for Reinforced Ultra-High Performance Fibre-Reinforced Concrete (R-UHPFRC) are poorly considered in UHPFRC codes or recommendations.

Many efforts have been made in experimental and theoretical research into the serviceability behaviour of RC or FRC structural elements in the last few decades. However, for R-UHPFRC, knowledge about tension and cracking behaviour must improve and serviceability design requirements have to be further studied.

Within this framework, the main purpose of the present PhD thesis is to evaluate the serviceability behaviour of R-UHPFRC. For this purpose, the evaluation of the deformation and cracking behaviour of R-UHPFRC tensile elements is essential. To that end, two main items were addressed and adequately met. The first one was to

design an innovative and adequate test methodology to carry out the experiments required for this PhD project. The second involved evaluating the tension stiffening response and cracking behaviour of R-UHPFRC, which are fundamental parameters for R-UHPFRC structures' serviceability design. To study these two parameters, important parameters were considered, such as fibre content, fibre type, size effect, reinforcement ratio and shrinkage effect.

In order to evaluate the aforementioned parameters, four experimental campaigns are presented. Each campaign represents a different study level. The first corresponds to the validation of the proposed tensile test methodology and to the examination of the obtained experimental data for future studies required for this PhD project. The second experimental study level corresponds to establishing and undertaking comprehensive experimental programmes with two different steel fibre types and fibre contents. Different cross-section and reinforcement ratios were used to evaluate the size effect and fibre content effect, respectively. The effect of the micro- and macro-steel fibres combination on the deformation and cracking behaviour of tensile R-UHPFRC elements was investigated in a specific experimental study. The third level corresponds to an intensive shrinkage test, which was conducted to obtain the shrinkage value of the UHPFRC used in this PhD study. The final level corresponds to a specific experimental study, done by modifying the specimen's geometry and using the dog bone-shaped specimens to evaluate the average and maximum crack width (real detected value) caused by tensile stresses in R-UHPFRC tensile elements. It is worth mentioning that different analyses were performed for each experimental research and appropriate results were achieved to fulfil the thesis aims.

**Keywords:** cracking behaviour, design criteria, durability, fragility curve, post-cracking tensile stiffness, serviceability behaviour, shrinkage, SLS requirements, structural design, tensile elements, tension stiffening, test method, tie, UHPFRC.



## *Resumen*

Todas estructuras, especialmente las conformadas con hormigón armado, no solo deben cumplir con la seguridad necesaria bajo los Estados Límites Últimos (ULS), además es imprescindible que garanticen un comportamiento adecuado frente a condiciones de servicio. En general, los requisitos fundamentales de servicio que debe cumplir este tipo de estructuras son: la funcionalidad, comodidad para el usuario y la apariencia. Sin embargo, estos no se pueden verificar de forma directa; por lo tanto, ha sido necesario definir criterios de desempeño tales como control de deflexión, control de vibración y control de agrietamiento para dar cumplimiento a lo indicado anteriormente.

Además, se dificulta el cálculo de la capacidad de servicio debido al fenómeno de agrietamiento, el efecto de rigidez por tensión, la contracción y los efectos de fluencia. Por lo tanto, el control de la fisuración en estructuras de hormigón armado generalmente se logra limitando la tensión en el refuerzo de acero y la matriz de hormigón. Siendo así que, en los diseños incluidos en códigos relevantes a hormigón, especifican la tensión máxima del refuerzo de acero después de la fisuración y el ancho máximo de fisura para los miembros estructurales de CR o FRC, no obstante los aspectos de capacidad de servicio del diseño para el hormigón reforzado con fibras de ultra alto rendimiento reforzado (R-UHPFRC), no han sido incluidos en los códigos o recomendaciones de UHPFRC.

A pesar de que se han realizado muchos esfuerzos en la investigación tanto experimental como teórica sobre el comportamiento de servicio de los elementos estructurales de CR o FRC durante las últimas décadas, para el R-UHPFRC se debe

desarrollar aún más su conocimiento relacionado con los requisitos para el diseño de capacidad de servicio, incluyendo su comportamiento de tensión y agrietamiento. En este marco, el objetivo principal de la presente tesis doctoral es evaluar el comportamiento de servicio de R-UHPFRC. Por tal razón, es fundamental realizar la evaluación del comportamiento de deformación y fisuración de los elementos de tracción R-UHPFRC. Para ello, se abordaron y cumplieron adecuadamente dos puntos principales. El primero, diseñar una metodología de prueba innovadora y adecuada para ejecutar los experimentos requeridos para este proyecto de doctorado. En segundo lugar, se llevó a cabo la evaluación de la respuesta de rigidez a la tensión y el comportamiento de agrietamiento del R-UHPFRC, que son parámetros primordiales para el diseño de capacidad de servicio. Para estudiar estos dos parámetros, se consideraron algunos parámetros importantes tales como: el efecto del volumen del contenido de fibra, el tipo de fibra, el efecto del tamaño, el efecto de la relación de refuerzo y el efecto de la contracción.

Finalmente, para evaluar los parámetros mencionados, se presentan cuatro campañas experimentales. Cada una de ellas, representa un nivel diferente de estudio. El primero corresponde a la validación de la metodología de ensayo de tracción propuesta y examinar los datos experimentales obtenidos, para emplearlos en futuros estudios de este proyecto. El segundo nivel consistió en establecer y realizar experimentos completos con dos tipos de fibra de acero, modificando además su cantidad, es así como se utilizaron diferentes proporciones de refuerzo y sección transversal para evaluar el efecto tanto del tamaño como del contenido de fibra, respectivamente. También, en un estudio experimental específico se indagó sobre el efecto de la combinación de micro y microfibras de acero en la deformación y el comportamiento de agrietamiento de los elementos R-UHPFRC de tracción. El tercer nivel corresponde a una prueba de contracción intensiva, necesaria para obtener el valor de contracción del UHPFRC utilizado en esta investigación. El último nivel comprende la modificación de la geometría de la probeta y el uso de probetas en forma de hueso de perro para evaluar el ancho medio y máximo de fisura (valor real detectado) provocado por esfuerzos de tracción en los elementos de tracción R-UHPFRC. Es importante mencionar que se realizaron diferentes análisis para cada investigación experimental y se lograron resultados óptimos para dar cumplimiento con los objetivos de la tesis.

**Palabras clave:** comportamiento de fisuración, criterios de diseño, durabilidad, curva de fragilidad, rigidez a la tracción posterior a la fisuración, comportamiento de servicio, retracción, requisitos SLS, diseño estructural, elementos de tracción, endurecimiento a tracción, método de ensayo, tirante, UHPFRC

## *Resum*

Totes les estructures, especialment les conformades amb formigó armat, no només han de complir amb la seguretat necessària sota els Estats Límits Últims (ULS), a més és imprescindible que garanteixin un comportament adequat davant de condicions de servei. En general, els requisits fonamentals de servei que ha de complir aquest tipus d'estructures són: la funcionalitat, la comoditat per a l'usuari i l'aparença. Això no obstant, aquests no es poden verificar de forma directa; per tant, ha calgut definir criteris d'acompliment com ara control de deflexió, control de vibració i control d'esquerdament per a donar compliment al que s'ha indicat anteriorment.

A més, es dificulta el càlcul de la capacitat de servei a causa del fenomen d'esquerdament, l'efecte de rigidesa per tensió, la contracció i els efectes de fluència. Per tant, el control de la fissuració en estructures de formigó armat generalment s'aconsegueix limitant la tensió al reforç d'acer i la matriu de formigó. És així que en els dissenys inclosos en codis rellevants a formigó, especifiquen la tensió màxima del reforç d'acer després de la fissuració i l'amplada màxima de fissura per als membres estructurals de CR o FRC, no obstant els aspectes de capacitat de servei del disseny per al formigó reforçat amb fibres d'ultra alt rendiment reforçat (R-UHPFRC), no han estat inclosos als codis o recomanacions d'UHPFRC.

Tot i que s'han realitzat molts esforços en la investigació tant experimental com

teòrica sobre el comportament de servei dels elements estructurals de CR o FRC durant les últimes dècades, per al R-UHPFRC s'ha de desenvolupar encara més el seu coneixement relacionat amb els requisits per al disseny de capacitat de servei, incloent el comportament de tensió i esquerdament.

En aquest marc, l'objectiu principal de la present tesi doctoral és avaluar el comportament de servei de R-UHPFRC. Per aquesta raó, és fonamental fer l'avaluació del comportament de deformació i fissuració dels elements de tracció R-UHPFRC. Per això, es van abordar i van complir adequadament dos punts principals. El primer, dissenyar una metodologia de prova innovadora i adequada per executar els experiments requerits per a aquest projecte de doctorat. En segon lloc, es va fer l'avaluació de la resposta de rigidesa a la tensió i el comportament d'esquerdament del R-UHPFRC, que són paràmetres primordials per al disseny de capacitat de servei. Per estudiar aquests dos paràmetres, es van considerar alguns paràmetres importants com ara l'efecte del volum del contingut de fibra, el tipus de fibra, l'efecte de la mida, l'efecte de la relació de reforç i l'efecte de la contracció.

Finalment, per avaluar els paràmetres mencionats, es presenten quatre campanyes experimentals. Cadascuna representa un nivell diferent d'estudi. El primer correspon a la validació de la metodologia d'assaig de tracció proposada i examinar les dades experimentals obtingudes, per a emprar-les en futurs estudis d'aquest projecte. El segon nivell va consistir a establir i realitzar experiments complets amb dos tipus de fibra d'acer, modificant-ne a més la quantitat, és així com es van utilitzar diferents proporcions de reforç i secció transversal per avaluar l'efecte tant de la mesura com del contingut de fibra, respectivament. També, en un estudi experimental específic, es va indagar sobre l'efecte de la combinació de micro i macrofibres d'acer en la deformació i el comportament d'esquerdament dels elements R-UHPFRC de tracció. El tercer nivell correspon a una prova de contracció intensiva, necessària per obtenir el valor de contracció de l'UHPFRC utilitzat en aquesta investigació. L'últim nivell comprèn la modificació de la geometria de la proveta i l'ús de provetes en forma d'os de gos per avaluar l'amplada mitjana i màxima de fissura (valor real detectat) provocat per esforços de tracció en els elements de tracció R-UHPFRC. És important esmentar que es van fer diferents anàlisis per a cada investigació experimental i es van aconseguir resultats òptims per a donar compliment als objectius de la tesi.

**Paraules clau:** comportament de fissuració, criteris de disseny, durabilitat, corba de fragilitat, rigidesa a la tracció posterior a la fissuració, comportament de servei, retracció, requisits SLS, disseny estructural, elements de tracció, enduriment a tracció, mètode d'assaig, tirant, UHPFRC

## *Thesis structure*

This doctoral thesis is presented as a compilation of six published articles. The thesis is divided into seven chapters in which those articles are included. The references of the articles, in order of appearance, are:

- 1<sup>st</sup> paper: Khorami, M., et al. (2019). A testing method for studying the serviceability behavior of reinforced UHPFRC tensile ties. IOP Conference Series: Materials Science and Engineering, IOP Publishing.
- 2<sup>nd</sup> paper: Khorami, M., et al. "Experimental methodology on the serviceability behaviour of reinforced ultra-high performance fibre reinforced concrete tensile elements." *Strain*: e12361.
- 3<sup>rd</sup> paper: Khorami, M., et al. (2021). "Tensile behaviour of reinforced UHPFRC elements under serviceability conditions." *Materials and structures* 54(1): 43.
- 4<sup>th</sup>: Book chapter (BEFIB -RILEM Book series): Khorami, M., et al. (2020). The Effect of Fiber Content on the Post-cracking Tensile Stiffness Capacity of R-UHPFRC. RILEM-fib International Symposium on Fibre Reinforced Concrete, Springer.
- 5<sup>th</sup> paper: Khorami, M., et al. (2022). An Experimental Study on the Behavior of reinforced UHPFRC Ties Under Serviceability Conditions. Proceedings of the VIII Congress of ACHE – Santander.
- 6<sup>th</sup> paper: M. Khorami, J. Navarro-Gregori, P. J. C. Serna, *Construction and Building Materials*, "Serviceability behaviour of reinforced UHPFRC tensile elements: Assessment of the ratio between maximum and average crack widths," vol. 303, No. 124513, 2021.

# *Table of contents*

<b>Acknowledgements .....</b>	<b>3</b>
<b>Abstract.....</b>	<b>5</b>
<b>Resumen .....</b>	<b>7</b>
<b>Resum .....</b>	<b>9</b>
<b>Thesis structure .....</b>	<b>11</b>
<b>Table of contents .....</b>	<b>12</b>
<b>Chapter 1. Introduction and objectives.....</b>	<b>17</b>
<i>1.1. Background and Justification .....</i>	<i>18</i>
<i>1.2. Objectives and Scope of the Thesis.....</i>	<i>24</i>
<i>1.3. Layout of the thesis .....</i>	<i>25</i>
<i>1.4. Summary and Interrelation of Papers.....</i>	<i>26</i>
<b>Chapter 2. State-of-the-art.....</b>	<b>31</b>
<i>2.1. Uniaxial tensile test methodology .....</i>	<i>32</i>
<i>2.1.1. Force transfer systems for the RC tensile element test .....</i>	<i>32</i>

2.1.2. Geometry of the specimens .....	34
2.1.3. Measurement techniques .....	38
2.2. Tension stiffening effect of conventional reinforcement concrete (RC) .....	40
2.2.1. Tension stiffening concept .....	40
2.2.2. Models of tension stiffening for RC elements.....	43
2.2.2.1. Empirical methods for tension stiffening modelling .....	44
2.2.2.2. Theoretical methods for tension stiffening modelling .....	48
2.3. Tension stiffening behaviour effect of fibre reinforced concrete (FRC).....	60
2.4. Tension Stiffening behaviour of R-UHPFRC .....	66
2.4.1. Background to UHPFRC .....	66
2.4.3 Inverse analysis methodology.....	72
2.4.4 Full tension stiffening concept .....	74
2.4.5. Models of tension stiffening for R-UHPFRC tensile elements .....	78
2.5. Shrinkage properties of UHPFRC.....	87
2.5.1. Background .....	87
2.5.2. Shrinkage values in codes and recommendations for UHPFRC.....	93
2.6. Crack width prediction and limitations for design of R-UHPFRC in serviceability limit states ....	101
2.7. Serviceability requirements for R-UHPFRC.....	105
<b>Chapter 3. Uniaxial tensile test methods for reinforcement concrete elements.....</b>	<b>121</b>
1 <sup>st</sup> Paper. A testing method for studying the serviceability behavior of reinforced UHPFRC tensile ties .....	123
Abstract .....	123
1. Introduction.....	123
2. Research Significance .....	124
3. Experimental Program .....	124
4. Description of the test system .....	126
2 <sup>nd</sup> Paper. Experimental methodology on the serviceability behaviour of reinforced ultra-high- performance fibre reinforced concrete tensile elements .....	136
Abstract .....	136
1. Introduction.....	137
2. Research significance .....	138
3. Test methodology.....	138

4. Test results and discussion .....	147
5. Summary and conclusions.....	152
Acknowledgments .....	153
<b>Chapter 4. Tensile behaviour and tension stiffening concept for RC, FRC, and R-UHPFRC elements .....</b>	<b>155</b>
3 <sup>th</sup> Paper. Tensile behaviour of reinforced UHPFRC elements under serviceability conditions.	157
Abstract .....	157
1. Introduction .....	158
2. Experimental programme .....	160
3. Experimental results of the R-UHPFRC ties .....	165
4. Analysis of the results .....	166
5. Conclusions .....	180
4 <sup>th</sup> Paper. The Effect of Fiber Content on the Post-cracking Tensile Stiffness Capacity of R-UHPFRC.....	187
Abstract .....	187
1. Introduction .....	187
2. Experimental program .....	189
3. Test results and general discussion.....	191
4. UHPFRC CONTRIBUTION IN TENSION.....	194
5. CRACKING BEHAVIOR.....	195
6. Conclusions .....	197
5 <sup>th</sup> Paper. An Experimental Study on the Behavior of Reinforced UHPFRC Ties Under Serviceability Conditions.....	201
Abstract .....	201
1. Introduction .....	202
2. Experimental Program .....	203
3. Tensile behavior of R-UHPFRC.....	206
4. UHPFRC tensile behavior characterization.....	208
5. Conclusions .....	212
<b>Chapter 5. Serviceability behaviour of reinforced UHPFRC tensile elements .....</b>	<b>215</b>
6 <sup>th</sup> Paper. Serviceability behaviour of reinforced UHPFRC tensile elements: Assessment of the ratio between maximum and average crack widths .....	217
Abstract .....	217



1. <i>Introduction</i> .....	217
2. <i>Research significance</i> .....	220
3. <i>Serviceability design and conditions</i> .....	220
4. <i>Experimental Program</i> .....	221
5. <i>Test results and discussion</i> .....	230
6. <i>Conclusions</i> .....	244
<b>Chapter 6. Resume and general discussion of the results</b> .....	<b>249</b>
6.1. <i>Proposed test method</i> .....	250
6.2. <i>Tensile behaviour and tension stiffening of R-UHPFRC tie elements</i> .....	266
6.3. <i>Shrinkage behaviour of UHPFRC</i> .....	281
6.4. <i>Cracking and serviceability behaviour</i> .....	290
<b>Chapter 7. Conclusions and future research lines</b> .....	<b>303</b>
7.1. <i>Summary and main conclusions</i> .....	304
7.2. <i>Partial conclusions</i> .....	305
7.3. <i>Global conclusions</i> .....	307
7.4. <i>Future research lines</i> .....	308
<b>Annex I. Justification of the impact index of the publications included in the thesis</b> .....	<b>311</b>



# ***Chapter 1. Introduction and objectives***

This chapter describes the problem that gives rise to this thesis. The objectives and scope of the thesis are also specified, and the structure of the document is explained, where the content of each thesis chapter is defined.

## **1.1. Background and Justification**

Modern civil engineering applications have needed to use high-performance engineering materials in novel ways. These new materials should have outstanding characteristics, such as high strength and toughness, high energy absorption, and also good durability characteristics [1]. UHPFRC material is an advanced cementitious and composite material with high compressive strength and non-negligible tensile strength. Because of its benefits, studies in this field have significantly grown in recent decades.

This composite material is ductile and provides multi-microcracking behaviour. The addition of fibres to the concrete matrix helps to control crack opening [2]. When UHPFRC develops cracks under service loads, crack bridging fibres help to transmit force from one side of the crack to the other, and this effect leads to reduced crack propagation and limits crack width [3].

Concrete structures should be designed in such a way that they are not only safe against failure, but also offer good performance during their working life. New structural design codes normally consider two types of limit states for structural design processes: Ultimate Limit States (ULS) and Serviceability Limit States (SLS). The fundamental serviceability requirements are functionality, user comfort and appearance [4]. These requirements are not easy to directly verify and, hence, the need to use indirect criteria, such as vibration control, deflection control and cracking control, to verify that the structure meets the serviceability limit states or not [5, 6]. With Reinforced Ultra-High Performance (R-UHPFRC) structures, due to high material resistance, structural members are normally slender, and more attention needs to be paid to deflection and cracking problems. The crack width limitation is an important design criterion for SLS. Cracks occur when the tensile strength of the concrete matrix is reached and can be caused by loads, shrinkages effects and the imposed deformation [7]. The main reasons for limiting crack width are resisting environmental actions and avoiding steel corrosion (durability), safety, tightness and aesthetics during concrete structures' working life [8]. Given the service loads predicted by an appropriate calculation method, the general design criteria for SLS requires crack widths ( $w_{cr}$ ) to be less than or to equal the maximum value ( $w_{max}$ ). The design serviceability requirements for R-UHPFRC are not included in FIB Model Code 2010 (MC10) [8] and are not completely considered in UHPFRC codes or recommendations, such as the French standard and recommendations NF P18-470, AFGC [9], the Japanese Standard and Guideline JSCE Concrete Committee [10], and Switzerland Technical Notebook for SIA 2052 [11].

### 1.1.1 UHPFRC in Standards and Codes

From a structural point of view, the SLS design requirements for UHPFRC (e.g., crack width limitation and permissible deformation) may differ from those for ordinary (reinforced) concrete (RC) or fibre-reinforced concrete (FRC). As UHPFRC is a new material that emerged about 25 years ago [12], design requirements are not substantially considered in codes. The first recommendation for designing prestressed UHPFRC beams was published in 2000 in Australia [13], and the French recommendations (AFGC-Sétra) were published later in 2002 [14]. Because of the good advantages of UHPFRC material, it became popular in the constructions field and new guidelines have appeared worldwide. In 2006, the Japanese recommendations were published by the Japanese Society of Civil Engineers (JSCE) [15]. In 2013, the revision of the interim recommendation of the 2002 French recommendation was published [9], and these recommendations became a standard in France in 2016 [16, 17]. In 2016 in Switzerland, a collection of all UHPFRC experiences acquired in the last few years was published as a standard draft (SIA 2052) [11]. In the current version of Eurocode 2: Background & Applications Design of Concrete (2014) [18], the UHPFRC requirements are not included, and the European Commission is developing the new revision of Eurocode 2. The Eurocode Committee is seeking to include UHPFRC design criteria in the 2022 version. The output of this PhD research (3<sup>rd</sup> paper) is cited in Chapter 6 of this new draft of Eurocode for the SLS design of R-UHPFRC structures.

Since the creation of this material to date, many research works have been conducted to understand the mechanical characteristic of UHPFRC, especially its tensile behaviour [19-27]. It should be mentioned that the majority of these research works have focused on unreinforced tensile UHPFRC behaviour, while real structural elements are reinforced with steel rebars. Hence further studies are needed to fully comprehend the behavior of reinforced UHPFRC (R-UHPFRC) elements.

### 1.1.2. The Tension-Stiffening Concept

In the concrete structure design, it is assumed that once concrete tensile strain exceeds the cracking strain, the tensile stress in concrete will be zero. Given this assumption, the tensile concrete zone is neglected in the design process. At the end of the 19th century, Considère et al. [28] tested small mortar specimens reinforced by steel wires under tensile force. They observed that the load-deformation response curve of members was parallel to the bare steel bar response and also above it, which means that the cracked member is carrying tensile force. To better describe this stiffening ability of RC in tension, the typical response of an RC element under tensile load is illustrated in Figure 1-1.

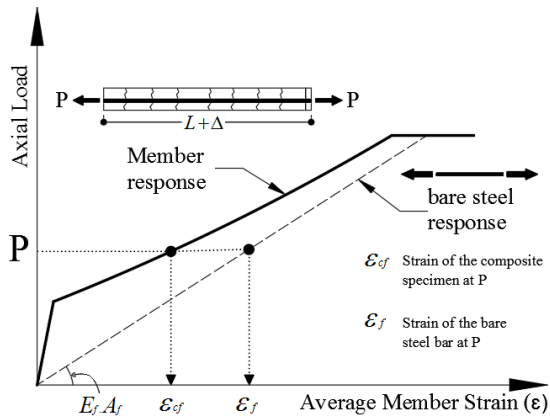


Figure 1- 1: The typical tensile response of a concrete reinforcement element [29]

This diagram compares the tensile behaviour of the RC element and the bare bar. Uncracked concrete between principal tensile cracks can carry a portion of the tensile load, because bond stress exists between the bar and concrete. These uncracked portions carry a portion of the tensile load and contribute to overall cracked composite stiffness [30]. For an applied force ( $P$ ), the bare bar would present a strain of ( $\epsilon_f$ ), and the overall member response would be less than ( $\epsilon_f$ ) and equal ( $\epsilon_{cf}$ ). This means that at the crack section, only the steel rebar carries the tensile force ( $P$ ) and strain ( $\epsilon_f$ ) is achieved. In all the other sections, the steel rebar stretches less than ( $\epsilon_f$ ) because it shares forces with concrete, which renders the overall RC element response less than ( $\epsilon_f$ ). However, at the sections between adjacent cracks, some tensile stress is restrained in the concrete around steel bars due to the bond's actions. This effect was called "tension-stiffening" by Mörsch in 1909 [31]. In other words, the tension stiffening effect reflects concrete's ability to carry tension between cracks and, due to this positive effect, the RC member's rigidity increases until bar reinforcement yields [32].

In the bending case, when the element is loaded under flexure, the cracking of RC results in reduced bending stiffness at the cracked section and all the stress must be carried by the bar crossing the cracks. Those uncracked portions carry a portion of the load due to the mechanical interaction between steel reinforcement and the surrounding. Hence the tension stiffening effect would appear. If the tension stiffening effect is neglected, the calculated deflection can be overestimated and, consequently, the tension stiffening effect in serviceability performance (deflection and crack width limitation) is significant. This phenomenon is also effective for concrete members' long-term behaviour due to concrete's creep and shrinkage.

### 1.1.3. Concrete's Shrinkage Phenomenon

Concrete shrinkage is a volumetric deformation caused by physic-chemical processes. During the hydration and hardening processes of cement paste, concrete volume will reduce when this process takes place in air, and this effect will be null in water. Shrinkage is the term for this reduction in volume, which can develop due to the loss of water [33]. In other words, shrinkage is a time-dependent decrease in concrete volume.

There are four main types of shrinkage for concrete depending on sources [34]:

- (1) Plastic shrinkage: it occurs as a result of fresh concrete losing its moisture and is transmitted to the surrounding environment.
- (2) Autogenous shrinkage: it is caused by water loss from capillary pores due to cement hydration. This deformation is known as early shrinkage and can happen with no environmental loss of water. However, when the water to cement (W/C) ratio is low or the cement content is high, autogenous shrinkage tends to increase in, for example, the case of UHPFRC material. This phenomenon can occur due to hydration chemical processes and internal water use (self-desiccation) in those concretes with a significantly low W/C ratio (0.2 to 0.42) [35].
- (3) Carbonation shrinkage: this occurs as a result of reactions between atmospheric carbon dioxide and several cement hydration products.
- (4) Drying shrinkage: it is a consequence of moisture migration and loss of water squeezing out from capillary pores in hardened concrete. Drying shrinkage is due to lowering capillary pressure because internal humidity attempts to make it uniform with environmental conditions.

The main parameters that affect shrinkage deformation magnitude are the concrete's mixture property (cement and water content), the properties of the employed materials (aggregates and cement properties, and chemical composition of cement), the curing process and method, the temperature and humidity conditions in the surroundings, and the geometrical conditions of the structure element [36-38]. It should be mentioned that aggregates' deformation properties strongly impact the drying shrinkage of concrete, while autogenous shrinkage is practically independent of aggregates' deformational properties [39].

In most structure applications, only two types of shrinkage are taken into account in the analysis of concrete elements as major components: drying and autogenous shrinkages. A schematic illustration of the drying shrinkage to autogenous shrinkages ratio for normal- and high-strength concrete at concrete's total shrinkage age are shown in Figures 1-2 (a) and (b) [40, 41]. As we can see, the autogenous shrinkage effect for normal-strength concrete has only a low percentage of long-term shrinkage (10-20% - between 20 and 110 micro strains [42]). Because of its minimal effect, a uniform consideration can be taken into account without separating between autogenous and drying shrinkages. Indeed, its effect has been ignored by designers for many years.

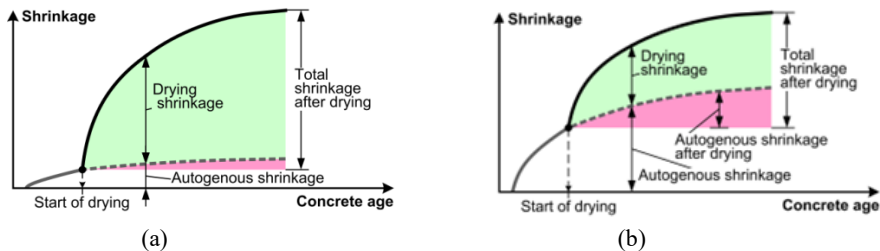


Figure 1-2: The drying and autogenous shrinkage ratio of: (a) normal-strength concrete; (b) high-strength concrete [40, 41].

Conversely to conventional concrete, the autogenous and drying components should be differentiated in high-strength concrete because the ratio of these shrinkages to total shrinkage fluctuate in relation to concrete age. The primary purpose of shrinkage measurement is to predict shrinkage cracking, which is a significant parameter for concrete structures' serviceability and durability behaviour.

The free shrinkage effect is another phenomenon that has been well covered by the literature. Free shrinkage is known as the contraction of hardened concrete exposed to air with relative humidity below 100%. Free shrinkage is a time-dependent phenomenon, and its rate rapidly lowers with time. The term "free" refers to the fact that the concrete element can shorten and generate no stresses without being restrained.

#### **1.1.4. Significance of Serviceability Design.**

For modern constructions and present demands for construction buildings, some requirements like durability, functionality and aesthetics are important. To fulfil these objectives, some solutions are becoming increasingly popular, and are sensitive to structural elements' deformation; for example, high-tech cladding, exposed concrete and white tank waterproofing systems. Simultaneously, cost and construction time limitations, along with new construction materials' increasing strengths and monolithically connected members according to rapid construction schedules lead to



slender structural elements, which all together result in less favourable serviceability conditions (see Figure 1-3).

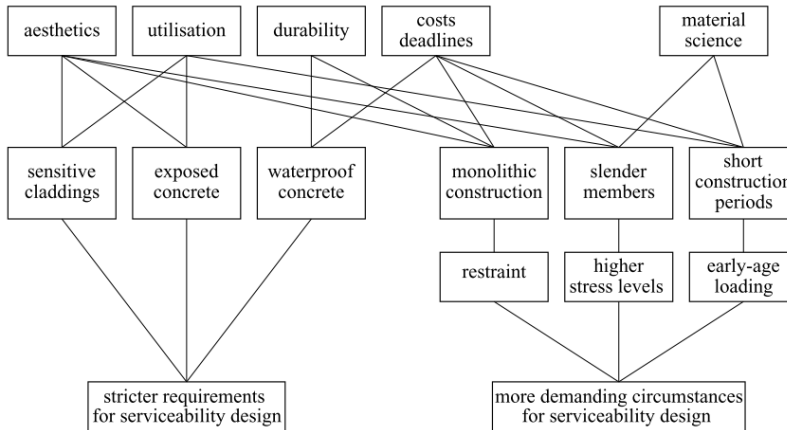


Figure 1-3: Significance of Serviceability Design [4].

Serviceability Limit States (SLS) requirements need to be applied to RC structures to guarantee their functionality and structure integrity under service conditions. Generally, the fundamental serviceability requirements that concrete structures should be meet are functionality, user comfort and appearance. These requirements cannot, however, be directly checked. Therefore, performance criteria like deflection control, vibration control and cracking control are defined to meet these requirements [5, 43]. Furthermore, RC structures' durability to environmental actions leads to the control of crack width under specific environmental conditions to prevent steel corrosion, which is caused by increasing chloride ions and carbon dioxide. Consequently, for the safety, serviceability and durability of the RC structures, crack control is essential during their designed working life.

Crack width control for concrete structure elements can be done so that cracks meet limitations to prevent steel reinforcement corrosion as determined under specific environmental conditions. Predicting the chloride ion concentration for steel reinforcement under specific environmental conditions is another parameter to examine RC elements' cracking behaviour, and it should be limited to the permissible concentration for steel corrosion onset during structures' working life. Note that concrete quality and concrete cover are important parameters to verify that steel reinforcement is protected from corrosion due to chloride ion ingress. Other parameters, such as structure appearance, water tightness and gas tightness, should be considered for examining cracking and the permissible crack width.

It is generally advised that the cracks which may pose user concern should be avoided for aesthetic and appearance reasons. Engineers and non-engineers may make various interpretations of cracks. However, the crack width value of 0.4 mm seems to be the

limit for them all. According to Beeby, A W [44], a crack width over 0.25 mm is likely to cause considerable dissatisfaction, In order to avoid casual observers' undue concern, Leonhardt, F [45] recommends limiting crack width on the surface for the concrete structural elements seen from short distances to 0.2 mm. It is worth mentioning that cracks on the surface may be accentuated by leaching or microorganisms. So restrictions for appearance purposes may be stricter than for other reasons [46]. When designing containers and reservoirs, both water tightness and gas tightness are governing parameters. Thus, limiting crack width values is critical to avoid leakage. This may also apply to bridge decks [47] and slabs in multi-story parking garages.

This thesis focuses on the tensile and cracking behaviour of R-UHPFRC elements under tensile axial loads (usually called tie elements) to evaluate the serviceability behaviour of R-UHPFRC elements. The tensile elements in this thesis are those prismatic UHPFRC elements with a central bar located over the entire element with a quadratic cross-section.

## **1.2. Objectives and Scope of the Thesis**

The main objective of this PhD study is to evaluate the tensile behaviour of R-UHPFRC under serviceability conditions and evaluate the SLS design code requirements for UHPFRC structures. This is done by:

1. Evaluating current experimental methods and designing a new test method based on the needs and objectives of this study.
2. Experimentally studying the influence of the fibre volume content effect, the size effect, and the reinforcement ratio effect on cracking behaviour of R-UHPFRC tensile elements.
3. Studying and evaluating the tension stiffening behaviour for R-UHPFRC tensile elements and the shrinkage effect on this behaviour
4. Evaluating the inverse analysis method proposed by our research group with the experimental results.

This thesis focuses on the deformation and cracking behaviour of R-UHPFRC tensile elements under serviceability conditions. In the serviceability field, other parameters should be considered, such as deflection limitation, vibration, etc. The work in this PhD is limited to the study of cracking limitations, and the following parameters are not considered in particular:

1. Fibre type: in this work, we used two types of steel fibres. There are many types of fibres with different kinds of materials that can be used in concrete and, depending on the employed fibre type, post-cracking behaviour can

differ. It should be mentioned that to understand the effect of utilising hybrid fibres on R-UHPFRC tensile elements' cracking behaviour (using large steel fibres mixed with micro-steel fibres), an experimental study was conducted. The complete description of this work is presented in Chapter 4.

2. Effect of high-strength reinforcement steel: combining the UHPFRC material (with high-strength and high-ductility characteristics under tensile and compression loads) with high-strength reinforcement steel could present a feasible means to solve undesirable damage patterns due to its delayed reinforcement yielding. In this work, we employ normal yield strength steel rebars.
3. Other parameters, such as load cycling (dynamic effects), load duration (creep effect), the effect of the bond between the matrix and aggregates on cracking and the size effect.

### 1.3. Layout of the thesis

This thesis is written based on six academic research papers presented in Chapters 3 to 5 of this document. Three of the papers are peer-reviewed and published in journal papers, and the other three are peer-reviewed conference papers and a book chapter.

This thesis has seven chapters, used to describe the process outlined above to meet the overall and specific objectives.

**Chapter 1.** The background, objectives and structure of the present document are included.

**Chapter 2.** A review of the main concepts related to the uniaxial tensile test methods, tensile concrete elements' (RC, FRC and UHPFRC) behaviour, tensile characterisation, and serviceability behaviour of the UHPFRC is presented.

**Chapter 3.** It contains the two published papers (1<sup>st</sup> and 2<sup>nd</sup> papers). It summarises the axial tensile test methods for RC elements and the details of the proposed novel tensile test methodology for serviceability to study R-UHPFRC tensile elements.

**Chapter 4.** It contains the 3<sup>rd</sup>, 4<sup>th</sup> and 5<sup>th</sup> published papers. It discusses the tensile behaviour of R-UHPFRC elements and describes the tension stiffening concept for R-UHPFRC tensile elements. This chapter also presents a comparison between the inverse analysis method and the experimental results. This chapter provides the deformation behaviour of R-UHPFRC tensile elements under serviceability conditions. It describes not only the effect of fibre content on the post-cracking tensile stiffness capacity of R-UHPFRC tensile elements, but also the importance of the shrinkage effect on the tension contribution of UHPFRC in tension.

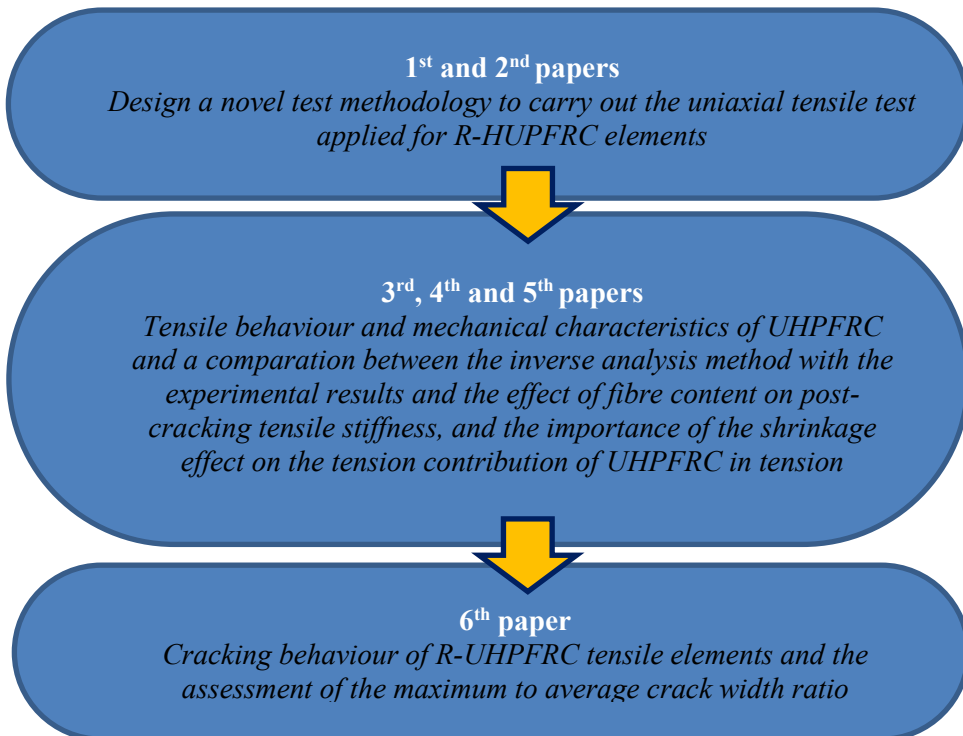
**Chapter 5.** It contains the 6<sup>th</sup> published paper, which presents an experimental study to evaluate the average and maximum crack widths caused by tensile stresses in R-UHPFRC tensile elements. The study presented in this chapter includes a statistical analysis to develop the fragility curves based on the obtained test data.

**Chapter 6.** It presents an overview of the six papers. It offers a brief description of the experimental work and discusses the main obtained results, together with an introduction that provides an overview of the work done in this thesis.

**Chapter 7.** It includes the main conclusions drawn from this PhD study and proposes future research lines.

#### **1.4. Summary and Interrelation of Papers**

Figures 1-4 show how the papers are interrelated to accommodate the main thesis objectives.



Figures 1-4: summary and interrelation of papers.

One of the commonest methods to study the tensile behaviour and cracking behaviour

of RC elements is carrying out the uniaxial tensile test using reinforced tie elements. For this purpose, (in the 1<sup>st</sup> and 2<sup>nd</sup> papers), an upgraded test methodology with all the details is proposed to study the deformation behaviour of R-UHPFRC under serviceability conditions. Two different types of R-UHPFRC tensile elements with variant fibre contents are tested. The preliminary results indicate that this test method could be useful and suitable for future studies for this PhD work. To better understand the tensile behaviour of R-UHPFRC elements (ties) and concrete's contribution behaviour of UHPFRC, an extensive experimental test was conducted, which is presented in the 3<sup>rd</sup> paper. Based on the achieved results in the 3<sup>rd</sup> paper, fibre content strongly influenced post-cracking tensile behaviour and serviceability behaviour. Hence a study was conducted to investigate this effect and the results are presented in the 4<sup>th</sup> paper.

In the 5<sup>th</sup> paper, the preliminary study about the shrinkage effect on the tensile response of R-UHPFRC elements was done. Finally in the 6<sup>th</sup> paper, a particular test programme with dog bone-shaped specimens was designed to run a specific study about the assessment ratio between the maximum and average crack widths and its importance in serviceability design for R-UHPFRC structures. Thus, these six papers accommodate the objectives of this PhD study.

## References:

- [1] M. Bajaber, I. J. J. o. M. R. Hakeem, and Technology, "UHPC evolution, development, and utilization in construction: A review," 2020.
- [2] A. Alani, M. Aboutalebi, M. J. J. I. J. o. C. King, Environmental, Structural, Construction, and A. Engineering, "Influence of fibre content on crack propagation rate in fibre-reinforced concrete beams," vol. 7, no. 9, pp. 1-7, 2013.
- [3] F. Rostásy, R. Koch, F. Leonhardt, and M. Patzak, Zur Mindestbewehrung für Zwang von Außenwänden aus Stahlleichtbeton: Minimum Reinforcement for Restrained External Lightweight Reinforced Concrete Walls. Ernst & Sohn, Berlin, Heft 267, 83 pp., 1976, p. 83pp.
- [4] C. Burns, "Serviceability analysis of reinforced concrete based on the tension chord model," IBK Bericht, vol. 342, 2012.
- [5] D. Honfi, Design for Serviceability-A probabilistic approach. Lund University, 2013.
- [6] A. Ghali, R. Favre, and M. Elbadry, Concrete structures: Stresses and deformations: Analysis and design for serviceability. CRC Press, 2018.
- [7] P. J. C. E. M. Claisse and M. Butterworth-Heinemann: Boston, USA, "Chapter 23—Creep, shrinkage, and cracking of concrete," pp. 241-249, 2016.
- [8] Model Code 2010-First complete draft-Volume 2: Model Code,

- 2883940967, 2010.
- [9] S. AFGC, "Bétons fibrés à ultra-hautes performances–Recommandations," AFGC, France, 2013.
  - [10] J. C. Committee, "Recommendations for design and construction of high performance fiber reinforced cement composites with multiple fine cracks," Japan Society of Civil Engineers, Tokyo, Japan, 2008.
  - [11] SIA 2052, "Béton fibré ultra-performant (BFUP)-Matériaux, dimensionnement et exécution. Draft," 2016.
  - [12] P. Richard and M. H. J. S. P. Cheyrezy, "Reactive powder concretes with high ductility and 200-800 MPa compressive strength," vol. 144, pp. 507-518, 1994.
  - [13] N. Gowripalan and R. J. R. A. Gilbert, The University of NSW, "Design guidelines for ductal prestressed concrete beams," 2000.
  - [14] A. Amin, S. J. Foster, and M. Watts, "Modelling the tension stiffening effect in SFR-RC," Magazine of Concrete Research, vol. 68, no. 7, pp. 339-352, 2016.
  - [15] C. C. JSCE, "Recommendations for design and construction of ultra high-strength fiber reinforced concrete structures (draft). JSCE Guidelines for Concrete No. 9.," 2006.
  - [16] P. J. A. NF, Paris, "P 18-470: Bétons fibrés à ultra-hautes performances–Spécification, performance, production et conformité," 2016.
  - [17] P. J. A. NF, Paris, "NF P 18-710, Complément national à l’Eurocode 2 — Calcul des structures en béton : règles spécifiques pour les Bétons Fibrés à Ultra-Hautes Performances (BFUP)."
  - [18] F. Biasioli, B. Poljansek, B. Nikolova, S. Dimova, and A. Pinto, "Eurocode 2: Background and applications: Design of concrete buildings," 2014.
  - [19] K. Wille, S. El-Tawil, A. E. J. C. Naaman, and C. Composites, "Properties of strain hardening ultra high performance fiber reinforced concrete (UHP-FRC) under direct tensile loading," vol. 48, pp. 53-66, 2014.
  - [20] K. Wille, D. J. Kim, A. E. J. M. Naaman, and structures, "Strain-hardening UHP-FRC with low fiber contents," vol. 44, no. 3, pp. 583-598, 2011.
  - [21] A. Hassan, S. Jones, G. J. C. Mahmud, and b. materials, "Experimental test methods to determine the uniaxial tensile and compressive behaviour of ultra high performance fibre reinforced concrete (UHPFRC)," vol. 37, pp. 874-882, 2012.
  - [22] K. Wille and A. E. J. A. M. J. Naaman, "Pullout Behavior of High-Strength Steel Fibers Embedded in Ultra-High-Performance Concrete," vol. 109, no. 4, 2012.
  - [23] E. J. Mezquida-Alcaraz, J. Navarro-Gregori, J. A. Lopez, and P. Serna-Ros, "Validation of a non-linear hinge model for tensile behavior of UHPFRC using a Finite Element Model," Computers and Concrete, vol. 23, no. 1, pp. 11-23, 2019.

- [24] J. Á. López, P. Serna, J. Navarro-Gregori, and H. J. C. P. B. E. Coll, "A simplified five-point inverse analysis method to determine the tensile properties of UHPFRC from unnotched four-point bending tests," vol. 91, pp. 189-204, 2016.
- [25] Y. Kusumawardaningsih, E. Fehling, M. Ismail, and A. A. M. J. P. E. Aboubakr, "Tensile strength behavior of UHPC and UHPFRC," vol. 125, pp. 1081-1086, 2015.
- [26] M. Gesoglu, E. Güneyisi, G. F. Muhyaddin, and D. S. J. C. P. B. E. Asaad, "Strain hardening ultra-high performance fiber reinforced cementitious composites: Effect of fiber type and concentration," vol. 103, pp. 74-83, 2016.
- [27] P. Maca, R. Sovjak, and T. J. P. E. Vavřiník, "Experimental investigation of mechanical properties of UHPFRC," vol. 65, pp. 14-19, 2013.
- [28] A. Considère, "Influence of metal reinforcement on the properties of the mortars and concrete (Influence des armatures métalliques sur les propriétés des mortiers et de béton)," (in French), *Le Génie Civil V. XXXIV*, vol. 15, pp. 229-233 1899.
- [29] H. Sooriyaarachchi, "Tension stiffening effect in GFRP reinforced concrete elements," University of Sheffield, 2006.
- [30] M. P. Collins and D. Mitchell, *Prestressed concrete structures*. Prentice Hall Englewood Cliffs, NJ, 1991.
- [31] E. Mörsch, "Concrete-Steel Construction (English Translation by EP Goodrich)," ed: McGraw Hill, New York, 1909.
- [32] P. H. Bischoff, "Tension stiffening and cracking of steel fiber-reinforced concrete," *Journal of materials in civil engineering*, vol. 15, no. 2, pp. 174-182, 2003.
- [33] P. J. Montoya, Á. G. Meseguer, and F. M. Cabré, *Hormigón armado*. Gustavo Gili, 2000.
- [34] G. Kaklauskas, V. Gribniak, D. Bacinskas, and P. J. E. s. Vainiunas, "Shrinkage influence on tension stiffening in concrete members," vol. 31, no. 6, pp. 1305-1312, 2009.
- [35] V. Gribniak, G. Kaklauskas, R. Kliukas, R. J. M. Jakubovskis, and Design, "Shrinkage effect on short-term deformation behavior of reinforced concrete—when it should not be neglected," vol. 51, pp. 1060-1070, 2013.
- [36] R. Bhandari, "Factors Influencing the Drying Shrinkage of Cement Stabilised Mixtures," in *Australian Road Research Board Conference Proc*, 1975, vol. 5, no. 7.
- [37] B. Tremper, "Factors influencing drying shrinkage of concrete," in *Meeting of Structural Engineers Association of Northern California*, San Francisco, 1961.
- [38] K. Ramamurthy, N. J. M. Narayanan, and Structures, "Influence of composition and curing on drying shrinkage of aerated concrete," vol. 33,

- no. 4, pp. 243-250, 2000.
- [39] P. Lura and K. Van Breugel, "Autogenous and drying shrinkage of high strength lightweight aggregate concrete," in *PRO 23: International RILEM Conference on Early Age Cracking in Cementitious Systems-EAC'01*, 2002, vol. 23, p. 335: RILEM Publications.
- [40] V. Gribniak, "Shrinkage influence on tension-stiffening of concrete structures," 2009.
- [41] V. Gribniak et al., "Investigation of shrinkage of concrete mixtures used for bridge construction in Lithuania," vol. 6, no. 2, pp. 77-83, 2011.
- [42] K. R. Silliman and C. M. Newton, "Effect of misting rate on concrete shrinkage," in *HPC: Build Fast, Build to Last. The 2006 Concrete Bridge Conference* Portland Cement Association Federal Highway Administration Nevada Department of Transportation American Concrete Institute (ACI), 2006.
- [43] T. Leutbecher and E. Fehling, "Design for serviceability of ultra high performance concrete structures," in *High Performance Fiber Reinforced Cement Composites 6: Springer*, 2012, pp. 445-452.
- [44] A. J. C. Beeby, "Cracking: what are crack width limits for?," vol. 12, no. 7, 1978.
- [45] F. J. P. J. Leonhardt, "Cracks and crack control in concrete structures," vol. 33, no. 4, pp. 124-145, 1988.
- [46] G. L. Balázs et al., "Design for SLS according to fib Model Code 2010," vol. 14, no. 2, pp. 99-123, 2013.
- [47] F. Toutlemonde, R. Pascu, G. Ranc, and T. J. B. D. L. D. P. C. Kretz, "Analysis of the structural effects of throughcracking within a reinforced concrete slab," pp. 193-213, 2005.



## ***Chapter 2. State-of-the-art***

The following chapter gives an overview of the uniaxial tensile test methodologies which were considered to design a novel test method for this PhD work. A state-of-the-art and historical perspective of the tensile stiffening behaviour modelling for RC, FRC and UHPFRC tensile elements is discussed. The general aspects of the structural serviceability and shrinkage influence on tension stiffening behaviour, and crack width prediction are described. The employed inverse analysis method is described, which is used to analyse and compare with experimental results. Finally, a discussion about the serviceability requirements for R-UHPFRC elements in different design codes is provided.

## **2.1. Uniaxial tensile test methodology**

This specific section attempts to explain and review the critical components of typical prototypes for performing the uniaxial tensile test, which is required in order to design a new test methodology.

The typical method for studying the cracking behaviour of reinforced concrete elements is carrying out the direct tensile test by using the tie elements. However, there is no standard for testing setup to carry out the tensile uniaxial test of reinforced concrete elements. Normally the concrete tie elements have a high length-to-width ratio with a prismatic shape with a steel bar reinforcement in the centre of the cross-section. Figure 2-1 illustrates a typical geometry of a tie element.

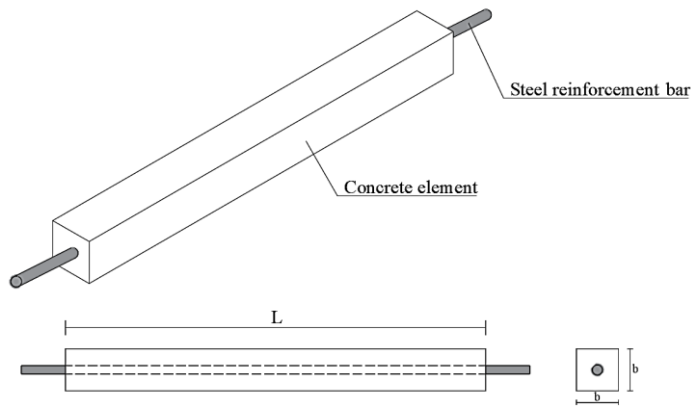


Figure 2-1: Typical tie element.

This test technique aims to determine the concrete structure SLS requirements. The tensile force is normally applied to bars protruding from the specimen's ends, and the main issue in performing a uniaxial tensile test is transferring the tensile load or deformation from the test machine devices to the end rebars. For that, special equipment requires for gripping and loading.

### **2.1.1. Force transfer systems for the RC tensile element test**

Researchers have presented several distinct approaches for force transmission and connecting systems. The most common method is using the jaw system or tensile grips and clamping two rebar's ends to be able to connect the concrete specimen to hydraulic jack devices.

Tables 2-1a and 2-1b show some of the grip types used by researchers to carry out the uniaxial tensile test of reinforced concrete elements.

Table 2-1a: Different types of grips used for uniaxial tensile test.



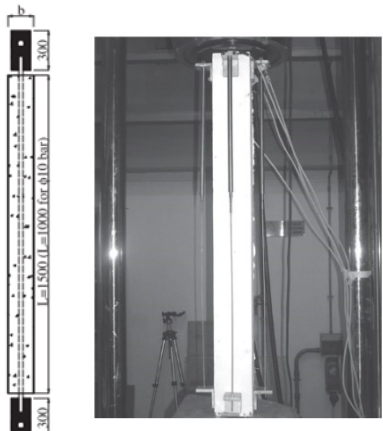
No.	Authors	General test setup view and connections	Descriptions
1	Al. Sokolov [1] LÁO Júnior [2]		The tie element were testes under monotonically increasing displacement by a displacement-controlled machine and using two vies grip wedges
2	M. HQ Wu [3]		The test was undertaken in an Instron universal testing machine by displacement control rate of 0.05 mm/min and using the hydraulic grips

Table 2-1b: Continue of Table 2-1a, Different types of grips used for uniaxial tensile test.

3	G. Tiberti [4] P. Bernardi [5]		<p>Tests were carried out by deformation control by using wedge tensile grips and clamping both the rebar ends. The deformation rate was varied from 0.1 to 0.2 mm/min.</p>
---	-----------------------------------	---	---

Researchers used several methodologies depending on their equipment capabilities and experimental test needs. As a sample, Shao-Bo Kang et al. [6] placed two steel plates at the end of the tie specimens with four welded reinforcing bars of 10 mm diameter. These bars were penetrated through the specimen to be able to directly apply the tension force to the element. To prevent the fracture in steel reinforcement at the outside of the specimen, they welded T-shaped steel brackets to the longitudinal reinforcement. These brackets were also welded to the endplates of the specimen. Figure 2-2 illustrate the proposed connection detail proposed by Shao-Bo Kang et al. [6].

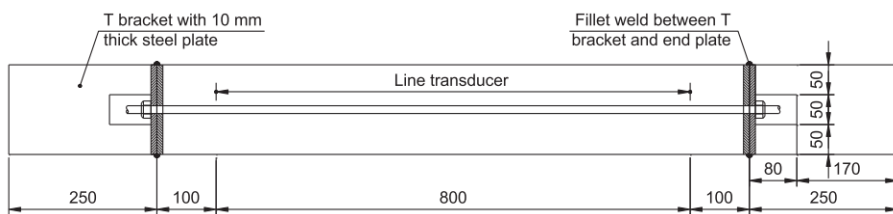


Figure 2-2: Using steel brackets for clamping the steel rebar's tie [6].

### 2.1.2. Geometry of the specimens

The most common geometry-shape for the ties is a prismatic shape with a quadratic cross-section. However, Kelvin Fields and Peter H. Bischoff [7] proposed an end corbel-shaped for specimens to apply tensile load to central 2 m long test length (see Figure 2-3). The tensile force was applied to specimen

by installing symmetrically four pull-rods at each end of the specimen with a concrete cover of 40mm. Due to existing a sharp stiffness difference between the central and end corbel parts, some localized cracks can be occurred out of the measurement zone and can affect the accuracy of measurement. This effect was called the end effect [8].

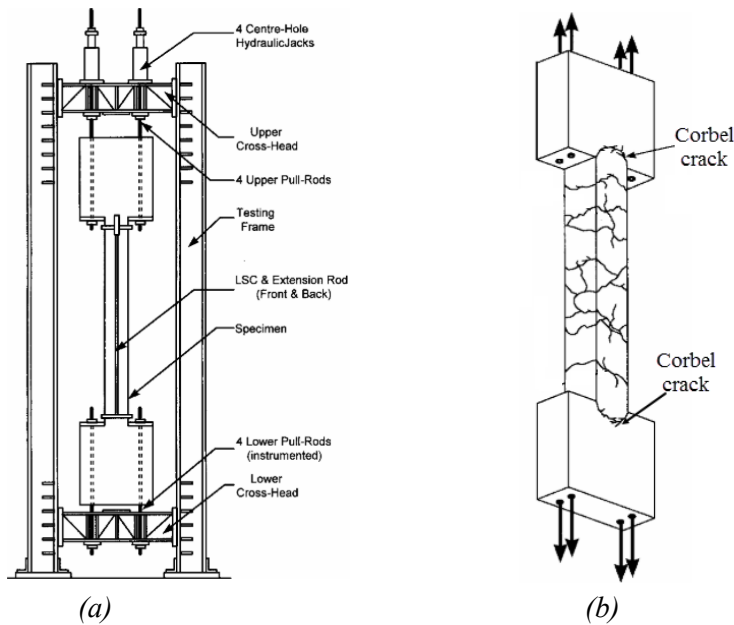


Figure 2-3: Corbel-shaped specimen for tensile element (a) General geometry of concrete specimen (b) Localized crack at the place of change of section width [7].

In order to reduce the unwanted end effect, R. Sahamitmongkol et al. [9] installed an additional spiral reinforcement at both ends of the specimen. These spiral reinforcements also help to prevent longitudinal cracks at the ends. The profile of the specimen and reinforcement details are shown in Figure.2-4.

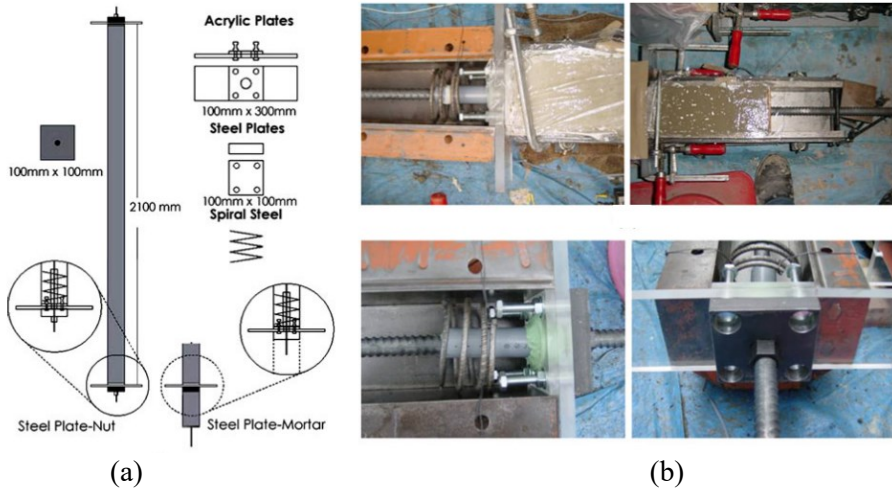


Figure 2-4: Restraining method applied to reduce the end effect for tie elements. (a) Specimen profile (b) Spiral reinforcement detail and localization [9].

Another similar method was proposed by Arvydas Rimkus et al. [8], M Qiu et al. [10], P Aghdasi et al. [11] with this difference that the width of the specimen at both ends was increased with a smooth slope (see Figure 2-5). Some scholars refer to this specimen geometry as "dog-bone shaped."

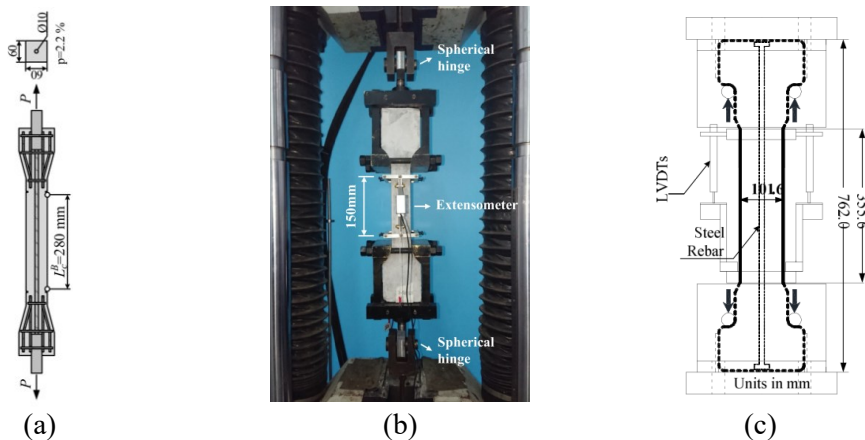


Figure 2-5: Proposed Dog-bone tensile elements geometry to reducing the end effect: (a) Arvydas Rimkus et al. [8] (b) M Qiu et al. [34] (c) P Aghdasi et al. [11].

Experimental evidence obtained by the authors [12, 13] and other researchers (e. g. [14, 15] ) shows that the crack pattern created by the uniaxial tensile test depends on the specimen's geometry and reinforcement arrangement. The typical tensile element with a bar at the centre of the cross-section might not be

representative of real structure elements. The typical tie elements are incapable to reflect the tensile behaviour of structural elements with a group of reinforcement bars. V. Gribniak et al. [16] proposed an innovative testing method that was capable to apply the uniformly distributed tension load to a series of reinforcement bars at a different location and monitoring the deformation of each bar. Their multi-bar equipment test and reinforcement arrangement at the cross-section are shown in Figure 2-6.

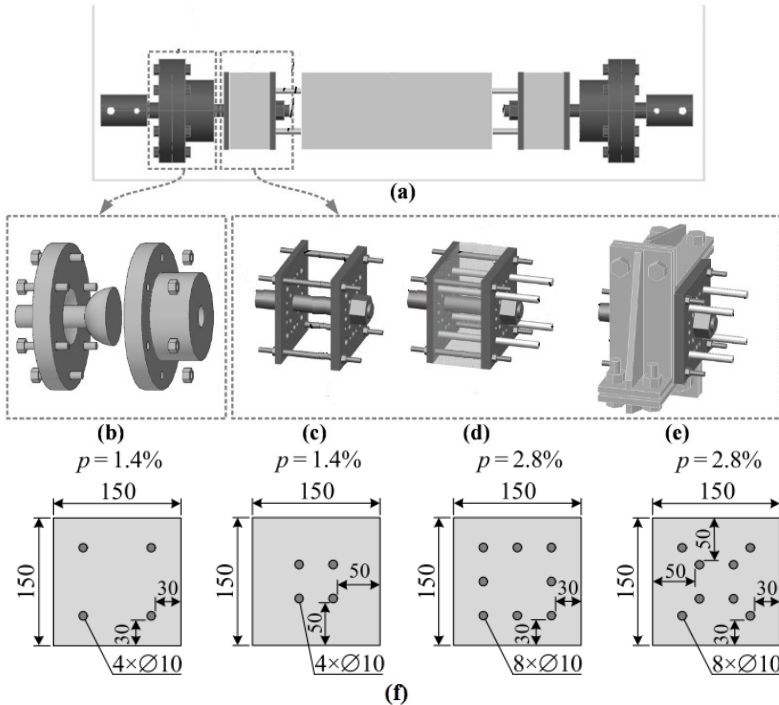


Figure 2-6: Multi-bar equipment test for tensile RC elements: (a) Concrete specimen with connection devices (b) spherical hinge (c) anchorage joint plate (d) reinforcement bar located in the anchorage joint plates (e) steel bracket (f) reinforcement arrangement over the cross-section [16].

It should be noted that the influence of reinforcement ratio or cover thickness can be also studied just by changing the cross-section dimension and reinforcement diameter. For instance, K. S Kang et al. [17] used specimens with cross-sections of  $90 \times 90$ ,  $120 \times 120$ , and  $150 \times 150$  mm<sup>2</sup> with longitudinal reinforcements of 13, 16, and 20 mm to study the influence of cross-section size of ties and ratio of steel reinforcement on tension stiffening effect. In this study, the ratio of longitudinal reinforcement ranged from 0.59% to 1.64% and the cover thickness ranged from 38.5 to 65.5 mm.

### 2.1.3. Measurement techniques

Different methods have been used for monitoring and measuring the strain or deformation of RC tensile elements. The most common method is measuring the displacement between two points over the surface of the RC tensile element to obtain the average strain over the gauge length. For that, it can be used the Linear Variable Differential Transformer (LVDTs) or Displacement Transducers (DTs), which they should be attached to the concrete surface. Monitoring the average tensile elongation of the RC elements under axial load can be performed by attaching four LVDT with the same length of the specimen on each side of the specimen. With this technique, by calculating the average elongation obtained by four LVDTs, the measurement accuracy will be increased and the errors due to curvature and rotation caused by cracking will be reduced. For instance, A. Amin et al. [18] fixed four LVDTs to each face of the specimen which the LVDT length was 900 mm to obtain the load-elongation behaviour of fibre reinforced concrete (SFRC) ties (see Figure 2-7).

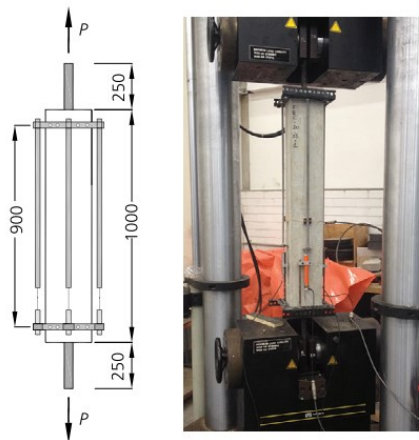


Figure 2-7: LVDT length and position [18].

Other researchers [19, 20] attached several small lengths of LVDTs through the element to perform a closer evaluation of tensile RC elements behaviour. Borosnyói and Snóbli [21] demonstrate that the crack width varied almost linearly from the concrete surface towards the reinforcing (see Figure 2-8). Consequently, the deformations of the concrete surface and internal bar reinforcement might be different and to have more realistic experimental results, monitoring the deformations at concrete surface and rebar surface is essential.



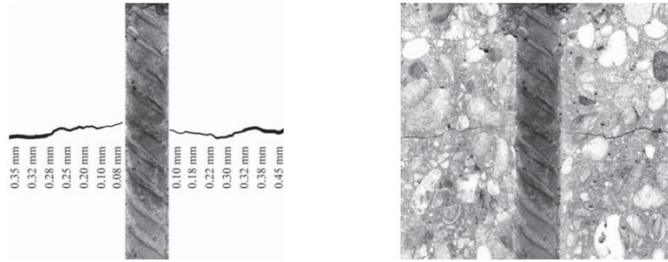


Figure 2-8: Variation of crack width for the specimen of RC tensile element with concentric steel reinforcement.

The average strains of the reinforcement can be obtained by an advanced monitoring system such as an internal gauging system. With this technique, the strain gradient variations through the specimen length can be obtained. RH Scott et al. [22], SB Kang et al. [17], H.Q Wu and R.I Gilbert [23], CC Hung [24] and I Vilanova et al. [25] used this technique to describe the strain profile along tie length. Some other researchers used optical fibre sensors to obtain the strain gradient along the reinforcement bar [26-29].

The Digital Image Correlation (DIC) technique is another method. This technique is used to get the crack propagation and strain distribution at the concrete surface of the concrete specimen during loading. Figure 2-9 shows the performance of the DIC technique for the uniaxial tensile test applied to RC ties.

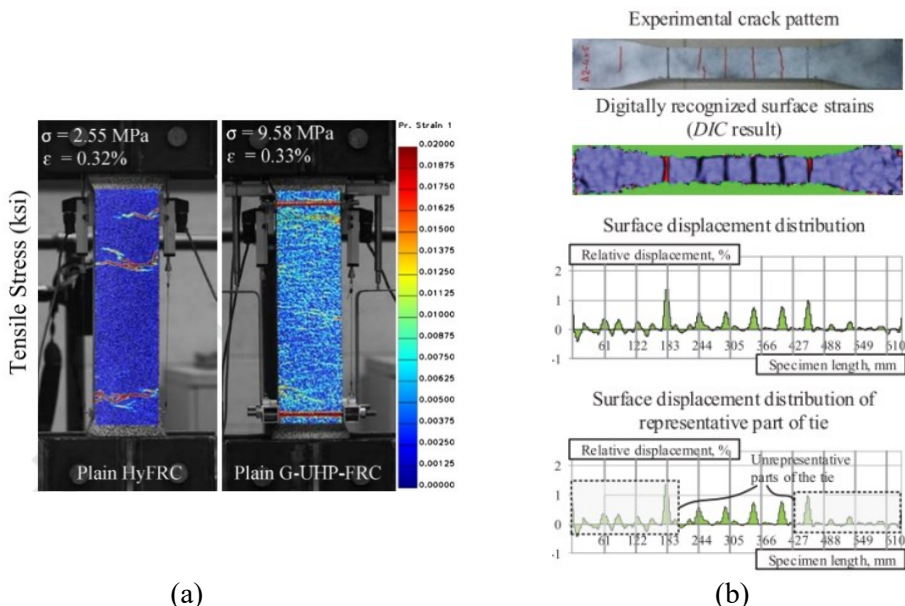


Figure 2-9: DIC images results (a) Strain counter at the peak stress for FRC and UHPFRC tie [11] (b) Strain distribution and relative displacement for RC tie [8].

Other indirect measurement techniques such as magnetic resonance imaging [30, 31], X-ray imaging [32, 33] and acoustic emission tomography [34] are available to detect the cracking behaviour of concrete specimens. These modern image back-scattering techniques need special equipment and a skilled person and the interpretation of the obtained results data from these methods is often complicated and needs the user's judgement.

Demountable mechanical gauge (DEMEC) is another measurement equipment that may be utilized to monitor the tensile deformation variation along with the concrete element. For using this mechanical measurement machine, the grid points should be defined over the surface of the specimen (see Figure 2-10).



Figure 2-10: DEMEC measurement machine and grid steel discs.

## **2.2. Tension stiffening effect of conventional reinforcement concrete (RC)**

### **2.2.1. Tension stiffening concept**

Plain concrete is not able to carry any tension stress at the cracks, while due to bonding between concrete and steel reinforcing, it is still able to carry a tension between cracks. This effect increases the member rigidity and causes a reduction of member deformation up to reinforcement yielding and consequently, the crack width under service loads is affected. For explaining the load sharing process and easy understanding of the tension stiffening concept, a reinforced concrete member loaded under axial tensile force and its load-deformation behaviour are illustrated in Figures 2-11 and 2-12, respectively.



proportional of their rigidity and their values theoretically remain constant along with the member (see Figure 2-11 (a)). In this stage, equilibrium and strain compatibility can be used by assuming linear elastic behaviour for both materials. The tensile force is transferred from reinforcement to the matrix by tending compressive forces surround the bar, and these forces cause internal cracks to form further primary cracks. By increasing the load (Force level  $N_2$ ), the tensile stress in the matrix reaches the concrete tensile strength capacity and the first crack takes place. The steel experiences a jump in stress at the crack and the distribution of stresses is no longer uniform and load carried by concrete ( $N_c$ ) and rebar ( $N_s$ ) are not constant. At the crack, due to bond failure along the short length of the bar, all the load must be carried by the steel bar and the stress value in the concrete would be zero (see Figure 2-11 (b)). In other words, after the first cracking, the contribution of steel and concrete for carrying the load is not equal. Collins and Mitchell [35] indicated that if force variation along the member is known, the strain variation along the member is possible to calculate. Consequently, it is possible to calculate the member deformation. Due to adhesion between two materials, by moving away from the crack, the tension in the matrix starts to increase and at a certain distance from the first crack (transfer length), tensile strength will achieve, and the second crack appears. By increasing the load, the element is fully cracked, and new cracks do not occur (load level  $N_3$  in Figure 2-11 (c)). The average strain in the steel bar can be calculated by:

$$\varepsilon_s = N_s / A_s \quad (2-1)$$

Where  $A_s$  is the bar area and  $N_s$  is the average force in the bar, which can be obtained by subtracting the concrete contribution from the total applied force:

$$\varepsilon_s = N_s / A_s \quad (2-2)$$

$$N_c = A_c \times f_c \quad (2-3)$$

The tension stress in the concrete ( $f_c$ ) is not constant, and its value is variable between zero at the cracks to a value less than cracking strength stress ( $f_c < f_{cr}$ ); hence, in Equation (2-3) is necessary to use an average value for ( $f_c$ ) [35]. The member's deformation can be calculated by the following Equation:

$$\Delta = \varepsilon_s \times L \quad (2-4)$$

where

$$\varepsilon_s = \varepsilon_c = \frac{N_s}{A_s \times E_s} \quad (2-5)$$

At the first cracking formation time, the average stress in the concrete is equal to cracking strength stress ( $f_c = f_{cr}$ ). Thanks to the tension stiffening effect, by increasing the load, the average tensile stress in the concrete will be reduced and

further cracks will develop. This reduction of average stress will continue, and the response curve will gradually close to the bare bar response. Figure 2-12 depicts this effect quite well. In Figure 2-12, the first stage refers to elastic deformations up to the first cracking (part OA). The region between first cracking up to final primary cracks (part AB) represents the crack formation region (stage 2), and in the third stage, cracks are fully developed (part BC).

### 2.2.2. Models of tension stiffening for RC elements

The tension stiffening effect can be expressed as the difference between the average member response and the bare rebar steel response, as is defined as the distance ( $N_{c,m}$ ) in Figure 2-13. The contribution of the cracked concrete to carry the tension stress in the reinforced member subjected to axial tensile force can be represented by the ( $f_c - \varepsilon_m$ ) diagram, where ( $f_c$ ) is the tension stress carried by cracked concrete and ( $\varepsilon_m$ ) is the average member strain as indicated by the inset in Figure 2-13. The initial response of reinforced concrete is linearly elastic and the distribution of stresses between steel and concrete is uniform and its value remains constant along the length of the member. Elastic behaviour will continue until the tensile strength of the concrete ( $f_{cr}$ ) and the first crack appears at a load ( $N_{cr}$ ).

It is assumed that at the cracked section, the concrete is not capable to carry tension, but the member is still able to develop tensile stresses away from the crack. The concrete stress value varies between cracks along the length of the member, causing the average tensile stress to decrease. The average tensile stress in the concrete after the first cracking is less than ( $f_{cr}$ ). By increasing the strain, the average tensile capacity of the concrete continues to decrease and more cracks develop; hence the tension stiffening decreases as the load ( $N$ ) increases. There are no more cracks after the crack stabilization, and the tension stiffening effect (average tensile stress in concrete) continues at a slower rate. Consequently, the member response curve will be closer to the bare bar response.

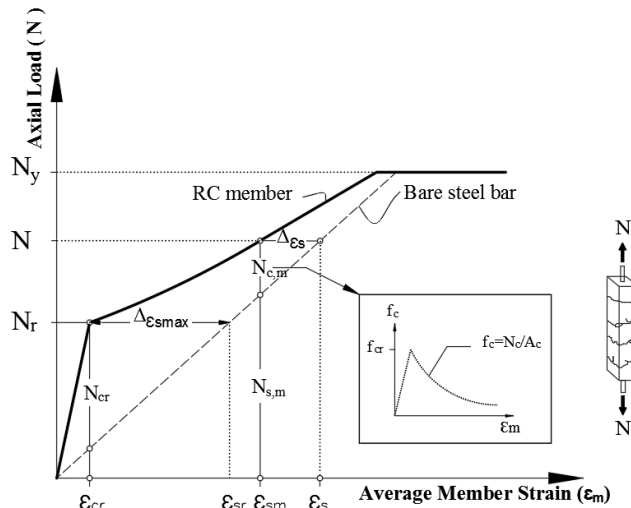


Figure 2-13: Tensile response and concrete contribution of axial tensile RC member [adapted from [7]].

There are two different approaches for modelling the tension stiffening behavior of RC tensile members: 1) Empirical methods and 2) Theoretical methods. These two approaches are described below.

### 2.2.2.1. Empirical methods for tension stiffening modelling

The empirical methods aimed to provide an idealistic behaviour for RC tensile members based on the post-cracking response obtained by a simple axial tensile test. Analytical models obtained by empirical methods have two main parts: I) Ascending portion, which assumes a unique stress-strain relationship up to peak stress value at the first cracking, II) Descending portion, which is a relationship between post-peak stress and crack width. Figure 2-14 depicts the typical analytical models for representing the post-cracking contribution of cracked concrete.

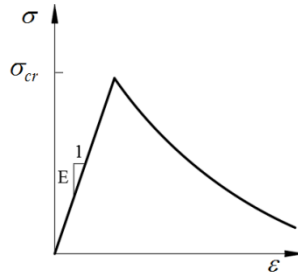


Figure 2-14: Typical analytical models used to represent for tension stiffening modelling.

The early modelling of tension stress-strain curves for concrete had been represented at the final of the 19<sup>th</sup> century. First attempts were made by Scanlon & Murray [37] using an approximate formulation to incorporate gradual loss of stress-strain capacity of plain concrete in tension in numerical schemes which used for the tension stiffening effects modelling for RC members. They proposed a stepwise stress-strain diagram by reducing secant stiffness. Figure 2-15 (a) gives the details of their model. Lin & Scordelis [38] tried to use a gradual unloading curve by a cubic polynomial for modelling the post-cracking behaviour (see Figure 2-15 (b)), and Gilbert & Warner [39] proposed a discontinuous unloading curve after cracking as shown in Figure 2-15 (c). Note that their model consisted of a small drop in strength immediately after cracking and flowed by linear behaviour.

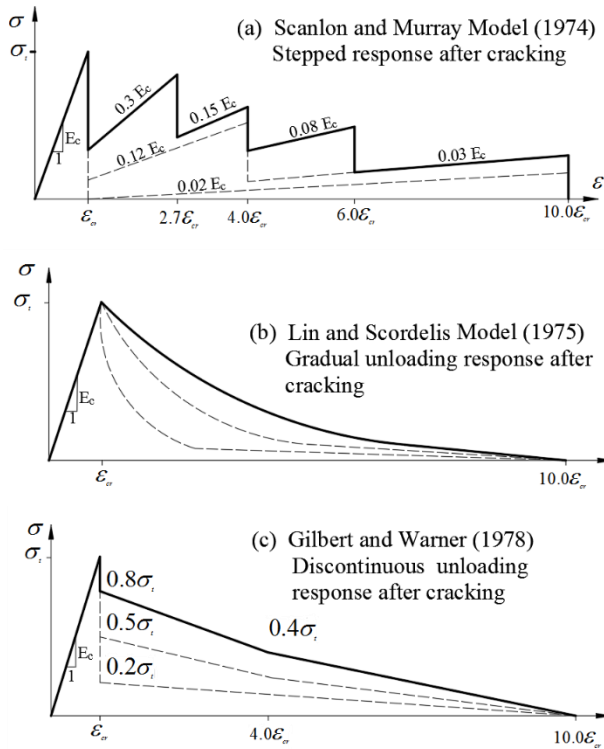


Figure 2-15: Stress-Strain diagram modelling for concrete in tension.

Vecchio & Collins [40] presented an analytical model that was capable to predict the load-deformation response of reinforced concrete elements subjected to pure plane shear. They obtained the stress-strain relationship for cracked concrete based on 30 reinforced concrete panels test results. They proposed a linear relationship before cracking (the ascending branch of the constitutive relation for determining the average stresses from the average strains):

$$f_{c1} = E_s \cdot \epsilon_1 \quad (2-6)$$

The suggested relationship for post-cracking response (tension stiffening effect) was:

$$f_{c1} = \frac{f_{cr}}{1 + \sqrt{200\epsilon_1}} \quad , \quad f_{cr} = 0.33\sqrt{f'_c} \quad (2-7)$$

Where ( $f_{c1}$ ) and ( $\epsilon_1$ ) are the stress and strain in the concrete in the principal direction, ( $f_{cr}$ ) is the cracking strength of concrete and ( $f'_c$ ) compressive strength of concrete cylinders. Figure 2-16 illustrate the tension stiffening proposed by Vecchio & Collins [40].



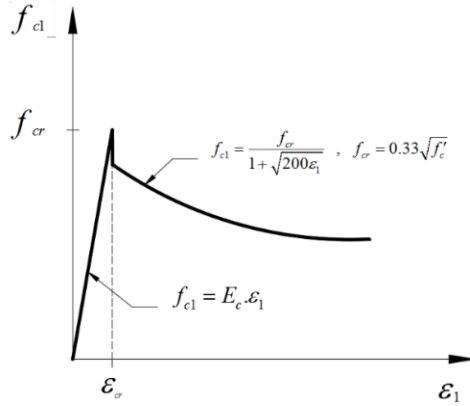


Figure 2-16: Average stress-strain relationship for cracked concrete in tension [40].

As can be observed in Figure 2-16, this proposed model includes a rapid drop in tension stiffening as the first crack form. Later, Collins & Mitchell [35] proposed a modification of this model and suggested flowing relationship expression for the descending part of the model :

$$f_c = \frac{\alpha_1 \alpha_2 f_{cr}}{1 + \sqrt{500} \epsilon_{cf}} \quad (2-8)$$

8)

where ( $\alpha_1$ ) is the factor accounting for bond characteristics of reinforcement and its value can be expressed as follows:

$$\alpha_1 = \begin{cases} 1.0 & \rightarrow \text{for deformed reinforcing bars} \\ 0.7 & \rightarrow \text{for plain bars, wires, or bonded strands} \\ 0 & \rightarrow \text{for unbounded reinforcement} \end{cases}$$

and ( $\alpha_2$ ) is the factor accounting for sustained or repeated loading and its value can be expressed as follows:

$$\alpha_2 = \begin{cases} 1.0 & \rightarrow \text{for short - term loading} \\ 0.7 & \rightarrow \text{for sustained and / or repeated loads} \end{cases}$$

Pang & Hsu [41] hypothesized another relationship for tension stiffening effect. The following analytical formulas were employed based on their results of 35 full-size panels tests:

ascending branch ( $\epsilon_1 \leq \epsilon_{cr}$ ):

$$\sigma_1^c = E_c \bar{\epsilon}_1 \quad (2-9)$$

descending branch ( $\epsilon_1 > \epsilon_{cr}$ ):

$$\sigma_1^c = f_{cr} \left( \frac{\epsilon_{cr}}{\bar{\epsilon}_1} \right)^{0.4} \quad (2-10)$$

Where ( $\varepsilon_{cr}$ ) is cracking strain of concrete, taken as  $0.00008(\text{mm/mm})$ , and ( $f_{cr}$ ) is cracking stress of concrete, obtained by:

$$f_{cr} = 0.31\sqrt{f_c(\text{MPa})} \quad (2-11)$$

The Equation (2-10) was first proposed by Tamai & Shima [42], and Hsu et al.[43] used that as well in his unified theory of reinforced concrete. The schematic diagram of this proposed tensile stress-strain relationship is shown in Figure 2-17.

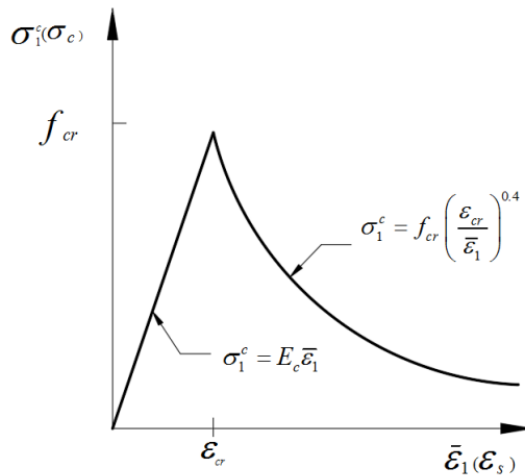


Figure 2-17: Tension stress-strain curve of concrete [41] and [43].

As previously stated, the tension stiffening relationship is usually driven by tensile experimental data. They are based on the modification of the constitutive law of concrete from the cracking stage. These models also can be applied for flexure behaviour modelling. However, their behaviour differs from that of tensile members.

### 2.2.2.2. Theoretical methods for tension stiffening modelling

This approach is based on modelling of the bond-action between concrete and reinforcement, and solution of the bond-stress distribution function or bond-slip function. Saliger [44] was the first one who has proposed this method.

#### **Basic assumption**

1. Concrete and steel reinforcement have linear elastic behaviour during the extension. Consequently, the maximum tensile load carried by steel

reinforcement due to applied load ( $P$ ) is equal to:

$$P_s = f_y \cdot A_s \quad (2-12)$$

where ( $f_y$ ), and ( $A_s$ ) are yield stress and the transversal section of steel reinforcement, respectively.

- It is assumed that the tensile stress is uniformly distributed in the concrete matrix.

### Equations for concrete and steel components

Figure 2-18 (a) depicts a section of reinforced concrete between two cracks that is subjected to a uniaxial tensile force ( $P$ ). The length of this segment is ( $\delta$ ), which is equal to the crack spacing. Figure 2-18 (b) indicates a free-body diagram of the left side. The applied load ( $P$ ) is carried partly by the matrix ( $P_{mx}$ ) and partly by the steel bar ( $P_{sx}$ ). The longitudinal equilibrium of forces in this section is determined as follows:

$$P = P_{mx} + P_{sx} \quad (2-13)$$

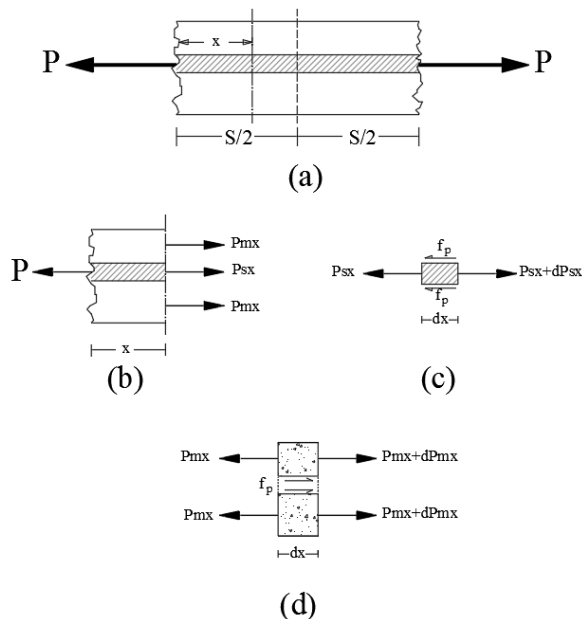


Figure 2-18: Free body diagram for RC member.

The load, strain, and bond stress distribution along the portion of reinforcement concrete and between two cracks are shown in Figure 2-19.

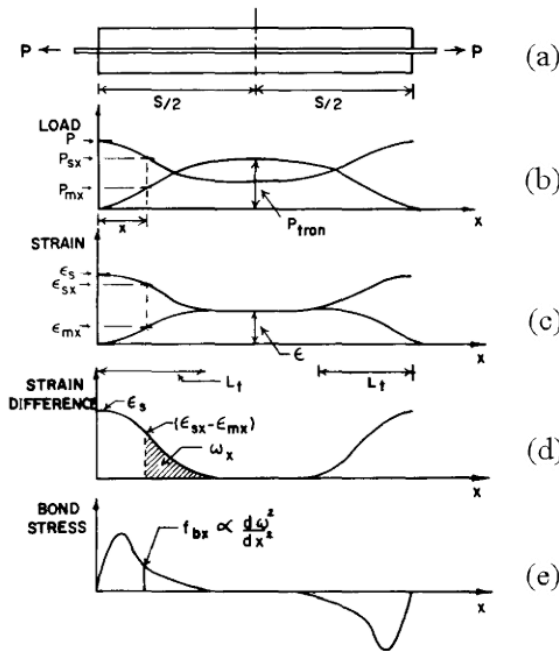


Figure 2-19: Load, strain, slip and bond stress distribution [45].

As can be seen in this diagram, the load value carried by reinforcement at the cracks ( $x=0$  and  $x=2(S/2)$ ) is equal to the total tensile force and is zero in concrete.

$$P_{mx} = A_m E_c \epsilon_{mx} \quad (2-14)$$

$$P_{sx} = A_s E_s \epsilon_{sx} \quad (2-15)$$

where ( $E$ ), ( $\epsilon$ ) and ( $A_m$ ) are the young's modulus, the axial strain, and cross-sectional area, respectively. Substituting Equations (2-14 and 2-15) into Equation (2-13) gives:

$$P = A_m E_c (\epsilon_{mx} + \epsilon_{sx} n) \quad (2-16)$$

The term ( $n$ ) is the modular ratio ( $E_s / E_m$ ). Also, the value of ( $P_{mx}$ ) is zero at the cracks, and its maximum amount is obtained at a distance of ( $l_f$ ) from the crack, which is shown in Figure 2-19 (b). The transfer length ( $l_f$ ) refers to the element length in which the strain value of steel bar and concrete is equal to each other.

The difference in elongations between the steel bar and the concrete indicates the local slip ( $w_x$ ) at the rebar-concrete interface and is measured along the section ( $x$ ) and the segment centre ( $S/2$ ).

$$w_x = \int_x^{S/2} (\epsilon_{sx} - \epsilon_{mx}) dx \quad (2-17)$$

Equation (2-18) is derived by differentiating of Equation (2-17) with respect to  $x$  :

$$\frac{dw_x}{dx} = -(\varepsilon_{sx} - \varepsilon_{mx}) \quad (2-18)$$

Substituting the  $(\varepsilon_{mx})$  obtained from (2-16) into (2-18) leads to:

$$\frac{dw_x}{dx} = (\varepsilon_s n \rho - \varepsilon_{sx} (1 + n \rho)) \quad (2-19)$$

In which  $(\varepsilon_s)$  is steel strain and its value at the crack ( $x=0$ ) is  $(\varepsilon_s = P / A_s E_s)$ . Differentiating Equation (2-19) leads to:

$$\frac{d^2 w_x}{dx^2} = -(1 + n \rho) \frac{d\varepsilon_{sx}}{dx} \quad (2-20)$$

The local bond stress  $(f_{bx})$  is expressed as the force reduction carried by the reinforcement over a differential length  $(d_x)$  at  $(x)$ , per unit surface area  $(\Sigma_0)$  of the bar, which can be demonstrated by the following Equation:

$$f_{bx} = -\frac{dP_{sx} / dx}{\Sigma_0} = -\frac{A_s E_s (d\varepsilon_{sx} / dx)}{\Sigma_0} \quad (2-21)$$

where  $(d\varepsilon_{sx} / dx)$  is obtained as follows:

$$\frac{d\varepsilon_{sx}}{dx} = \frac{f_{bx} \Sigma_0}{A_s E_s} \quad (2-22)$$

Substituting (2-22) into Equation (2-20) leads to:

$$\frac{d^2 w_x}{dx^2} - \frac{(1 + n \rho) \Sigma_0}{A_s E_s} f_{bx} = 0 \quad (2-23)$$

Equation (2-23) represents the basic relationship between the second derivative of local slip  $(w_x)$  and local bond stress  $(f_{bx})$ . The boundary conditions should be applied for solving this Equation [45]. The boundary conditions are: at  $(x = S / 2 \rightarrow w_x = 0)$ ; The slip is zero at the centre of the segment (see Figure 2-19(d)).

- a) at  $(x = 0 \rightarrow \frac{dw_x}{dx} = -\varepsilon_s)$ ; from Equation (2-18), (see Figure 2-19(d)).
- b) at  $(x = l \rightarrow \frac{dw_x}{dx} = 0)$ ; from Equation (2-18), (see Figure 2-19(d)).
- c) at  $(x = 0 \rightarrow \frac{d^2 w_x}{dx^2} = 0)$ ; bond stress at the crack face is zero (see Figure 2-19(e)).
- d) at  $(x = S / 2 \rightarrow \frac{d^2 w_x}{dx^2} = 0)$ ; bond stress at the centre is zero (see Figure 2-19(e)).

The local bond stress  $(f_{bx})$  is a function of local slip  $(w_x)$ , which can be seen in Equation (2-23).

Somayaji & Shah [45] assumed that the local bond stress-slip relationship is an exponential distribution function and the resulting solution is given as follows:

$$\frac{d^2 w_x}{dx^2} = Ae^x + Be^{-x} + C \quad (2-24)$$

( $w_x$ ) can be obtained by twice integrating the above Equation:

$$w_x = Ae^x + Be^x + Cx^2 / 2 + D_x + E \quad (2-25)$$

By applying the boundary conditions mentioned above (a to e), the constants (A to E) can be obtained and consequently, the reinforcement strain, the concrete strain, and bond stress at any section can be derived by successive differentiation of Equation (2-25) and using Equations (2-18), (2-19) and (2-23). The tension stiffening effect along the specimen's length can be obtained by integrating the contribution at various sections.

Somayaji & Shah [45] assumed that the transfer length is proportional to the transferred loading. This linear relationship can be defined by using the pull-out test results, which is expressed by:

$$l_t = K_p \frac{P}{(1+n\rho)\pi D} \quad (2-26)$$

where ( $K_p$ ) is the constant value, which is obtained from the pull-out test, and ( $D$ ) is rebar diameter.

Another approach that can be used to model post-crack behaviour, including the stress-stiffening effect is a model based on the function of bond stress distribution. In this method, the equilibrium of free bodies for concrete and steel is obtained by considering a segment of composite material (concrete and steel) with the length of ( $dx$ ), (see Figure 2-20) as follows:

$$u.\pi.Ddx = -A_c.d\sigma_{cx} \rightarrow u = -\frac{A_c}{\pi D} \frac{d\sigma_{cx}}{dx} \quad (2-27)$$

and

$$u.\pi.Ddx = -A_s.d\sigma_{sx} \rightarrow u = -\frac{A_s}{\pi D} \frac{d\sigma_{sx}}{dx} \quad (2-28)$$

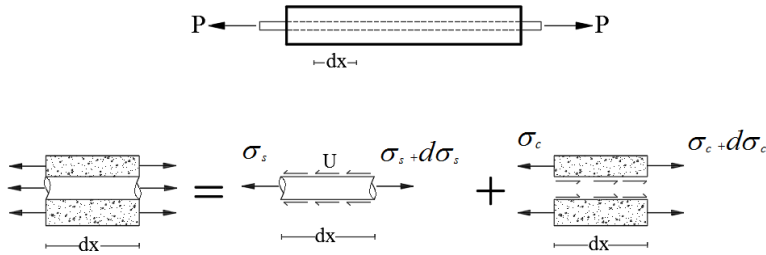


Figure 2-20: Tension member and free bodies for modelling the post-crack behaviour [46].

( $u$ ) represents the bond stress at the concrete-steel interface, while ( $\sigma_{cx}$ ) and ( $\sigma_{sx}$ ) represent concrete and steel stresses, respectively. There are different methods for determining bond stress. Nilson et al. [47] used a third-degree polynomial Equation for the local bond stress-slip relationship ( $u-d$ ) to fit in with the test results in the following Equation and Figure 2-21.

$$u = 3606 \times 10^3 d - 5356 \times 10^6 d^2 - 1986 \times 10^9 d^3 \quad (2-29)$$

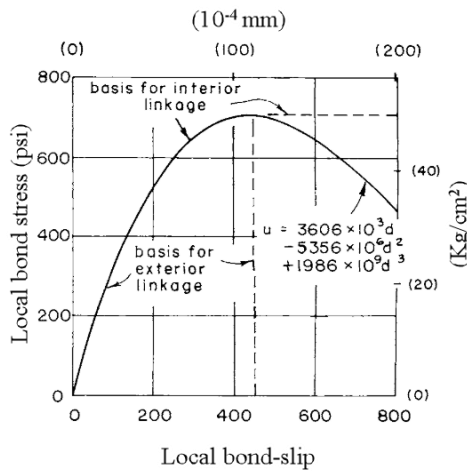


Figure 2-21: Proposed bond-slip curve used in the Nilson et al. modelling [47].

In further research, the bond stress-slip relationship was obtained experimentally by Nilson et al. [48], and Gupta & Maestrini [49] used a bilinear curve for approximating this experimental data, as seen in Figure 2-22.

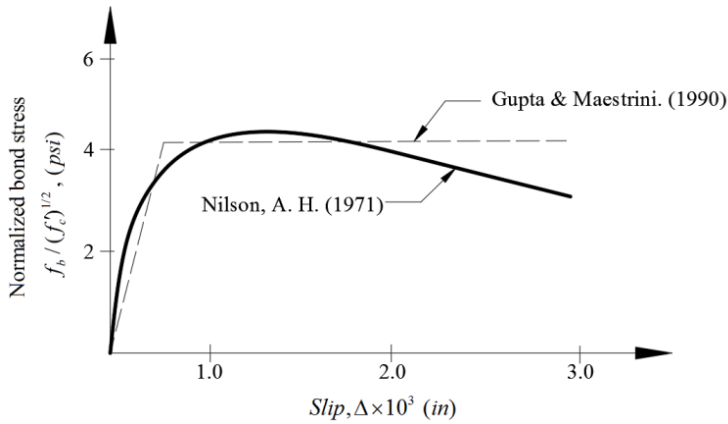


Figure 2-22: Bond-slip curve and bilinear approximation.

Their approach was based on two steps: first, they applied the linear bond stress-slip relationship to solve Equation (2-23) and obtain the average stress-strain relationship for concrete.

$$f_b = A \times \Delta \tag{2-30}$$

Where ( $\Delta$ ) is equal to ( $u_s - u_c$ ), and ( $A$ ) is the slope of the bond-slip curve. By using the same equilibrium and boundary conditions to the prior procedure and assuming that both steel and concrete are linear elastic, it is possible to determine the concrete tensile contribution (tension stiffening effect). The obtained relationship for the four values of the area parameter ( $n\rho$ ) is depicted in Figure (2-23).

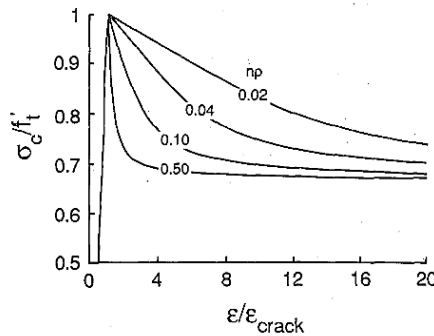


Figure 2-23: Tension stiffening model with a linear bond stress-slip relationship [49].

In this diagram, ( $\sigma_c$ ) and ( $\varepsilon$ ) are the effective tensile stress in concrete and the average strain in the reinforcing steel bar, respectively. ( $\rho$ ) is the member reinforcement ratio and ( $n$ ) is the steel-to-concrete modular ratio ( $n = E_s / E_c$ ).



In the second step, they considered the bilinear bond stress-slip relationship as follows (see also Figure 2-22):

$$\begin{cases} f_b = A \times \Delta \rightarrow f_b < f_m, \Delta < \Delta_m \\ f_b = f_m \rightarrow \Delta \geq \Delta_m \end{cases} \quad (2-31)$$

In the problem-solving method, they defined the parameter ( $f$ ) called “bond parameter,” which is a ratio of the concrete cracking force and bond force transferred at the interface area between concrete and steel over the characteristic length. ( $f=0$ ) implies that the maximum bond stress ( $f_m$ ) is considerable, and the linear bond stress-slip relationship is applied. The effective tensile stress-strain curve of concrete is plotted for ( $n\rho=0.500$ ) and for different values of the bond parameter (0 to 5). Figure 2-24 is shown this tension stiffening model.

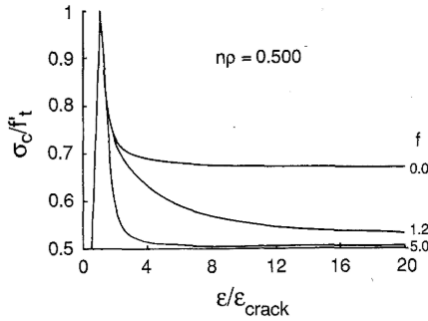


Figure 2-24: Tension stiffening model with a bilinear bond stress-slip relationship proposed by Gupta & Maestrini [49].

Most of the models for tension stiffening effect are just considered to describe the post-cracking range of the tensile stress-strain curve without considering the reinforcement ratio and material properties. Many researchers have been conducted parametric studies to investigate the influence of reinforcement ratio ( $\rho$ ) and material properties on tension stiffening. Stramandinoli & La Rovere [50] proposed an exponential decay curve for modelling the post-cracking branch of the tensile stress-strain of concrete, which was a function of the ( $\rho$ ) and ( $n$ ) by applying an exponential decay parameter ( $\alpha$ ). The decay curve was adopted until yielding of reinforcement took place, and it was specified by the following Equation:

$$\sigma_{ct} = f_{ct} e^{-\alpha \left( \frac{\epsilon}{\epsilon_{cr}} \right)} \quad (2-32)$$

Where, ( $f_{ct}$ ) and ( $\epsilon_{cr}$ ) are the concrete tensile strength and the corresponding strain, respectively. In order to determine the ( $\alpha$ ), another method could be

applied by adjusting the experimental results from the direct tensile tie test, by changing the reinforcement ratio ( $\rho$ ) and material properties; however, Stramandinoli & La Rovere [50] suggested an expression for ( $\alpha$ ), which was defined as a function of ( $\rho$ ) and ( $n$ ) based on the CEB, 1984 model [51]. Obtained parameter ( $\alpha$ ) was:

$$\alpha = 0.016(n\rho)^3 - 0.106(n\rho)^2 + 0.255(n\rho) + 0.017 \quad (2-33)$$

Unlike the simplified models, which are not able to consider the different reinforcement ratio on tension stiffening, this model considers this effect. A comparison of the proposed model with the model of Collins & Mitchell [35] is shown in Figure 2-25.

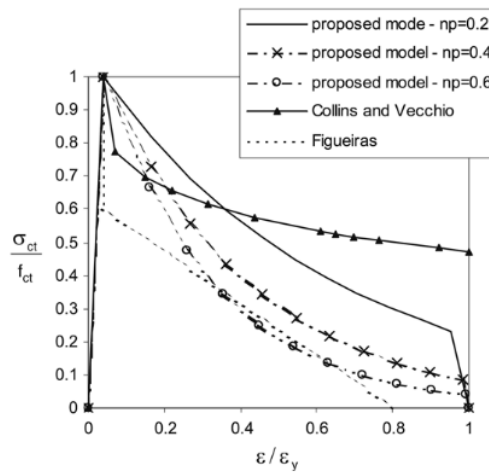


Figure 2-25: Comparison of tension-stiffening models Stramandinoli & La Rovere [50] with Collins & Mitchell [35].

### 2.2.3. Tension stiffening bond factor

As previously stated, in order to evaluate the concrete contribution and obtain the average concrete tensile stress for the reinforced members, it is helpful to introduce a relationship between the average tensile stress carried by cracked concrete ( $f_c$ ) and the average tension stiffening strain ( $\varepsilon_m$ ), (see inset in Figure 2-13). This approach was first presented by Johnson [52]. The parameters mentioned above can be defined as follows:

$$f_c = \frac{N_{cm}}{A_c} \quad (2-34)$$

Where ( $N_{cm}$ ) is the load carried by concrete, and ( $\varepsilon_m$ ) is the tension strain of the element.

There are two methods to evaluate the tension stiffening behaviour: I) Using the

tension stiffening strain ( $\Delta\epsilon_s$ ) which can be obtained by subtracting the average member deformation from the bare steel bar response. (see Figure 2-13). II) Using the average load carried by cracked concrete ( $N_{c,m}$ ), which can be calculated by subtracting the bare bar response ( $N_{s,m}$ ) from the measured member response ( $N$ ).

The average strain of the cracked member ( $\epsilon_m$ ) for any given load ( $N$ ), which is equal to the average strain in the steel reinforcement could be obtained by subtracting the tension stiffening strain ( $\Delta\epsilon_s$ ) from the average bare steel strain ( $\epsilon_s$ ) as follows [7]:

$$\epsilon_{sm} = \epsilon_s - \Delta\epsilon_s \quad (2-35)$$

The tension stiffening factor ( $\beta$ ) can be defined as a ratio between the tension stiffening strain for a given load ( $\Delta\epsilon_s$ ), and the jump in steel strain at the first crack ( $\Delta\epsilon_{s,max}$ ) by the following Equation:

$$\beta = \frac{\Delta\epsilon_s}{\Delta\epsilon_{s,max}} \quad (2-36)$$

where

$$\Delta\epsilon_{s,max} = \epsilon_{sr} - \epsilon_{cr} \quad (2-37)$$

Substituting (2-36) into (2-35) leads to:

$$\epsilon_{sm} = \epsilon_s - \beta \cdot \Delta\epsilon_{s,max} \quad (2-38)$$

The tension stiffening factor also is called the “bond factor” by some researchers, which shows the variation of strains in the steel bar along the member length [7]. While ( $\beta$ ) at the first crack can vary between one and zero, the member response and bare bar response are the same, and also the bond between them is destroyed. ( $\Delta\epsilon_{s,max}$ ) can be obtained by equating the slope of the bare steel bar using load carried at the first crack ( $P_{cr}$ ) and ( $\Delta\epsilon_{s,max}$ ):

$$A_s \cdot E_s = \frac{P_{cr}}{\Delta\epsilon_{s,max}} \rightarrow \Delta\epsilon_{s,max} = \frac{P_{cr}}{A_s \cdot E_s} = \frac{A_c \cdot f_{cr}}{A_s \cdot E_s} = \frac{f_{cr}}{\rho \cdot E_s} \quad (2-39)$$

Where ( $A_s$ ) and ( $E_s$ ) are the area, and elastic modulus of reinforcement, respectively and ( $A_c$ ) is the concrete area in tension and ( $\rho$ ) is equal to the steel reinforcing ratio. Finally, by substituting the Equation (2-39) into (2-38), the term ( $\epsilon_{sm}$ ) can be expressed as:

$$\epsilon_{sm} = \frac{1}{E_s} \left( f_s - \beta \frac{f_{cr}}{\rho} \right) \quad (2-40)$$

Johnson [52] proposed the expression (2-37), which was also expressed in another way by Fields & Bischoff [7]:

$$\varepsilon_{sm} = \varepsilon_s - \frac{\beta}{1+n\rho} \varepsilon_{sr} = \frac{f_s}{E_s} \left( 1 - \frac{\beta}{1+n\rho} \frac{f_{sr}}{f_s} \right) \quad (2-41)$$

where ( $f_{sr}$ ) is the stress in the reinforcement at first cracking.

$$f_{sr} = \frac{N_r}{A_s} \quad (2-42)$$

42)

As discussed previously, the load carried by cracked concrete can be applied to evaluate the tension stiffening, and hence ( $\beta$ ) expression can be presented as a load ratio or stress ratio [53]

$$\beta = \frac{N_{cm}}{N_{cr}} = \frac{f_c}{f_{cr}} \quad (2-43)$$

The bond factor ( $\beta = f_c / f_{cr}$ ) indicates the material property for cracked concrete, which is independent of the strength of concrete and reinforcement ratio. In other words, the average tensile strength of cracked concrete ( $f_c = \beta f_{cr}$ ) performs as a material property by defining an empirical expression for tension stiffening bond factor ( $\beta$ ), which shows the variation of concrete tensile stress between cracks [7] and [54].

Rostásy, Koch, Leonhardt, & Patzak [55] proposed an inverse form for the value of ( $\beta$ ), which is a ratio of the steel stress at first cracking ( $f_{sr} = N_r / A_s$ ) and bare steel stress at the crack ( $f_s = N / A_s$ ). Their expression has a benefit that is based on the steel ratio [53].

$$\beta = \frac{f_{sr}}{f_s} \quad (2-44)$$

44)

By substituting this expression into Equation (2-55) leads to:

$$\varepsilon_{sm} = \varepsilon_s \left( 1 - \frac{1}{1+n\rho} \frac{f_{sr}^2}{f_s^2} \right) = \varepsilon_s \left( 1 - \frac{f_{sr}^2}{f_s^2} \right) + \frac{f_{sr}}{f_s} \varepsilon_{cr} \quad (2-45)$$

In order to simplify this Equation, the cracking strain of the concrete ( $\varepsilon_{cr}$ ) can be neglected in the second part of the Equation. This approach was applied in the CEB-FIP Model Code-1978 to consider the tension stiffening effect for RC structures, as well as Eurocode 2 for the crack limit checking. In the CEB-FIP Model Code-2010 [56] the value of ( $\beta$ ) is constant ( $\beta = 0.4$ ). It should be mentioned that this parameter was defined experimentally for R-UHPFRC tensile elements in work reported in Chapter 5 (paper 6<sup>th</sup>).

Figure 2-26 compares different constitutive laws for tension stiffening bond factor for RC members which were developed by researchers and some of them were discussed previously. The empirical model proposed by Fields & Bischoff [7] provides the normalized concrete stress value (bond factor  $\beta = f_c / f_{cr}$ ). Their

model was based on experimental test results of the seven large-scale tensile tie specimens with normal strength (44 to 55 MPa) and high strength (80 MPa) with two types of reinforcement steel bars (15M and 22M). Their proposed prediction Equation was:

$$\beta = \frac{f_c}{f_{cr}} = e^{-0.8(\varepsilon_{cf} - \varepsilon_{cr}) \times 10^3} \quad (2-46)$$

where ( $\varepsilon_{cf}$ ) is the elastic strain in the concrete before cracking obtained by ( $\varepsilon_{cf} = f_c / E_c$ ).

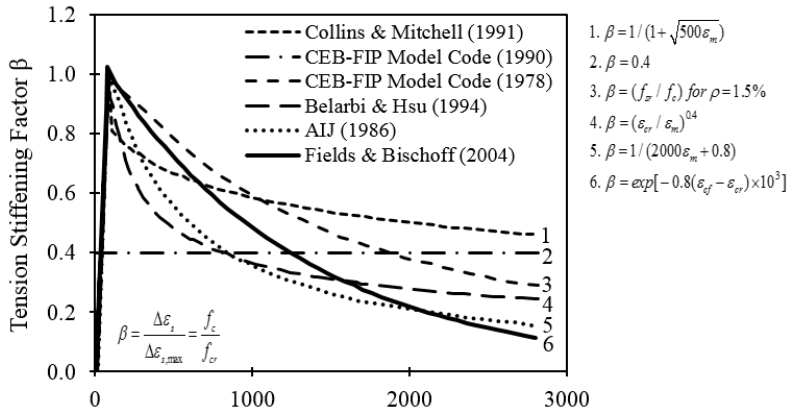


Figure 2-26: Different models for tension stiffening bond factor ( $\beta$ ) [adapted by [7]].

Hwang & Rizkalla [57] proposed an expression similar to Bischoff's model for the average concrete tensile stress after cracking, as indicated in the following Equation and Figure 2-27:

$$\beta = \frac{f_c}{f_{cr}} = e^{-1000(\varepsilon_m - \varepsilon_{cr})} \quad (2-47)$$

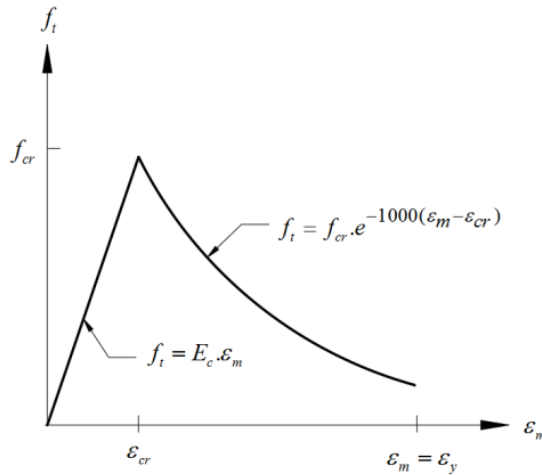


Figure 2-27: Tension stiffening bond factor ( $\beta$ ) proposed by Hwang & Rizkalla [57].

### 2.3. Tension stiffening behaviour effect of fibre reinforced concrete (FRC)

The concept of using fibres as reinforcement began before recorded history. The oldest fibre application has probably been the use of natural fibres such as flax or wool, and historically horsehair was used to reinforce masonry mortar and plaster. In the 19th century, the Industrial Revolution animated the further invention of machines to use natural fibres, and at this time, the asbestos fibres were used in concrete. Once scientists discovered that human health is affected by long-term usage of asbestos, the replacement substance was needed and the glass, steel, and synthetic fibres were applied in concrete. In the 1950s using composite material in construction came into being and fibre-concrete was one of the topics of interest.

Earlier research on Steel Fibre Reinforced Concrete (SFRC) was conducted by J. Romualdi & Batson [58] and J. P. Romualdi & Mandel [59]. They carried out the indirect tension test (bending test) on specimens reinforced with the closely spaced and randomly orientated wire reinforcement forming. These studies were the first significant steps toward the development of (SFRC) technology. Using fibres in concrete leads to be compensating the innate low tensile strength and the brittle tensile response of concrete. Fibre incorporation with a concrete matrix makes it more isotropic and homogeneous. Once concrete cracks, the randomly oriented fibres detain the microcracking mechanism and limit crack propagation, which significantly leads to improving the toughness, ductility, and tensile response. Unlike the plain concrete, the FRC provides a post cracking (or residual) strength due to bridging of cracks by fibres and consequently provides

post cracking resistance in tension. Adding fibres to the concrete matrix improves most of the mechanical and material properties of cement-based composites, according to numerous experimental studies. A summary of relevant experimental and analytical findings was reported by ACI Committee 544. These fibres can be considered as smeared reinforcement in concrete; hence, FRC provides favourable crack distribution and limits crack width at Serviceability Limit State (SLS) [60]. Also, fibre reinforcement concrete substantially increases the bond-slip behaviour under both monotonic and cyclic loadings and leads to a significant improvement in ductility in comparison to plain concrete [61].

Fibres improve the bonding performance of concrete while also allowing it to transfer tension across cracks, resulting in a significant improvement in the tension response of reinforced concrete members. The tensile behaviour of FRC members with conventional reinforcements (R/FRC) is considerably different from that of conventional reinforced concrete [60]. This fundamental difference is indicated in Figure 2-28.

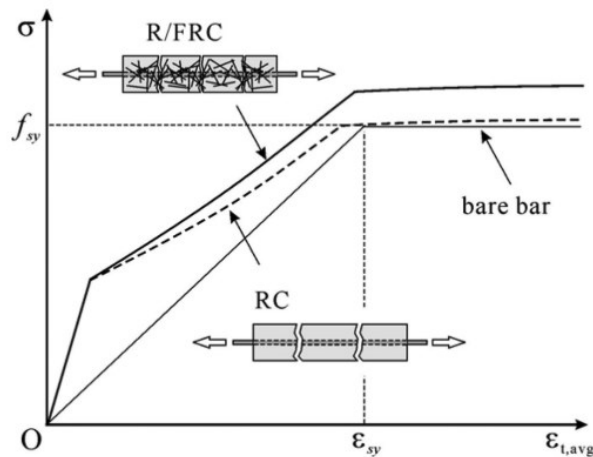


Figure 2-28: Tension behaviour of R/FRC and RC members [62].

The overall tensile response of RC member gradually approaches that of the bare bar after appearing the first crack. Then, the yielding of the reinforcing bar is achieved. After yielding, a little or no increase in tensile strength and stiffness will remain over the bare bar response. In the R/FRC members, both reinforcement and fibres bridge a crack and the transmitted tensile stress across the crack will share between the fibres and reinforcement bar. Due to the contribution of fibres in tensile strength, the R/FRC member can resist higher tensile stresses, not only after initial cracking but also after yielding the reinforcing bar. This post-cracking tensile resistance at a crack depends on the

fibre type and dosage of fibres [63]. The average crack spacings and crack widths in R/ FRC members by applying fibres in concrete would be smaller compared to those in RC members.

The general load-deformation behavior of reinforced axial member loaded in tension can be described in four stages. These strategies are shown in Figure 2-29 and are explained as follows:

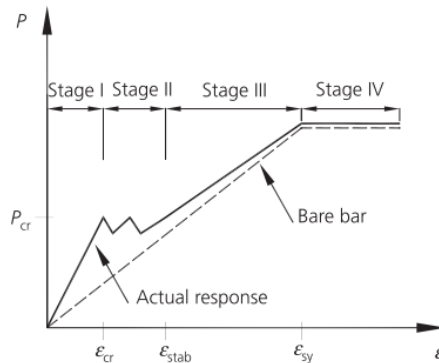


Figure 2-29: Typical load-deformation of R/FRC member under tensile load [64].

- ❖ Stage I: The applied tensile load is shared between concrete and steel based on their relative stiffnesses. The stresses and strains are uniform along the entire length of the member, and the contribution of the fibres in this stage is negligible, and this stage remains until the first crack is formed.
- ❖ Stage II: This stage starts after the first crack formation. Therefore, the stresses in the concrete matrix and steel are not constant along the length of the element. Due to the bridging effect of fibres on cracks, fibres become engaged, and this leads to carrying the tension. Consequently, the tension load will be shared by reinforcing bar and fibres. The strain difference between concrete and steel becomes small, and the strain in the concrete is approximately equal to that of the reinforcing bar. As the additional load is applied to the section, strain compatibility will recover, and once the tensile strength of the concrete is reached, a second crack will occur at the next weakest section. This process continues and cracks stabilization occurs when the distance between the cracks is not large enough to develop a sufficient bond to reach the concrete tension stress strength.
- ❖ Stage III: In this stage, the crack pattern has been stabilized, and the crack spacing remains constant. By increasing the tension load, an increment in crack width will only happen.



- ❖ Stage IV: The average member strain reaches the yield strain of the reinforcing bar, and the concrete contribution begins to diminish. In this stage, the overall response of the member is dominated by fibres and the behaviour of steel reinforcing bar.

### Bond factor aspect for FRC

One of the most cited researches about tension stiffening of steel fibre reinforced concrete was done by Bischoff [63] to develop the tension stiffening relationship of R/FRC and comparing with RC tensile members under monotonic and cyclic load with experimental data. The tension stiffening bond factor ( $\beta$ ) was determined similar to Equation (2-43), which was explained in section 2.2.3. This parameter represents the average load carried by the cracked concrete ( $P_{c,m}$ ) through normalizing with force carried by the concrete at first cracking, “cracking strength” ( $P_{cr}$ ), which could be determined as follows:

$$\beta = \frac{P_{c,m}}{P_{cr}} \quad (2-48)$$

( $P_{c,m}$ ) and ( $P_{cr}$ ) are illustrated in Figure 2-30, and also the tension stiffening relationship is shown in the inset part of the Figure.

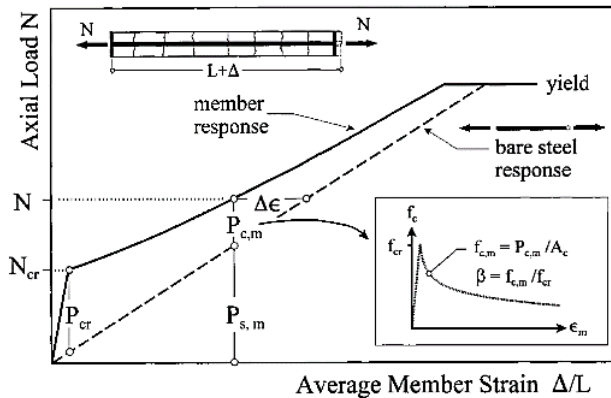


Figure 2-30: Typical tensile response of axial R/FRC member [63].

Two basic assumptions were used for determining the bond factor. The first one was based on the average crack spacing ( $S_m$ ) indicated in CEB 1993. Once the cracking pattern has been stabilized, and the formation of cracks is completed, the distance between cracks can vary between ( $l$ ) and ( $2l$ ). By taking into

account the random nature of cracking, the average crack spacing is calculated as  $2/3$  of the maximum crack spacing.

$$S_m = \frac{2}{3}(2l_f) \tag{2-49}$$

This result leads to assuming that the corresponding transferred force is equal to  $2/3$  of the concrete cracking force.

$$P_{max} = \frac{2}{3} P_{cr} \tag{2-50}$$

The second assumption was to consider the nonlinearity aspect in bond force, which was transferred to the concrete. As shown in Figure 2-31, for plain concrete, the average load carried by the cracked concrete ( $P_{c,m}$  or  $P_{avg}$ ) is a proportion of maximum force transferred to the concrete ( $P_{max}$ ). This aspect was indicated in CEB 1993.

$$P_{c,m} = 0.6P_{max} \tag{2-51}$$

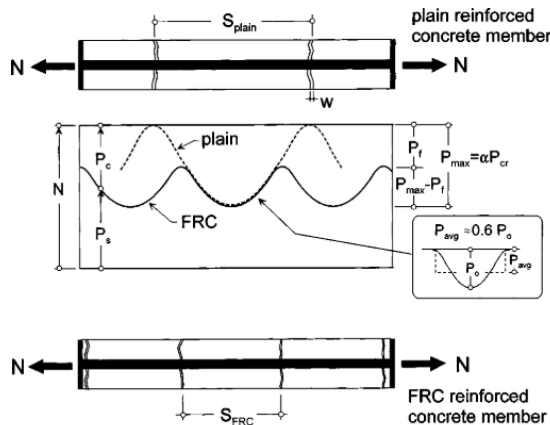


Figure 2-31: Axial tension force distribution in RC and R/FRC member for stabilized cracking [63].

substituting the (2-50) into (2-51) leads to:

$$P_{c,m} = 0.6 \times \frac{2}{3} P_{cr} = 0.4P_{cr} \tag{2-52}$$

Based on two indicated assumptions, the bond factor ( $\beta_c$ ) for plain concrete can be expressed by:

$$\beta_c = \frac{P_{c,m}}{P_{cr}} = 0.4 \tag{2-53}$$

The same approach can be used to develop an expression for the bond factor of FRC ( $\beta_f$ ). As can be seen in Figure 2-22, the tensile load transferred into the

concrete matrix due to the bond effect is  $0.6(P_{\max} - P_f)$ , and the average load value carried by fibre concrete is the sum of two components as follows:

$$P_{c,m} = P_f + 0.6(P_{\max} - P_f) \quad (2-54)$$

By dividing two sides of this expression to  $(P_{cr})$ , and substituting the Equation (3-53),  $(\beta_f)$  will be obtained by the following Equation:

$$\beta_f = 0.4 \frac{P_f}{P_{cr}} + \beta_c \quad (2-55)$$

This expression indicates that the bond factor for FRC ( $\beta_f$ ) is related to the tensile capacity of the FRC at the crack ( $P_f$ ), the first cracking capacity of the concrete ( $P_{cr}$ ), and the bond factor for plain concrete ( $\beta_c$ ). In the post-yield stage, the bond factor is controlled by the capacity of the fibres at the crack, and the bond factor expression is defined as a residual load ratio, which is different from the expression of Abrishami & Mitchell [65], as discussed earlier.

$$\beta_f = \frac{P_f}{P_{cr}} \quad (2-56)$$

The obtained results of RC and R/FRC members were compared with a constant value of 0.4 recommended by CEB-FIB Model Code (1990 and 1993) and the relationship proposed by Collins & Mitchell [35], which are explained in section 2.2.2.1 and 2.2.3, respectively. This comparison between bond factors is shown in Figure 2-37. In this graph, the residual load ratio is replaced by the residual stress ratio ( $P_f / P_{cr} \Leftrightarrow f_f / f_{cr}$ ). The difference between the bond factor of RC and R/FRC is due to the tension force carried by the steel fibres at the cracks.

For calculating the bond factor, the post cracking stress of the fibre concrete was used immediately after the first cracking. The post cracking fibre concrete stress ( $f_f$ ) and tensile cracking stress values ( $f_{cr}$ ) were obtained by experimental results, which were 3.0 MPa and 4.8 MPa, respectively. By substituting these values in the Equation (3-55), the tension stiffening bond factor is obtained as follows:

$$\beta_f = \beta_c + 0.4 \left( \frac{3.0}{4.8} \right) = \beta_c + 0.25 \quad (2-57)$$

The proposed relationship well agrees with experimental results in the serviceability range after cracking, as shown in Figure 2-32. Note that the tensile strength of fibre concrete immediately after cracking is a critical part of the material characteristic, which affects the tension stiffening and parameters related to serviceability stage such as crack width.

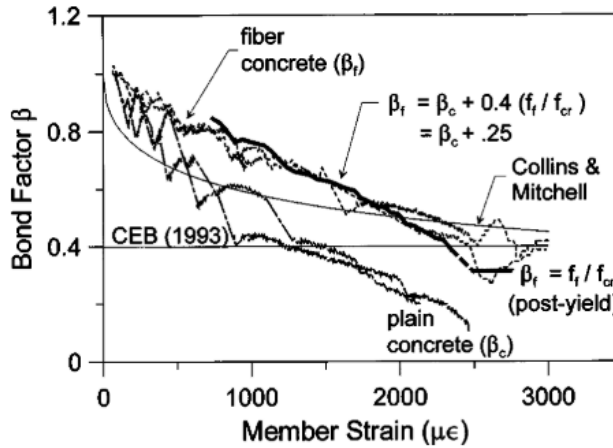


Figure 2-32: Different bond factors models for FRC [63].

## 2.4. Tension Stiffening behaviour of R-UHPFRC

### 2.4.1. Background to UHPFRC

Over many years, numerous studies have been conducted in order to develop innovative construction materials with exceptional strength, ductility and durability, with the aim of the design and creating lighter, stronger, and safer structures. In the mid-1990s, ultra-high performance fibre-reinforced concrete (UHPFRC) developed from ultra-high performance concrete (UHPC) [66]. UHPFRC is an emerging cement-based composite with extraordinary mechanical and durability properties. Its compressive strength of at least is 150 MPa [67-69] due to high cementitious material content and optimized gradation of granular materials. They are characterized by an ultra-compact matrix with very low permeability. Because of the incorporation of high strength steel fibres, UHPFRC is primarily distinguished for its tensile behaviours, which include sustained post-cracking tensile strength (greater than 7 MPa). The addition of fibres reduces the brittleness of the UHPFRC and transmits stress across crack faces, making UHPFRC one of the most ductile concretes in the industry [70]. UHPFRC can develop a hardening stage in tension characterized by uniform matrix microcracking prior to macrocracking localization [71]. Outstanding tensile ductility and energy absorption capacity achieved in strain hardening process accompanied with multi-cracking due to fibre bridging at the crack surfaces [72].

The combination of UHPFRC and steel rebar, subsequently called R-UHPFRC, can be considered as a novel technology for improving concrete structures. The markable merit of steel reinforcement can be largely exploited in the case of compatible deformation between a strain hardening UHPFRC and tensile

reinforcing bars prior to yielding. Furthermore, due to the predetermined rebar layout along the direction of tensile stress, continuous rebars are extremely effective in increasing the load-carrying capacity of reinforced UHPFRC. In addition, due to the predictability and stability of the position of the reinforcements in the structure elements, the reinforcing rebar strength in the R-UHPFRC reduce the variation in the tensile strength caused by the random orientation and distribution [73].

In recent years, the applications of UHPFRC have been increasing in infrastructural systems due to its superior properties. The mechanical properties of UHPFRC have been widely studied up to the present time. However, there are limited design provisions for the structural design of UHPFRC in international codes and standards. Therefore, it is necessary to develop design approaches that allow it to be used effectively.

The UHPFRC can be categorized as a particular type of FRC with improved characteristics, so the same fundamental categorization method that applies to FRC can also be used for UHPFRC. Figure 2-33 depicts a simple classification of fibre reinforced concrete based on its tensile stress-strain response and flexure load-deflection response proposed by Naaman and Reinhardt [74].

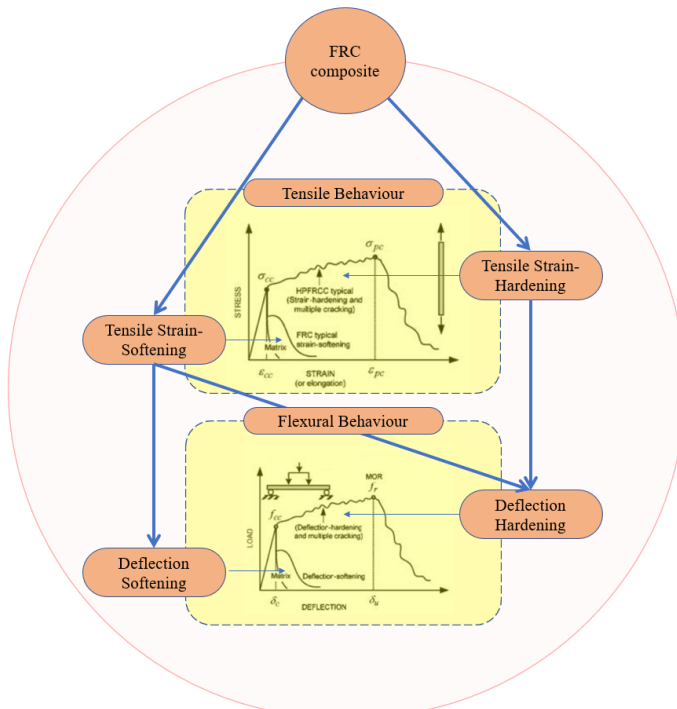


Figure 2-33: FRC composite classification based on their tensile and flexure behaviour [74].

A definition for performance levels of cementitious composites (i.e. FRC or UHPFRC) was proposed by Wille et al. [75]. This definition was based on the criteria established by Naaman and Reinhardt [74], as illustrated in Figure 2-34. This categorization is based on the concrete's direct tensile and bending behaviour and divides the cementitious performance into five levels as follows: *Level 0*: is related to plain concrete without fibres reinforcement. Therefore, their failure mode under tensile or bending load is brittle, and after reaching the tensile strength of the matrix ( $\sigma_{cc}$ ) or modulus of rupture ( $\sigma_{f1}$ ), they do not present significant post cracking strength.

*Level 1*: refer to traditional FRC with strain-softening and deflection-softening. At this level, the performance of cementitious composites exhibits crack controlling with little enhancement in mechanical properties.

*Level 2*: is defined by tensile strain-softening and deflection-hardening. At this level, the equivalent bending strength ( $\sigma_{f2}$ ) is bigger than the modulus of rupture ( $\sigma_{f2} > \sigma_{f1}$ ).

*Level 3*: the cementitious composites under both tensile and bending load exhibit a hardening behaviour. In other words, tensile strain-hardening ( $\sigma_{pc} > \sigma_{cc}$ ) and deflection-hardening ( $\sigma_{f2} > \sigma_{f1}$ ) behaviours can happen. The parameter ( $\sigma_{pc}$ ) is the post-cracking tensile strength.

*Level 4*: this level is the same as level 3. The only difference between this level and level 3 is that the energy absorption is substantially higher ( $g > 50 \text{kJ} / \text{m}^3$ ).

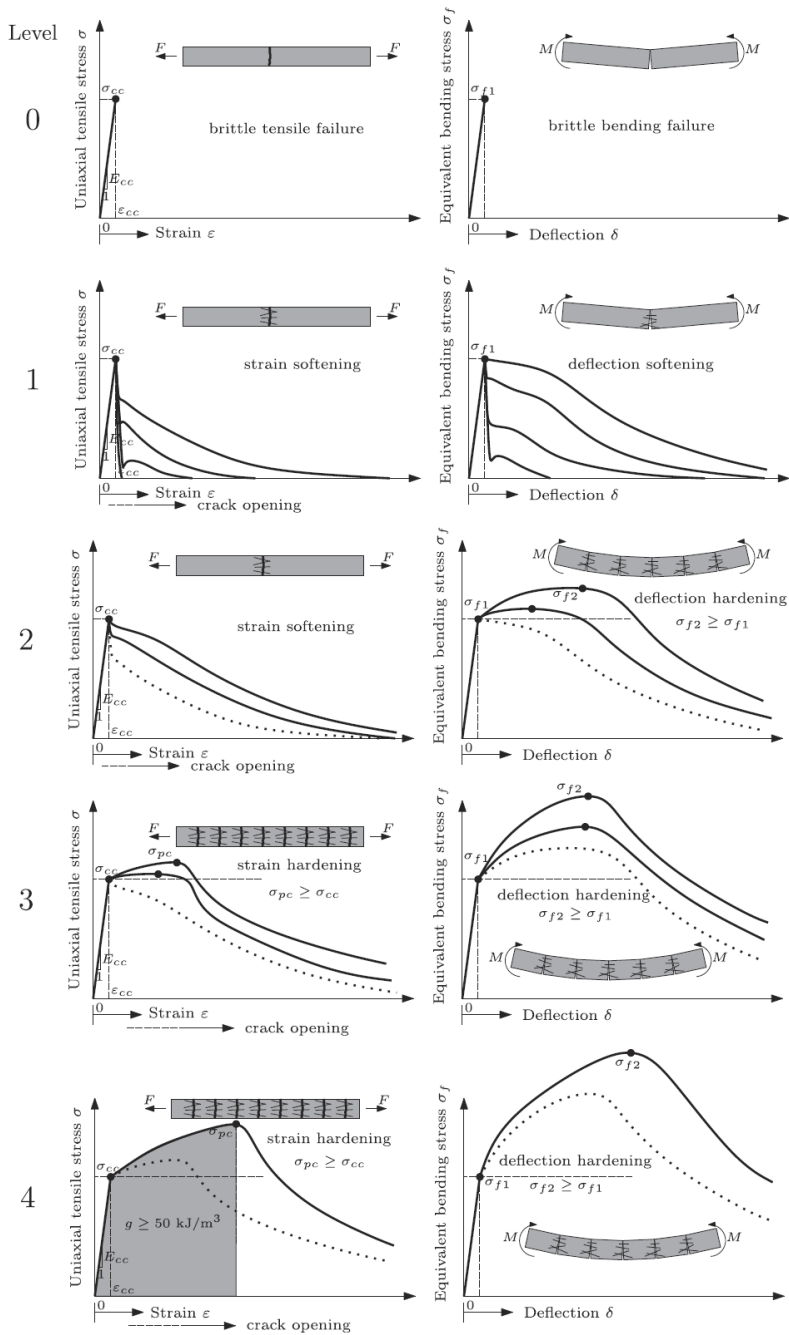


Figure 2-34: Performance levels of cementitious composites [75].

Figure 2-35 depicts the differences in behaviour between FRC and HPRCC composites.

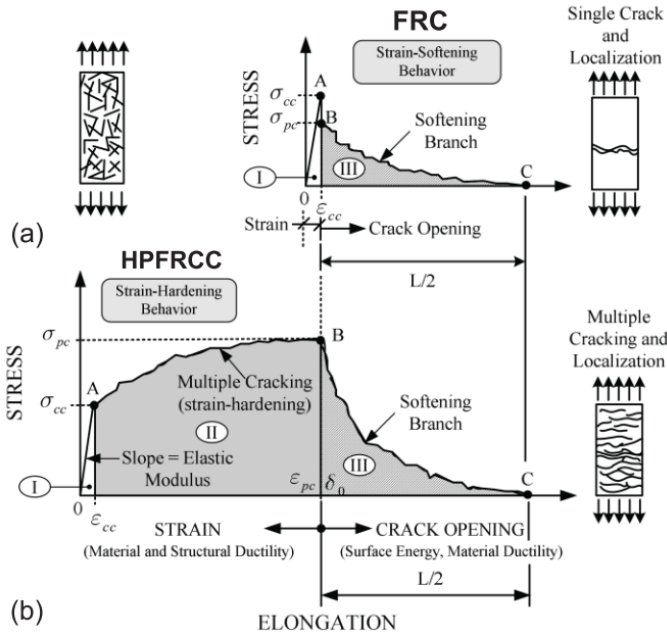


Figure 2-35: Comparison of the typical stress-strain response of conventional FRC vs HPRCC; (a) Fiber-reinforced concrete (FRC) composites with strain-softening behaviour, (b) HPRCC with strain-hardening behaviour [76].

Phase I is the linear elastic behaviour in which the composite's elastic modulus characterizes by the stiffness. The stress-strain response of the FRC composite (Figure 2-35 (a)) goes directly from phase I to phase III (softening branch) because the matrix at the crack is not strong enough to open up another crack. In contrast, the HPRCC composite exhibits phase II, where multiple cracking occurs after cracking and before softening branch.

Before the macrocrack forms, the fibres were activated due to microcracking phase. Activated fibres bridge over the crack and resist the further opening and propagation of the crack. This function is similar to steel reinforcement bars in the concrete; however, fibres are considerably finer, which is why they are activated as early as the microcrack formation phase.

Factors that influence the tensile behaviour of UHPFRC are matrix properties, fibre volume fraction, geometry and type of fibres, fibre stiffness, fibre orientation and distribution, the size effect of the element and curing conditions [77, 78].

The tensile mechanical characterization of UHPFRC is defined by the constitutive



law, and it can be obtained directly by standard uniaxial direct tensile tests. However, the eccentricity of the load and the specimen, as well as the boundary conditions (fixed-end and rotating-end conditions) and stress concentrations, all affect to the tensile tests. Regarding these difficulties, the bending tests are recommended by main standards. Two types of test procedures have been recommended, such as three-point bending tests (EN-14651 [79], ASTM C1609 [80]) and four-point bending tests (UNI 11039-1 [81], UNI 11039-2 [82]). Both the European and the Italian standards suggest the use of notched specimens, while the American Standard recommend prismatic specimens without the notch.

The French standard (NF P 18-470 [83]), which is based on recommendations AFGC 2013 [84] considers three types of UHPFRCs depending on their post-cracking behaviour. The UHPFRC type 1 has a strain-softening behaviour for its post-cracking stage, type 2 is low strain-hardening and type 3 is high strain-hardening. This standard recommends using notched prisms and conducting a three-point bending test to determine the constitutive post-cracking law for UHPFRC types 1 and 2. The obtained moment-crack width ( $M-w$ ) should be converted to the stress-crack width ( $\sigma_f-w$ ) law using an associated inverse analysis procedure. The Swiss standard (Swiss Society of Engineers and Architects SIA 2016 [85]) classifies UHPFRC into three different types (U0, UA and UB) according to tensile parameters such as ( $f_{t,k}$ ), ( $f_{tu,k} / f_{t,k}$ ) and ( $\varepsilon_{tu,k}$ ) as shown in Figure 2-36. This standard use two test methods to define the tensile behaviour of UHPFRCs. One of those is the doge-bone direct tensile test by defining the force-displacement relationship and the other one is the four-point bending test (4PBT) by using a simplified inverse analysis to derive the tensile response from the load-deflection response. The proposed tensile constitutive law has a bilinear stress-strain behaviour for elastic and hardening regions and a stress-crack opening for the softening region (see Figure 2-36).

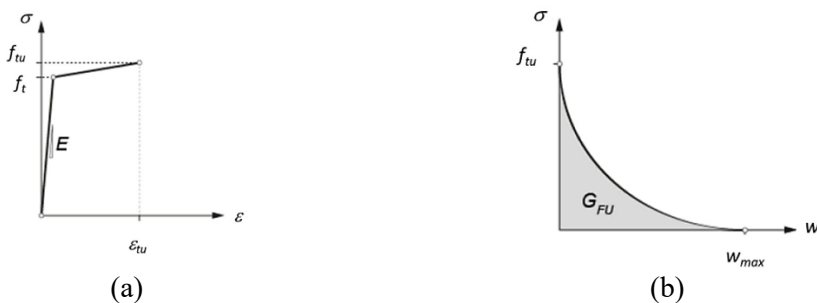


Figure 2-36: Constitutive tensile behaviour proposed by SIA 2016 [85], (a) elastic and hardening region, (b) softening region (stress-crack opening behaviour).

The proposed parameters values for defining the constitutive tensile behaviour

for three types of UHPFRCs are provided in Table 2-2.

Table 2- 2: Parameters values for defining the constitutive tensile behaviour for UHPFRCs based on SIA 2016 [85].

UHPFRC types	U0	UA	UB
$f_{t,k}$ (MPa)	$\geq 7.0$	$\geq 7.0$	$\geq 8.5$
$f_{tu,k}/f_{t,k}$	0.7	$>1.1$	$>1.2$
$\varepsilon_{tu,k}$ (‰)	$f_{t,k}/E_t$	$>1.5$	$>2.0$

### 2.4.3 Inverse analysis methodology

In this section, the inverse analysis method proposed by López, J.A et al. [86, 87] is explained, which was used to obtain the characteristic parameters to define the UHPFRC tensile behaviour of the employed UHPFRCs.

As explained in the previous section, one of the best test methods to obtain the characteristic parameters that define the UHPFRC tensile behaviour is the four-point bending test and using an associated inverse analysis procedure recommended in several standards.

The unnotched Four-Point Bending Test (4PBT) was conducted to obtain the tensile behaviour of the UHPFRC. Therefore, for each concrete batch, two prismatic specimens with dimensions of 500×100×100 mm were cast and the 4PBT were conducted according to geometrical conditions indicated by López, J.A et al. [86, 87]. The specimens were tested in an Instron 3382J8440 universal testing machine with a capacity of 100 kN. The test setup and specimen detail are presented in Figures 2-37 (a) and (b).

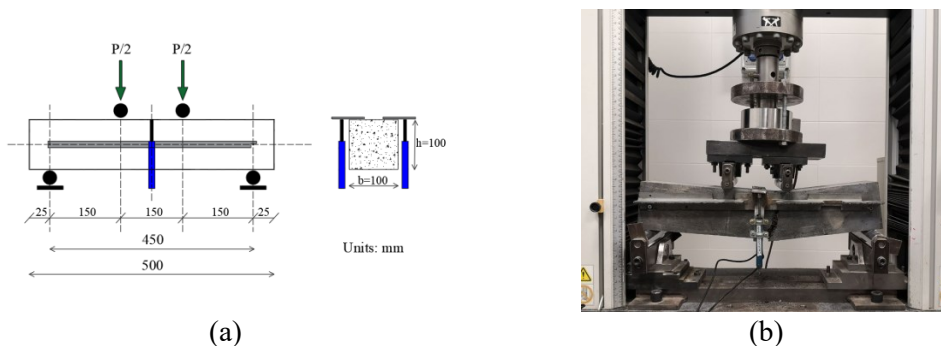


Figure 2-37: Employed Four-point Bending Test (4PBT) to obtain the tensile behaviour of UHPFRC, (a) specimen geometry, (b) experimental test setup.

The load-displacement curve was obtained by using two Displacement Transducers in the middle of the span located on both sides of the specimen. The following parameters define constitutive UHPFRC behaviour:

- ( $f_t$ ): cracking strength
- ( $f_{tu}$ ): ultimate tensile strength
- ( $\varepsilon_{tu}$ ): tensile strain corresponding to Ultimate tensile strength ( $f_{tu}$ )
- ( $w_d$ ): crack opening at the change of slope
- ( $w_c$ ): crack opening at the zero stress
- ( $E$ ): elastic modulus
- ( $E^*$ ): unloading modulus

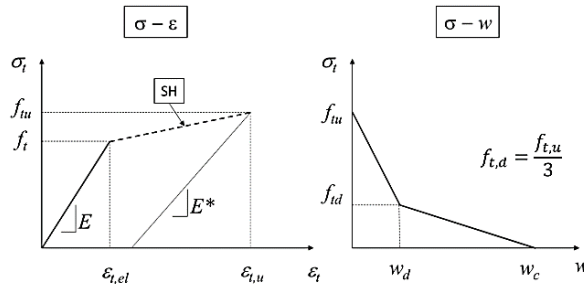


Figure 2-38: Constitutive tensile behaviour used for non-linear hinge model [87].

López, J.A [87, 88] proposed a simplified methodology (called five-point inverse analysis, 5P-IA) based on the closed-form nonlinear hinge model to define the tensile parameters of the constitutive tensile behaviour. The method consists of selecting five specific key points extracted from the experimental equivalent bending strength-displacement at the mid-span curve shown in Figure 2-39.

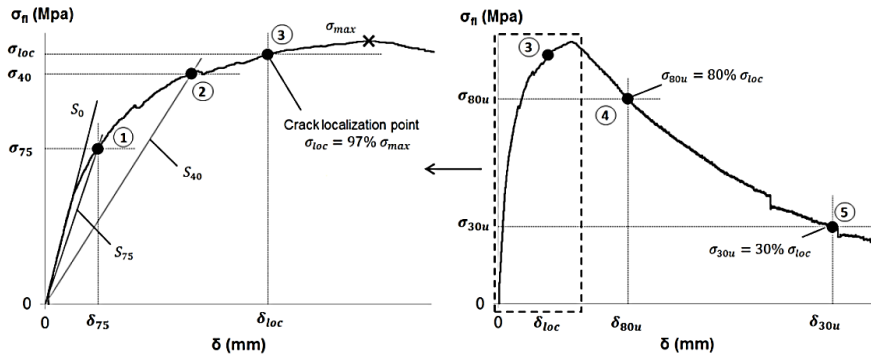


Figure 2-39: Key points of the proposed five-point model, López, J.A [87].

Figure 2-40 presents the formulations of the simplified model to determine the stress-strain relationship of the UHPFRC based on five key points obtained from the experimental bending test for both  $l/h=3$  and  $4.5$  ( $l$  is the support distance of and ( $h$ ) is the section high). Four normalized parameters ( $\alpha, \gamma, \beta, \mu$ ) were introduced to simplify the formulation, as shown in Figure 2-63.

Stress-strain	$L/h = 3$	$L/h = 4.5$	Normalized parameters
$S_l$	$\sigma_n = k_{12,40h} \frac{E_s^2}{h}$	$\sigma_n = k_{14,75h} \frac{E_s^2}{h}$	$k_0 = 1$ $k_{75} = 0.75$ $k_{40} = 0.40$
$f_t$	$\frac{\sigma_{75}}{1.63} \left( \frac{\sigma_{22}}{\sigma_{40}} \right)^{0.19}$	$\frac{\sigma_{75}}{1.59} \left( \frac{\sigma_{22}}{\sigma_{40}} \right)^{0.21}$	Normalized parameters
$\epsilon_{t,u}$	$\frac{f_t}{E} (7.65 \frac{\sigma_{loc}}{\sigma_{75}} - 10.53)$	$\frac{f_t}{E} (6.65 \frac{\sigma_{loc}}{\sigma_{75}} - 9.40)$	$\epsilon_{t,el} = f_t/E$
$f_{t,u}$	$\alpha^{-0.18} (2.46 \frac{\sigma_{loc}}{\sigma_{75}} - 1.76) f_t$	$\alpha^{-0.17} (2.24 \frac{\sigma_{loc}}{\sigma_{75}} - 1.55) f_t$	$\alpha = \epsilon_{t,u} / \epsilon_{t,el}$
Stress-crack opening	$\epsilon_{t,d}$	$\gamma^{-0.38} \alpha^{0.89} (2.82 \frac{\sigma_{loc}}{\sigma_{75}} - 1.68) \frac{f_t}{E}$	$\gamma = f_{t,u} / f_t$
$\epsilon_{t,max}$	$2.81 \beta^{-0.76} \gamma^{-0.19} \alpha^{1.42} \left( \frac{\sigma_{loc}}{\sigma_{75}} \right)^{1.85} \frac{f_t}{E}$	$2.17 \beta^{-0.76} \gamma^{-0.26} \alpha^{1.48} \left( \frac{\sigma_{loc}}{\sigma_{75}} \right)^{1.86} \frac{f_t}{E}$	$\beta = \epsilon_{t,d} / \epsilon_{t,el}$
$w_d$	$w_0 + (\epsilon_{t,d} - \epsilon_{t,u} + \frac{2f_t \mu}{3E}) \frac{l}{3}$	$w_0 = \epsilon_{t,u} \cdot s_{av}$	If no data are available $w_0 = 0$ ; $E^* = \infty$
$w_{max}$	$w_0 + (\epsilon_{t,max} - \epsilon_{t,u} + \frac{f_t \mu}{3E}) \frac{l}{3}$		

Figure 2-40: Simplified five-point inverse analysis formulation [88].

### 2.4.4 Full tension stiffening concept

As stated before, tension stiffening plays a significant role in the deformation behaviour of reinforced concrete at the serviceability limit states. When these elements are under tension or bending, the tensile force carried by the uncracked concrete can be transmitted across cracks via the reinforcement and fibres due to the bond interaction. The tension stiffening is most commonly included in reinforced concrete models by adjusting the tension concrete's constitutive laws. The tension stiffening must be adequately modelled to accurately simulate the reinforced concrete elements for serviceability behaviour. The load-carrying capacity of the concrete and the bond stress-slip property between the concrete

and reinforcement are both important factors in tension stiffening. The local bond stress is dependent on the local slip, stress and strain magnitude in the steel reinforcement, the duration of the applied load and dry shrinkage level [89]. Tension stiffening is highly influenced by early shrinking [90-92], and it causes a reduction in the cracking load level. The shrinkage produces additional primary cracks with time and creates a time-dependent deterioration of the bond behaviour. The effect of the shrinkage on the tensile behaviour of R-UHPFRC tensile elements is discussed in section 2.5 and chapter 4.

In order to comprehend the full tension stiffening concept, it's essential to understand the difference between RC and R-UHPFRC cracking behaviour. Multiple cracking formation is an essential characteristic deformation behaviour of R-UHPFRC compared to RC, and it has a consequential effect on performance of the reinforced UHPFRC elements. Before reaching the first cracking strength of the cementitious matrix, the applied tensile load is shared between the steel reinforcement and matrix proportional to their stiffness and volume fraction. In this stage, the stresses are uniformly distributed throughout both steel and concrete matrix components (see Figure 2-41(a)). The formation of the transverse crack in the RC tensile element leads to a redistribution of stresses in the matrix and reinforcement, as shown in Figure 2-41(b).

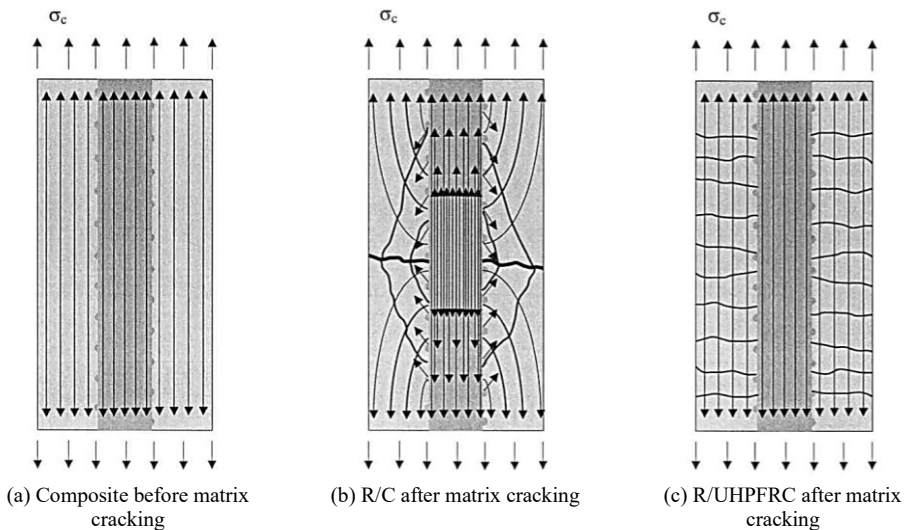


Figure 2-41: Schematic internal stresses and crack formation in R/C and R-UHPFRC [93].

Because the concrete matrix cannot transfer stresses across the crack, the applied load must be transferred to the reinforcement through bond action. Hence, the total tensile load should be carried by the reinforcement at the crack location where the concrete matrix is stress-free. At the crack location, the stress

concentration in the reinforcement occurs and both materials experience relatively large strain differences; consequently, the bond deterioration and local slip happen. After appearance the first crack and with a gradual increase in tensile force, more cracks appear alternately. Consequently, deterioration in the bond between reinforcement and concrete matrix happens progressively (a reduction in tension stiffening with increasing load) and the overall tensile response of RC member gradually approaches that of the bare bar.

In the case of exiting the fibres in the composite matrix (i.e. R-FRC or R-UHPFRC elements), both reinforcement and fibres bridge a crack and the transmitted tensile stress across the crack will share between the fibres and reinforcement bar. Thus, the element can resist higher tensile stresses and the strain difference between matrix and reinforcement would be lower than the RC elements. However, with increasing the crack width, the fibre activation is started (fibre pull-out and/or yielding of the steel fibres). Hence, the tensile load-carrying capacity of the element presents a higher tension stiffening and higher ( $\beta$ ) factor. On the other hand, the multiple cracking property of the R-UHPFRC element can eliminate the strain difference between reinforcement and UHPFRC matrix material and local deterioration does not happen and the composite element can carry tension upper than the yield strength of the reinforcement. The cracking behaviour of R-UHPFRC demonstrates very fine cracks with small spacing between them (see Figure 2-41(c)) and the tension stiffening is extremely high due to the high bond between the reinforcement-UHPFRC matrix and the fibre-UHPFRC matrix, as well as the high tensile strength of UHPFRC [94].

As a consequence, the overall tensile behaviour remains parallel to the bare response due to the almost constant tensile contribution of the UHPFRC matrix (see Figure 2-65). Hence, the tensile R-UHPFRC element may be considered as a composite of two materials having an elastic/plastic deformation behaviour with individual yield strength and strain and the ( $\beta$ ) factor would be one (post cracking stress/cracking strength). This phenomenon was called the full tension stiffening effect by Bischoff [53, 95, 96].

Regarding the experimental studies [94, 97-99], it was observed that the general behaviour of R-UHPFRC elements under tensile load could be presented a peak tensile force strength (the ultimate load capacity of the tensile members, the peak point in Figure 2-42) higher than the yield strength or ultimate strength of the steel reinforcement due to the combination of the fibres and the steel reinforcement across cracks only for a very high amount of ordinary steel reinforcement.

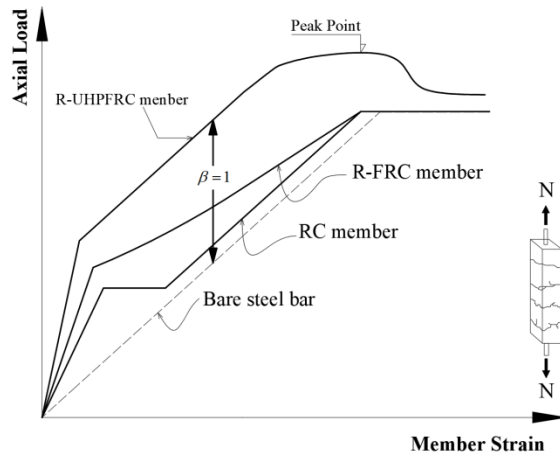


Figure 2-42: Comparison between the tension stiffening behaviour of RC, R-FRC and R-UHPFRC elements [adopted from[97]].

The experimental study conducted by Moreno, D. M., et al. [100] present the full tension stiffening effect compared with RC tension stiffening effects. Figure 2-43 demonstrate the strong potential of the R-UHPFRC tensile element to carry the tension after post cracking phase. In contrast, the tension stiffening behaviour for RC elements has a descending form.

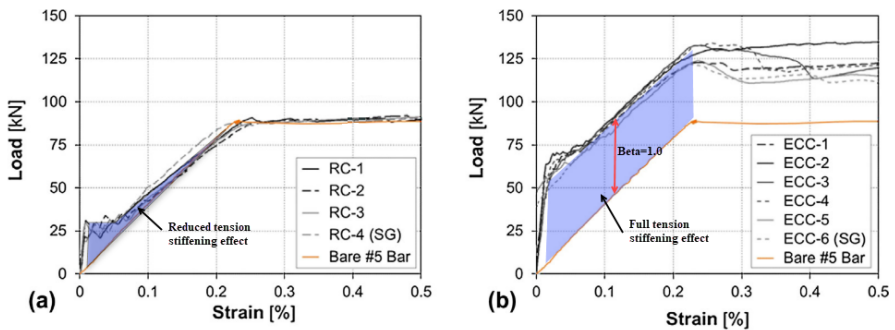


Figure 2-43: Tension stiffening effect; (a) reduced tension stiffening effect for RC tensile elements, (b) full tension stiffening effect for R-UHPFRC tensile elements [100].

Experimental results obtained by Leutbecher and Fehling [101], Lárusson, L., et al. [102] and Hollmann, C. P. [103] confirm this fact as well (see Figure 2-44). It can be seen that tension stiffening behaviour for R-UHPFRC tensile elements exhibits a nearly constant contribution of the concrete over a wide strain range. The tension stiffening curve is parallel to the bare bar response, which leads to having ( $\beta = 1$ ).

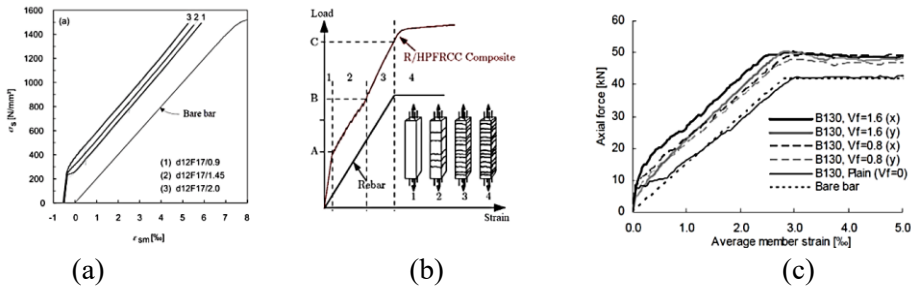


Figure 2-44: Full tension stiffening effect observed in experimental studies for R-UHPFRC tensile elements; (a) Leutbecher and Fehling [101], (b) Lárusson, L., et al. [102], (c) Hollmann, C. P. [103].

### 2.4.5. Models of tension stiffening for R-UHPFRC tensile elements

Various methods have been proposed for modelling the tension stiffening for R-UHPFRC tensile elements. Numerical calculations are used to assess the relative merits of these methods and to test the validity of the models. Jungwirth et al. [104] presented a model to describe the structural response on R-UHPFRC tensile elements based on mechanical processes. They examined the cracking mechanism of R-UHPFRC tensile elements by considering the relevant double multi-cracking behaviour in their model. First, multiple meso-cracks form controlled by the fibres and then multiple macro-cracks form controlled by the bond between the UHPFRC and the reinforcing steel. In their model, the contribution of steel fibres is implicitly taken into account in the composite's homogenous model. Its contribution to the load-bearing capability is simply added to the bare rebar. This model, however, is limited to the UHPFRC with strain-hardening behaviour, and inductive reasoning is necessary when the UHPFRC enters the softening stage.

On the other hand, the majority of modelling approaches are based on the concept of parallel discrete cracks. In these models, the tension stiffening effect is considered to have an explicit consideration of the bond transfer mechanism between cracks. The steel fibre's contribution must be explicitly considered at the crack section with a fibre engagement model based on crack width. The modelling approaches based on discrete cracks are more suitable for FRC or UHPFRC elements since they usually simulate the reinforced tensile element with composites showing strain-softening or strain-hardening behaviour under tensile loads [104].

Leutbecher [101] proposed a model in which the variability of the post-cracking strength was incorporated, which was only validated in the rebar's elastic phase. In this model, the possibility of additional crack formation after the initial crack formation stage was considered as the tensile load increased. However, the Leutbecher model [101] does not provide an integrated approach for simulating



R-UHPFRC tension ties in both the elastic and plastic phases of the rebar. In contrast, the model proposed by Valente, R., et al. [105] describe the total load-deformation response of R-UHPFRC tensile element from elastic to failure. Their theoretical model is capable of providing the tension stiffening effects in the service conditions and estimating the deformation capacity at the ULS. Their model was based on dividing the tensile tie element into a series of cracked elements (parallel discrete cracks) and applying an incremental and iterative procedure (by ensuring equilibrium at each load step) to obtain the overall load-deformation behaviour of the element. The suggested modelling technique takes into account the variety of the post-cracking strength as well as the potential of progressive cracking after the initial cracking formation stage. They adopted the Tension Chord Model (TCM) to resolve the bond problem by accounting the fibre contribution and matrix stresses at the crack section.

TCM is an analytical model which helps to resolve problems such as cracking, minimum reinforcement, tension stiffening and deformation of the reinforced concrete members [106]. Figure 2-50 depicts the TCM model for R-UHPFRC tensile element proposed by Valente, R., et al. [105] (called crack element), which is based on Marti, P., et al. [106] model. TCM models the interaction between the reinforcement and concrete between the cracks in cracked tensile chords. A crack and the parts up to the distance ( $s_{rm} / 2$ ) between the two closed cracks form the model. According to TCM, the bond-slip problem simplifies by assuming the bond law follows a two-step rigid-perfectly plastic stress relationship (see Figure 2-45(b)). The bond-slip relationship depends on the rebar stress at the crack section ( $\sigma_{s,r}$ ) and it has two different values of ( $\tau_{bs0}$ ) and ( $\tau_{bs1}$ ) when the rebar is in the elastic and plastic phase, respectively. As a result, the TCM gives closed-form solutions for the distribution of stresses (Figure 2-45(d)) and strains (Figure 2-45 (e)) along the cracked tensile element. The equilibrium between the crack section and the section at a null-slip section can be established since the crack behaviour is symmetrical (Figure 2-45(c)). The tension stiffening effect due to bond transfer is accounted by the relationship between the maximum rebar stress and the average deformation of the cracked tensile element ( $\sigma_{s,r} - \varepsilon_{sm}$ ).

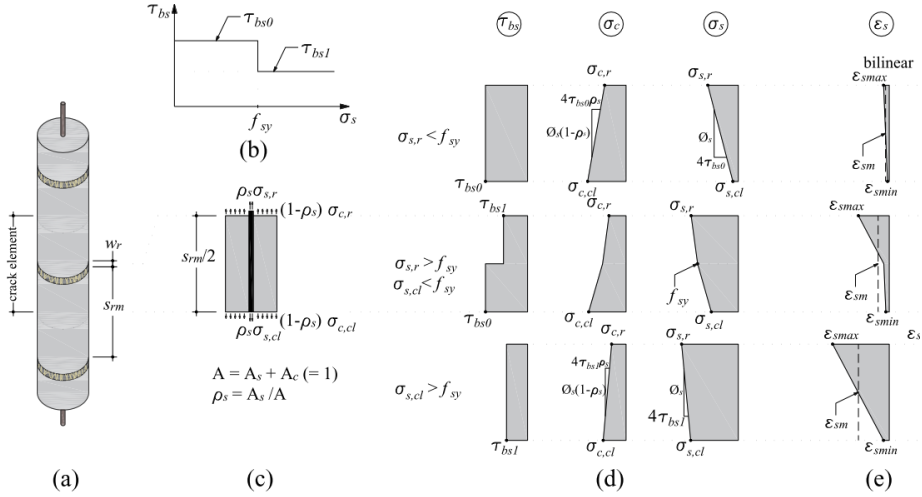


Figure 2-45: Tensile chord model: (a) cracked element; (b) bond shear stress-slip relationship; (c) equilibrium between two cracks; (d) stress and (e) strain distributions in elastic, elastic-plastic and plastic cracked tensile element [105].

The crack width of the tensile element can be obtained from the compatibility of deformations as indicated in Equation (2-58). Where  $(\epsilon_{sm})$  is the average strain value of the steel rebar and  $(\epsilon_{cm})$  is the average strain value of the composite. The parameter  $(S_{rm})$  is the average crack spacing of the cracked tensile element.

$$wr = S_{rm}(\epsilon_{sm} - \epsilon_{cm}) \tag{2-58}$$

A crack forms when the composite stress reaches the tensile strength of the matrix  $(f_{ct})$ . Therefore, the maximum crack spacing  $(S_{rm0})$  as indicated in Equation (2-59) can be determined by the equilibrium condition between the crack and null-slip sections for  $(\sigma_{c,cl} = f_{ct})$ .

$$S_{rm0} = \frac{\phi_s \times f_{ct} \times (1 - \rho_s)}{2\tau_{bs0} \times \rho_s} \left( 1 - \frac{\sigma_{c,r}}{f_{ct}} \right) \tag{2-59}$$

where  $(\phi_s)$  and  $(\rho_s)$  are the diameter and ratio of the steel reinforcement, respectively. The parameter  $(\sigma_{c,r})$  is the composite stress at the crack section. The maximum crack spacing  $(S_{rm0})$  can be turned into  $(s_{rm})$  by the factor  $(\lambda)$  due to the variability of the matrix cracking strength  $(f_{mt})$  as is indicated in Eq. (2-60).

$$s_{rm} = \lambda \times S_{rm0} \geq s_{r,min} \tag{2-60}$$

The minimum crack spacing  $(s_{r,min} = l_f / 2)$  is set to guarantee that the steel fibres'

post-cracking strength ( $\sigma_{cf0}$ ) is adequately transferred to the matrix. The parameter ( $l_f$ ) is the steel fibre's length. As can be seen, an iterative model is required to obtain ( $w_r$ ), which must be established the average strains in composite ( $\varepsilon_{cm}$ ) and steel reinforcement ( $\varepsilon_{sm}$ ). The value of ( $w_r$ ) is iterated using a numerical approach to attain deformation compatibility and equilibrium at the same time by using the Equations (2-58) and (2-61). The equilibrium Equation (2-61) also is used to determine the load-deformation response of the cracked tensile element by finding the internal load ( $\sigma_N$ ) for each value of ( $\varepsilon_{sm}$ ).

$$\sigma_N = \rho_S \sigma_{S,r} + (1 - \rho_S) \sigma_{C,r} \quad (2-61)$$

The rebar and crack bridging stresses at the crack section contribute to the value of ( $\sigma_N$ ). The rebar stress at the crack section ( $\sigma_{s,r}$ ) should be obtained directly from TCM Equations. On the other hand, the value of ( $\sigma_{c,r}$ ) is obtained by iterating the value of ( $w_r$ ) until the compatibility of deformation is met according to Equation (2-58).

The cracking load can be calculated by replacing ( $\sigma_{c,r} = f_{ct}$ ) and ( $\sigma_{s,r} = E_s / E_c$ ) values into Equation (2-61), where leads to having:

$$\sigma_{N,cr} = \rho_s (E_s / E_c) + f_{ct} (1 - \rho_s) \quad (2-62)$$

For considering the crack bridging stress, the steel fibres contribution ( $\sigma_{c,f}$ ) and matrix contribution ( $\sigma_{bri}$ ) were added together. The softening behaviour of the matrix was assumed as a linear behaviour, as shown in Figure 2-46(a). For the engagement of the fibre and simulating the contribution of fibres in the debonding and pull-out phase, the proposed model by Pfyl [107] were used, as shown in Figure 2-46(b). According to Pfyl [107], the crack width setting and the transmission between the debonding and pull-out phase ( $w_{deb}$ ) was estimated depending on the average bond strength value between the matrix and the steel fibres ( $\tau_f$ ) and the fibre geometry.

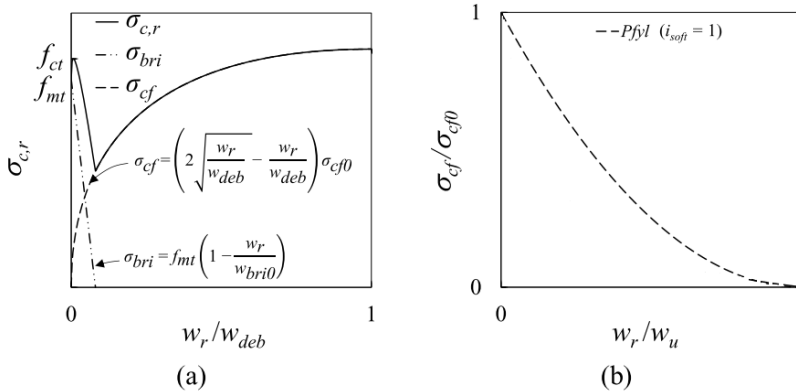


Figure 2-46: Stresses due to crack bridging: (a) matrix softening and debonding of steel fibres; (b) pull-out of steel fibres [107].

One of the most cited research about the cracking and tensile behaviour of R-UHPFRC elements was carried out by Leutbecher, T. [108]. He proposed a mechanical model based on compatibility and equilibrium at the crack cross-section to determine the crack width and deformation calculation by considering the tension stiffening due to the contribution of fibres. This model is explained below.

In the reinforcement concrete elements with fibres, the fibres help to transfer the load in the cracked cross-section and consequently, the stress in the reinforcement is reduced. Figure 2-47 shows the contribution of fibres in tension and equilibrium of forces in the crack for elements subjected to tension or bending. The contribution of the fibres in tension can be determined depending on the actual crack width (see Figure 2-47(c)).

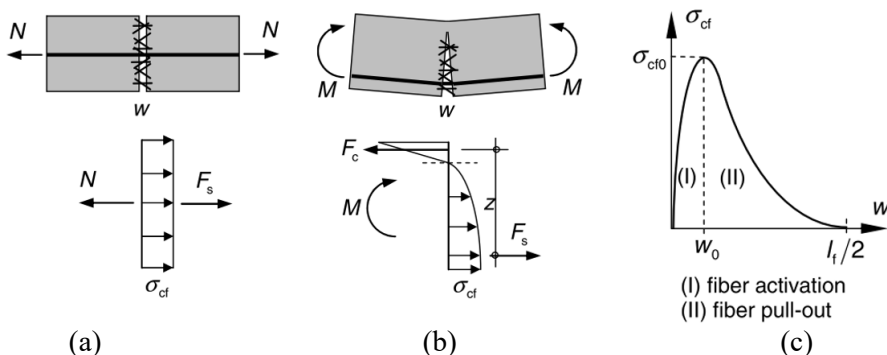


Figure 2-47: Contribution of the fibres in the cracked-section (a) and (b) Equilibrium of forces for element subjected to tension and bending, (c) Typical stress-crack opening relationship of concrete with fibres [109].

As can be observed in Figure 2-47(c), the fibres' contribution in tension is determined by the actual crack width based on the stress-crack opening relationship of the FRC or UHPFRC.

For obtaining the crack width, it is necessary to evaluate the steel rebar strain ( $\varepsilon_s^f$ ) at the crack by taking into account the force transfer of the fibres at the crack cross-section. By assuming the compatibility of deformation, the relative displacement between steel reinforcement and matrix and also between fibres and matrix lead to having the same crack width, and the distribution of the internal forces can be determined with the following Equation (see also Figure 2-48):

$$F_s = N - F_f = N - \sigma_{cf} \cdot A_c \quad (2-63)$$

where ( $F_s$ ) is the tensile force in the steel reinforcement, ( $N$ ) is applied axial force, ( $A_c$ ) is the concrete cross-section and ( $\sigma_{cf}$ ) is the tensile stress transferred by steel fibres at crack. The value of ( $\sigma_{cf}$ ) can be obtained by the experimental stress-crack opening relationship of UHPFRC and should be calculated at the centre line of the steel reinforcement.

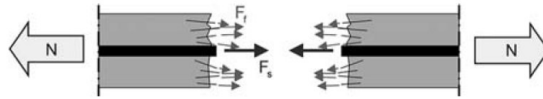


Figure 2-48: External and internal force equilibrium at crack cross-section under tensile load.

Figure 2-49 (a) and (b) illustrate the experimental and schematical ( $\sigma_{cf} - w$ ) relationship, respectively, for the hardening ( $\sigma_{cf0} > \sigma_{cf,cr}$ ) and softening ( $\sigma_{cf0} < \sigma_{cf,cr}$ ) behaviour of UHPFRC [107] and [108].

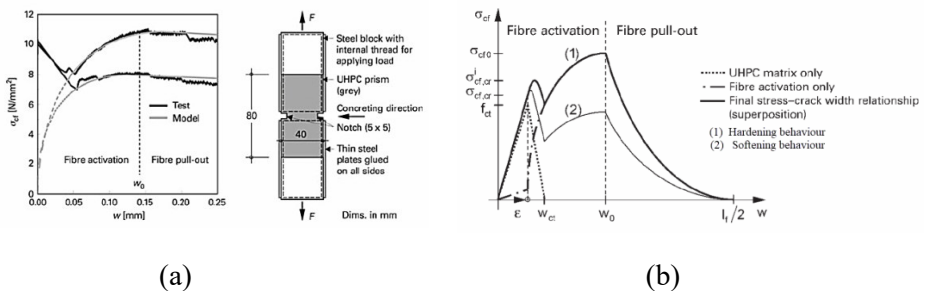


Figure 2-49: Stress-crack opening relationship for UHPFRC, (a) experimental results, (b) schematical illustration [107] and [108].

The relative tensile stress ( $\sigma_{cf}$ ) can be determined as follows:

$$\sigma_{cf} = \sigma_{cf0} \left( 2\sqrt{\frac{w}{w_0}} - \frac{w}{w_0} \right) \rightarrow \text{fibre activation phase; } w \leq w_0 \quad (2-64)$$

$$\sigma_{cf} = \sigma_{cf0} \left(1 - \frac{2w}{l_f}\right)^2 \rightarrow \text{fibre pull - out phase; } w > w_0 \quad (2-65)$$

where:

( $\sigma_{cf0}$ ) is the fibre efficiency, ( $w$ ) is the actual crack width, ( $l_f$ ) is the length of the fibre, and ( $w_0$ ) is the corresponding crack width when ( $\sigma_{cf0}$ ) is reached.

Equations (2-64) and (2-65) are found in studies of [107, 108, 110-112], and they are valid for concrete reinforced with fibres in general and UHPC. However, based on the test results, the value of the fibre efficiency ( $\sigma_{cf0}$ ) should be adjusted accordingly. For SLS, the Equation (2-65) can be simplified as ( $\sigma_{cf} = \sigma_{cf0,k}$ ) [109]. The value of ( $\sigma_{cf0,k}$ ) is the maximum tensile stress transferred by fibres. When the embedment length of the fibre is ( $l_f/2$ ) and it is fully activated, the characteristic value of the fibre efficiency can be reached. Based on the theoretical study carried out by Leutbecher, T. [108], the value of the ( $w_0$ ) can be obtained by the following Equation:

$$w_0 = \frac{\tau_{fm} \cdot l_f^2}{E_f \cdot d_f} \quad (2-66)$$

where:

( $\tau_{fm}$ ) is the average value of the bond stress between matrix and fibre by assuming a rigid plastic bond law, ( $d_f$ ) is fibre's diameter, and ( $E_f$ ) is the elasticity's modulus of the fibre.

Finally, the strain of the steel reinforcement at the crack is calculated by:

$$\varepsilon_S^f = \sigma_S / E_S = F_S / (A_S \cdot E_S) \quad (2-67)$$

By evaluating Equations (2-64) and (2-65) seems to be that the tensile stress transferred by steel fibres at the crack ( $\sigma_{cf}$ ) depends on the crack width. The characteristic value of the crack width ( $w_k$ ) can be obtained by the basic crack width formula as was indicated in section 2.3 by using Equation ( $w_k = s_{r,max} \cdot (\varepsilon_{sm} - \varepsilon_{cm})$ ). The maximum crack spacing ( $s_{r,max}$ ) is the maximum length over which the slip between steel reinforcement and matrix occurs in the stabilized cracking state. ( $\varepsilon_{sm}$ ) and ( $\varepsilon_{cm}$ ) are the average strain in the reinforcement and matrix over ( $s_{r,max}$ ), respectively. Figure 2-50 illustrate the qualitative distribution of strains in the steel reinforcement and concrete matrix by including the shrinkage effect at the stabilised cracking state [109, 113-115].

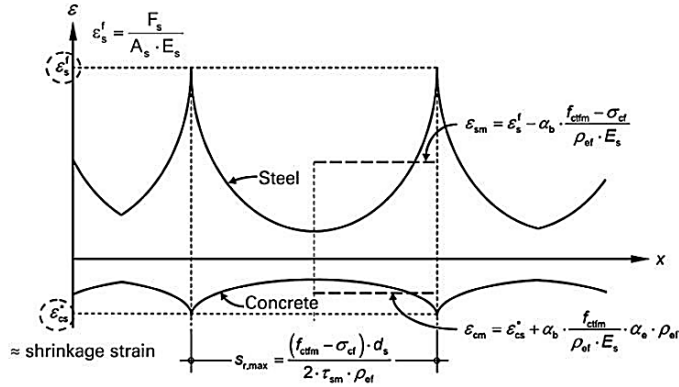


Figure 2-50: Qualitative strain distribution in R-UHPFRC element with concrete shrinkage consideration [115].

Based on the average values indicated in Figure 2-50, the mean strain difference ( $\varepsilon_{sm} - \varepsilon_{cm}$ ) can be stated as follows:

$$\varepsilon_{sm} - \varepsilon_{cm} = \varepsilon_s^f - \varepsilon_{cs}^* - \alpha_b \cdot \frac{f_{ctfm} \cdot (1 + n \cdot \rho_{ef}) - \sigma_{cf}}{\rho_{ef} \cdot E_s} \quad (2-68)$$

where:

( $\varepsilon_{sm}$ ) the average strain in the reinforcement.

( $\varepsilon_{cm}$ ) the average strain in the UHPFRC matrix.

( $\varepsilon_s^f$ ) steel rebar strain at the cracks obtained by Equations 2-63 and 2-67.

( $\varepsilon_{cs}^*$ ) the shrinkage strain in the UHPFRC matrix. For more details, see section 2.5 and chapter 4.

( $\alpha_b$ ) the shape coefficient for defining the strain distribution diagram. For the short-term loads and long-term loads, its value is 0.6 and 0.4, respectively.

( $n$ ) the modular ratio ( $n = E_s / E_c$ ). ( $E_s$ ) and ( $E_c$ ) are elastic modulus of the steel rebar and UHPFRC, respectively.

( $\rho_{ef}$ ) the effective reinforcement ratio ( $\rho_{ef} = A_s / A_{c,ef}$ ).

( $A_{c,ef}$ ) the effective tension area according to Figure 7-1 in Eurocode 2 [116].

( $\sigma_{cf}$ ) the tensile stress transferred by the fibres in the crack.

The value of the ( $s_{r,max}$ ) can be calculated with the following Equation:

$$s_{r,max} = \frac{(f_{ctfm} - \sigma_{cf}) \cdot d_s}{2 \cdot \tau_{sm} \cdot \rho_{ef}} \quad (2-69)$$

where

( $\tau_{sm}$ ) is the average bond stress over ( $s_{r,max}$ ) and ( $d_s$ ) is the diameter of the steel

reinforcement.

The average bond stress value ( $\tau_{sm}$ ) can be found in Figure 2-51, which is based on the pull-out test [108].

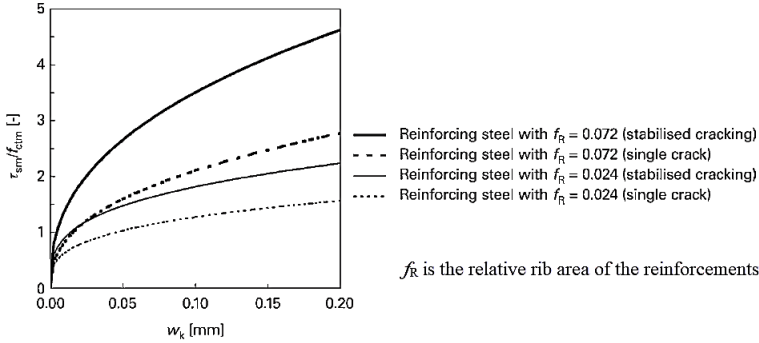


Figure 2-51: Bond stress-crack width relationship [108].

By an interaction process and using Equations (2-68) and (2-69), the crack width ( $w_k = s_{r,max} \cdot (\epsilon_{sm} - \epsilon_{cm})$ ) can be found.

The average steel reinforcement strain and average concrete stress in the stabilized cracking phase can be calculated by the following expressions [115]:

$$\epsilon_{sm} = \epsilon_s - \frac{\beta_t \cdot (f_{ctfm} - \sigma_{cfm}) + \sigma_{cfm} \cdot \rho_{ef} / \rho_s}{\rho_{ef} \cdot E_s} \quad (2-70)$$

$$\sigma_{cm} = \beta_t \cdot (f_{ctfm} - \sigma_{cfm}) \cdot A_{c,cf} / A_c + \sigma_{cfm} \quad (2-71)$$

where

( $\beta_t$ ) the shape factor, 0.4 for short-term loading and 0.25 for long-term or repeat loading.

( $\beta_t$ ) the strain in the bare steel reinforcement at the crack by neglecting the fibre's contribution.

Equation 2-71 shows that the tension stiffening has a constant value, and the full-tension stiffening can be accurately modelled.

The proposed tension stiffening model was evaluated with the experimental uniaxial tensile test results with three different fibre content for the R-UHPFRC element (see Figure 2-52), and a good agreement was achieved.



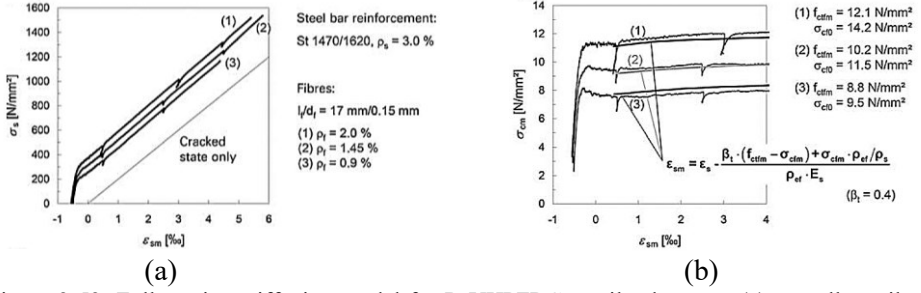


Figure 2-52: Full-tension stiffening model for R-UHPFRC tensile elements, (a) overall tensile response, (b) comparison of test results with proposed full-tension stiffening model.

It is possible to use a constant value for stress in the tensile stress transferred by steel fibres at the crack ( $\sigma_{cfm}$ ) as 80 percent of the mean fibre efficiency to simplify the calculation process ( $\sigma_{cfm} = 0.80 \times \sigma_{cf0m}$ ). Figure 2-53 shows a comparison of the simplified model and test results, and as can be seen, a good agreement was achieved.

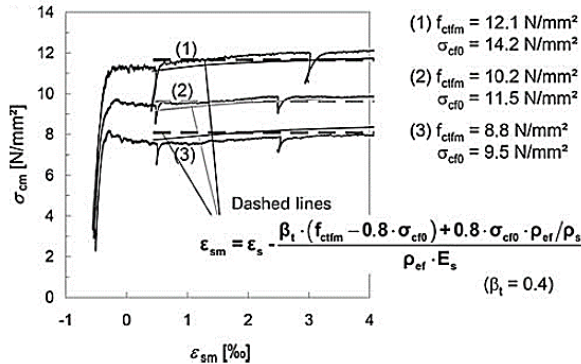


Figure 2-53: Simplified full-tension stiffening model by approximating the value of the ( $\sigma_{cfm} = 0.80 \times \sigma_{cf0m}$ ).

## 2.5. Shrinkage properties of UHPFRC

### 2.5.1. Background

The mix design of the UHPFRC contains a high binder content (cement and silica fume) and a low water-to-cement ratio (W/C) of 0.2 or below compared with the conventional concrete. Pore sizes and densified microstructure would be reduced due to existing fineness admixtures and filler in the UHPFRC matrix [117], and according to Laplace's law, the capillary pressure in the pore network

increase due to the consumption of water by hydration [118]. Thus, the smaller pore size combined with higher capillary pressure results in a higher autogenous shrinkage strain for UHPFRC when compared to drying shrinkage. With a very low (W/C), there would be less pore water available, and thus the evaporation transport mechanisms would be very limited. As a result, drying shrinkage is reduced. Generally, UHPFRC's long-term drying shrinkage will be lower, but its autogenous shrinkage is considerable and the autogenous shrinkage of UHPFRC can account for a significant part of the total shrinkage value [119-122].

Due to exiting the steel reinforcement in the UHPFRC structural elements, this high autogenous shrink is restrained by internal steel reinforcements and a significant residual tensile stress and shrinkage cracks can be generated in the matrix without exiting any external load. The value of the autogenous strain of UHPFRC can be between 220 to 760  $\mu m / m$  (see Table 2-3), and it could generate microcracks and macrocrack propagation due to the development of high induced tensile stress (called self-equilibrated stresses).

Steel fibres can limit shrinkage through the interfacial band; hence the shrinkage behaviour can be varied by the fibre content value. According to Zhang, J. and Li, Victor [123], decreasing the shrinkage strain happens only for fibre content value up to 3 vol%. They observed that specimens with 4 vol% of steel fibres have the same shrinkage value. Yoo, D, Y et al. [124] obtained the same conclusion, as illustrated in Figures 2-54 (a) and (b). On the other hand, the fibre content has a lower effect on shrinkage for the hardened concrete and it can be caused due to the increase of the matrix's modulus with age [123].

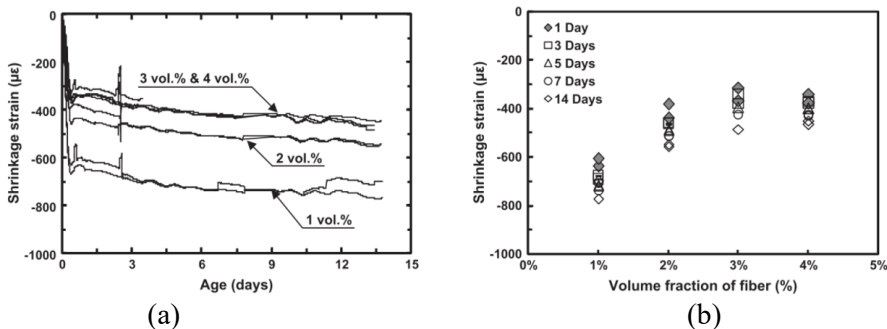


Figure 2- 54: Fibre content effect on shrinkage behaviour of UHPFRC, (a) shrinkage diagram for 1%, 2%, 3% and 4% fibre content, (b) early age shrinkage values for 1% to 4% fibre content [124].

Due to the importance of characterizing shrinkage strains, a lot of recent research has been conducted to understand better the fundamental mechanisms governing autogenous shrinkage of UHPC and UHPFRC and its impact on performance. For example, comprehensive experimental studies were conducted by Şahmaran

et al. [125-127] and Yoo et al. [124, 128-130] to study the effects of parameters such as mixing proportion, curing conditions, geometry effect and specimen restraint on autogenous shrinkage. Table 2-3 present the obtained values for autogenous and drying shrinkage strain of some experimental studies for UHPFR and UHPC material.

**Table 2-3a:** Summary of shrinkage behaviour studies and values of autogenous and drying shrinkage of UHPFRC and UHPFRC.

Author	Aims, parameters of studying and findings	Obtained autogenous value ( $\mu m / m$ )
Islam M.M.U. 2022 [131]	The aim of this experimental work was to study the long-term tension stiffening mechanism of UHPFRC under the influence of shrinkage strain. They studied the interrelation between the instantaneous and sustained tensile loading conditions. The autogenous shrinkage and drying shrinkage at 180-day were obtained by conducting testing method [132] in accordance with the ASTM C512 [133] for UHPFRC with small steel fibres content of 215 kg/m <sup>3</sup> . They recommend that the shrinkage effect should be considered even before applying any loads to prevent any failure for the serviceability behaviour of the structural element.	<p style="text-align: center;"><u>At 25-days:</u></p> Autogenous shrinkage: 221 Drying shrinkage: 115 Total shrinkage: 334  <p style="text-align: center;"><u>At 180-days:</u></p> Autogenous shrinkage: 392 Drying shrinkage: 170 Total shrinkage: 562
Cédric Androuët et al. 2021 [134]	The impact of several mixing and curing methods, as well as different curing starting times and curing duration on shrinkage of UHPFRC was investigated. It was found that the water immersion curing method led to reducing the shrinkage value up to 65% for early-age and 30% for long-term. Additionally, the shrinkage of UHPC reduced more than 20% when the temperature of the fresh UHPC was 20 °C. The fibre dosage for casting the specimens were 3 and 4 %. Half of the shrinkage deformation that happened at 28 days occurred in the first 24 hours.	<p style="text-align: center;"><u>Early age shrinkage:</u></p> Total shrinkage: 200-800  <p style="text-align: center;"><u>Long-term shrinkage:</u></p> Total shrinkage: 800-1400

**Table 2-3b:** Continue of Table 2-3a, Summary of shrinkage behaviour studies and values of autogenous and drying shrinkage of UHPFRC and UHPFRC.

<p>Fang C. et al. 2020 [122]</p>	<p>The influence of fibre type, fibre aspect ratio and fibre volume content on the shrinkage mechanism of UHPFRC was experimentally quantified. Four different steel fibres were used in this study. Three of those four fibres were macro-fibres with hooked end type with different diameters and lengths, whereas the fourth was micro-straight fibre. Additionally, the effect of the hybridization of steel fibres (micro and macro fibres) were investigated. The fibre volume fraction of the mixtures were 1.5%, 2 %, 2.5%, and for the hybrid mixture, the proportion of the micro to macro fibres were 1:1 (1% for each type). It was discovered that the presence of randomly distributed steel fibres reduced both total and autogenous shrinkage. Total and autogenous shrinkages were significantly reduced when the fibre volume fraction or aspect ratio was increased. Hooked-end fibres provide better restraining autogenous shrinkage compared to straight fibres.</p>	<p><u>At 180-days:</u> Autogenous shrinkage: 200-700  Drying shrinkage: 110-200  Total shrinkage: 300-900</p>
<p>Weina Meng et al. 2018 [135]</p>	<p>The key material properties such as compressive and tensile flexural strength, viscosity and autogenous shrinkage of UHPFRC made by hybridization of fibres with both micro-macro steel fibres and steel-synthetic fibres were investigated. The fibre volume content varied between 0 to 5%. It was reported that using UHPFRC mixture made with hybrid fibres (1% micro steel fibres and 1% macro steel hooked-end fibres) reduce 25% of the autogenous compared with UHPFRC with 2% of micro straight fibres as a reference. The autogenous shrinkage was reduced by 40% in the case of using 1.5% of micro straight fibres with 0.5% polyvinyl alcohol (PVA) fibres. Additionally, it was observed that the increase of the fibre content (1% to 5%) caused a significant reduction of the autogenous shrinkage compared with UHPC (0% of fibre) by 15, 30, 35, 45 and 60% measured at 56-days.</p>	<p><u>At 56-days:</u> Autogenous shrinkage: 200-500</p>

**Table 2-3c:** Continue of Table 2-3a, Summary of shrinkage behaviour studies and values of autogenous and drying shrinkage of UHPFRC and UHPFRC.

<p>T. Xie et al. 2018 [120]</p>	<p>Three different technics were experimentally investigated to reduce the impact of shrinkage, which were binder content reduction, using shrinkage reduction admixture and replacing the mixing water partially with crushed ice. It was observed that the autogenous shrinkage predominated the overall UHPC shrinkage and mentioned techniques significantly reduced the shrinkage effect. The optimal binder-to-sand and shrinkage reducing admixture content for decreasing the shrinkage effect were suggested in the range of 1-1.1 and 1%, respectively. Furthermore, they reported that replacing 50% of mixing water with crushed ice led to a significant reduction in shrinkage. Five distinct mixes with b/s ratios of 0.8, 0.9, 1.0, 1.1, and 1.266 were made and the autogenous and total shrinkage after 180 days were experimentally obtained to evaluate the binder-to-sand (b/s) influence on shrinkage of UHPC.</p>	<p style="text-align: center;"><u>At 180-days:</u></p> <p>Autogenous shrinkage: 440-640</p> <p>Total shrinkage: 650-800</p>
<p>Yalçinkaya and Yazıcı 2017 [136]</p>	<p>The effect of exposure temperature and relative humidity on autogenous and dry shrinkage at the early age of UHPFRC with high-volume mineral admixture was investigated. Three main types of climate conditions were applied by varying the temperature (20, 30, 40 °C) and relative humidity (50, 60, and 70 %). The UHPFRC mixtures designed by W/C ratio between 0.25-0.50 and steel straight fibres with 2% in volume by 6 mm length and 0.16 mm diameter were employed. The obtained autogenous shrinkage values under controlled temperature conditions of 20, 30, and 40 °C were near 450, 600 and 750 micro-strain, respectively. The shrinkage of UHPFRC increases and accelerates in the first few hours due to increasing the ambient temperature.</p>	<p style="text-align: center;"><u>On first days:</u></p> <p>Autogenous shrinkage: 380-750</p> <p>Drying shrinkage: 520-2020</p>

**Table 2-3d:** Continue of Table 2-3a, Summary of shrinkage behaviour studies and values of autogenous and drying shrinkage of UHPFRC and UHPFRC.

<p>Yoo D. Y. et al. 2015 [137]</p>	<p>The aim of this study was to describe the effect of shrinkage-reducing admixture (SRA) on the free and autogenous shrinkage of reinforced UHPFRC. Specimens were reinforced by steel rebars with ratios of 1.3, 2.9, and 8% and three different shrinkage-reducing admixture content were used. A higher SRA content contributed to a slightly higher tensile strength and a lower autogenous shrinkage. In addition, a higher SRA content and a lower reinforcement ratio resulted in better restrained autogenous shrinkage behaviours, such as lower autogenous shrinkage stress and cracking potential. Therefore, it can be concluded that the use of SRA or a lower reinforcement ratio is favourable for improving the restrained shrinkage behaviours of UHPFRC. Furthermore, tensile strength development was measured to evaluate the cracking potential of UHPFR. Smooth steel fibres with a diameter of 0.2 mm and a length of 13 mm, and 2% volume fraction were used in the mix design. The Water-to-binder ratio was 0.2, and SRA to cement weight ratios were 0, 1, and 2%. It was observed that increasing the SRA content caused to slightly reduced the autogenous shrinkage. Additionally, better autogenous shrinkage behaviour was obtained with a higher SRA content and lower reinforcement ratio. The tensile strength slightly increased with an increase in the SRA content. 30-day autogenous shrinkage was measured at different zeroing points. After nearly 17 hours, the autogenous strain's increased rate rapidly decreased, and only a slight expansion was observed.</p>	<p><u>At 30-days:</u> Autogenous shrinkage: 520-760</p>
<p>Fehling, 2015 [115]</p>	<p>According to Fehling's book, for structural UHPFRC elements made under non-heat-treated conditions, depending on cement content and mix design, the total shrinkage strain can be assumed about 600-900 <math>\mu m / m</math> for UHPFRCs with W/C ratios of 0.25 or below.</p>	<p>Total; shrinkage: 600-900</p>

**Table 2-3e:** Continue of Table 2-3a, Summary of shrinkage behaviour studies and values of autogenous and drying shrinkage of UHPFRC and UHPFRC.

Yoo D. Y. et al. 2014 [138]	The combined effect of shrinkage-reducing (SRA) and expanding and expanding (EA) admixtures on the early age shrinkage and cracking behaviour of UHPFRC slabs was investigated. Six full-scale slabs with different thicknesses of 40, 60, and 80 mm were fabricated with two different mixtures. The 7-day free shrinkage of UHPFRC with 1% SRA and 7.5% of EA reduced about 36-42%. This mixture design improved the cracking behaviour significantly, and the maximum crack width was reduced from 0.2 mm to 0.04 mm by referencing UHPFRC without SRA and EA.	<u>At 7-days:</u> Free shrinkage: 800-950
-----------------------------	---	--

### 2.5.2. Shrinkage values in codes and recommendations for UHPFRC

There are not many international codes and recommendations for designing the UHPFRC structures around the world. The first technical recommendation on UHPFRC for structural design and material properties were established when this material was first developed by Frances's research group and called AFGC-SETRA recommendation [84], published in 2002 (and its revised edition in 2013 [139]). Based on this recommendation, two French standards for UHPFRC (Association Francaise de Normalisation) were released in 2016. The first standard [140] contributed the UHPFRC specification, performance, production and conformity and the second standard [141] stands as a national complement to Eurocode 2 for the design of RUHPFRC structures. Thereafter, in Germany in 2003, a state-of-art reported all aspects of material and design on UHPFRC (DAfStB) [142]. Then, in 2008, the concrete Committee of the Japan Society of Civil Engineers (JSCE) released a recommendation for design of the UHPFRC structures called (Recommendation for design and construction of High-Performance Fibre Reinforced Cement Composites with multiple fine cracks (HPFRCC)) [143]. In 2014, the Korea Institute of Construction Technology (KICT) also released a design guideline for UHPFRC [144] based on the design recommendations published in 2012 [145]. In recent years, the Swiss standard (fprSIA 2052-2016) [85], Australian [146] and American [77] are available.

According to the Japanese recommendation [143] the shrinkage value must be determined by experimental results test by considering parameters such as material properties, mix proportions, curing conditions, shape and dimensions of the member cross-section and ambient humidity. The shrinkage experiment should be performed according to JIS A 6202 appendix or JIS A 1129.

The Korean design guideline [144] consider the same parameters mentioned above to determine the UHPFRC shrinkage value and propose total shrinkage values (autogenous plus drying shrinkage) of 550 and 600  $\mu\text{m} / \text{m}$  for UHPFRC subjected to high-temperature wet curing range and standard curing range, respectively. This guideline also provides equations to predict the autogenous and drying shrinkage values for UHPFRC as follows:

Drying shrinkage:

$$\varepsilon_{ds}(t, t_s) = \varepsilon_{ds0} \cdot \beta_s(t - t_s) \quad (2-72)$$

$$\beta_s(t, t_s) = \left[ \frac{(t-t_s)/t_1}{87.5(h/h_0)^2 + (t-t_s)/t_1} \right]^{0.5} \quad (2-73)$$

Autogenous shrinkage:

$$\varepsilon_{as}(t) = \varepsilon_{as0} \cdot (f_{cm}) \cdot \beta_{as}(t) \quad (2-74)$$

$$\varepsilon_{as0}(f_{cm}) = \alpha_{as} \left( \frac{f_{cm} / f_{cm0}}{6 + f_{cm} / f_{cm0}} \right)^{0.25} \times 10^{-6} \quad (2-75)$$

$$\beta_{as}(t) = 1 - e^{\left[ -0.7 \left( \frac{t}{t_1} \right)^{0.5} \right]} \quad (2-75)$$

where

$\varepsilon_{ds}(t, t_s)$  : drying shrinkage of UHPFRC in a specific time.

$\varepsilon_{ds0}$  : conceptual drying shrinkage.

$\beta_s(t - t_s)$  : coefficient to considering the development of drying shrinkage with time.

$t$  : age of UHPFRC.

$t_s$  : age  $\varepsilon_{ds}(t, t_s)$  of UHPFRC at which the drying shrinkage was started.

$t_1$  : time function in dimensionless form and represents 1-day age

$h$  : member dimension defined as  $(2A_c / u)$ , where  $(A_c)$  is cross-sectional area and  $(u)$  is the circumferential length of the cross-section.

$h_0$  : is equal to 100 mm.

$f_{cm}$  : average compressive strength.

$f_{cm0}$  : is equal to 10 MPa.



$\alpha_{as}$  : coefficient which its value is determined by characteristics of UHPFRC and should be determined based on autogenous shrinkage test results. In the absence of experimental evidence, the recommended value of ( $\alpha_{as}$ ) is 470.

It should be noted that Equation (2-74) is for calculating the autogenous shrinkage of UHPFRC and it is based on the fib Model Code (2010). The drying and autogenous shrinkage test result for UHPFRC provided in this design guide is shown in Figures 2-55 (a) and (b).

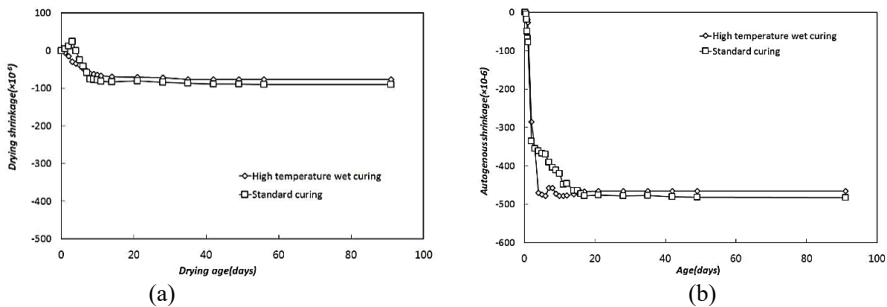


Figure 2-55: Drying and autogenous shrinkage test result for UHPFRC provide by design guideline [144], (a) drying shrinkage behaviour, (b) autogenous shrinkage behaviour.

As can be seen, the drying shrinkage strain ranged between 70-80 and 90-100  $\mu\text{m} / \text{m}$  for cases of high-temperature wet curing and standard curing, respectively. On the other hand, the autogenous shrinkage strain was partially similar for two high-temperature and standard curing and ranged between 450-500  $\mu\text{m} / \text{m}$ .

The Australian design guidelines [146] use a constant shrinkage value of 500  $\mu\text{m} / \text{m}$  for shrinkage of Ductal's Reactive Powder Concrete (RPC) in the case of the element was exposed to steam curing at 90oC for at least 2 days. If the element were cured at room temperature, the shrinkage value increases slowly during the long period of time, as illustrated in Figure 2-56.

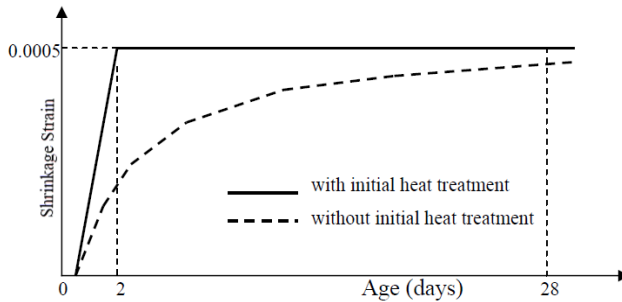


Figure 2-56: Shrinkage behaviour during the 28 days with and without initial heat treatment.

In the United States of America, the Federal Highway Administration (FHWA) has reported a state-of-the-art [77] about research, development and deployment of UHPC. This report for obtaining the shrinkage value of UHPFRC refers to the standard test ASTM C157 [147], which is specific for measuring the drying shrinkage after the concrete has hardened. Other methods are recommended by this standard for measuring the autogenous shrinkage immediately after casting. The proposed total shrinkage strain range is between 620 to 766  $\mu m / m$  depending on the treatment method and value of 555  $\mu m / m$  for untreated elements [148] (see Figure 2-57). Additionally, this report indicates that for untreated elements, almost 400  $\mu m / m$  of the total shrinkage strain occurs in the first 24 hours.

The report “Material Property Characterization of Ultra-High Performance Concrete” [148] published by (FHWA) presents results from their first research program to characterize the material behaviour of UHPC in terms of accepted concrete test methodologies [148]. Based on this research, both tempered steam-treated and untreated specimens showed continued shrinkage after 4 months of age, as illustrated in Figure 2-57, and all specimens were reached to 95% of their ultimate shrinkage after 2 months.

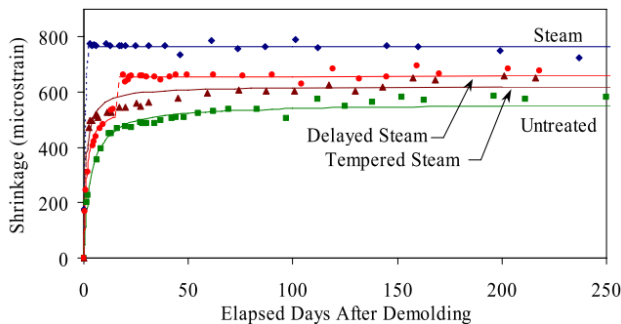


Figure 2-57: Long term shrinkage of steam-treated and untreated UHPC specimens [148].

The early age shrinkage was measured using an embedded strain gage (Geokon 4202 Vibrating Wire Strain Gage) for two steam treatment and an untreated curing regime. Results showed that the UHPC with steam-treated reached a total shrinkage of  $850 \mu m / m$  and untreated UHPC's total shrinkage were obtained beyond the  $790 \mu m / m$  (see Figure 2-58).

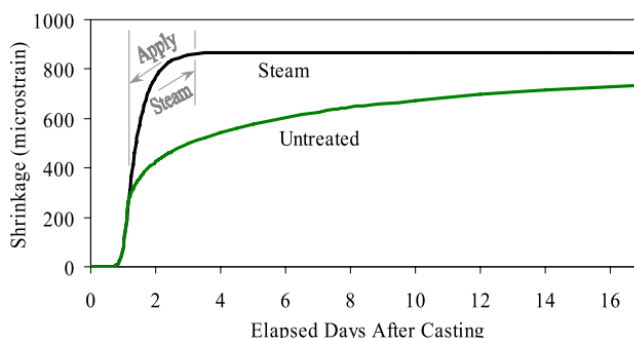


Figure 2-58: Early age shrinkage of steam-treated and untreated UHPC specimens [148].

The French standard [140] defines two kinds of heat treatment that can cure the UHPFRC elements. The first type of heat treatment is applied during the first few hours, and the second type is applied when the UHPFRC has hardened. The first type of heat treatment aims to anticipate the moment in which the concrete will begin to set and to accelerate the initial hardening process. The second type aims to develop new hydrates to increase the cement strength.

For the preliminary design phase of UHPFRC elements, when nothing is known about the heat treatment, the following recommendations can be used for long term effects:

- ❖ For heat treatment type one (first type): for outdoor environmental conditions with a relative humidity of 50-70 %, the total shrinkage strain is  $550 \mu m / m$ .
- ❖ For heat treatment type two (second type): the total shrinkage value can be used with a value of  $550 \mu m / m$  before the end of the heat treatment, after which the total shrinkage is nil.
- ❖ For the case of applying any heat treatment: for outdoor environmental conditions with a relative humidity of 50-70 %, the total shrinkage strain is  $700 \mu m / m$ . This total shrinkage strain is composed of drying shrinkage ( $150 \mu m / m$ ) and autogenous shrinkage ( $550 \mu m / m$ ).

In Annex 7 of the French recommendations [139], the expression (2-76) is provided to compute the autogenous shrinkage of UHPFRC.

$$\varepsilon_{sh}(t) = A \cdot \exp \left[ \frac{B}{\sqrt{t+C}} \right] \quad (2-76)$$

Where ( $A = 525$ ), ( $B = -2.5$ ), and ( $C = -0.5$ ). The parameter ( $t$ ) is the age of the concrete for which the shrinkage is computed.

According to the Swiss standard (fprSIA 2052) [85], shrinkage is mainly due to autogenous shrinkage. The total shrinkage strain (drying plus autogenous shrinkage) for UHPFRC made with cement type CEM I and CEM III with heat treatment can be obtained by using Equation (2-77).

$$\varepsilon_{Us}(t) = \varepsilon_{Us\infty} \cdot \exp \left[ \frac{c}{\sqrt{t+d}} \right] \quad (2-77)$$

where the coefficients are a function of the cement type:

For cement type CEM I:

$$c = -2.48$$

$$d = -0.86$$

$$\varepsilon_{Us\infty} = 0.6 - 0.8 \mu m / m$$

and for cement type CEM III:

$$c = -1.3$$

$$d = -0.86$$

$$\varepsilon_{Us\infty} = 0.95 \mu m / m$$

For UHPFRC made with cement type CEMI, the final value of shrinkage ( $\varepsilon_{Us\infty}$ ) is 600 to 800  $\mu m / m$ . If the cement used in the UHPFRC is not CEMI, the shrinkage effect can be significant and the shrinkage test is advised. The coefficients ( $c$ ) and ( $d$ ) in Equation (2-76) are (-2.48) and (-0.86), respectively. Equation (2-77) is similar to the equation suggested in the French recommendation (Equation (2-76)), only with different coefficients values. Figure 2-59 shows a comparison between the Swiss standard [85] and French recommendations [139].

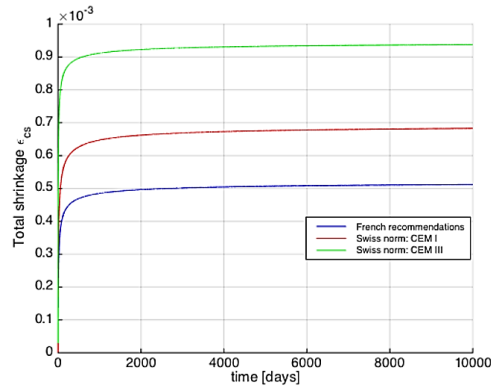


Figure 2-59: Comparison between shrinkage values provide by equations in Swiss standard and French recommendation [149].

### 2.5.3. Shrinkage influence on tension stiffening behaviour

As illustrated in Figures 2-60 (a) and (c), free shrinking of an isolated UHPFRC member would simply shorten the member, while the embedded steel reinforcement provides restraint to shrinkage leading a negative pre-strain ( $\epsilon_{s,sh}$ ) with a compressive stress in the steel reinforcement ( $\Delta\sigma_{s,sh}$ ) and initial tensile strain in UHPFRC ( $\epsilon_{c,sh}$ ) with a tensile stress ( $\Delta\sigma_{c,sh}$ ), (see Figures 2-60 (b), (d) and (e)).

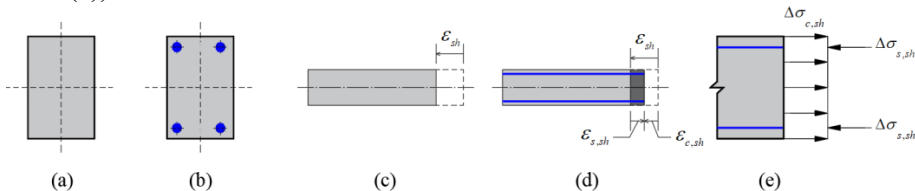


Figure 2-60: Deformation of UHPFRC due to shrinkage: (a) and (b) UHPFRC section without and with reinforcement, (c) free shrinkage deformation, (d) shrinkage-influenced deformation in R-UHPFRC element, (e) stress distribution in the reinforced cross-section due to shrinkage.

Bischoff [91] reported that the member response of RC specimens drops as shrinkage increases and results in a lower cracking load and less apparent tension stiffening. The same phenomenon can occur for R-UHPFRC tensile tie elements. Shrinkage strain is influenced by variables such as mixture properties, temperature, curing conditions, material properties, and geometry of the element [150]. Shrinkage of concrete leads to an initial shortening of the R-UHPFRC member and causes a reduction in the cracking load and effects on the tensile response and tension stiffening response as indicated in Figure 2-61 (a) and (b). However, the high shrinkage strain of UHPFRC needs to be paid special

attention for elements under tensile stresses.

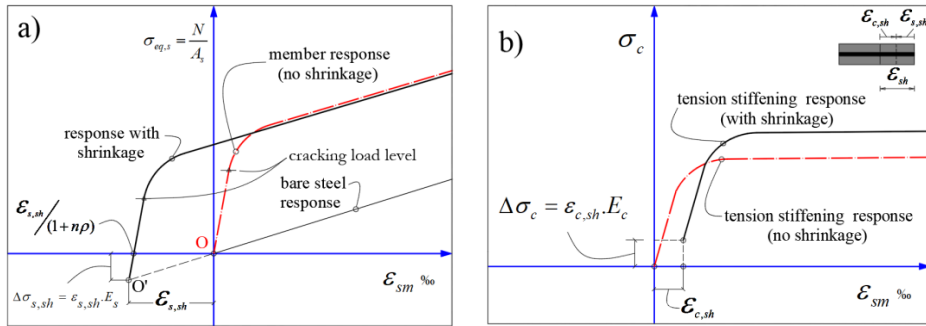


Figure 2-61: Effect of the shrinkage on the tensile response of R-UHPFRC; (a) average stress-strain response, (b) UHPFRC's contribution in tension.

The origin of the stress-strain behaviour of the tensile R-UHPFRC element should be modified as shown in Figure 2-61. The UHPFRC's matrix would be already in tension, even without considering the effects of external actions. Thus, the cracking load level lowered, see Figure 2-61(a).

The free shrinkage strain of the UHPFRC ( $\epsilon_{sh}$ ) can be derived as the sum of the steel reinforcement strain and concrete strain:

$$\epsilon_{sh} = |\epsilon_{s,sh}| + |\epsilon_{c,sh}| \quad (2-78)$$

By applying the compatibility equation and assuming the elastic behaviour for steel and concrete (non-cracked section), the stress in each of the materials can be obtained by the following expressions:

$$\Delta\sigma_{c,sh} = E_c \cdot \epsilon_{c,sh} \quad (2-79)$$

$$\Delta\sigma_{s,sh} = E_s \cdot \epsilon_{s,sh} \quad (2-80)$$

where ( $E_s$ ) and ( $E_c$ ) are elastic modulus of the steel rebar and UHPFRC, respectively.

The equilibrium of the tensile and compression forces in the section leads to having:

$$F_s = F_c \rightarrow \sigma_c \cdot A_c = \sigma_s \cdot A_s \Rightarrow \sigma_c = \frac{A_s}{A_c} \cdot \sigma_s \quad (2-81)$$

by defining the effective reinforcement ratio as ( $\rho = A_s / A_c$ ) and substituting in the Equation (2-81) gives:

$$\sigma_c = \rho \cdot \sigma_s \quad (2-82)$$

the strain in the reinforcement can be derived as:

$$\epsilon_{s,sh} = \epsilon_{sh} - \epsilon_{c,sh} \quad (2-83)$$

by substituting the Equation (2-83) into Equation (2-80) and defining parameter ( $n = E_s / E_c$ ), we have:

$$\begin{aligned}
 \Delta\sigma_{s,sh} &= E_s \cdot (\varepsilon_{sh} - \varepsilon_{c,sh}) = E_s \cdot \varepsilon_{sh} - \frac{E_s}{E_c} \cdot E_c \cdot \varepsilon_{c,sh} \\
 &= E_s \cdot \varepsilon_{sh} - n \cdot E_c \cdot \varepsilon_{c,sh} \\
 &= E_s \cdot \varepsilon_{sh} - n \cdot \Delta\sigma_{c,sh} \\
 \Delta\sigma_{s,sh} &= E_s \cdot \varepsilon_{sh} - n \cdot \rho \cdot \Delta\sigma_{s,sh} \\
 &\Downarrow \\
 (\Delta\sigma_{s,sh} + n \cdot \rho \cdot \Delta\sigma_{s,sh}) &= E_s \cdot \varepsilon_{sh} \\
 &\Downarrow \\
 \Delta\sigma_{s,sh} (1 + n \cdot \rho) &= E_s \cdot \varepsilon_{sh}
 \end{aligned} \tag{2-84}$$

Consequently, the compressive stress in the steel reinforcement ( $\Delta\sigma_{s,sh}$ ) and tensile stress in the concrete ( $\Delta\sigma_{c,sh}$ ) derive by following expressions:

$$\Delta\sigma_{s,sh} = \frac{E_s \cdot \varepsilon_{sh}}{(1 + n \cdot \rho)} \tag{2-85}$$

and by using Equation (1-81):

$$\Delta\sigma_{c,sh} = \frac{\rho}{(1 + n \cdot \rho)} \cdot E_s \cdot \varepsilon_{sh} \tag{2-86}$$

dividing two sides of Equation (2-84) to ( $E_s$ ) and extract ( $\varepsilon_{sh}$ ) leads to:

$$\varepsilon_{sh} = \varepsilon_{s,sh} \cdot (1 + n \cdot \rho) \tag{2-87}$$

By using Equation (2-87), the compression strain in the reinforcement caused by shrinkage converts into the free shrinkage strain.

The free shrinkage value can be determined experimentally or can be used the recommended values provided by codes, as discussed in the previous section. With the aim of obtaining the free shrinkage value for the used UHPFRC in this PhD study, an incentive shrinkage test was conducted, which is described in the following section of the present document.

## 2.6. Crack width prediction and limitations for design of R-UHPFRC in serviceability limit states

Controlling crack width in UHPFRC is essential for resisting environmental actions, serviceability behaviour and safety, and for avoiding steel corrosion and aesthetics during UHPFRC structures' working life. To design UHPFRC

structural elements, resistance to environmental actions should be examined by controlling crack width, while cracks should be tested (due to stresses) to control impaired structures' serviceability and safety [151, 152].

Based on the Euro Code 2 [153] and The French code NF P 18-710 for UHPFRC structures [154], a durable structure should meet the requirements of serviceability. It also needs to consider the effect of direct and indirect actions, environmental conditions and consequential effects. The French code is based on Euro code 2, and they classified exposure conditions related to environmental conditions in accordance with EN 206-1 [155]. Note that the exposure conditions are chemical and physical conditions to which the structure is exposed in addition to the mechanical actions. The environmental conditions are classified into four main categories and their subcategories:

- (1) No risk for corrosion or attack (X0)
- (2) Corrosion induced by carbonation (XC1, XC2, XC3, XC4)
- (3) Corrosion induced by chlorides (XD1, XD2, XD3)
- (4) Corrosion induced by chlorides from seawater (XS1, XS2, XS3)
- (5) Freeze/Thaw Attack (XF1, XF2, XF3, XF4)
- (6) Chemical attack (XA1, XA2, XA3)

In structural design, the limitation of the crack width is done by complying with design rules and the limitation of the maximum crack width under the decisive load combination.

The proper combination of actions must be used to calculate the characteristic crack width value and its value should be less than the allowable value recommended by design codes [56, 156-159]. The maximum crack width limitation recommended by French code NF P 18-710 for R-UHPFRC structures [154] for relevant exposure classes are given in Table 2-4.



Table 2-4: Maximum crack width limit values for R-UHPFRC elements for relevant exposure classes recommended by French code NF P 18-710 [154].

Exposure class	Reinforced UHPFRC element and prestressed UHPFRC elements with unbonded tendons	UHPFRC prestressed elements with bonded tendons
	Quasi-permanent load combination	Frequent load combination
X0, XC1	0.3	0.2
XC2, XC3, XC4	0.2	0.1
XD1, XD2, XD3, XS1, XS2, XS3	0.1	Tensile stress limitation: $\min : - \left( f_{cm,el}, \frac{f_{ctfm}}{K_{global}} \right)$
$f_{cm,el}$ : mean value of the tensile limit of elasticity $f_{ctfm}$ : mean value of the post-cracking strength $K_{global}$ : orientation factor associated with global effects		

The maximum crack width of the reinforced concrete structures, on the other hand, is not easy to predict and has been much debated over the past decades and for that, a large variety of solutions had been proposed, as indicated in references [160-168].

Four different categories for crack width calculation approaches can be considered based on summarization done by Borosnyói and Balász [169]:

- Calculating the crack width by using an analytical approach based on differential equation solution of bond-slip.
- A semi-analytical approach for calculating the average crack width ( $w_m$ ) as the product of the mean crack spacing ( $s_{rm}$ ), and the difference between the mean strain in the reinforcement ( $\varepsilon_{sm}$ ) and the mean strain in the concrete between cracks ( $\varepsilon_{cm}$ ).

With this approach, the characteristic crack width value ( $w_k$ ) is obtained by multiplying the average crack width ( $w_m$ ) to factor ( $\beta$ ), which is a coefficient relating the average crack width value to the characteristics value, as shown by the following expression:

$$w_k = \beta \cdot w_m = \beta \cdot s_{rm} \cdot (\varepsilon_{sm} - \varepsilon_{cm}) \quad (2-88)$$

The Spanish design code for conventional concrete structures (EHE-08) [170] use a value of ( $\beta = 1.3$ ) for indirect actions and ( $\beta = 1.7$ ) for other circumstances;

however, generally, based on literature [12, 170-173], the value of the ( $\beta = 1.3$  to  $2.0$ ) is recommended. Other design codes, such as CEB-FIP Model code 2010 [56], Eurocode 2 [153], and French code NF P 18-710 [154], do not explicitly use this approach. The characteristics value of crack width is calculated directly by considering the maximum crack spacing and difference of average tensile strain of concrete and reinforcement strain as described in chapter 6.

Considering Equation (2-88), the coefficient ( $\beta$ ) can be defined as a ratio of the characteristic to average crack width values, as follows:

$$\beta = \frac{w_k}{w_m} \tag{2-89}$$

Borosnyói and Balász [169] calculated the ( $\beta$ ) value for rectangular reinforced concrete with reinforcement ratio of 0.5% to 2.5% and compressive strength from 30 to 50 N/mm<sup>2</sup> by using the recommended equation provided in MC90 [174] and they demonstrate that ( $\beta$ ) is independent of concrete strength and reinforcement ratio and its value is constant ( $\beta = 1.5$ ), as shown in Figure 2-62.

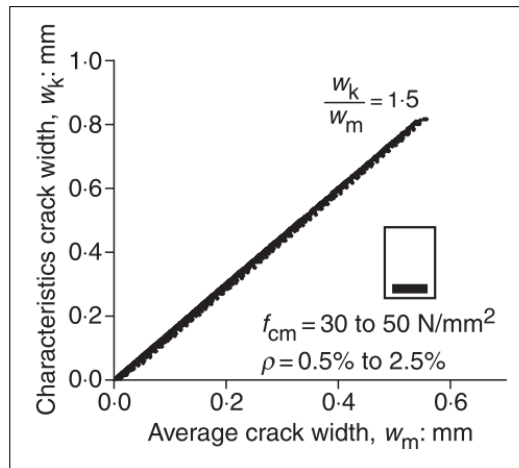


Figure 2-62: beta value for rectangular concrete reinforcement section calculated according to MC90 [169].

- (c) An empirical relation based on fitting a large number of experimental data.
- (d) A numerical model, such as FEM models, fracture mechanics models or damage models.

As mentioned in sections 2.3 and 2.4.5, if steel fibres are induced in the concrete matrix, the crack width calculation can be similar to the normal reinforcement concrete and the general equation for calculating the characteristic crack width

( $w_r = s_{rm}(\varepsilon_{sm} - \varepsilon_{cm})$ ) can be used by considering that the tensile stress in the crack section is not zero [56]. However, in the RILEM TC 162-TDF recommendation for test and design for steel fibre reinforced concrete [175] used Equation (2-88) for calculation the characteristic crack width value (called design crack width) by using the of ( $\beta$ ):

=1.7 for load induced cracking and for restrained cracking in sections with a minimum dimension in excess of 800 mm.

=1.3 for restrained racking in section with a minimum depth, breadth or thickness of 300 mm or below.

For R-UHPFRC, a well-established model was proposed by Leutbecher, T. [108]. This model is completely explained in section 2.4.5.

## 2.7. Serviceability requirements for R-UHPFRC

Serviceability design and analysis is an essential aspect of the design process for concrete structures, particularly when the intention is to reflect the behaviour of the structure in use. It is recognized that crack width and deformation for concrete structural elements must be kept to reasonable limits. Both excessive cracking and deformation can have a negative impact on the performance of the structure in SLS.

The serviceability specifications and requirements provided by design codes must be as simple as possible and also transparent [162]. These specifications should be implemented to concrete structures in order to guarantee their functioning and structural integrity under service conditions. The process for verification of the concrete structures for SLS must be easy to apply for designers. Simple rules mean indirect control of cracking or deflections without calculations.

The serviceability check for concrete structures is often controlled by limiting stresses in the material, crack width and crack spacing restriction, vibration limit of the structure elements, and restraining of deflections (long term or short term). Simple rules (indirect control) are needed to control the cracks or deflection; for example, the crack controlling under service conditions may include the restraining of stresses and selection of maximum reinforcement diameter or maximum reinforcement spacing and the indirect deflection control normally is done by limiting the span-to-depth ratio. Therefore, concrete design codes provide serviceability design requirements with or without calculation. Table 2-5 indicate the related sections for cracking and deflection control for serviceability design for conventional concrete structures provided in ModelCode 2010 [56].

Table 2- 5: Cracking and deflection control, with or without calculations [162].

SLS	Type of control	Method	Section in MC2010
Cracking	Indirect crack control	Limitation of stresses	7.6.3
		Selection of max. rebar $\emptyset$	7.6.4.6
		Selection of max. rebar spacing	7.6.4.6
	Detailed crack control	Calculation of design crack width ( $w_d$ )	7.6.4.3
Deflection	Indirect deflection control	Limitation of L/d	7.6.5.2.4
	Detailed deflection control	Simplified method	7.6.5.2.2
		Integration of curvatures, General method	7.6.5.2.1

For UHPFRC structures as well as conventional concrete structures, the SLS requirements must be applied to guarantee their functionality and structural integrity. The same requirements such as stress control, crack width and spacing limitation, vibration and deflection must be applied for UHPFRC structural elements. The tensile and compressive stress levels in reinforcements and the UHPFRC matrix should be controlled under service loads. The compressive stress limitations under SLS loads are provided by design codes to avoid excessive compression, which produces irreversible strains and longitudinal cracks (parallel with the compressive strains) and excessive creep deformations. The French code NF P 18-710 [154] specifications for UHPFRC elements for limiting the compressive stress in the UHPFRC matrix is resemble the RC and FRC elements specifications provided by Eurocode 2 [153], and compressive stress limitation is a value of  $(0.6f_{ck})$ , where  $(f_{ck})$  is the compressive concrete strength. In comparison, the Japanese UHPFRC design recommendations [143] takes a more cautious value of  $(0.4f_{ck})$  under permanent loads. The Korean design guideline for UHPFRC [144] takes the same value limitation as Eurocode 2 [153]  $(0.6f_{ck})$  for compressive stress caused by bending moment and axial force.

With respect to stress limitation for reinforcements, the tensile stresses are limited with an appropriate safety margin to be set below the yielding strength to prevent uncontrolled, large, permanently open cracks due to inelastic deformations of steel bars. [153]. Inelastic reinforcing deformation should be avoided under serviceability conditions to avoid large and permanent cracks.

ModelCode 2010 [56] specifies that tensile rebar stress not exceed  $(0.8f_{yk})$  for RC and FRC structural elements, and French code NF P 18-710 [154] specifies the same tensile stress restriction requirement for UHPFRC elements. According to Japanese UHPFRC design recommendations [143], steel reinforcement behaviour should be elastic under compression and perfectly elastoplastic under

tensile stress with the limited value of characteristic tensile strength ( $f_{yk}$ ). The Korean design guideline for UHPFRC [144] recommends the same limit value ( $f_{yk}$ ) for the tensile stress of the steel reinforcement under bending moment or axial force.

In terms of concrete stress verification, the post-cracking behaviour under uniaxial tensile stress (strain-hardening or strain-softening behaviour) is used to verify concrete stress in the SLS for UHPFRC. For example, for SLS designing, the French code NF P 18–710 [154] uses the post-cracking strength determined from experimental curves in accordance with standard NF P18-470 [83] ; as stated in section 2.4.2, the French code NF P 18–710 [154] classified the UHPFRC in three categories of T1, T2, and T2 depending on their post-cracking behaviour. The Swiss standard fprSIA 2052 [85] restricts the maximum tensile concrete stress for SLS verification up to 90% of the characteristic elastic tensile strength value for UHPFRC with strain-hardening tensile behaviour and up to 70% for UHPFRC with tension-softening behaviour.

The Korean design guideline for UHPFRC [144] indicates that for examining the serviceability, the tensile stress caused by bending moment, shear force, torsional moment and axial force shall not exceed the design tensile strength ( $f_{td}$ ). The design tensile strength is determined by multiplying the characteristic tensile strength by the material reduction factor, including the influence of the steel fibre orientation effect. It is possible that the orientation of the steel fibres of the cast prism specimens to determine the post-cracking law and the actual orientation of fibres in the constructed structures be different. The French UHPFRC Recommendation of AFGC-SETRA [84] uses a fibre orientation factor ( $k_f$ ) to consider this difference. The factor ( $k_f$ ) only applies to the post-cracking part of the tensile law, as shown in Figure 2-63.

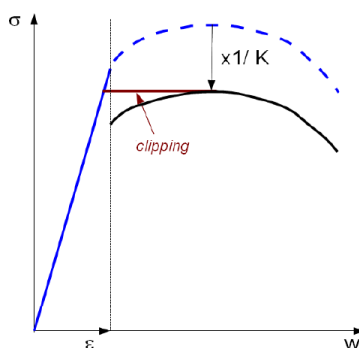


Figure 2-63: 1/k factor applied to the post-cracking characteristic tensile law obtained on cast specimens.

It should be noted that the tensile stresses induced by the shrinkage of the

UHPFRC must be considered for examinations of the tensile stresses for SLS.

#### References

- [1] A. Sokolov et al., "Experimental investigation of tension stiffening in RC ties," *Advances in Materials Science and Engineering*, vol. 2016, 2016.
- [2] L. Á. O. Júnior, D. de Lima Araújo, R. D. Toledo Filho, E. M. R. Fairbairn, and M. A. S. Andrade, "< b> Tension stiffening of steel-fiber-reinforced concrete," *Acta Scientiarum. Technology*, vol. 38, no. 4, pp. 455-463, 2016.
- [3] M. H. Q. Wu, "Tension stiffening in reinforced concrete: instantaneous and time-dependent behaviour," University of New South Wales, Sydney, 2010.
- [4] G. Tiberti, F. Minelli, G. A. Plizzari, and F. J. Vecchio, "Influence of concrete strength on crack development in SFRC members," *Cement and Concrete composites*, vol. 45, pp. 176-185, 2014.
- [5] P. Bernardi, E. Michelini, F. Minelli, A. Sirico, and G. Tiberti, "Non-linear analyses and cracking process of FRC tension ties," *Proceedings of computational modelling of concrete structures (EURO-C 2014)*. CRC Press/Balkema, Leiden, pp. 883-892, 2014.
- [6] S.-B. Kang, K. H. Tan, X.-H. Zhou, and B. Yang, "Influence of reinforcement ratio on tension stiffening of reinforced engineered cementitious composites," *Engineering Structures*, vol. 141, pp. 251-262, 2017.
- [7] K. Fields and P. H. Bischoff, "Tension stiffening and cracking of high-strength reinforced concrete tension members," *Structural Journal*, vol. 101, no. 4, pp. 447-456, 2004.
- [8] A. Rimkus, R. Jakstaite, R. Kupliauskas, L. Torres, and V. Gribniak, "Experimental identification of cracking parameters of concrete ties with different reinforcement and testing layouts," *Procedia Engineering*, vol. 172, pp. 930-936, 2017.
- [9] R. Sahamitmongkol and T. Kishi, "Tension stiffening effect and bonding characteristics of chemically prestressed concrete under tension," *Materials and structures*, vol. 44, no. 2, pp. 455-474, 2011.
- [10] M. Qiu, Y. Zhang, S. Qu, Y. Zhu, and X. Shao, "Effect of reinforcement ratio, fiber orientation, and fiber chemical treatment on the direct tension behavior of rebar-reinforced UHPC," *Construction and Building Materials*, vol. 256, p. 119311, 2020.
- [11] P. Aghdasi and C. P. Ostertag, "Tensile fracture characteristics of Green Ultra-High Performance Fiber-Reinforced Concrete (G-UHP-FRC) with longitudinal steel reinforcement," *Cement and Concrete Composites*, vol. 114, p. 103749, 2020.

- [12] B. B. Broms and L. A. Lutz, "Effects of arrangement of reinforcement on crack width and spacing of reinforced concrete members," in *Journal Proceedings*, 1965, vol. 62, no. 11, pp. 1395-1410.
- [13] R. Jakubovskis, G. Kaklauskas, V. Gribniak, A. Weber, and M. Juknys, "Serviceability analysis of concrete beams with different arrangements of GFRP bars in the tensile zone," *Journal of Composites for Construction*, vol. 18, no. 5, p. 04014005, 2014.
- [14] A. Pérez Caldentey, H. Corres Peiretti, J. Peset Iribarren, and A. Giraldo Soto, "Cracking of RC members revisited: influence of cover,  $\phi/ps$ ,  $e_f$  and stirrup spacing—an experimental and theoretical study," *Structural Concrete*, vol. 14, no. 1, pp. 69-78, 2013.
- [15] A. Rimkus and A. Vilėniškytė, "An experimental study of the influence of reinforcement bar arrangement on deformation behaviour and cracking of reinforced concrete members," in *Proc. of the 18th Conference for Junior Researchers „Science–Future of Lithuania “*, Vilnius, Lithuania, 2015, pp. 1-4.
- [16] V. Gribniak, R. Jakubovskis, A. Rimkus, P.-L. Ng, and D. Hui, "Experimental and numerical analysis of strain gradient in tensile concrete prisms reinforced with multiple bars," *Construction and Building Materials*, vol. 187, pp. 572-583, 2018.
- [17] S.-B. Kang, K. H. Tan, X.-H. Zhou, and B. J. E. S. Yang, "Influence of reinforcement ratio on tension stiffening of reinforced engineered cementitious composites," vol. 141, pp. 251-262, 2017.
- [18] A. Amin, S. J. Foster, and M. J. M. o. C. R. Watts, "Modelling the tension stiffening effect in SFR-RC," vol. 68, no. 7, pp. 339-352, 2016.
- [19] F. Ceroni, M. Pecce, and S. J. J. o. C. f. C. Matthys, "Tension stiffening of reinforced concrete ties strengthened with externally bonded fiber-reinforced polymer sheets," vol. 8, no. 1, pp. 22-32, 2004.
- [20] H.-R. Kim, W.-C. Choi, S.-C. Yoon, T. J. I. J. o. C. S. Noguchi, and Materials, "Evaluation of bond properties of reinforced concrete with corroded reinforcement by uniaxial tension testing," vol. 10, no. 3, pp. 43-52, 2016.
- [21] A. Borosnyói and I. Snóbli, "Crack width variation within the concrete cover of reinforced concrete members," *Építőanyag*, vol. 62, no. 3, pp. 70-74, 2010.
- [22] R. H. Scott and A. W. Beeby, "Long-term tension-stiffening effects in concrete," *ACI Structural Journal*, vol. 102, no. 1, p. 31, 2005.
- [23] H. Wu and R. Gilbert, "An experimental study of tension stiffening in reinforced concrete members under short-term and long-term loads," UNICIV Report no, 2008.
- [24] C.-C. Hung, H.-S. Lee, and S. N. Chan, "Tension-stiffening effect in steel-reinforced UHPC composites: constitutive model and effects of steel

- fibers, loading patterns, and rebar sizes," *Composites Part B: Engineering*, vol. 158, pp. 269-278, 2019.
- [25] I. Vilanova, L. Torres, M. Baena, G. Kaklauskas, and V. Gribniak, "Experimental study of tension stiffening in GFRP RC tensile members under sustained load," *Engineering structures*, vol. 79, pp. 390-400, 2014.
- [26] P. Marchand et al., "Bond behaviour of reinforcing bars in UHPFRC," *Materials and structures*, vol. 49, no. 5, pp. 1979-1995, 2016.
- [27] A. Khadour et al., "Distributed strain monitoring of reinforcement bars using optical fibers for SHM," in *CONSEC13-7th International Conference on Concrete under Severe Conditions-Environment and Loading*, 2013.
- [28] A. Michou, A. Hilaire, F. Benboudjema, G. Nahas, P. Wyniecki, and Y. Berthaud, "Reinforcement-concrete bond behavior: Experimentation in drying conditions and meso-scale modeling," *Engineering Structures*, vol. 101, pp. 570-582, 2015.
- [29] M. Quiertant et al., "Deformation monitoring of reinforcement bars with a distributed fiber optic sensor for the SHM of reinforced concrete structures," in *NDE*, 2012, p. 10p.
- [30] E. Marfisi, C. Burgoyne, M. Amin, and L. J. M. o. c. r. Hall, "The use of MRI to observe the structure of concrete," vol. 57, no. 2, pp. 101-109, 2005.
- [31] E. Marfisi, C. Burgoyne, M. Amin, and L. J. M. o. C. R. Hall, "Observation of flexural cracks in loaded concrete beams using MRI," vol. 57, no. 4, pp. 225-234, 2005.
- [32] Y. Cheng, P. C. Hagan, R. Mitra, and S. J. A. M. J. Wang, "Defects Visualization Using Acoustic Emission Tomography Technique," vol. 112, no. 6, 2015.
- [33] A. du Plessis, W. P. J. C. Boshoff, and B. Materials, "A review of X-ray computed tomography of concrete and asphalt construction materials," vol. 199, pp. 637-651, 2019.
- [34] K. F. Liu, "Detection of defect in concrete using elastic wave tomography reconstruction technique/Liu Kit Fook," *University of Malaya*, 2017.
- [35] M. P. Collins and D. Mitchell, *Prestressed concrete structures*. Prentice Hall Englewood Cliffs, NJ, 1991.
- [36] V. Gribniak, H. A. Mang, R. Kupliauskas, and G. Kaklauskas, "Stochastic Tension-Stiffening Approach for the Solution of Serviceability Problems in Reinforced Concrete: Constitutive Modeling," *Computer-Aided Civil and Infrastructure Engineering*, vol. 30, no. 9, pp. 684-702, 2015.
- [37] A. Scanlon and D. W. Murray, "Time-dependent reinforced concrete slab deflections," *Journal of the Structural Division*, vol. 100, no. Proc. Paper 10833, 1974.
- [38] C.-S. Lin and A. C. Scordelis, "Nonlinear analysis of RC shells of general



- form," *Journal of the Structural Division*, vol. 101, no. 3, pp. 523-538, 1975.
- [39] R. I. Gilbert and R. F. Warner, "Tension stiffening in reinforced concrete slabs," *Journal of the structural division*, vol. 104, no. 12, pp. 1885-1900, 1978.
- [40] F. J. Vecchio and M. P. Collins, "The modified compression-field theory for reinforced concrete elements subjected to shear," *ACI J.*, vol. 83, no. 2, pp. 219-231, 1986.
- [41] X.-B. D. Pang and T. T. Hsu, "Behavior of reinforced concrete membrane elements in shear," *Structural Journal*, vol. 92, no. 6, pp. 665-679, 1995.
- [42] S. Tamai and H. Shima, "Average stress-strain relationship in post yield range of steel bar in concrete," *Concrete Lib. JSCE*, no. 11, pp. 117-129, 1988.
- [43] T. T. Hsu, *Unified theory of reinforced concrete*. Routledge, 2017.
- [44] R. Saliger, "High grade steel in reinforced concrete," in *Preliminary Publication, 2nd Congress of IABSE*. Berlin-Munich: IABSE Publications, 1936, pp. 293-315.
- [45] S. Somayaji and S. Shah, "Bond stress versus slip relationship and cracking response of tension members," in *Journal Proceedings*, 1981, vol. 78, no. 3, pp. 217-225.
- [46] H. Chan, Y. Cheung, and Y. Huang, "Crack analysis of reinforced concrete tension members," *Journal of Structural Engineering*, vol. 118, no. 8, pp. 2118-2132, 1992.
- [47] A. H. Nilson, "Nonlinear analysis of reinforced concrete by the finite element method," in *Journal Proceedings*, 1968, vol. 65, no. 9, pp. 757-766.
- [48] A. H. Nilson, *Bond stress-slip relations in reinforced concrete*. Research Report No. 345. Ithaca, N.Y., 1971.
- [49] A. K. Gupta and S. R. Maestrini, "Tension-stiffness model for reinforced concrete bars," *Journal of Structural Engineering*, vol. 116, no. 3, pp. 769-790, 1990.
- [50] R. S. Stramandinoli and H. L. La Rovere, "An efficient tension-stiffening model for nonlinear analysis of reinforced concrete members," *Engineering Structures*, vol. 30, no. 7, pp. 2069-2080, 2008.
- [51] CEB, "Design Manual Cracking and Deformations ", B. d. i. N. 158, Ed., ed. Paris, 1984.
- [52] A. I. Johnson, "Deformations of reinforced concrete," *International Association for Bridge and Structural Engineering Publications*, vol. 11, pp. 253-290, 1951.
- [53] P. H. Bischoff, "Effects of shrinkage on tension stiffening and cracking in reinforced concrete," *Canadian Journal of Civil Engineering*, vol. 28, no. 3, pp. 363-374, 2001.

- [54] L.-Y. Xu, X. Nie, and M.-X. Tao, "Rational modeling for cracking behavior of RC slabs in composite beams subjected to a hogging moment," *Construction and Building Materials*, vol. 192, pp. 357-365, 2018.
- [55] F. Rostásy, R. Koch, F. Leonhardt, and M. Patzak, *Zur Mindestbewehrung für Zwang von Außenwänden aus Stahlleichtbeton: (Minimum Reinforcement for Restrained External Lightweight Reinforced Concrete Walls)*. Ernst & Sohn, Berlin, Heft 267, 83 pp., 1976, p. 83pp.
- [56] *Model Code 2010-First complete draft-Volume 2: Model Code*, 2883940967, 2010.
- [57] L. Hwang and S. Rizkalla, "Effective tensile stress-strain characteristics for reinforced concrete," *Proceedings of the Canadian Society of Civil Engineering*, pp. 129-147, 1983.
- [58] J. Romualdi and G. Batson, "Mechanics of crack arrest in concrete beam with closely spaced reinforcement," *J. Am. Inst.*, vol. 60, pp. 775-789, 1963.
- [59] J. P. Romualdi and J. A. Mandel, "Tensile strength of concrete affected by uniformly distributed and closely spaced short lengths of wire reinforcement," in *Journal Proceedings*, 1964, vol. 61, no. 6, pp. 657-672.
- [60] M. Di Prisco, G. Plizzari, and L. Vandewalle, "Fibre reinforced concrete: new design perspectives," *Materials and structures*, vol. 42, no. 9, pp. 1261-1281, 2009.
- [61] M. Harajli, B. Hamad, and K. Karam, "Bond-slip response of reinforcing bars embedded in plain and fiber concrete," *Journal of Materials in Civil Engineering*, vol. 14, no. 6, pp. 503-511, 2002.
- [62] S.-C. Lee, J.-Y. Cho, and F. J. Vecchio, "Tension-Stiffening Model for Steel Fiber-Reinforced Concrete Containing Conventional Reinforcement," *ACI Structural Journal*, vol. 110, no. 4, 2013.
- [63] P. H. Bischoff, "Tension stiffening and cracking of steel fiber-reinforced concrete," *Journal of materials in civil engineering*, vol. 15, no. 2, pp. 174-182, 2003.
- [64] A. Amin, S. J. Foster, and M. Watts, "Modelling the tension stiffening effect in SFR-RC," *Magazine of Concrete Research*, vol. 68, no. 7, pp. 339-352, 2015.
- [65] H. H. Abrishami and D. Mitchell, "Influence of steel fibers on tension stiffening," *Structural Journal*, vol. 94, no. 6, pp. 769-776, 1997.
- [66] P. Serna et al., "Upgrading the concept of UHPFRC for high durability in the cracked state: the concept of Ultra High Durability Concrete (UHDC) in the approach of the h2020 project resilience," in *Sustainable Materials Systems and Structures SMSS 2019*, 2019, vol. 128, pp. 764-771: RILEM Publications SARL.

- [67] K. Wille, A. E. Naaman, and G. J. J. A. m. j. Parra-Montesinos, "Ultra-High Performance Concrete with Compressive Strength Exceeding 150 MPa (22 ksi): A Simpler Way," vol. 108, no. 1, 2011.
- [68] W. Meng and K. H. J. C. P. B. E. Khayat, "Mechanical properties of ultra-high-performance concrete enhanced with graphite nanoplatelets and carbon nanofibers," vol. 107, pp. 113-122, 2016.
- [69] O. M. Abdulkareem, A. B. Fraj, M. Bouasker, A. J. C. Khelidj, and B. Materials, "Mixture design and early age investigations of more sustainable UHPC," vol. 163, pp. 235-246, 2018.
- [70] M. Bajaber, I. J. J. o. M. R. Hakeem, and Technology, "UHPC evolution, development, and utilization in construction: A review," vol. 10, pp. 1058-1074, 2021.
- [71] C. Zanuy and G. S. J. E. S. Ulzurrun, "Bending model for composite UHPFRC-RC elements including tension stiffening and crack width," vol. 209, p. 109958, 2020.
- [72] Z. Zhang, X.-D. Shao, P. J. C. Zhu, and B. Materials, "Direct tensile behaviors of steel-bar reinforced ultra-high performance fiber reinforced concrete: Effects of steel fibers and steel rebars," vol. 243, p. 118054, 2020.
- [73] C. Oesterlee, "Structural response of reinforced UHPFRC and RC composite members," 2010.
- [74] A. E. Naaman, H.-W. J. M. Reinhardt, and structures, "Proposed classification of HPFRC composites based on their tensile response," vol. 39, no. 5, pp. 547-555, 2006.
- [75] K. Wille, S. El-Tawil, A. E. J. C. Naaman, and C. Composites, "Properties of strain hardening ultra high performance fiber reinforced concrete (UHP-FRC) under direct tensile loading," vol. 48, pp. 53-66, 2014.
- [76] A. Naaman, "Strain hardening and deflection hardening fiber reinforced cement composites," in Proc. 4th Int. RILEM Workshop on High Performance Fiber Reinforced Cement Composites, Ann Arbor, University of Michigan, 2003, pp. 95-113.
- [77] H. G. Russell, B. A. Graybeal, and H. G. Russell, "Ultra-high performance concrete: A state-of-the-art report for the bridge community," United States. Federal Highway Administration. Office of Infrastructure ...2013.
- [78] D.-Y. Yoo, Y.-S. J. I. J. o. C. S. Yoon, and Materials, "A review on structural behavior, design, and application of ultra-high-performance fiber-reinforced concrete," vol. 10, no. 2, pp. 125-142, 2016.
- [79] E. C. f. Standardization, "EN 14651 test method for metallic fibered concrete—Measuring the flexural tensile strength (limit of proportionality (LOP), residual)," ed: Belgian standards (NBN) Brussels, Belgium, 2005.
- [80] A. J. S. T. M. f. F. P. o. F.-R. C. A. I. Standard, West Conshohocken, PA,

- "C1609," 2012.
- [81] "UNI 11039-1: Steel Fibre Reinforced Concrete - Definitions, Classification and Designation. National Italian Unification centre, (2003), Italy.."
- [82] "UNI 11039-2: Steel Fibre Reinforced Concrete - Test Method for Determination of First Crack Strength and Ductility Indexes. National Italian Unification centre, (2003), Italy.."
- [83] P. J. A. NF, Paris, "P 18-470: Bétons fibrés à ultra-hautes performances—Spécification, performance, production et conformité," 2016.
- [84] Association Française de Génie Civil (AFGC)/ Service d'études techniques des routes et autoroutes (SETRA), Bétons fibrés à ultra-hautes performances, Recommandations provisoires, Janvier 2002.
- [85] SIA 2052, "Béton fibré ultra-performant (BFUP)-Matériaux, dimensionnement et exécution. Draft," 2016.
- [86] J. Á. López, P. Serna, J. Navarro-Gregori, and E. Camacho, "An inverse analysis method based on deflection to curvature transformation to determine the tensile properties of UHPFRC," *Materials and Structures*, vol. 48, no. 11, pp. 3703-3718, 2015.
- [87] J. A. López Martínez, "Characterisation of The Tensile Behaviour of UHPFRC by Means ff Four-Point Bending Tests," 2017.
- [88] J. Á. López, P. Serna, J. Navarro-Gregori, and H. J. C. P. B. E. Coll, "A simplified five-point inverse analysis method to determine the tensile properties of UHPFRC from unnotched four-point bending tests," vol. 91, pp. 189-204, 2016.
- [89] H. Wu and R. J. E. S. Gilbert, "Modeling short-term tension stiffening in reinforced concrete prisms using a continuum-based finite element model," vol. 31, no. 10, pp. 2380-2391, 2009.
- [90] R. I. Gilbert and H. Q. J. A. J. o. S. E. Wu, "Time-dependent stiffness of cracked reinforced concrete elements under sustained actions," vol. 9, no. 2, pp. 151-158, 2009.
- [91] P. H. J. C. J. o. C. E. Bischoff, "Effects of shrinkage on tension stiffening and cracking in reinforced concrete," vol. 28, no. 3, pp. 363-374, 2001.
- [92] G. Kaklauskas, V. Gribniak, D. Bacinskas, and P. J. E. s. Vainiunas, "Shrinkage influence on tension stiffening in concrete members," vol. 31, no. 6, pp. 1305-1312, 2009.
- [93] G. Fischer and V. C. J. S. J. Li, "Influence of matrix ductility on tension-stiffening behavior of steel reinforced engineered cementitious composites (ECC)," vol. 99, no. 1, pp. 104-111, 2002.
- [94] J. Jungwirth and A. Muttoni, "Structural behavior of tension members in Ultra High Performance Concrete," in *International symposium on ultra high performance concrete*, 2004, no. CONF: International Symposium on Ultra High Performance Concrete.

- [95] P. H. Bischoff and S. P. J. J. o. c. f. c. Gross, "Design approach for calculating deflection of FRP-reinforced concrete," vol. 15, no. 4, pp. 490-499, 2011.
- [96] P. H. Bischoff and S. P. J. J. o. C. f. C. Gross, "Closure to "Design Approach for Calculating Deflection of FRP-Reinforced Concrete" by Peter H. Bischoff and Shawn P. Gross," vol. 17, no. 1, pp. 164-165, 2013.
- [97] D. Redaelli, "Testing of reinforced high performance fibre concrete members in tension," in Proceedings of the 6th Int. Ph. D. Symposium in Civil Engineering, Zurich 2006, 2006, no. CONF, p. 8: Proceedings of the 6th Int. Ph. D. Symposium in Civil Engineering, Zurich 2006.
- [98] T. Leutbecher and E. Fehling, "Structural behaviour of UHPC under tensile stress and biaxial loading," in Proceedings of the International Symposium on Ultra High Performance Concrete, Kassel, Germany, 2004, pp. 435-448.
- [99] D. Redaelli and A. Muttoni, "Tensile behaviour of reinforced ultra-high performance fiber reinforced concrete elements," in fib Symposium, Dubrovnik 2007, 2007, no. CONF, pp. 267-274: fib Symposium, Dubrovnik 2007.
- [100] D. M. Moreno, W. Trono, G. Jen, C. Ostertag, S. L. J. C. Billington, and C. Composites, "Tension stiffening in reinforced high performance fiber reinforced cement-based composites," vol. 50, pp. 36-46, 2014.
- [101] T. Leutbecher and E. J. B. u. S. Fehling, "Rissbildung und Zugtragverhalten von mit Fasern verstärktem Stahlbeton am Beispiel ultrahochfesten Betons: Teil 1: Rissmechanische Zusammenhänge," vol. 104, no. 6, pp. 357-367, 2009.
- [102] L. Lárusson, G. Fischer, and J. Jönsson, "Mechanical interaction between concrete and structural reinforcement in the tension stiffening process," in High Performance Fiber Reinforced Cement Composites 6: Springer, 2012, pp. 247-254.
- [103] C. P. Hollmann, "Tensile Behavior of Ultra-High Performance Fiber Reinforced Concrete and Reinforcement Bar," 2014.
- [104] J. JUNgWIRTH, "Zum tragverhalten von zugbeanspruchten bauteilen aus ultra-hochleistungs-faserbeton," EPFL2006.
- [105] R. Valente, M. Pimentel, and S. Nunes, "Tensile response of reinforced UHPFRC elements."
- [106] P. Marti, M. Alvarez, W. Kaufmann, and V. J. S. E. I. Sigrist, "Tension chord model for structural concrete," vol. 8, no. 4, pp. 287-298, 1998.
- [107] T. Pfyl, Tragverhalten von stahlfaserbeton. vdf Hochschulverlag AG, 2003.
- [108] T. Leutbecher, Rissbildung und Zugtragverhalten von mit Stabstahl und Fasern bewehrtem ultrahochfesten Beton (UHPC). Kassel University Press, 2008.

- [109] T. Leutbecher and E. Fehling, "Design for serviceability of ultra high performance concrete structures," in *High Performance Fiber Reinforced Cement Composites 6*: Springer, 2012, pp. 445-452.
- [110] V. C. Li and C. K. J. J. o. e. m. Leung, "Steady-state and multiple cracking of short random fiber composites," vol. 118, no. 11, pp. 2246-2264, 1992.
- [111] M. Behloul, "Analyse et modélisation du comportement d'un matériau à matrice cimentaire fibrée à ultra hautes performances: bétons de poudres réactives, du matériau à la structure," Cachan, Ecole normale supérieure, 1996.
- [112] M. Behloul, "Les micro-bétons renforcés de fibres: de l'éprouvette aux structures," in *14es rencontres universitaires de génie civil (Clermont Ferrand, 9-10 mai 1996. 1, COS'96: comportement des ouvrages en service. 2, Prix des jeunes chercheurs)*, 1996, pp. 25-32.
- [113] T. Leutbecher and E. J. B.-u. S. Fehling, "Crack Formation and Tensile Behaviour of Concrete Members Reinforced with Rebars and Fibres exemplified by Ultra-High-Performance Concrete Part 1: Crack Mechanical Relationships," vol. 104, no. 6, pp. 357-367, 2009.
- [114] T. Leutbecher and E. J. B.-u. S. Fehling, "Crack Formation and Tensile Behaviour of Concrete Members Reinforced with Rebars and Fibres exemplified by Ultra-High-Performance Concrete Part 2: Experimental Investigations and Examples of Application," vol. 104, no. 7, pp. 406-415, 2009.
- [115] E. Fehling, M. Schmidt, J. Walraven, T. Leutbecher, and S. Fröhlich, *Ultra-high performance concrete UHPC: Fundamentals, design, examples*. John Wiley & Sons, 2015.
- [116] B. EN, "1-1. Eurocode 2: Design of concrete structures–Part 1-1: General rules and rules for buildings," European Committee for Standardization (CEN), 2004.
- [117] M. U. Khan, S. Ahmad, A. A. Naqvi, and H. J. J. P. i. N. E. Al-Gahtani, "Shielding performance of heavy-weight ultra-high-performance concrete against nuclear radiation," vol. 130, p. 103550, 2020.
- [118] D.-Y. Yoo, S. Kim, M.-J. J. C. Kim, and B. Materials, "Comparative shrinkage behavior of ultra-high-performance fiber-reinforced concrete under ambient and heat curing conditions," vol. 162, pp. 406-419, 2018.
- [119] K. Koh, G. Ryu, S. Kang, J. Park, and S. J. A. S. L. Kim, "Shrinkage properties of ultra-high performance concrete (UHPC)," vol. 4, no. 3, pp. 948-952, 2011.
- [120] T. Xie, C. Fang, M. M. Ali, P. J. C. Visintin, and C. Composites, "Characterizations of autogenous and drying shrinkage of ultra-high performance concrete (UHPC): An experimental study," vol. 91, pp. 156-173, 2018.
- [121] L. Wu, N. Farzadnia, C. Shi, Z. Zhang, H. J. C. Wang, and B. Materials,

- "Autogenous shrinkage of high performance concrete: A review," vol. 149, pp. 62-75, 2017.
- [122] C. Fang, M. Ali, T. Xie, P. Visintin, A. H. J. C. Sheikh, and B. Materials, "The influence of steel fibre properties on the shrinkage of ultra-high performance fibre reinforced concrete," vol. 242, p. 117993, 2020.
- [123] J. Zhang and V. C. J. J. o. e. m. Li, "Influences of fibers on drying shrinkage of fiber-reinforced cementitious composite," vol. 127, no. 1, pp. 37-44, 2001.
- [124] D.-Y. Yoo, H.-O. Shin, J.-M. Yang, and Y.-S. J. C. P. B. E. Yoon, "Material and bond properties of ultra high performance fiber reinforced concrete with micro steel fibers," vol. 58, pp. 122-133, 2014.
- [125] M. Şahmaran, M. Lachemi, K. M. Hossain, V. C. J. C. Li, and c. research, "Internal curing of engineered cementitious composites for prevention of early age autogenous shrinkage cracking," vol. 39, no. 10, pp. 893-901, 2009.
- [126] M. Sahmaran, M. Lachemi, K. M. Hossain, R. Ranade, and V. C. J. A. M. J. Li, "Influence of aggregate type and size on ductility and mechanical properties of engineered cementitious composites," vol. 106, no. 3, p. 308, 2009.
- [127] M. Şahmaran et al., "High-early-strength ductile cementitious composites with characteristics of low early-age shrinkage for repair of infrastructures," vol. 48, no. 5, pp. 1389-1403, 2015.
- [128] D.-Y. Yoo, J.-J. Park, S.-W. Kim, Y.-S. J. M. Yoon, and structures, "Influence of ring size on the restrained shrinkage behavior of ultra high performance fiber reinforced concrete," vol. 47, no. 7, pp. 1161-1174, 2014.
- [129] D.-Y. Yoo, M.-J. Kim, S. Kim, G.-S. Ryu, K.-T. J. C. Koh, and B. Materials, "Effects of mix proportion and curing condition on shrinkage behavior of HPRFRCs with silica fume and blast furnace slag," vol. 166, pp. 241-256, 2018.
- [130] D.-Y. Yoo, N. Banthia, and Y.-S. J. K. J. o. C. E. Yoon, "Geometrical and boundary condition effects on restrained shrinkage behavior of UHPFRC slabs," vol. 22, no. 1, pp. 185-195, 2018.
- [131] M. M. U. J. C. Islam and B. Materials, "Investigation of long-term tension stiffening mechanism for ultra-high-performance fiber reinforced concrete (UHPFRC)," vol. 321, p. 126310, 2022.
- [132] M. M. U. J. C. Islam and B. Materials, "Investigation of tensile creep for Ultra-High-Performance Fiber Reinforced Concrete (UHPFRC) for the long-term," vol. 305, p. 124752, 2021.
- [133] "ASTM C512 / C512M-15, Standard Test Method for Creep of Concrete in Compression, ASTM International, West Conshohocken, PA, www.astm.org, 2015."

- [134] C. Androuët and J.-P. J. M. Charron, "Shrinkage Mitigation of an Ultra-High Performance Concrete Submitted to Various Mixing and Curing Conditions," vol. 14, no. 14, p. 3982, 2021.
- [135] W. Meng and K. H. J. J. o. M. i. C. E. Khayat, "Effect of hybrid fibers on fresh properties, mechanical properties, and autogenous shrinkage of cost-effective UHPC," vol. 30, no. 4, p. 04018030, 2018.
- [136] Ç. Yalçinkaya, H. J. C. Yazıcı, and B. Materials, "Effects of ambient temperature and relative humidity on early-age shrinkage of UHPC with high-volume mineral admixtures," vol. 144, pp. 252-259, 2017.
- [137] D.-Y. Yoo, N. Banthia, Y.-S. J. C. Yoon, and C. Composites, "Effectiveness of shrinkage-reducing admixture in reducing autogenous shrinkage stress of ultra-high-performance fiber-reinforced concrete," vol. 64, pp. 27-36, 2015.
- [138] D.-Y. Yoo, K.-H. Min, J.-H. Lee, Y.-S. J. C. Yoon, and B. Materials, "Shrinkage and cracking of restrained ultra-high-performance fiber-reinforced concrete slabs at early age," vol. 73, pp. 357-365, 2014.
- [139] S. AFGC, "Bétons fibrés à ultra-hautes performances—Recommandations," AFGC, France, 2013.
- [140] "Association Francaise de Normalisation. (2016a). "Concrete-Ultra-high performance fibre- reinforced concrete-specifications, performance, production and conformity." NFP 18 470 : 2016."
- [141] "Association Francaise de Normalisation. (2016b). "National addition to Eurocode 2- Design of concrete structures: specific rules for ultra-high performance fibre-reinforced concrete (UHPFRC)." NFP 18 710 : 2016.."
- [142] U. J. D. A. f. S. G. A. f. R. C. DAfStB, Berlin, Germany, draft, "State-of-the-art report on ultra high performance concrete—Concrete technology and design," vol. 3, 2003.
- [143] J. C. Committee, "Recommendations for design and construction of high performance fiber reinforced cement composites with multiple fine cracks," Japan Society of Civil Engineers, Tokyo, Japan, 2008.
- [144] F. KCI, "Design Guidelines for K-UHPC," ed: Korea Concrete Institute Seoul, Korea, 2014.
- [145] KCI-M-12-003, "Design recommendations for ultra-high performance concrete K-UHPC," ed: Korea Concrete Institute Seoul, 2012.
- [146] N. Gowripalan and R. J. R. A. Gilbert, The University of NSW, "Design guidelines for ductal prestressed concrete beams," 2000.
- [147] "C157, A. (2006). "Standard test method for length change of hardened hydraulic-cement mortar and concrete." annual book of ASTM standards, 4, 96–101.."
- [148] B. A. Graybeal, "Material property characterization of ultra-high performance concrete," United States. Federal Highway Administration. Office of Infrastructure ...2006.



- [149] J. Grosjean, "Effect of shrinkage on the ultimate behaviour of UHPFRC-strengthened reinforced concrete members," 2017.
- [150] V. Gribniak, G. Kaklauskas, D. J. T. B. J. o. R. Bacinskas, and B. Engineering, "State-of-art review of shrinkage effect on cracking and deformations of concrete bridge elements," vol. 2, no. 4, pp. 183-193, 2007.
- [151] A. Boschmann Käthler, U. M. Angst, M. Wagner, C. K. Larsen, and B. Elsener, "Effect of cracks on chlorideinduced corrosion of steel in concrete-a review: Etatsprogrammet Varige konstruksjoner 2012-2015," 2017.
- [152] N. El-Joukhadar and S. Pantazopoulou, "Effectiveness of UHPFRC cover in delaying bar corrosion," *Construction and Building Materials*, vol. 269, p. 121288, 2021.
- [153] Eurocode2:, *Design of concrete structures: Part 1-1: General rules and rules for buildings*. British Standards Institution, 2004.
- [154] P. J. A. NF, Paris, "NF P 18-710, Complément national à l'Eurocode 2 — Calcul des structures en béton : règles spécifiques pour les Bétons Fibrés à Ultra-Hautes Performances (BFUP)."
- [155] B. S. J. B. S. I. EN, "206-1 Concrete-Part 1: Specification, performance, production and conformity," 2000.
- [156] A. C. I. Committee, I. American Concrete, A. C. I. Committee, and A. C. I. Committee, *Building code requirements for structural concrete (ACI 318-19) : an ACI standard ; Commentary on building code requirements for structural concrete (ACI 318R-19)*. 2019.
- [157] D. Sunaga, K. Namiki, and T. Kanakubo, "Crack width evaluation of fiber-reinforced cementitious composite considering interaction between deformed steel rebar," *Construction and Building Materials*, vol. 261, p. 119968, 2020.
- [158] M. Basteskår, M. Engen, T. Kanstad, and K. T. J. S. C. Fosså, "A review of literature and code requirements for the crack width limitations for design of concrete structures in serviceability limit states," vol. 20, no. 2, pp. 678-688, 2019.
- [159] A. J. S. P. Beeby, "Crack control provisions in the new eurocode for the design of concrete structures," vol. 204, pp. 57-84, 2001.
- [160] H. Lin et al., "State-of-the-art review on the bond properties of corroded reinforcing steel bar," vol. 213, pp. 216-233, 2019.
- [161] I. J. E. J. o. S. E. Gilbert, "Shrinkage, cracking and deflection-the serviceability of concrete structures," vol. 1, no. 1, pp. 15-37, 2001.
- [162] G. L. Balázs et al., "Design for SLS according to fib Model Code 2010," vol. 14, no. 2, pp. 99-123, 2013.
- [163] I. Löfgren, "Calculation of crack width and crack spacing," in *Nordic Mini Seminar: Fibre reinforced concrete*, Trondheim, Norway, 2007, pp.

- 1-12.
- [164] R. R. Zhu, W. Wanichakorn, T. T. Hsu, and J. J. S. J. Vogel, "Crack width prediction using compatibility-aided strut-and-tie model," vol. 100, no. 4, pp. 413-421, 2003.
  - [165] G. Creazza, S. J. M. Russo, and structures, "A new model for predicting crack width with different percentages of reinforcement and concrete strength classes," vol. 32, no. 7, pp. 520-524, 1999.
  - [166] C.-Q. Li and S. J. J. o. e. m. Yang, "Prediction of concrete crack width under combined reinforcement corrosion and applied load," vol. 137, no. 11, pp. 722-731, 2011.
  - [167] S. Yang, K. Li, C. Q. J. C. Li, and Structures, "Numerical determination of concrete crack width for corrosion-affected concrete structures," vol. 207, pp. 75-82, 2018.
  - [168] N. Dawood and H. J. C. J. o. C. E. Marzouk, "Crack width model for thick reinforced concrete plates subjected to in-plane forces," vol. 38, no. 11, pp. 1262-1273, 2011.
  - [169] A. Borosnyói and G. L. Balázs, "Models for flexural cracking in concrete: the state of the art," *Structural Concrete*, vol. 6, no. 2, pp. 53-62, 2005.
  - [170] "Instrucción de Hormigón Estructural EHE-08." Comisión Permanente Del Hormigón. Ministerio De Fomento, 2008.
  - [171] A. S. G. Bruggeling, *Structural concrete: theory and its application*. 1991.
  - [172] S. Rizkalla and L. Hwang, "Crack prediction for members in uniaxial tension," in *Journal Proceedings*, 1984, vol. 81, no. 6, pp. 572-579.
  - [173] CNR-DT 203. (2006). *Guide for the Design and Construction of Concrete Structures Reinforced with Fiber-Reinforced Polymer Bars.* Advisory Committee on Technical Recommendations for Construction.
  - [174] M. CEB-FIP, "90, Design of concrete structures. CEB-FIP Model Code 1990," British Standard Institution, London, 1993.
  - [175] L. Vandewalle et al., "Rilem TC 162-TDF: Test and design methods for steel fibre reinforced concrete: Uni-axial tension test for steel fibre reinforced concrete," vol. 34, no. 235, pp. 3-6, 2001.

## ***Chapter 3. Uniaxial tensile test methods for reinforcement concrete elements***

A novel uniaxial tensile test methodology for the characterisation of the tensile R-UHPFRC elements under service loads were designed. This chapter contain the two published papers (1<sup>st</sup> and 2<sup>nd</sup> papers) given a summary of the proposed uniaxial tensile test methods for reinforced UHPFRC elements and test procedure for serviceability studying of R-UHPFRC tensile elements. Preliminary experimental studies were conducted to evaluate the proposed test method.

**1<sup>st</sup> PAPER**

Details:

---

Type of paper	Conference paper
Title	<i>A testing method for studying the serviceability behavior of reinforced UHPFRC tensile ties</i>
Authors	<u>Majid Khorami</u> Juan Navarro-Gregori Pedro Serna Ros Miguel Ángel Navarro-Laguarda
Congress	<i>IOP Conference Series: Materials Science and Engineering</i>
Date	17 <sup>th</sup> -20 <sup>th</sup> September, 2019
City	Prague (Czech Republic)
Status	Accepted and presented
Full reference	Khorami, M., et al. (2019). A testing method for studying the serviceability behavior of reinforced UHPFRC tensile ties. IOP Conference Series: Materials Science and Engineering, IOP Publishing.

---

**1<sup>st</sup> Paper. A testing method for studying the serviceability behavior of reinforced UHPFRC tensile ties**

M. Khorami<sup>1,2</sup>, J. Navarro-Gregori<sup>1</sup>, P. Serna<sup>1</sup>, M.A . Navarro-Laguarda<sup>1</sup>

J. Navarro-Gregori, [juanagre@cst.upv.es](mailto:juanagre@cst.upv.es)

<sup>1</sup>: Institute of Science and Concrete Technology, ICITECH, Universitat Politècnica de València, València, 46022, Spain.

<sup>2</sup>: Universidad UTE, Facultad de Arquitectura y Urbanismo, Calle Rumipamba s/n y Bourgeois, Quito, Ecuador

**Abstract**

Structural control under the serviceability limit state is a requirement of design codes to ensure the durability of structural elements. As it is possible to consider fibers to be reinforcement in concrete, UHPFRC can be used to guarantee properly distributing cracks and limiting crack width in the serviceability limit state. This research presents an experimental testing method for direct tensile tests on UHPFRC specimens. The results obtained from the proposed method, such as the specimen's average tensile stress-strain curve, tensile stress in concrete, number and width of cracks, can be used to consider the behavior and design requirements of UHPFRC under serviceability conditions.

**Keywords:** reinforced concrete, composite beam, horizontal shear, shear strength, interface roughness.

**1. Introduction**

Ultra high-performance fiber-reinforced concrete (UHPFRC) is a material with high compression stress, and great ductility and toughness due to the inclusion of steel fibers. The addition of fibers to the concrete matrix leads to significant energy being absorbed and helps control crack opening [1,2]. The presence of fibers in cracks limits the width of cracks, and results in their proper distribution and increases their serviceability [3,4]. In all concrete structure design codes, controls related to the serviceability state and cracking control are important. Many research works have been conducted to study only the tensile behavior of UHPFRC [5–9]. They have focused on the mechanical properties of UHPFRC without reinforcements. However, in real structural elements, concrete is usually accompanied by reinforcement. One method for recognizing this behavior is to test the direct tensile tie (a prismatic concrete member with a high length-to-width

ratio and a reinforcing steel bar in the center of the cross-section). In order to understand the tensile behavior of concrete as a simple material, and of concrete combined with conventional reinforcement, parameters like crack width, distance between cracks and tension stiffening have been studied for many years [10–13]. As adding fibers to concrete limits the cracking phenomenon by narrowing cracks with short distances among them, it is important to analyze how the aforementioned parameters could be affected when UHPFRC is combined with a steel bar. In recent years, very few studies have analyzed the tensile behavior of UHPFRC by including steel bar reinforcement [14–16].

The present paper focuses on providing an appropriate testing method to investigate the UHPFRC cracking behavior under the serviceability limit state (SLS). For this purpose, tensile tie experiments were proposed and developed. A new method is provided to measure the ability to transfer tensile force to a concrete member. Some parameters were evaluated by this testing method, such as the element's average tensile stress-strain diagram, the element's strain behavior in small segments and the development of cracks and their frequency.

## **2. Research Significance**

Performing a direct tensile test on reinforced concrete specimens and applying tensile force to concrete specimens are not easy tasks. This present work provides a simple testing method for studying the behavior of reinforced UHPFRC under uniaxial tension load. This method is able to analyze the multicracking behavior of a UHPFRC tensile tie using different types of measurements equipment. It also helps us to analyze the interaction between concrete and steel reinforcement and the possible synergy between them under SLS.

## **3. Experimental Program**

The experimental program was considered for one type mixture to evaluate the behavior of the UHPFRC tensile tie. Due to the capacity limitation of the laboratory mixer and the number of molds, five batches with the same dose were prepared (C1 to C5). The mixture design of UHPFRC is reported in Table 1. The achieved average 28-day compressive strength test of concrete cubs of 10 cm x 10 cm was 158.41 MPa and the average Young's Modulus was 48.88 GPa. The fibrous reinforced concrete was typified as Fiber 13/02 (in which 13 refers to a length of 13 mm and 02 implies a diameter of 200  $\mu\text{m}$ ) and tensile strength was more than 2000 MPa.

**Table 1.** The UHPFRC Mixture Design.

Component	Content (kg/m <sup>3</sup> )
Cement I 42.5 R/RS	800
Silica Fume 940 D Elkem UD	175
Silica Flour U-S500	225
Fine Sand 0.5 mm	302
Medium Sand 0.6-1.2 mm	565
Water	160
Superplasticizer, Viscocrete 20 HE	30
Fiber	160

All the specimens were made as follows: the considered specimen length was 1000 mm and a central bar was located over the entire element with a length of 1450 mm. Two complementary rebars were located at both ends with a length of 450 mm. These reinforcement bars were welded to the main bar. This experimental research was conducted for one cross-section type (i.e. 80 × 80 mm) and three tie series with rebars ratios of 1.23 %, 1.77% and 3.14% (rebars were 10 mm, 12 mm and 16 mm). The nominal yield stress of the rebars was 500 MPa. To identify specimens, the first number represents the reinforcement diameter, whereas the second number refers to the number of series per specimen; e.g., for the tensile tie with a 10-mm reinforcing bar, the ID specimens were named (T-10-1), (T-10-2) and (T-10-3). Figure 1 illustrates specimen details.

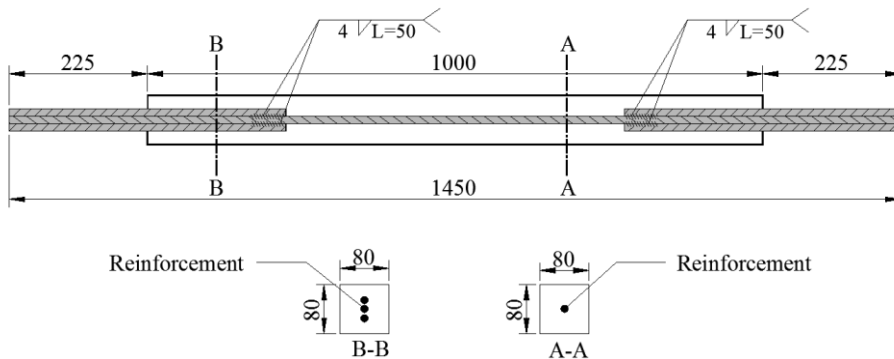


Figure 1: Specimen reinforcement details (units in mm).

During the manufacturing procedure, an attempt was made to locate the rebar exactly on the center section to avoid eccentricity and bending effects. Specimens were stored in a curing chamber at 95% relative humidity and a temperature of  $T = 20 \pm 2^\circ\text{C}$  until 2 or 3 days before testing. UHPFRC was cast horizontally so that the casting process would start from one extreme to the other extreme by applying

a uniform velocity to ensure a good alignment of the steel fibers in the concrete mixture.

## **4. Description of the test system**

### **4.1. Description of the test system**

In order to perform this test, a 2-meter steel structural frame was used, as outlined in [17] 'Figure 2.a'. This structure was made using two plates whose thicknesses were 5 cm on both extremes, along with four 60 × 60-mm rectangular tube sections of 8 mm thickness. As tensile force had to be transferred to the specimen, two two-piece steel jaws (2 mm high) with indented corrugations were used as shown in Figure 2.b.

In order to prevent the main bar from yielding and failing on both ends without concrete, two 45-cm long rebars were used in the external region of the specimen, and penetrated 22.5 cm into the concrete specimen (Figure 1). The test zone lay in the center part of the member where only one rebar existed.

As previously mentioned, two st52 steel jaws were used to transfer tensile force from the system to both the concrete specimen and the ending reinforcing bars. Each jaw consisted of two segments with six high-strength bolts whose diameters were 13 mm. By tightening these bolts, tensile force was transferred by the hydraulic jack to the bar embedded in the concrete specimen because of the frictional force between the rebar and the interior side of the jaw. In order to distribute the force caused by tightening the bolts uniformly, this process was done in a zigzag manner. Figure 2. b. provides details of the jaw and the assembled connection.

Hydraulic jacks are designed as cylinders and a bar can be passed to their centers. A Ø20-mm high-strength steel bar ( $f_y=1000\text{MPa}$ ) was used to transfer the tensile force caused by the movement of the hydraulic jack. At the end of these bars, a circular steel rod end bearing was embedded (Figure 2.c). At both ends of the jaws, there was a Ø25-mm bolt that allowed the steel jaw to be connected to the bars through the steel rod end bearing. This connecting system displayed a hinge behavior and allowed bending or twisting at both specimen ends (Figure 2.d).



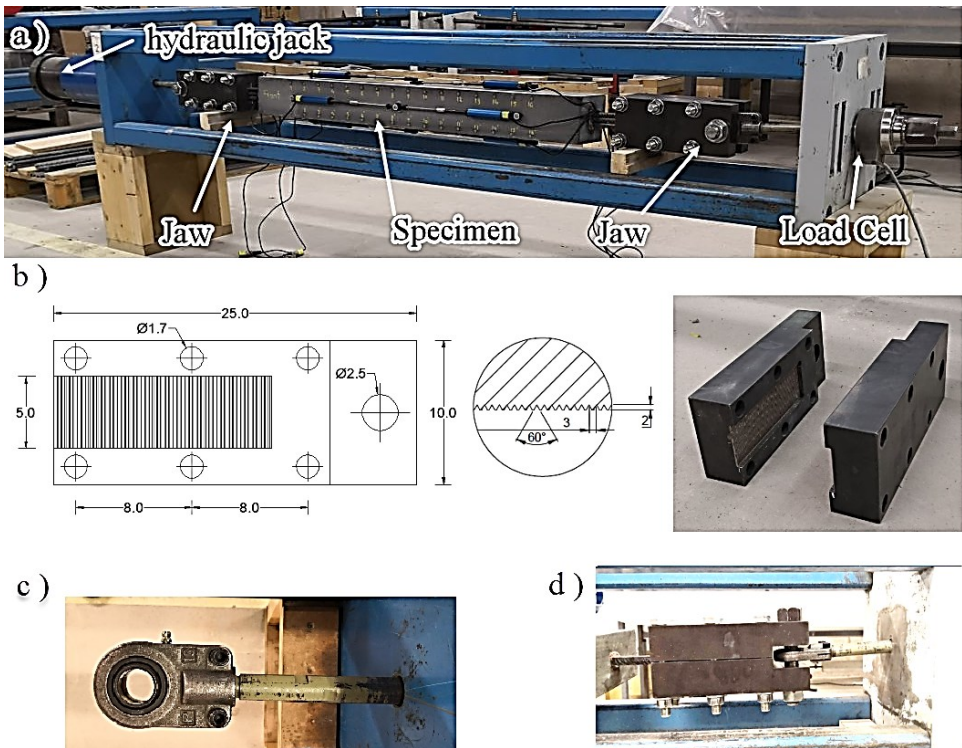


Figure 2: a) Tensile test equipment. b) Jaw details. c) rod end bearing. d) assembled Jaw connection.

## 4.2. Instrumentation and experimental procedure

As previously mentioned, this experiment aimed to study the tensile behavior of the UHPFRC reinforced tie. To conduct this study, the behavior of the member was studied at both the general and local levels. To investigate the general behavior, displacement transducers were employed, while local behavior was evaluated using demountable mechanical gauges (DEMEC points). The position of the measurement equipment is illustrated in Figure 3.

For this purpose, specimens were tested under the displacement control. On both sides of the concrete specimen and on four surfaces, four 35-cm long displacement transducers were installed (Figure 3). In this method, it was assumed that the strain of the rebar located in the center of the section would equal the average value of the strains recorded for four external surfaces. For the local level measurement, #16 DEMEC steel discs were installed at a 1-cm distance from the upper and lower edges on each specimen edge (see Figure 3). The reason for using four displacement transducers on the four specimen surfaces was to study the possible

bending and rotations due to asymmetric cracks occurring.

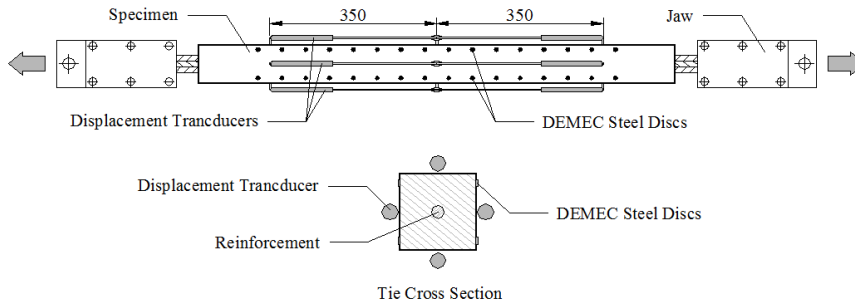


Figure 3: Measurement equipment: positions of the displacement transducers and the DEMEC points along the element.

After installing the concrete specimen within the test equipment, force was applied by the hydraulic jack and the increase in force was stopped in strains of 0.03‰, 0.05‰, 0.10‰, 0.15‰, 0.5‰, 1‰, 1.5‰ and 2‰. Then the changes in length between the DEMEC disks were measured. While testing, an attempt was made to maintain force at constant levels.

As the average displacement recorded by the displacement transducers reached an equivalent strain of 2‰, the experiment was stopped, and the number of cracks on the upper and lower edges between the DEMEC points was recorded by plotting the crack pattern on the specimen surfaces. For the specimens containing the  $\varnothing 16$  bars, it was difficult to reach the tension strain of 2‰ because the bars slipped at a high load value. Therefore, the experiment continued for these specimens until a displacement corresponding to a strain of 1.5‰ took place.

## 5. Results and Discussion

A tensile stress-strain diagram of specimens was obtained from the average of the four displacement transducers located on the left and right specimen sides. Figure 4 illustrates the displacement-force curves due to the tensile force on both the left and right sides of specimen T-12-2, respectively.

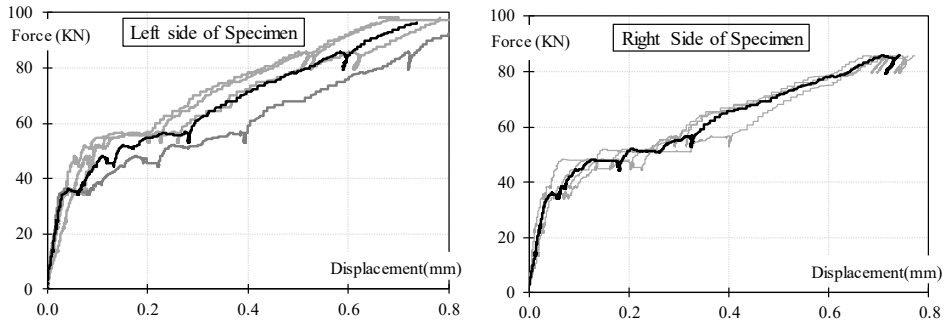


Figure 4: Displacement-force curve for specimen #T-12-2.  
Displacement transducers on the four surfaces and their average values.

As previously stated, a slight difference in the diagrams was due to asymmetric cracks appearing on the specimen's cross-section, as well as very small localized bending because of the difference in the cracking inertia along the member. Figure 5 presents the average tensile stress-strain curve for both the specimen's left and right sides. These two diagrams are similar to one another, and the average behavior diagrams for the specimen's left and right sides can be described as the tensile behavior of the tensile tie. The stress expressed in this diagram is shown as the equitant steel stress, which was obtained by dividing the total tensile force by the area of the reinforcing steel. The results obtained for each series of specimens are shown in Figures 6, 7 and 8.

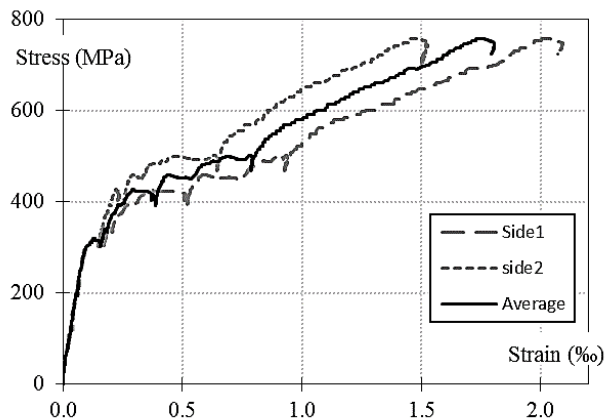


Figure 5: Tensile stress-strain diagram for specimen #T-12-2 and the average values.

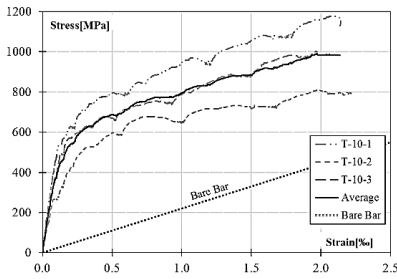


Figure 6: Stress-strain diagram based on the rebar area for tie 8x8cm with the Ø10-mm bar.

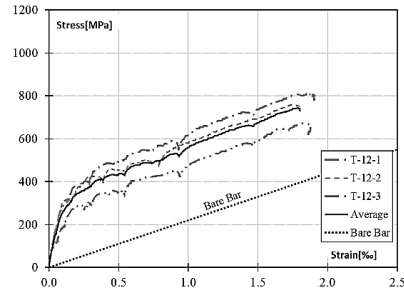


Figure 7: Stress-strain diagram based on the rebar area for tie 8x8cm with the Ø12-mm bar.

As the equivalent stresses shown in the above diagrams are based on the area of the reinforcing steel, the numerical value of this stress is higher for the bars with smaller areas. As observed in the diagrams, the tie's stress-strain behavior is relatively in parallel to that of the steel bar after the member cracked under tensile force, and reducing of the stiffness and change in slope of the stress-strain diagram.

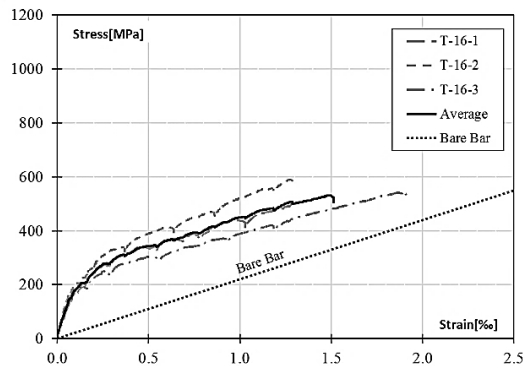


Figure 8: Stress-strain diagram based on the stress on rebar area for tie 8x8cm with the Ø16-mm bar.

Regarding the above diagrams, the elastic stiffness in the linear region varied from 39 to 42 GPa for the ties with the Ø10-mm bar, from 19 to 25 GPa for the ties with the Ø12-mm bar, and from 15 to 18 GPa for the ties with the Ø16-mm bar. By assuming the simultaneous participation of concrete and steel in tension and with the same strain, it was possible to obtain tensile stresses in concrete by subtracting the strain-stress curve of the bare rebar from the total stress-strain curve; e.g., the tensile stress of concrete is calculated in Figure 9. The average tensile stresses for

all three tie series are shown in Figure 10. It should be noted that no significant strain-hardening behavior was observed for UHPFRC. With this diagram, it is possible to compute the tensile stresses that correspond to the desired strains and to compare them with the allowable SLS values.

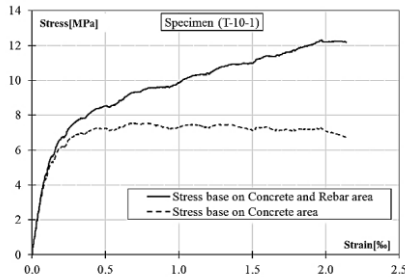


Figure 9: Tensile stress-strain curve for specimen T-10-1 (stress based on concrete area).

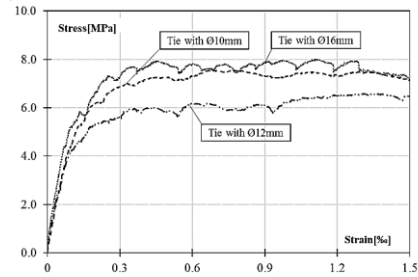


Figure 10: Average tensile stress-strain curve calculated according to the concrete area for all three specimens per series.

It should be noted that due to the asymmetry and uniformity of cracking in concrete, strains would not be identical on the element's four edges.

By way of example, for specimen T-12-2 at the force level of 2.31 kN, the average value of the strains of all the elements obtained by DEMEC was  $\varepsilon=0.066\%$  and the average value obtained by the displacement transducer was  $\varepsilon=0.059\%$ , with a difference of 10.5%.

It is worth noting that in some specimens, it was not possible to record the increased length using DEMEC within the required strain intervals because cracks and a sudden increase in the longitudinal strain occurred.

At the end of the test and after accessing the tensile strain of 2‰ (1.5‰ for the specimen with the Ø16-mm bars), the number of cracks between the disks installed on the specimen's six edges was recorded by wetting the surface with water. Due to the rough surface created on the specimen surface that did not come into contact with the steel mold, no cracks were seen (see Table 1).

Table 1: The average number of cracks recorded between DEMEC disks and the average width of cracks for specimen T-12-2 (force value 2.31kN, strain obtained= 2 ‰).

Point Number		Total Number of Cracks	Achieved Elongation (mm)	Mean Crack Width (µm)
Upside	Edge1	70	0.632	9
	Edge2	91	0.632	7
Front Side	Edge1	69	0.632	9
	Edge2	86	0.632	7
Back Side	Edge1	92	0.632	7
	Edge2	56	0.632	11
			Mean	8

The number of cracks and the average crack widths are shown for specimen T-12-2. A large number of cracks and the short distance among them are some of the important characteristics of UHPFRC, as evidenced by the crack pattern shown in Figure 11.

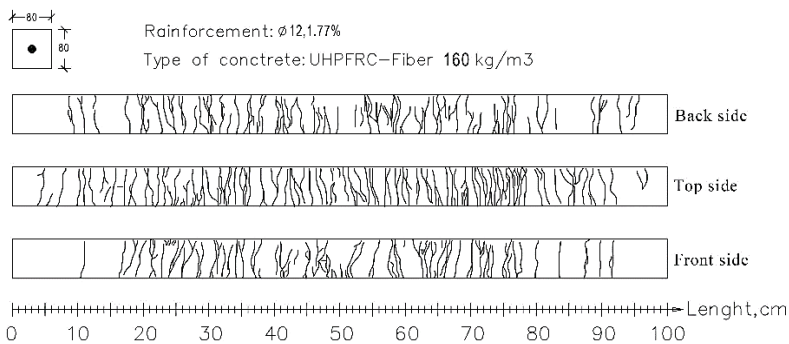


Figure 11: Cracks pattern for specimen T-12-2.

## 6. Conclusion

In order to study the necessary UHPFRC design requirements under SLS, a new testing method was developed to perform direct tensile tests. This method is able to examine the behavior of these elements under serviceability conditions and can determine tensile strains from the multi-cracking phase to the localized crack development stage.

In this method, the average tensile stress-strain curve of tensile ties was obtained by installing four displacement transducers on the specimen's four surfaces on both sides. Some parameters were obtained, such as the stiffness of elastic region, the tensile stress-strain diagram of concrete, and the width and number of cracks. The tensile strain on the 5-cm elements was acquired by installing DEMEC equipment on the four edges of the cross-section. Using the data obtained by this method, the tensile strain variations along the member were studied. In the final loading stage, after reaching the strain of 2 ‰ recorded by the displacement transducers, the cracking pattern along the specimen, the number of cracks on each 5-cm element on four edges and the average crack widths of the specimens were obtained. The proposed testing method and the obtained results will enable the study of UHPFRC behavior under direct tension under serviceability conditions.

**Acknowledgement.** This work forms part of Project “BIA2016-78460-C3-1-R” supported by the State Research Agency of Spain.

## References

- [1] Wille K, El-Tawil S and Naaman A E 2014 Properties of strain hardening ultra high performance fiber reinforced concrete (UHP-FRC) under direct tensile loading *Cem. Concr. Compos.* 48 53–66
- [2] Japan Society of Civil Engineers 2008 Recommendations for Design and Construction of High Performance Fiber Reinforced Cement Composites with Multiple Fine Cracks (HPFRCC ) *Concr. Eng. Ser.* 82 Testing Method 6-10
- [3] di Prisco M, Plizzari G and Vandewalle L 2009 Fibre reinforced concrete: new design perspectives *Mater. Struct.* 42 1261–81
- [4] R. Yu et al. 2015 Development of Ultra-High Performance Fibre Reinforced Concrete (UHPFRC) : towards an efficient utilization of binders and fibres *Constr. Build. Mater.* 273–82
- [5] Naaman A E 2006 Proposed classification of HPFRC composites based on their tensile response *Mater. Struct.* 39 547–55
- [6] Kusumawardaningsih Y 2015 Tensile strength behavior of UHPC and UHPFRC *Procedia Eng.* 125 1081–6
- [7] Hun S, Joo D, Sung G and Taek K 2012 Tensile behavior of Ultra High Performance Hybrid Fiber Reinforced Concrete *Cem. Concr. Compos.* 34 172–84
- [8] Eduardo J. Mezquida-Alcaraz, Juan Navarro-Gregori, Juan Ángel López and Pedro Serna-Ros 2019 Validation of a non-linear hinge model for tensile behavior of UHPFRC using a Finite Element Model *Comput. Concr.* 23 11–23
- [9] López J Á, Serna P, Navarro-Gregori J and Coll H 2016 A simplified five-

- point inverse analysis method to determine the tensile properties of UHPFRC from unnotched four-point bending tests *Compos. Part B Eng.* 91 189–204
- [10] Bernardi P, Michelini E, Minelli F and Tiberti G 2016 Experimental and numerical study on cracking process in RC and R/FRC ties *Mater. Struct. Constr.* 49 261–77
- [11] Rimkus A, Jakstaite R and Kupliauskas R 2017 Experimental identification of cracking parameters of concrete ties with different reinforcement and testing layouts *Procedia Eng.* 172 930–6
- [12] Bernardi P, Cerioni R, Ferretti D and Michelini E 2014 Role of multiaxial state of stress on cracking of RC ties *Eng. Fract. Mech.* 123 21–33
- [13] Tan R, Eileraas K, Opkvitne O, Giedrius Ž, Hendriks M A N, Geiker M and Terje D B 2018 Experimental and theoretical investigation of crack width calculation methods for RC ties 1–12
- [14] Redaelli D and Muttoni A 2007 Tensile Behaviour of Reinforced Ultra-High Performance Fiber Reinforced Concrete Elements *Symp. Dubrovnik. Concr. Struct.* 267–74
- [15] Sigrist V and Rauch M 2010 Deformation behavior of reinforced UHPFRC elements in tension *Tailor Made Concr. Struct.* 106–106
- [16] Redaelli D 2006 Testing of reinforced high performance fibre concrete members in tension *Proc. 6th Int. Ph.D. Symp. Civ. Eng.* 9
- [17] Caro L A, Serna P and Martí J R 2013 Experimental Technique for Measuring the Long-term Transfer Length in Prestressed Concrete 125–34



---

**2<sup>nd</sup> PAPER**  
Details:

---

Type of paper	Journal article
Title	<i>Experimental methodology on the serviceability behaviour of reinforced ultra-high-performance fibre reinforced concrete tensile elements</i>
Authors	<u>Majid Khorami</u> Juan Navarro-Gregori Pedro Serna Ros
Journal	Strain
Publisher	Wiley
ISSN	1475-1305
JIF	1.848 (2020)
Quartiles	Q2, Mechanics of Materials
Status	Published
Date	Accepted: 07 April 2020 Available online: 03 June 2020
Full reference	Khorami, M., et al. "Experimental methodology on the serviceability behaviour of reinforced ultra-high performance fibre reinforced concrete tensile elements." Strain: e12361.

---

***2<sup>nd</sup> Paper. Experimental methodology on the serviceability behaviour of reinforced ultra-high-performance fibre reinforced concrete tensile elements***

M. Khorami<sup>1,2</sup>, J. Navarro-Gregori<sup>1</sup>, P. Serna<sup>1</sup>

<sup>1</sup>: Institute of Science and Concrete Technology, ICITECH, Universitat Politècnica de València, València, 46022, Spain.

<sup>2</sup>: Facultad de Arquitectura y Urbanismo, Calle Rumipamba s/n y Bourgeois, Universidad UTE, Quito, Ecuador

**Correspondence**

Majid Khorami, ICITECH, Av. Dels Tarongers, 4D, 46022 Valencia, Spain.

Email: [makho2@doctor.upv.es](mailto:makho2@doctor.upv.es)

**Funding information**

State Research Agency of Spain, Grant/Award Number: BIA2016-78460-C3-1-R.

**Abstract**

Design codes include Serviceability Limit States (SLS) provisions for stress, crack and deflection control in concrete structures, which may limit the structural design. When drawing on reinforced ultra-high performance fiber reinforced concrete (R-UHPFRC), the process of cracking differs significantly from traditional concretes. Thus, it remains unclear whether the traditional provisions are applicable to R-UHPFRC or should be reviewed. Uniaxial tensile tie test is an excellent option to analyze and review these criteria. This work proposes a novel test methodology to study the behavior of R-UHPFRC under serviceability conditions, which lets the study of the global and local deformation behavior by using different measurement equipment. Two different types of R-UHPFRC ties with variant fibre content were tested. The global average tensile stress-strain curve, cracking behavior, number and width of cracks were obtained. Promising preliminary results admitted that this methodology can be useful to propose design criteria of R-UHPFRC under SLS.

**Keywords:** design criteria, R-UHPFRC, serviceability, SLS requirements, test method, tie.

## 1. Introduction

The addition of fibers in concrete as reinforcement in the matrix improves post-cracking tensile behavior, energy dissipation capacity, and proper crack distribution. Hence, investigating the tensile properties of ultra-high performance fiber-reinforced concrete (UHPFRC) as a new alternative material for construction is needed. In recent decades, research on this field has increased. From a structural design point of view for UHPFRC, the design criteria, such as crack width limitation and allowable deformation, for serviceability limit state (SLS) may be different from that of conventional concrete; however, studying these requirements is necessary.

Many studies have analyzed the mechanical properties and behavior of conventional concrete and UHPFRC, and have covered various mechanical properties, including shear and flexural behavior, or durability and permeability of concrete among others. A large number of studies were conducted to examine the tensile behavior of fiber concrete without rebar reinforcement [1-4].

Given that almost all structural elements include steel rebar reinforcement, the mechanical properties of ultra-high performance concrete by using short steel fibers and rebar reinforcement should be evaluated to increase the structural applications of UHPFRC. High compression strength and improved ductility due to the addition of short steel fibers and well-bonded property between the UHPFRC and the reinforcing bar have of reinforcing bar, and rebar's cover.

The tensile force is generally applied to bars coming out from the specimen's ends. The influence of reinforcement ratio and specimen's shape on cracking distribution was studied by Sasaki et al. [5], and their results showed that the crack distribution of R-UHPFRC could be increased by decreasing the amount of reinforcement. The experimental result reported by Kunieda et al. [6], Leutbecher and Fehling [7] supported the latter inference. An experimental study conducted by Rimkus and Gribniak [8] considered the influence of the distribution of reinforcing rebar on cracking behavior and crack distance. A particular device that could apply uniform tensile force to all rebars was needed to perform this experiment because of the rebar arrangement and presence of more than one rebar on the specimen's ends. Hence, studies on the distribution of rebar reinforcing effect are limited due to the need for special devices when conducting experimental tests. Therefore, researchers must follow the tensile tie test by only using single rebar reinforcement.

The other method to measure the local deformation of tensile tie is using the digital image correlation technique (DIC) for monitoring the crack propagation and strain distribution at the concrete surface of the tensile tie [8, 10]. Since DIC is a powerful and useful tool to crack detection and measurement, but this technique cannot express the actual cracking and deformation behaviors because only one side of the tensile element is under monitoring. By contrast, carrying out this

method would result in difficulties because of possible movements out of the longitudinal axis. In addition, due to having a large length for the reinforced tensile element, it is needed to set the camera at a long-distance of the specimen losing the image quality. Hence, the identification of the microcracks could be challenging. However, investigating the local tension deformations is necessary to understand the cracking behavior of R-UHPFRC effectively. In the proposed test method, a demountable mechanical strain gauge (DEMEC) with 5 cm distance and measurement accuracy of  $\pm 1 \mu\text{m}$  was used.

This study proposed a test method to carry out the uniaxial tensile test for reinforcement UHPFRC ties. The proposed test method was easy to carry out and prepare compared with other techniques without the need for special or complicated equipment. The aim of this work was studying the cracking behavior of R-UHPFRC tensile ties and verifying that for serviceability analysis of R-UHPFRC tensile tie the tension stiffening phenomenon by considering crack formation and crack stabilization, that is used for conventional concrete ties, can be applied, or on the contrary, it is necessary to provide a different approach by considering the micro cracking branch of UHPFRC for this analysis. The results, such as global stress–strain of the tensile tie, local deformations measured via DEMEC equipment, and average crack width were obtained.

The proposed test method could be used to consider the design requirements of UHPFRC under serviceability conditions.

## **2. Research significance**

Defining the design requirements for UHPFRC under SLS was not strongly considered in codes. The uniaxial tensile test is an experimental method that investigates these requirements. Performing a direct tensile test on reinforced concrete specimens and applying tensile force to concrete specimens are difficult tasks. This work provided a simple testing method for exploring the behavior of R-UHPFRC under the uniaxial tension loads in order to analyze the interaction effect between the UHPFRC matrix and the reinforcement. The proposed experimental methodology was easy to perform, used specimens easy to produce in a lab, and the analysis of the experimental results was simple. The proposed method could analyze the deformation behavior of R-UHPFRC tensile elements under SLS conditions by using different types of measurement equipment.

## **3. Test methodology**

### **3.1 Test setup**

#### **3.1.1 Main frame**

In this experimental test, a structural frame was necessary in applying the tension force to the R-UHPFRC specimen. The system test should be able to support the maximum force that could be applied to specimens during the test procedure. The system was designed as a horizontal structure for the easy installation of measurement equipment that allows suitable access to the front and back sides of the specimen. The main structure was composed of two plates joined with four rectangular steel tube sections. The distance between two plates was 2000 mm. The plate's dimension was 320 mm × 320 mm with 50 mm-thick. Connector elements were designed to support compression reactions. The elastic buckling capacity was also considered. A 6 mm-thick tube section with 60 × 60 mm size was used based on the allowable stress design for the four connector elements. The st37 (steel material type) was used for all frame members. Figs. 1 and 2 show the details of the main frame.

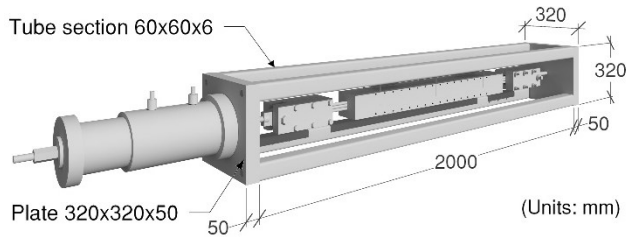
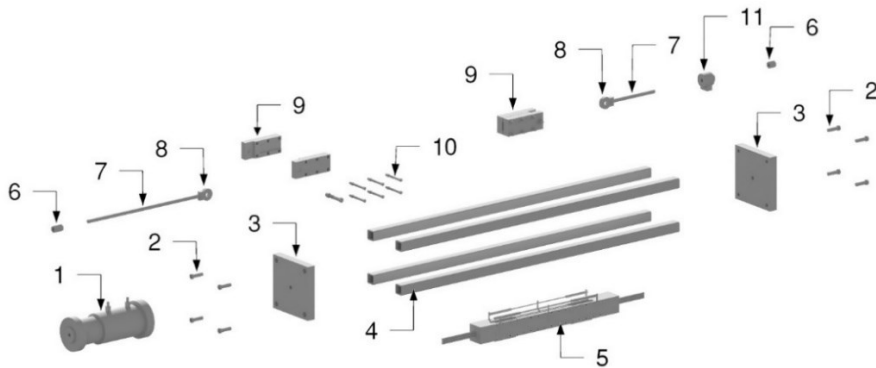


Figure 1: Main frame and installed concrete specimen.



Test set-up assembly parts

- 1.- Hydraulic jack
- 2.- Bolt Ø20 mm
- 3.- Plate 320 x 320 x 50 mm
- 4.- Tube section 60 x 60 mm
- 5.- Concrete specimen
- 6.- Anchorage

- 7.- Steel rebar Ø20 mm
  - 8.- Steel rod end bearing
  - 9.- Steel Jaw
  - 10.- Bolts Ø13 mm
  - 11.- Cell-force
- (Units: mm)

Figure 2: Test setup of assembly parts.

### **3.1.2 Force transfer and connection systems**

A primary challenge when conducting a uniaxial tensile tie test is the transfer of tensile force or application of displacements from devices to the end rebars of the specimen; hence, different methods were proposed by researchers. Some authors [7, 11-13] used a jaw system by clamping both rebar ends to connect the concrete specimen to a hydraulic jack device and apply displacement on both ends. Sasaki et al. [5] used a 22 mm-thick steel plate at each end of the specimen to transfer the tensile force to the specimen. Four rebars were used to ensure sufficient bonding between the plates and UHPFRC. These rebars were welded to the plate and penetrated the UHPFRC tie. On the outside, a screw type reinforcing bar with a 29 mm diameter was welded to apply and transfer the tensile force from devices to the specimen. This connection method is rarely used by researchers due to its difficulties, such as the welding process, special performing details, and possible out-of-plane plate deformation.

Makita and Brühwiler [9] presented a method to explore the fatigue behavior of UHPFRC reinforced by steel rebars. In this technique for loading and unloading the specimen, a 2 mm-thick aluminium plate was used and guided by epoxy resin to both surfaces of the specimen. These plates were part of the strengthening element. Two U-shaped jaws were used on both sides of the specimens. A fraction force was produced by applying lateral force at the jaw, and the tensile force could transfer to the specimen. This method was unsuitable for specimens with large section sizes due to low fraction capacity. Amin et al. [14] used a large section size for SFRC tensile ties with screw-type reinforcing bars at Ø20 and Ø28 mm. The screwed reinforcement was directly connected to the universal joint machine. This technique made it easy to cast, install, and connect the specimen to devices. However, the probability of failure at the end zone is high due to the yielding fracture of rebar considering the different stiffnesses between the bare bar and the end part of the specimen where concrete and reinforcement exist. The spherical hinge joint is another technique used by Rimkus et al. [10]. In this method, the mechanical anchorage joint is used, and the specimen is connected to machine transfer force devices via the spherical hinge. Notably, the joint detail and method must avoid the fracture by using the yielding mechanism of the bare rebar and end parts of the tensile tie.

The direct tensile test was generally performed by directly applying tension force to the rebar. The rebar should be located exactly along the tie longitudinal axis and pass from the center of the cross-section of the tie element. The hydraulic jack was installed on the left side of the frame, and the movement of the interior cylinder caused displacement at the end border of the hydraulic jack. This test was carried out by using the deformation control method.

The hydraulic jack should be designed as a circular tube with a longitudinal hole

to transfer the cylinder's displacement to the specimen. This form helps the steel bar to pass through the interior hole and transfer end border movements of the hydraulic jack to the specimen located inside the frame (see Fig. 2 segment #7).

Given that this investigation focused on SLS of R-UHPFRC, hence it was not needed to achieve the specimen fracture. The applied force value was dependent on the specimen's cross-section and reinforcement diameter. Hence, the steel bar was designed by using a high-strength steel material with  $f_y=1000$  MPa and the achieved rebar diameter was 20 mm to support the 200 kN tension force. The hydraulic jack's length was 800 mm; thus, the chosen length for the steel bar that passed through the hydraulic jack was 1000 mm. The same 600 mm-long steel bar was used on the right side of the frame. A screw thread was designed on both extremes of the steel rebars to connect and fix the rebar to the frame with the anchorage and washer at the back side of the right plate and end border of the hydraulic jack (Fig. 2). Another side of these steel rebars was embedded with a circular bearing to connect the jaw system.

A primary challenge in conducting the direct tensile test was the connection system in fixing the reinforced concrete element to the transfer force device. As previously mentioned, common methods, such as the wedge-shaped clamp, spherical hinge connection, and end welded to steel anchor plates, were used by researchers. Such systems and methods need special preparation techniques and exhibit difficulties.

The proposed connection system in this research included two-piece steel jaws with 2 mm-high indented corrugations. Each segment was symmetric with the other segment and assembled by using six bolts with a diameter of 13 mm. Indentations that occurred on the rebar body produced sufficient friction force to transfer the tensile force to the specimen by tightening the bolts. Jaw details are provided in Fig. 3b.

Bolts ( $\text{Ø}25$  mm) were placed at both ends of the jaws and allowed the steel jaw to be connected to the bars through the steel rod end bearing. This connecting system displayed a hinge behavior and avoided any bending or twisting on the specimen ends (Fig. 3d).

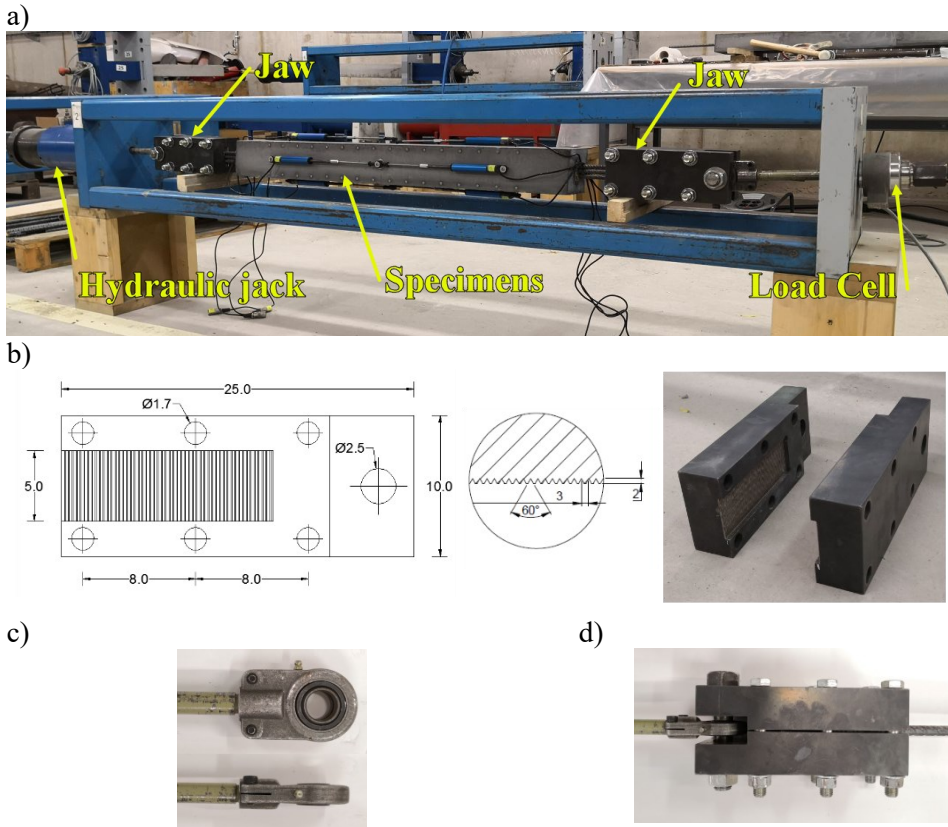


Figure 3: a) Tensile test equipment. b) Jaw details. c) Rod end bearing. d) Assembled jaw connection.

### 3.2 Materials and specimens

In this experimental research were considered for two types of UHPFRC to evaluate the proposed direct tensile test method and compare the measurement parameters obtained by the test. The dosage of steel fibers for the first (C1) and second (C2) mix designs were 160 and 80 kg/m<sup>3</sup>, respectively. The length and diameter of applied steel fibers in this study were 13 and 0.2 mm, respectively, and their tensile strength was more than 2000 MPa. Table 1 lists the proposed mixed design.



Table 1: UHPFRC mixture design.

<b>Component</b>	<b>Content (kg/m<sup>3</sup>)</b>
Cement I 42.5 R/SR	800
Silica fume 940 D Elkem UD	175
Silica flour U-S500	225
Fine sand 0.5 mm	302
Medium sand 0.6–1.2 mm	565
Water	160
Superplasticizer, Viscocrete 20 HE	30
Fiber	160

The procedure was initiated by mixing the dry materials in the mixing chamber for 1 minute to combine all the components well. Water and superplasticizer were added, and the concrete was mixed for approximately 10 minutes until a visible flow was achieved. After the concrete started to flow, steel fibers were added, and the mixing procedure continued for 5 minutes.

The cross-section dimensions usually depend on the machine capacity and reinforcement ratio used for the specimen. Tiberti et al. [13] and Berbaridi P [11] tested a wide range of RC and SFRC tensile ties by using seven different square section dimensions (50, 80, 100, 120, 150, 180, and 200 mm) and three different rebar diameters ( $\text{Ø}10$ ,  $\text{Ø}20$ , and  $\text{Ø}30$  mm) to evaluate the crack behavior of ties at SLS. Previous studies [15–17] have demonstrated that section shape, dimension section, and distribution of reinforcements are significant parameters on the deformation behavior of tensile reinforced ties. Sigrist and Rauch [12] used large dimensions, such as 110, 160, and 170 mm, for tie square sections and examined the UHPFRC tensile tie reinforced with high-strength steel and conventional steel rebar to investigate the deformation behavior. The obtained experimental results indicated that the stress–strain characteristic and steel rebar type had a significant effect on deformation behavior and the failure mechanism.

In this experimental study, the R-UHPRC tensile tie elements had a prismatic shape. The element length was  $1000 \pm 2$  mm, and its cross-section was a square with  $100 \text{ mm} \times 100 \text{ mm}$  size. The 1450 mm-long steel reinforcement rebar with  $\text{Ø}12$  mm used for all specimens. The nominal yield stress was 522 MPa and Young's modulus was 200 GPa. During the manufacturing procedure, an attempt was made to locate the rebar exactly in the center section to avoid eccentricity and bending effects. Given the different axial stiffnesses at the end of the specimen (the region with and without concrete), two 45 cm-long rebars were used in the external region of the specimen and penetrated 22.5 cm into the concrete specimen to prevent the main bar from yielding and failing on both ends without concrete (Fig. 4). The reinforcement bars were welded at a length of 3–5 cm to the main bar to ensure that no pull-out would occur. The width of indented corrugations

located inside the jaw was set to 50 mm to place the three rebars. The test zone was in the center part of the member where only one rebar existed.

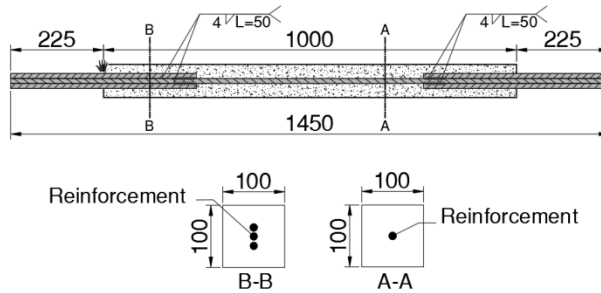


Figure 4: Specimen reinforcement details (units in mm).

The average compression strength values of UHPFRC were 157.73 and 152.41 MPa for concrete types C1 and C2, and the average Young's modulus values obtained by using 150X300 mm cylindrical specimens were 48.53 and 46.49 GPa, respectively. Tensile properties of UHPFRC were obtained by an inverse analysis method developed by López et al. [18]. For that, prismatic specimens (500×100×100 mm) were tested under four-point bending test. Table 2 provides the constitutive parameters for each specimen and concrete type. In this table ( $E$ ) is elastic modulus, ( $f_t$ ) cracking strength, ( $\epsilon_t$ ) strain at cracking strength, ( $f_{t,u}$ ) tensile strength, ( $\epsilon_{t,u}$ ) strain at tensile strength, ( $w_d$ ) crack opening at change of slope, and ( $w_0$ ) intersection of the first line of the bilinear  $\sigma_w$  to the  $w$  axis.

Table 2: Main characteristics of R-UHPFRC ties.

Material code	Fiber dosage (kg/m <sup>3</sup> )	Tie code	E (GPa)	$f_t$ (MPa)	$\epsilon_t$ (‰)	$f_{t,u}$ (MPa)	$\epsilon_{t,u}$ (‰)	$w_d$ (mm)	$w_0$ (mm)
C1	160	T10-12-C1-1	52.73	7.91	0.15	6.52	2.11	2.27	3.40
	160	T10-12-C1-2	49.66	8.94	0.18	8.03	4.04	1.90	2.84
	160	T10-12-C1-3	51.50	10.30	0.20	9.58	5.09	1.99	2.99
C2	80	T10-12-C2-1	62.62	7.40	0.11	4.87	3.32	2.20	3.30
	80	T10-12-C2-2	54.64	7.58	0.13	4.69	2.94	3.98	5.97
	80	T10-12-C2-3	62.06	7.44	0.12	4.27	2.90	2.46	3.69

### 3.3 Instrumentation

Relevant data from the experimental tensile test should be obtained to study the tensile behavior of R-UHPFRC and evaluate the required design parameters under serviceability conditions. These data reflected the specimen's tensile average stress-strain relationship, average tensile stress in the concrete matrix and

reinforcement, cracking behavior, and crack width.

### 3.3.1 Global and local deformation measurement

In this study, the behavior of the member was studied at the global and local levels. Displacement transducers (DTs) were used to investigate the global behavior. The average value of deformations recorded by DTs was used for rebar deformation by assuming that surface deformations of concrete with steel rebar reinforcement were equal. However, Rimkus and Gribniak [8] considered this method for investigating the cover effect on reinforced tensile tie with conventional concrete and found that a significant difference existed between the average deformation of the concrete surface and the rebar. The local behavior was evaluated by using demountable mechanical gauges (DEMEC). On both sides of the concrete specimen, four 35 cm-long DTs were utilized to obtain the total tensile elongation of the element (Fig. 5).

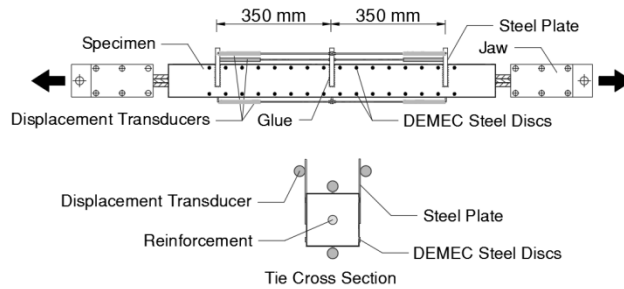


Figure 5: Measurement equipment: positions of DTs and DEMEC points along the element.

For local level measurement, #16 DEMEC steel discs were installed at a 1 cm distance from the upper and lower edges on each specimen edge. DEMEC discs were installed on the front and back faces of the element by following the required space for DEMEC machine measurement. Thus, the DTs were installed on the same surface but on top of the concrete specimen by using small plates and hard glue.

### 3.3.2 Force measurement

The specimens were tested under manually displacement control at a rate about of 0.5 mm/min. The load cell was used to measure the force values located at the right side of the frame behind the plate. The steel bar with 20 mm diameter was connected to the jaw and passed through the hole of the plate where the anchorage and washer were fixed. The applied displacement from the hydraulic jack on the

left side of the frame transferred from the steel rebar to the specimen. The tension force in the steel bar caused a compression reaction force between the anchorage and the right plate where an electronic load cell was located. Fig. 3a illustrates the details and position of the cell force.

### **3.4 Procedure**

This experiment was carried out in two stages. The first determined the tension stress-strain relationship of the specimen in the global level. For this purpose, the applied tension force value was measured via load cell and then the rebar tension stress was calculated. Rebar deformation was obtained by using the surface concrete deformation measured by the DTs at the right and left side of specimen. With regard to DTs location and distance from the center of the section, sectional analysis was used, and the rebar elongation (in the center of the section) was obtained via the linear regression method. The average of tension stress-strain relationship obtained for right and left side of specimen was used as a global specimen behavior. The local deformations were obtained by using the DEMEC equipment. The second stage obtained the cracking parameters of specimens and measured the number of cracks to calculate the average crack width. After attaching the DEMEC discs on the front and back surfaces, the specimen was placed inside the jaw and fixed by tightening the six bolts. This process was conducted in a zigzag manner to uniformly distribute the force caused by the tightening of bolts. A specimen axis was installed along the jaw centerline to avoid applying any bending or torsion to the specimen ends. Before applying the force, the distance between DEMEC discs was measured. This distance will be used to calculate the relative elongation after the force was applied to the element. Force application should be stopped because the measuring process of DEMEC equipment is time-consuming, and the amount of specimen elongation should be measured in every stopped force level. The applied force for all specimens was stopped in the value strains of 0.03%, 0.05%, 0.10%, 0.15%, 0.5%, 1%, 1.5%, and 2%. When the distance between DEMEC discs was measured, the force was maintained at a constant level. The first phase of the test was completed as the average element tensile strain reached 2%, and the experiment was stopped. Then, the crack propagation scheme drawn on the specimen's surfaces without unloading the specimen to keep the cracks open. The number of cracks on the upper and lower edges between the DEMEC discs on the specimen's six edges was recorded by wetting the surface with water.

## 4. Test results and discussion

### 4.1. Global tensile behavior

In this work, the concrete surface strain monitored by DTs was used to obtain the reinforcement strain, which was located in the center of the tie section. As previously mentioned, four DTs were present in each side of the specimen to record element tensile elongation. A slight difference in the force-displacement diagrams obtained by each DT was observed. This characteristic likely occurred due to the asymmetric cracks that appeared on the specimen's cross-section and very small rotations. Fig. 6 illustrates the average force-displacement curves recorded by four DTs on the left and right sides of specimen T10-12-C1-1 as an example.

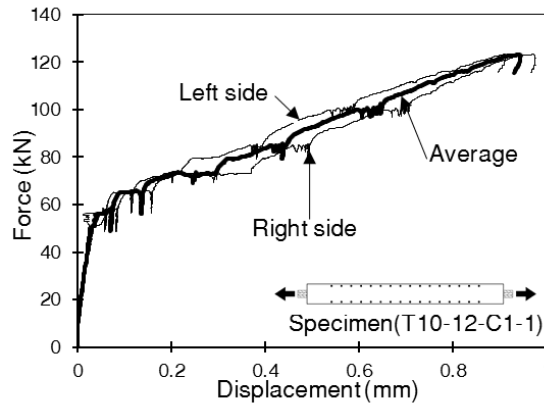


Figure 6: Displacement–force relationship of specimen T10-12-C1-1.

Figs. 7a and 7b present the results obtained for the two categories of R-UHPFRC by two different concrete types (C1 and C2) and three specimens for each category. These diagrams demonstrated the global stress-strain relationship of tie elements. The stress expressed in this diagram was shown as the equitant steel stress, which was obtained by dividing the total tensile force by the area of the reinforced steel.

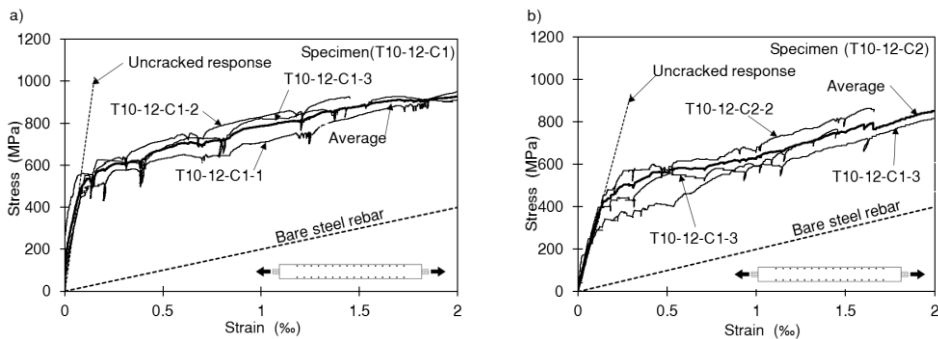


Figure 7: Tensile stress–strain diagram: a) concrete type C1 (fiber dosage = 160 kg/m<sup>3</sup>); b) concrete type C2 (fiber dosage = 80 kg/m<sup>3</sup>).

A significant difference was observed for the first cracking strength by increasing the fiber content in the concrete matrix. The first cracking strength for tie type C1 and C2 were 533 and 426 MPa, respectively. Note that in this study, the difference between the fiber contents was twofold. The average stiffness values in the elastic branch obtained by the three test samples of concrete types C1 and C2 were 6800 and 3123 GPa, respectively. In the elastic region due to force equilibrium and strain compatibility was not observed crack in the matrix. This outcome indicated that the applied force was shared between the rebar and UHPFRC. For fibre activation, a small opening at the crack was necessary to allow slip between the matrix and the fiber. At the first cracking, a small portion of the rebar will lose bond from the concrete. If this process continues, then an increasing number of microcracks along the element will develop [8]. It can be seen that after the first cracking a significant reduction in stiffness happened and the member response curve of ties by concrete type C1 moved forward parallel to the bare steel response, while for ties by concrete type C2 the tension response curve became diminish and response line has a small curve similar to the tension behavior for conventional concrete or FRC ties.

In addition, another result, which can be obtained from the general tensile response of R-UHPFRC tensile element, is the tension stiffening effect. The tension stiffening refers to the ability of the concrete to carrying the tension between cracks. This phenomenon has an effect on member stiffness, and it is essential for determining the serviceability deflection, and crack widths [19]. The tension stiffening effect should be included in the analysis to predict member behavior by employing an appropriate model. Sturm, A et al [20] proposed a tension stiffening model for FRC and UHPFRC by considering the strain-softening and strain-hardening with an allowance for the long-term creep and shrinkage effects of the concrete. The obtained tension stiffening effect for concrete type C1 and C2 is

presented in Fig. 8. The R-UHPFRC specimens exhibit a quasi-constant tension stiffening effect (refer to the horizontal branch of the curve), even at high-tension strain rates closed to 2‰. Moreover, the increment of the UHPFRC concrete contribution due to the increasing fiber content can be seen. It is important to outline that the fiber collaboration in the UHPFRC tensile elements has two fundamental effects: (a) fibers provide a significant residual post-cracking strength, and (b) a state of stabilized microcracking is generated thanks to the bond between the UHPFRC matrix and the fibers improving ductility behavior even for UHPFRC with only 80 kg/m<sup>3</sup>.

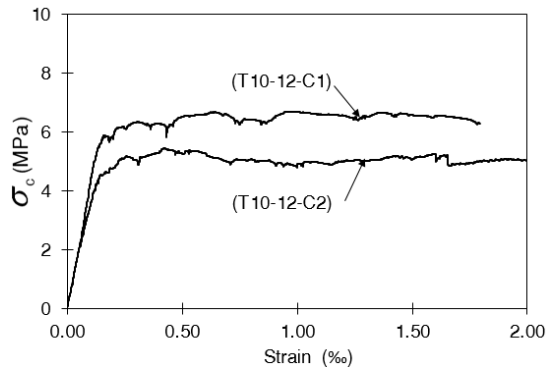


Figure 8: Tension stiffening response for concrete type C1, and C2.

The stress–strain diagrams, and the tension stiffening response obtained by the proposed method demonstrated the efficiency of this method in carrying out future research and studying the tensile behavior of R-UHPFRC structural elements.

## 4.2 Local tensile behavior

The measured local deformations obtained by the DEMEC equipment helped evaluate the strain distribution along the tensile element length and its variation in different force stages. The same evaluation was initiated [21] by installing DEMEC discs on the four cross-sectional corners in a symmetric form. The average elongation measured by the four corner points was used to obtain the steel rebar strain in the center of the section. Figs. 9 and 10 show the results obtained for two different concrete types of tensile R-UHPFRC ties.

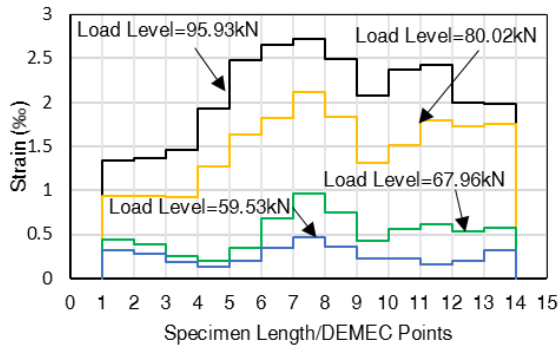


Figure 9: Strain distribution along the tie length of R-UHPFRC tensile tie #T10-12-C1-1.

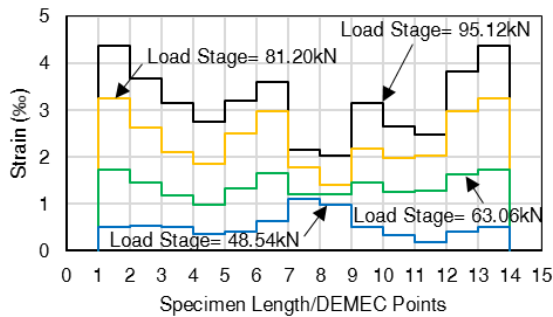


Figure 10: Strain distribution along the tie length of R-UHPFRC tensile tie #T10-12-C2-1.

Certain crack amounts of the tie element and crack opening differed with the other parts due to the stochastic nature of concrete cracking. Thus, the local strain distribution diagrams along the element length varied.

By comparing the local deformation results obtained for the two types of concrete, the ties that include  $80 \text{ kg/m}^3$  fibers demonstrated a significant difference with those with a fiber dosage of  $160 \text{ kg/m}^3$ . Consequently, the amount of fiber content in tensile R-UHPFRC tie elements exhibited an influence on deformation behavior, and their design parameters under SLS conditions. Thus, the proposed measurement method could be used to investigate these parameters.

The results of the proposed measurement method showed that this method is able to capture the maximum tensile strains along the specimen, its position, and its variation. Using together the experimental data obtained by DEMECs and DTs leads to having a potential experimental methodology for studying the serviceability behavior of R-UHPFRC.



### 4.3 Cracking behavior (propagation of cracks and crack width)

Cracking behavior parameters, such as width and crack spacing, were influenced by the reinforcement ratio and rebar diameter for conventional concrete. The fiber content exhibited a significant effect on this behavior [22]. The observed first cracks at the concrete surface were very small (called microcracks). The crack width was increased with increasing tensile force. At the end of the test and after obtaining the tensile strain of 2‰, the number of cracks between the DEMEC discs installed on the specimen's six edges was recorded by wetting the surface with water. The average crack width was calculated by dividing the total achieved elongation at the 2‰ tensile strain (total elongation recorded from the right and left sides by DTs) by the number of cracks. The number of cracks in each edge was slightly different due to the inhomogeneous cracking manner. Table 3 lists the number of cracks on each side of the specimen and the average crack width of two different R-UHPFRC ties as examples. No cracks were clearly observed due to the rough surface created on the specimen that did not come into contact with the steel mold.

Table 3: Average number of cracks recorded between DEMEC discs and the average width of cracks for specimens T10-12-C1-1 and T10-12-C2-1

		T10-12-C1-1 (Force level value = 122.82)			T10-12-C2-1 (Force level value = 110.72)		
Measurement surface side	Edges	Total Number of Cracks	Achieved Elongation (mm)	Mean Crack Width (mm)	Total Number of Cracks	Achieved Elongation (mm)	Mean Crack Width ( $\mu\text{m}$ )
Top side	Edge1	78	1.890	0.0242	39	2.299	0.0589
	Edge2	78	1.890	0.0242	39	2.299	0.0589
Front Side	Edge1	77	1.890	0.0245	50	2.299	0.0459
	Edge2	64	1.890	0.0295	47	2.299	0.0489
Back Side	Edge1	87	1.890	0.0217	45	2.299	0.0510
	Edge2	59	1.890	0.0320	38	2.299	0.0605
			Mean	0.026		Mean	0.054

The medium crack width for the R-UHPFRC tensile tie with 80 and 160 kg/m<sup>3</sup> fiber content was obtained 0.054 and 0.026 mm, respectively. The main crack space was obtained by dividing the entire length of the measurement zone by average number of cracks. The crack spacing of concrete type C1 and C2 was 10.16 and 17.44 mm, respectively. This difference emphasized the clear influence of fiber volume content on crack width and serviceability behavior. Figs. 11a and 11b illustrate the crack propagation for the prior specimens. The crack pattern obtained for the two types of UHPFRC showed that substantial microcracks (with minor width) occurred in the tie with high fiber content and the high fiber content caused the cracking process by mines distance between them. Considering the

difference of cracks amounts and crack distance for two types of ties, the microcracking effect can be taken into account for tension stiffening analysis.

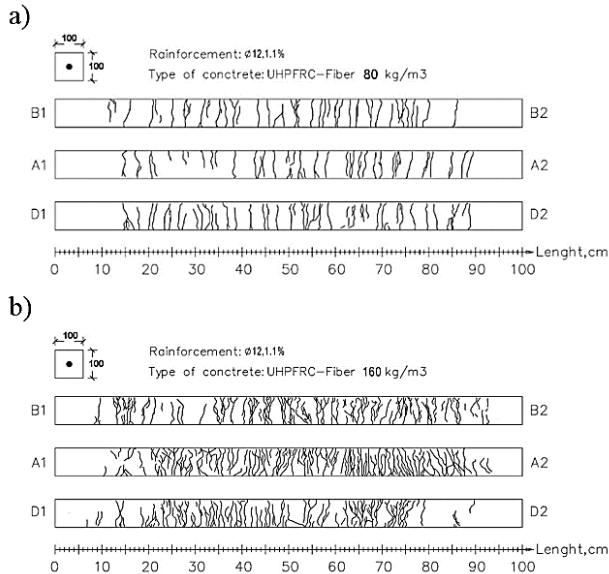


Figure 11: Crack pattern of specimens a) T10-12-C1-1 and b) T10-12-C2-1

## 5. Summary and conclusions

In this research, a new test method is proposed to carry out the uniaxial tensile test for R-UHPFRC tie. This method can evaluate the tensile behavior of R-UHPFRC under serviceability conditions, and help understand the deformation and cracking behaviors of tie elements. The experimental test was designed with two stages; in the first stage, defined the global tension behavior, and in the second stage obtained the local deformation behavior along the member length in small distances. Six specimens with two different fiber contents were examined.

The experimental study showed that the increase in fiber volume content of concrete has a significant influence on first cracking strength. In this study fiber content for concrete type C1 = 80 kg/m<sup>3</sup> and C2 = 160 kg/m<sup>3</sup>. The local deformation behavior in small segments along the member length was analyzed. The result showed that R-UHPFRC tensile ties with concrete type C2 had more significant local tensile strain than those with C1 concrete type due to the enlarged crack width. The fiber volume content had an important influence on the cracking and serviceability behaviors of R-UHPFRC.

The obtained results of the proposed test method demonstrated the suitability of

this test method in carrying out the uniaxial R-UHPFRC tensile test, and in analysing the interaction effect between the UHPFRC matrix and the reinforcement. Consequently, the proposed test methodology is appropriate for future studies on serviceability design criteria for R-UHPFRC.

## **Acknowledgments**

This work was supported by the State Research Agency of Spain and formed a part of Project “BIA2016-78460-C3-1-R”.

## **References**

- [1] Y. Kusumawardaningsih, E. Fehling, M. Ismail, A. A. M. Aboubakr, *Procedia Engineering* 2015, 125, 1081-1086.
- [2] A. E. Naaman, H.-W. Reinhardt, *Materials and structures* 2006, 39, 547-555.
- [3] S. H. Park, D. J. Kim, G. S. Ryu, K. T. Koh, *Cement and Concrete Composites* 2012, 34, 172-184.
- [4] K. Wille, S. El-Tawil, A. E. Naaman, *Cement and Concrete Composites* 2014, 48, 53-66.
- [5] K. Sasaki, R. Mori, M. Kunieda, in *International Conference on Strain-Hardening Cement-Based Composites*, Springer, 2017, pp. 502-508.
- [6] M. Kunieda, M. Hussein, N. Ueda, H. Nakamura, *Journal of Advanced Concrete Technology* 2010, 8, 49-57.
- [7] T. Leutbecher, E. Fehling, *ACI Structural Journal* 2012, 109.
- [8] A. Rimkus, V. Gribniak, *Construction and Building Materials* 2017, 148, 49-61.
- [9] T. Makita, E. Brühwiler, *International Journal of Fatigue* 2014, 59, 145-152.
- [10] A. Rimkus, R. Jakstaite, R. Kupliauskas, L. Torres, V. Gribniak, *Procedia Engineering* 2017, 172, 930-936.
- [11] M. E. Bernardi P, Minelli F, Sirico A and Tiberti G, in *Computational Modelling of Concrete Structures - Proceedings of EURO-C 2014*, Vol. 2, Taylor and Francis - Balkema, 2014, pp. 883-892.
- [12] V. Sigrüst, M. Rauch, *Taylor Made Concrete Structures-Walraven & Stoelhorst (eds)* 2008, 405-410.
- [13] G. Tiberti, F. Minelli, G. A. Plizzari, F. J. Vecchio, *Cement and Concrete composites* 2014, 45, 176-185.
- [14] A. Amin, S. J. Foster, M. Watts, *Magazine of Concrete Research* 2015, 68, 339-352.
- [15] I. Vilanova, L. Torres, M. Baena, G. Kaklauskas, V. Gribniak, *Engineering Structures* 2014, 79, 390-400.

- [16] N. J. Carino, N. J. Carino, Prediction of cracking in reinforced concrete structures, US Department of Commerce, National Institute of Standards and Technology, 1995.
- [17] V. Gribniak, A. Rimkus, L. Torres, R. Jakstaite, Structural Concrete 2017, 18, 634-647.
- [18] J. Á. López, P. Serna, J. Navarro-Gregori, E. Camacho, Materials and Structures 2015, 48, 3703-3718.
- [19] A. Sturm, P. Visintin, D. Oehlers, Journal of Structural Engineering 2019, 145, 04019138.
- [20] A. Sturm, P. Visintin, D. Oehlers, R. Seracino, Journal of Structural Engineering 2018, 144, 04018122.
- [21] T. Pfyl, P. Marti, Versuche an stahlfaserverstärkten Stahlbetonelementen, Vol. 268, ETH Zurich, 2001.
- [22] J. R. Deluce, F. J. Vecchio, ACI Structural Journal 2013, 110.

## ***Chapter 4. Tensile behaviour and tension stiffening concept for RC, FRC, and R-UHPFRC elements***

This chapter contains the 3<sup>rd</sup>, 4<sup>th</sup> and 5<sup>th</sup> published paper and discusses the tensile behaviour of R-UHPFRC elements and describes the tension stiffening concept for R-UHPFRC tensile elements and present the experimental behaviour of the UHPFRC ties behaviour under serviceability conditions. This chapter also presents a comparison between the inverse analysis method and experimental results. In this chapter, the deformation behaviour of R-UHPFRC tensile elements under serviceability conditions is provided and the effect of fibre content on the post-cracking tensile stiffness capacity of R-UHPFRC tensile elements are described. In this chapter, the importance of the shrinkage effect on the tension contribution of the UHPFRC in tension is described as well.

**3<sup>th</sup> PAPER**

Details:

---

Type of paper	Journal article
Title	<i>Tensile behaviour of reinforced UHPFRC elements under serviceability conditions</i>
Authors	<u>Majid Khorami</u> Juan Navarro-Gregori Pedro Serna Ros
Journal	Materials and Structures
Publisher	Springer
ISSN	1871-6873 / 1359-5997
JIF	3.428 (2020)
Quartiles	Q1, Civil and Structural Engineering, Material Science
Status	Published
Date	Accepted: 16 January 2021 Available online: 10 February 2021
Full reference	Khorami, M., et al. (2021). "Tensile behaviour of reinforced UHPFRC elements under serviceability conditions." Materials and structures 54(1): 43.

---

**3<sup>th</sup> Paper. Tensile behaviour of reinforced UHPFRC elements under serviceability conditions**

M. Khorami<sup>1,2</sup>, J. Navarro-Gregori<sup>1</sup>, P. Serna<sup>1</sup>

<sup>1</sup>: Institute of Science and Concrete Technology, ICITECH, Universitat Politècnica de València, València, 46022, Spain.

<sup>2</sup>: Facultad de Arquitectura y Urbanismo, Calle Rumipamba s/n y Bourgeois, Universidad UTE, Quito, Ecuador

**Correspondence**

J. Navarro-Gregori

Email: [juanagre@cst.upv.es](mailto:juanagre@cst.upv.es)

**Abstract**

Tension stiffening is an essential effect that influences the behaviour of concrete structures under serviceability conditions, mainly regarding crack control and deflection behaviour. Serviceability conditions can be studied experimentally by running the so-called uniaxial tensile test. This paper reports extensive experimental research conducted to study the tensile behaviour of reinforced Ultra-High Performance Fibre-Reinforced Concrete (R-UHPFRC) under service conditions by uniaxial tensile testing. The parameters studied were the reinforcement ratio and the steel fibre content in a experimental programme including 36 specimens. Special testing equipment and methodology to measure the post-cracking deformation of R-UHPFRC ties were developed, and special attention was paid to the shrinkage effect. The tensile elements' axial stiffness was approximately parallel to the bare bar response after microcracking formation showing a full tension-stiffening response. The average tensile capacity of the reinforced elements (tension stiffening response) was achieved. Concrete's contribution in the R-UHPFRC ties with the tensile properties deriving from four-point bending tests (4PBTs) on non-reinforced UHPFRC specimens was also compared. The experimental results revealed a slight increase in concrete's contribution with the higher reinforcement ratio. Moreover, the concrete's contribution in the tensile elements was higher than the characteristic tensile properties deriving from 4PBTs.

**Keywords:** reinforcement, serviceability, tensile elements, tension stiffening, UHPFRC.

## **1. Introduction**

For modern constructions and current demands for constructing buildings, some requirements like durability, functionality and aesthetics are important. These requirements are becoming an important key aspect for structural design, and most design codes include mandatory provisions in terms of serviceability conditions. The fundamental requirements associated with serviceability are functionality, user comfort and appearance [1]. However, as these requirements cannot be directly verified, performance criteria like deflection control, vibration control and cracking control are defined to meet these requirements [2]. In other words, serviceability in reinforced concrete structures refers to behaviour upon working loads with particular references made to deflections and cracking. In many structural design situations, and practically in systems such as houses and medium-sized commercial buildings, acceptable structure performance is seldom defined by ultimate limit states, but is controlled by serviceability requirements.

The tensile behaviour of reinforced concrete elements is closely related with the bond property between concrete and the embedded rebars. At a cracked section, the tensile force is mainly carried out by the rebar. However, due to the bond stresses between the rebar and the concrete interface, a fraction of the tensile force is transferred between cracks by the concrete. This effect is termed tension stiffening. In the case of reinforced concrete, the major fraction of the tensile force is carried out by the rebar, and therefore the residual concrete stress at the crack drops to zero rapidly. This effect is termed tension softening and can be characterized by the fracture energy obtained under the tensile stress-crack width relationship. Under serviceability conditions the most important effect that governs the global tensile behaviour is only the tension stiffening effect. On the contrary, UHPFRC provides a significant residual tensile stress in the crack due to the bridging effect of the fibres. Thus, the sum of both tension stiffening and tension softening effects will govern the R-UHPFRC global tensile behaviour. For the sake of simplicity, the combination of both effects together (tension stiffening and tension softening) is expressed as “tension stiffening” in this paper.

Serviceability verifications are, to some extent, complex to apply because of the cracking phenomenon, tension stiffening, shrinkage, and creep effects. According to the tension stiffening effect, concrete can carry tension between cracks in the reinforced concrete member, which helps to control not only member deformation, but also crack spacing, crack width and the formation of multiple cracks. Consequently, if the reinforced concrete member exhibits major tension stiffening, this effect helps to meet serviceability requirements [3-5].

Crack control in reinforced concrete structures is generally achieved by limiting



the increase of the stress in steel reinforcement to an appropriate value that never reaches its yield stress. Many structural concrete design codes specify maximum steel reinforcement stress after cracking and maximum crack width such as [6].

The design serviceability aspects for reinforced UHPFRC structures are not included in CEB-FIP Model Code 2010 (MC2010) [6] and are barely considered in UHPFRC codes or recommendations, such as French code NF P18-470 [7], Japanese standard and guideline JSCE concrete Committee [8], or Swiss standard fprSIA 2052 [9], among others. Thus, research in this area is still required as less knowledge is acquired in UHPFRC structures than that acknowledged in RC constructions. By way of example, the French code NF P 18-710 [7] indicates that it is not necessary to perform the control of cracking for strain hardening UHPFRC (T3). However, for the strain softening UHPFRC (T1 and T2) it provides an expression for the calculation of the crack widths in reinforced UHPFRC elements, which includes explicitly both the tension-softening and tension-stiffening effects. On the other hand, the Swiss standard fprSIA 2052 [9] indicates that the verification under serviceability conditions must be carried out by limiting the maximum tensile concrete stresses. For example, in the case of sections under bending forces, the concrete tensile stress is limited to the 90% of the characteristic value of the elastic tensile strength  $f_t$  in strain-hardening concretes (UA and UB), while this limitation is reduced to 70% for strain-softening concretes (U0). There is a disparity of criteria when verifying service conditions. Thus, research in this area is still required as less knowledge is acquired in UHPFRC structures than that acknowledged in RC constructions.

In analysis approaches, in which the average stresses and strains used to predict the concrete member behaviour, such as smeared finite elements, truss modelling or a layered beam section analysis, the tension stiffening effect plays a main role and needs to be included in such analyses [10-12]. These types of analysis approaches require a convenient material model for cracked concrete, and the suitable tension stiffening relations for obtaining the stress-strain response of the cracked concrete member. Many constitutive models have been proposed to predict the post-cracking behaviour of conventional reinforcement concrete (RC) [13-17] and fibre-reinforced concrete (FRC) [18-22].

To predict the structural behaviour of UHPFRC concrete members, simple models to represent the tensile behaviour of UHPFRC material are required. Inverse analysis methods can be used to derive the tensile material properties from the load-deflection response obtained from four-point bending tests (4PBTs) [23-26]. In line with this, a new inverse analysis method based on deflection to curvature transformation has been proposed to determine the tensile properties of UHPFRC in the authors' previous research [27, 28]. It remains unclear whether it is possible to also use the tensile properties that directly derive from inverse analysis methods in the analysis of reinforced UHPFRC structures under serviceability conditions.

The present study focuses on the behaviour of reinforced UHPFRC ties under serviceability conditions. The experimental programme consisted of 36 prismatic tensile elements classified into six series with varying reinforcement ratios and two concrete types with different fibre contents. The tension stiffening response and concrete's contribution to the overall response of tensile elements, including the shrinkage effect, were obtained. The influence of the steel fibre content and the reinforcement ratio on tension stiffening under service loads was also studied. Finally, concrete's contribution was compared to the tensile properties deriving from the characterisation tests done using 4PBTs.

## **2. Experimental programme**

The experimental program was developed to carry out the uniaxial tensile test applied to the R-UHPFRC elements [29]. Tensile elements with a square cross-section and one central reinforcement bar along its longitudinal length were prepared. The complete details of specimens are offered in Section 2.2. The experimental programme aimed to characterise the tension stiffening effect of R-UHPFRC elements and to compare it with the tensile properties obtained from bending tests in specimens without reinforcement [27]. The parameters related to fibres, such as type, content and fibre length, affect UHPFRC properties. Therefore, the influence of each factor on the mix design of concrete should be considered. This study focused on how fibre content influenced tensile behaviour under Serviceability Limit State (SLS) loads. However, the influences of the reinforcement ratio and section dimensions are also presented to provide a comprehensive conclusion. Therefore, the main parameters for this study were section size, reinforcement diameter and fibre content. The test-measured parameters were tensile elongation and tensile force. The test procedure and measurement equipment are explained in Section 2.3. Finally, a study was done to take into account the shrinkage effect.

### **2.1. Mixture proportion and material properties of UHPFRC**

The test programme was conducted with two concrete mixture types that only vary in fibre content terms. The fibre dosage 160 kg/m<sup>3</sup> (concrete C1) and 80 kg/m<sup>3</sup> (concrete C2) were used in this study. The bases of the mixture proportion and aggregate properties were as in previous research conducted by the authors [29, 30]. These chosen dose values were based on both resistant and moderate economic cost criteria. The main components of the mixtures were cement, silica fume, silica flour, fine sand and medium sand. The mix proportion is described in Table 1. The cement used in the experimental programme is Portland cement, obtained from a local plant, and it is classified as CEM I 42.5 R-SRS, with properties according to specification EN 197-1:2011. Its compression strength was

52.5 MPa on the 28th day according to the supplier. The silica sand specific gravity was  $2.61 \text{ g/cm}^3$ , and two size ranges were used. The fine sand and the medium sand were 0.5 and 0.6-1.2 mm in size. With its small grain size, silica fume and silica flour fill the space in between cement grains, and improve the density and reduce the porosity of UHPFRC [31]. Small steel fibres were herein used with a diameter of 0.2 mm, a length of 13 mm, and a tensile strength beyond 2,000 MPa strength.

Table1: Mix proportions of UHPFRC for concrete types C1 and C2-units content ( $\text{kg/m}^3$ ).

Medium sand 0.6–1.2 mm	Fine sand 0.5 mm	Silica flour U- S500	Silica fume (Elkem Microsilica, grade 940)	Cement	Superplasticiser	Water	Fibre content	
565	302	225	175	800	30	160	Concrete type (C1) $V_f=2\%$	160
							Concrete type (C2) $V_f=1\%$	80

A standard horizontal pan mixer was used. Firstly, the dry ingredients, the medium and fine silica sands, silica flour, silica fume and cement were mixed for approximately 1 min. Next water and the superplasticiser were added, and the materials were mixed for 10 min until a homogeneous mixture was obtained and the dry powder mix became a wet paste concrete. The small straight steel fibres were slowly spread by hand into the wet concrete paste in the mixer. The concrete was further mixed for 5 min to ensure proper fibre dispersion. Finally, the fresh UHPFRC material was cast into standard prismatic and cube specimen moulds. As the superplasticizer was used, the concrete did not need to undergo vibration. The specimens from both mixes were cured for 24h at laboratory temperature ( $25\pm 2^\circ\text{C}$ ) before demoulding. All of the specimens were placed in a high-humidity curing room at 95% relative humidity and temperature of  $T = 20\pm 2^\circ\text{C}$  for 28 days.

Six batches were prepared for each concrete type. Four cubic specimens (100 mm), two 150 diameter by 300 mm cylinders and two prismatic specimens ( $500\times 100\times 100 \text{ mm}$ ) for the compressive strength test, Young's modulus test and flexural characterization test were taken from each batch. The average, among all batches, compression strength values of UHPFRC were obtained, which were 154.0 MPa (CV=4.3%) and 139.2 (CV=7.0%) MPa for concrete types C1 and C2, and the average Young's modulus values were 48.4 (CV=1.1%) GPa and 46.5 (CV=1.1%) GPa. Concrete type C1 generally shows a higher modulus of elasticity compared to concrete type C2, but this difference is not significant. Beigi et al. [32], Li [33], and Edgington [34] indicated that using fibres has no significant

influence on the Young’s modulus of concrete, especially with a low fibre content.

The tensile properties of the herein used concrete were obtained by carrying out the 4PBTs and applying an inverse analysis method, which was proposed by the authors in a previous research project [27]. The prismatic specimens were tested under flexural loading. Fig. 1a, and 1b present the test results including the average and characteristic values obtained.

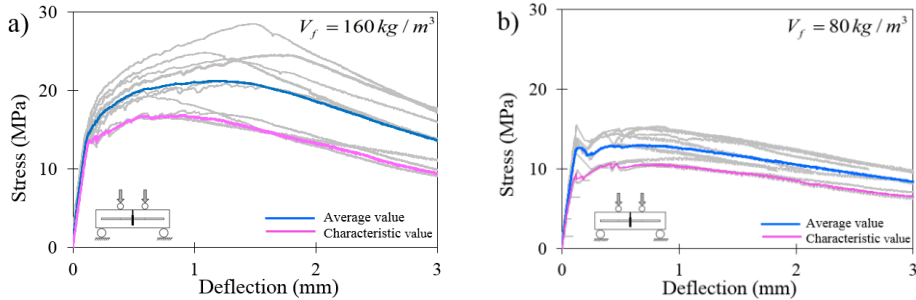


Figure 1: Tensile stress - midspan deflection for 4-PBTs: (a) concrete C1 and (b) concrete C2.

The inverse analysis method was applied to derive constitutive UHPFRC behaviour. The constitutive  $\sigma - \varepsilon$  law of UHPFRC can be described with four parameters [27, 28]: cracking strength ( $f_i$ ), strain at cracking strength ( $\varepsilon_{i,el}$ ), ultimate tensile strength ( $f_{t,u}$ ) and its corresponding strain ( $\varepsilon_{t,u}$ ). In Table2, the average and characteristic tensile properties are presented.

Table 2: UHPFRC tensile properties per batch.

Constitutive Relation Model Parameters	$f_i$ (MPa)	$\varepsilon_{i,el}$ (‰)	$f_{t,u}$ (MPa)	$\varepsilon_{t,u}$ (‰)
C1 ( $V_f=160 \text{ kg/m}^3$ )				
Values of characteristic results	7.65	0.17	6.79	4.95
Average result value	9.41	0.18	8.49	6.56
C2 ( $V_f=80 \text{ kg/m}^3$ )				
Values of characteristic results	4.82	0.11	4.48	1.57
Average result value	6.41	0.13	5.81	1.98

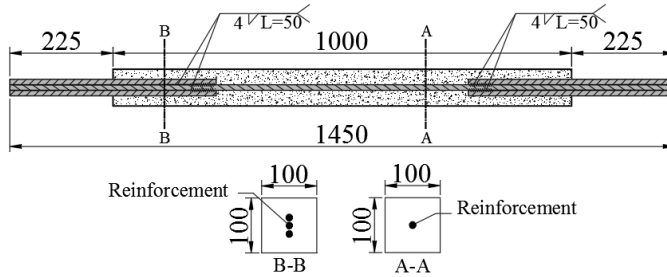
## 2.2. Specimen preparation

Specimens were made to take a prismatic shape that had a square cross-section with a central rebar. Element length was 1,000 mm, and the rebar was extended 225 mm from both ends. Two complementary rebars were welded to the main rebar (length of 450 mm) to be able to connect the concrete specimen to the steel jaws. In this experimental study, three different cross-section sizes (60, 80, and 100 mm) and two steel reinforcement rebar diameters ( $\text{Ø}10$  and  $\text{Ø}12$ ) were used to consider the reinforcement ratio effect on R-UHPFRC behaviour. The nominal yield stress of rebars was 500 MPa. Three specimens were cast for every group of section size and rebar diameter. Thirty-six specimens were tested in the experimental programme. The IDs of the specimens were as follows  $\phi xx Fxxx Sxx - \#$ , where ( $\text{Ø}$ ) is the rebar diameter in millimetres, (F) is the fibre content in  $\text{kg}/\text{m}^3$ , (S) is the section size in millimetres, and (#) is the number of specimens of each group (see Table 3). Specimen details are shown in Fig. 2a.

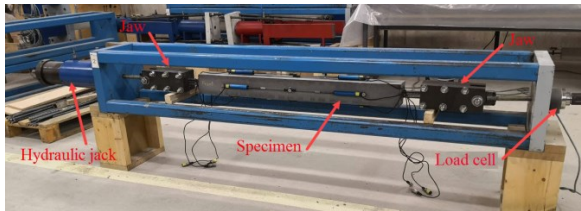
Table3: Description of test specimens

Concrete type and fibre content				Section Size	Rebar diameter	$\rho$ (%)	Cover (mm)
C1 ( $V_f = 160\text{kg} / \text{m}^3$ )		C2 ( $V_f = 80\text{kg} / \text{m}^3$ )					
Concrete batch number	Specimen ID	Concrete batch number	Specimen ID				
3	$\text{Ø}10\text{F}160\text{S}60\text{-}1$	3	$\text{Ø}10\text{F}80\text{S}60\text{-}1$	60×60 mm <sup>2</sup>	$\text{Ø}10$	2.18	25
2	$\text{Ø}10\text{F}160\text{S}60\text{-}2$	3	$\text{Ø}10\text{F}80\text{S}60\text{-}2$				
5	$\text{Ø}10\text{F}160\text{S}60\text{-}3$	4	$\text{Ø}10\text{F}80\text{S}60\text{-}3$				
6	$\text{Ø}12\text{F}160\text{S}60\text{-}1$	5	$\text{Ø}12\text{F}80\text{S}60\text{-}1$		$\text{Ø}12$	3.13	24
6	$\text{Ø}12\text{F}160\text{S}60\text{-}2$	5	$\text{Ø}12\text{F}80\text{S}60\text{-}2$				
2	$\text{Ø}12\text{F}160\text{S}60\text{-}3$	6	$\text{Ø}12\text{F}80\text{S}60\text{-}3$				
6	$\text{Ø}10\text{F}160\text{S}80\text{-}1$	6	$\text{Ø}10\text{F}80\text{S}80\text{-}1$	80×80 mm <sup>2</sup>	$\text{Ø}10$	1.23	35
3	$\text{Ø}10\text{F}160\text{S}80\text{-}2$	6	$\text{Ø}10\text{F}80\text{S}80\text{-}2$				
3	$\text{Ø}10\text{F}160\text{S}80\text{-}3$	5	$\text{Ø}10\text{F}80\text{S}80\text{-}3$				
2	$\text{Ø}12\text{F}160\text{S}80\text{-}1$	4	$\text{Ø}12\text{F}80\text{S}80\text{-}1$		$\text{Ø}12$	1.77	34
5	$\text{Ø}12\text{F}160\text{S}80\text{-}2$	4	$\text{Ø}12\text{F}80\text{S}80\text{-}2$				
3	$\text{Ø}12\text{F}160\text{S}80\text{-}3$	4	$\text{Ø}12\text{F}80\text{S}80\text{-}3$				
1	$\text{Ø}10\text{F}160\text{S}100\text{-}1$	3	$\text{Ø}10\text{F}80\text{S}100\text{-}1$	100×100 mm <sup>2</sup>	$\text{Ø}10$	0.79	45
2	$\text{Ø}10\text{F}160\text{S}100\text{-}2$	5	$\text{Ø}10\text{F}80\text{S}100\text{-}2$				
1	$\text{Ø}10\text{F}160\text{S}100\text{-}3$	3	$\text{Ø}10\text{F}80\text{S}100\text{-}3$				
1	$\text{Ø}12\text{F}160\text{S}100\text{-}1$	1	$\text{Ø}12\text{F}80\text{S}100\text{-}1$		$\text{Ø}12$	1.13	44
2	$\text{Ø}12\text{F}160\text{S}100\text{-}2$	1	$\text{Ø}12\text{F}80\text{S}100\text{-}2$				
1	$\text{Ø}12\text{F}160\text{S}100\text{-}3$	2	$\text{Ø}12\text{F}80\text{S}100\text{-}3$				

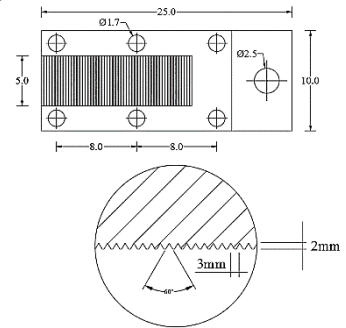
a)



b)



c)



d)

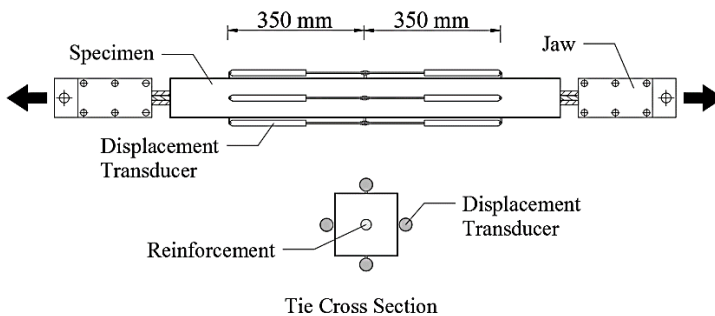


Figure 2: Uniaxial tensile test equipment: a) Specimen reinforcement details, b) test setup and installed specimen; c) jaw details, d) Position of displacement transducers.

### 2.3. Experimental test setup

A novel test system for performing the uniaxial tensile test has been proposed [30]. The proposed test system and method were suitable for carrying out the

experimental test of the R-UHPFRC ties under SLS loads. To apply the tensile force to the concrete specimen, a proposed connection system was used, which included two-piece steel jaws with 2 mm-high indented corrugations assembled by six bolts. The main steel test frame, hydraulic jack, installed specimen and jaw details are shown in Fig. 2b, and 2c. A load cell was placed between the main plate and the end of the anchored rebar to measure force values.

Specimens were tested under manual displacement control at a rate of approximately 0.5 mm/min. Eight displacement transducers (DTs) were installed on the specimen surfaces (four to the right and four to the left of the specimen) to record element elongation during the test, and to capture any bending applied to the specimen due to unforeseen load eccentricities. The length of each DT was 350 mm, and was attached from the centre of specimens to the ends. The position of the installed DTs is shown in Fig. 2d.

### 3. Experimental results of the R-UHPFRC ties

#### 3.1. Tensile stress-strain behaviour

The experimental method aimed to obtain the average tensile strains and stresses carried by reinforcement and UHPFRC under service loads. The element's total tensile elongation was calculated by the average value recorded by DTs installed on the left and right sides of the specimen (Fig. 2d). It was assumed that the surface deformations of concrete with steel rebar deformation were equal. The test results are presented with the stress-strain curve format insofar as the horizontal axis presents the average tensile strain ( $\epsilon_{sm}$ ) obtained by the mean elongation recorded by DTs with units *mm / m* (%), and the vertical axis shows the total applied force in the tensile element (N) expressed in terms of equivalent concrete tensile stress ( $\sigma_{eq,c}$ ) or equivalent steel stress ( $\sigma_{eq,s}$ ) as follows:

$$\sigma_{eq,c} = \frac{N}{A_c}; \quad A_c = A - A_s$$

$$\sigma_{eq,s} = \frac{N}{A_s} = \rho \cdot \sigma_{eq,c} \quad (1)$$

where ( $A_s$ ) is the cross-sectional area of reinforcement, ( $A$ ) is the element's cross-sectional area, and  $\rho = A_s/A_c$  is the reinforcement ratio.

#### 3.2. Tensile response

The tensile response of all the specimens with concrete types C1 and C2 is shown in Fig. 3a, and 3b. Each curve represents the average result of three specimens

(same section size and rebar diameter). Tensile elongation was measured at the test start time (after the curing and storage times). This means that the results shown in Fig. 3 do not take into account the shrinkage effect occurred so far. The shrinkage effect is discussed in Section 4.3. Diagrams were labelled with reinforcement ratios ( $\rho$ ) and ( $\rho/D$ ) to evaluate the influence of the reinforcement ratio and diameter on the tensile elements' general behaviour.

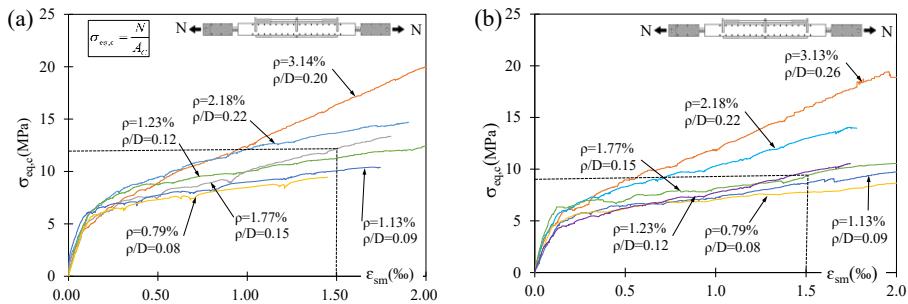


Figure 3: Tensile response of the R-UHPFRC elements: (a) concrete C1 and (b) concrete C2.

## 4. Analysis of the results

### 4.1. Effect of the steel fibre content

The fibre content considerably influenced the tensile properties of UHPFRC. An efficient method to improve the tensile performance of UHPFRC was to increase the amount of fibres in order to increase both tensile strength and toughness. Accordingly, this research aims to investigate the effect of fibre content on the mechanical properties of the two UHPFRC types used: C1 (160 kg/m<sup>3</sup>) and C2 (80 kg/m<sup>3</sup>).

The increase of the tensile strength was observed by comparing the results obtained for two identical R-UHPFRC ties; e.g., for a given tensile strain (1.5%), the tensile strength for tensile elements types C1 and C2 with a reinforcement ratio of 1.77% were 12.14 and 9 MPa (see Fig. 3), respectively, where shows enhanced tensile capacity. However, the tensile elements with concrete type C1 showed a higher slope in the elastic region.

Energy absorption is a parameter used to evaluate a material's toughness, which is the material's inherent property that describes the nature of the material to break. Therefore, one way to measure toughness is to calculate the total area under the stress-strain curve with a uniaxial tensile test. In the present study, this concept was applied to define the energy capacity of the tensile elements. Hence in order to evaluate the influence of fibre content on the tensile response of the R-UHPFRC



ties, energy absorption (toughness) is calculated as the area under the stress-strain curve, which is herein called energy absorption capacity. Therefore, the area between both curves can be defined as the Increase of Energy Absorption (IEA) due to the fibre content difference.

Figs. 4a to 4f show the tensile stress-strain behaviour of the specimens with identical properties in section size and reinforcement ratio terms for both concrete types. Each curve presents the average behaviour curve of three identical specimens. The IEA capacity (the area between two curves) shows that the cracked specimens with  $160 \text{ kg/m}^3$  present more toughness than those ones with  $80 \text{ kg/m}^3$ . The average IEA value for all the specimens herein included came close to 21.4%. This increase of the capacity and the improvement in post-cracking behaviour were due to greater fibre bridging over the cracks caused by an additional number of fibres [35, 36]. The obtained result indicated that using a high-fibre dose for the R-UHPFRC ties did not remarkably influence the cracked specimen's energy absorption capacity. So, from an economic point of view, employing the double fibre dose in R-UHPFRC ( $160$  and  $80 \text{ kg/m}^3$  in this case study) only improved tensile capacity by 21.4% on average. However, the cracking behaviour (crack opening and spacing) of the tensile elements under SLS load and durability performance could lead to a more marked improvement.

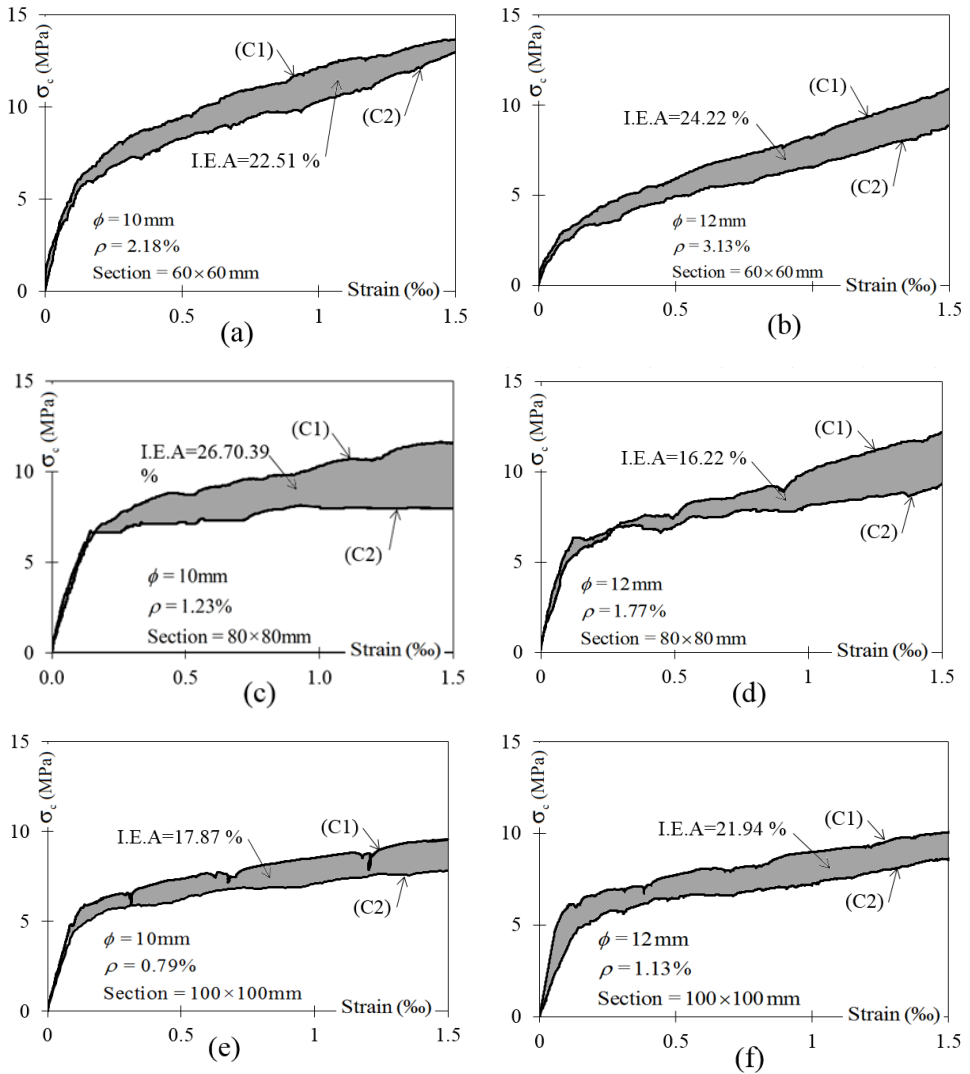


Figure 4: Increment of Energy Absorption (IEA) due to fibre content increment from 80 to 160  $\text{kg/m}^3$ .

#### 4.2. Effect of the reinforcement ratio and rebar diameter

The typical load-strain diagram of a R-UHPFRC tie obtained from the uniaxial tensile test can be described as a bilinear curve with a parabolic part in the interaction zone, as shown in Fig. 5.

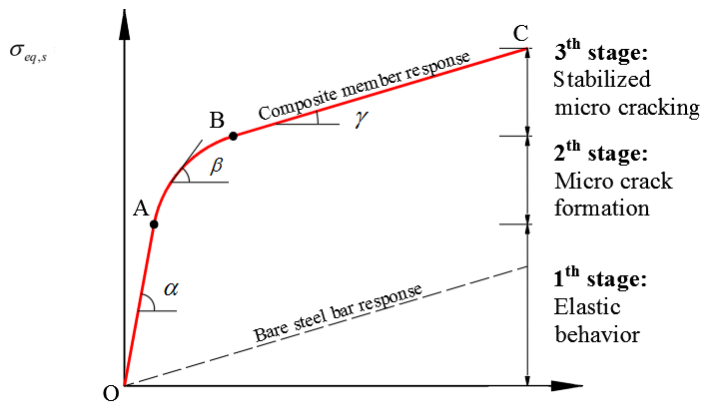


Figure 5: Load-deformation response of R-UHPFRC tensile element

The deformation behaviour consists of three stages. The first stage presents the elastic behaviour up until microcracking starts (part OA). The second stage (part AB) refers to microcracking formation. In this stage, cracks are very thin, and it is difficult to see them by the naked eye. Additionally, most of the cracks in this stage are internal cracks and cannot reach the specimen surface. In the microcracking stage, element stiffness sharply reduces (refer to the curve slope:  $\beta$ ) by increasing deformation. At the end of microcracking (point B), the crack pattern starts to become stable, and a full crack pattern develops (part BC).

The overall tensile response in the crack stabilisation stage (3<sup>rd</sup> stage) of the RC and FRC ties gradually approaches the bare bar due to the deterioration of the bond surrounding the reinforcement. Given the high bond property of UHPFRC with the reinforcement, the tensile response remains parallel to the bare bar and presents a high tension capacity for the cracked specimen.

One of the most important parameters involved with the cracked specimen's stiffness is the reinforcement ratio and reinforcement diameter. By observing the tension stress-strain relation obtained from the tensile elements (Figs. 3a and 3b), the effect of the aforementioned parameters on tensile deformation behaviour is clearly revealed. The cracked specimen's stiffness (slope of the overall response in the stabilised microcracking stage), which refers to ( $\gamma$ ), was evaluated in this study. To do so, slope ( $\gamma$ ) was calculated for all the specimens in the third stage

between points B and C. To apply the same criteria to calculate the slope of the curve for all the specimens, two reference points at deformations 0.3‰ and 1.5‰ were chosen (points M and N), where the response curve came close to linear behaviour, as shown in Fig. 6. The main points of the tension response curve obtained from the test results for all the specimens are presented in Table 4a and 4b.

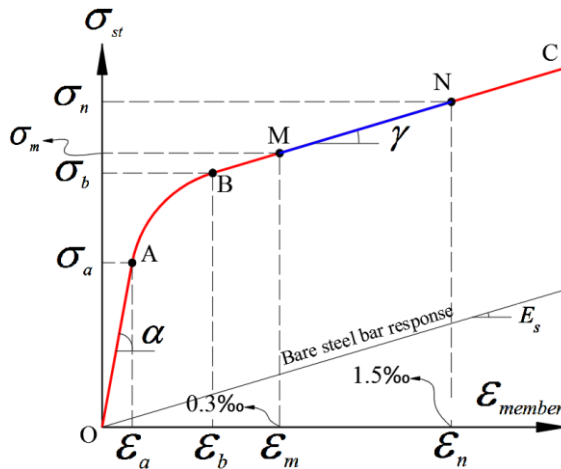


Figure 6: Slope calculation criteria of the tensile response in the stabilised microcracking stage.

The start point of microcrack formation (point A) was chosen as the point of the change in the slope of the curve. The elastic tensile stiffness of reinforced UHPFRC ( $\alpha$ ) was calculated by dividing the  $(\sigma_a)$  by  $(\epsilon_a)$ . The average proportion of elastic tensile stiffness value for concrete types C1 and C2 ( $\alpha_{c1} / \alpha_{c2}$ ) calculated for identical specimens was 1.13, which shows that the increased fibre volume ( $V_f = 1\%$  to  $V_f = 2\%$  in this study) had no significant influence on the elastic tensile stiffness of R-UHPFRC. However, the incorporation of the steel fibres into the concrete matrix improved the bond-slip between the matrix and reinforcement, and increased the elastic stiffness of the UHPFRC ties according to [33, 34, 37].

Table 4.a: Stress-strain relation curve of the tensile elements for concrete C1 and C2.

Specimen ID	$\sigma_a$ (MPa)	$\varepsilon_a$ (‰)	$\alpha$ (GPa)	$\sigma_b$ (MPa)	$\varepsilon_b$ (‰)	$\gamma$ (GPa)
Concrete type C1 ( $V_f = 160 \text{ kg / m}^3$ )						
Ø10F160S60-1	340.97	0.14	2384.41	412.92	0.27	235.23
Ø10F160S60-2	228.27	0.13	1783.36	299.84	0.26	201.22
Ø10F160S60-3	237.44	0.13	1855.00	316.97	0.27	172.89
Ø12F160S60-1	91.38	0.05	1791.76	190.00	0.24	224.34
Ø12F160S60-2	134.92	0.14	992.06	185.41	0.25	232.75
Ø12F160S60-3	155.80	0.09	1832.94	244.69	0.25	234.05
Ø10F160S80-1	520.00	0.11	4727.27	707.00	0.30	245.00
Ø10F160S80-2	512.00	0.15	3413.33	628.00	0.30	185.83
Ø10F160S80-3	483.00	0.15	3220.00	623.00	0.30	218.33
Ø12F160S80-1	279.00	0.09	3100.00	372.00	0.27	241.67
Ø12F160S80-2	339.00	0.15	2306.12	460.00	0.30	240.00
Ø12F160S80-3	222.00	0.07	3171.43	318.00	0.27	219.17
Ø10F160S100-1	603.27	0.09	6703.00	809.81	0.23	230.21
Ø10F160S100-2	643.37	0.10	6433.70	819.18	0.21	209.70
Ø10F160S100-3*	-	-	-	-	-	-
Ø12F160S100-1	458.98	0.10	4413.27	560.92	0.23	215.83
Ø12F160S100-2	448.64	0.08	5340.95	563.35	0.24	218.98
Ø12F160S100-3	536.02	0.13	4254.13	611.95	0.20	212.54
CV (%)	46.96	27.07	49.74	43.04	12.31	8.90
Average	366.71	0.11	3395.46	477.83	0.26	219.87
Concrete type C2 ( $V_f = 80 \text{ kg / m}^3$ )						
Ø10F80S60-1	232.13	0.11	2210.76	298.03	0.24	214.60
Ø10F80S60-2	244.81	0.12	2003.36	338.73	0.30	209.55
Ø10F80S60-3*	-	-	-	-	-	-
Ø12F80S60-1	143.09	0.11	1266.28	202.45	0.24	224.10
Ø12F80S60-2	144.74	0.13	1130.78	208.65	0.30	234.82
Ø12F80S60-3*	-	-	-	-	-	-
Ø10F80S80-1	281.44	0.08	3518.00	364.56	0.30	78.34
Ø10F80S80-2	350.67	0.12	2922.25	393.51	0.27	59.43
Ø10F80S80-3*	-	-	-	-	-	-
Ø12F80S80-1	267.77	0.07	3771.41	308.27	0.21	183.18
Ø12F80S80-2	285.95	0.10	2749.52	381.41	0.30	116.50
Ø12F80S80-3	363.22	0.12	3078.14	419.50	0.30	98.02

Table 4.b: Continue of Table 4.a, Stress-strain relation curve of the tensile elements for concrete C1 and C2.

Ø10F80S100-1	574.00	0.09	6377.78	734.22	0.30	202.32
Ø10F80S100-2	551.71	0.11	5254.38	749.80	0.30	177.58
Ø10F80S100-3	601.88	0.12	4853.87	748.93	0.30	200.55
Ø12F80S100-1	364.92	0.11	3475.43	457.04	0.30	194.34
Ø12F80S100-2	459.93	0.11	4181.18	523.20	0.28	233.73
Ø12F80S100-3	267.19	0.10	2754.54	348.00	0.22	247.89
CV (%)	42.65	15.36	43.79	42.08	11.59	40.45
Average	342.23	0.11	3303.18	431.75	0.28	438.82

\*These tests failed due to the sliding rebar in the steel jaw.

The stiffness of the cracked R-UHPFRC ties is related to the bridging effect provided by fibres and reinforcement. To evaluate this effect, the variations in ( $\gamma$ ) according to the reinforcement ratio ( $\rho$ ) obtained for the two concrete types are shown in Fig. 7.

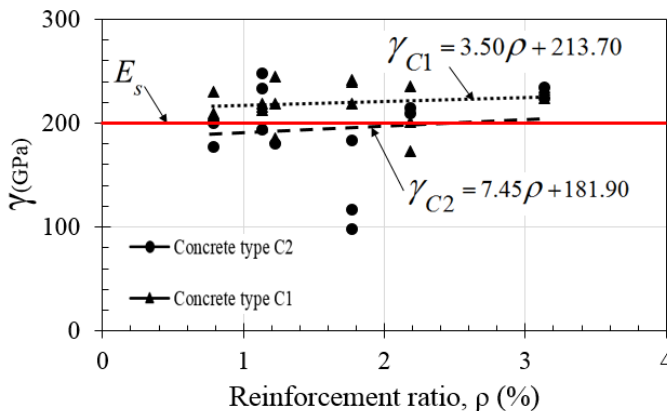


Figure 7: Influence of the reinforcement ratio ( $\rho$ ) on the tensile behaviour response.

The two trend lines obtained for all the specimens for concretes C1 and C2 are nearly parallel. The cracked R-UHPFRC specimens with a higher fibre content show more axial tension stiffness. This increment can be observed as an offset distance between the two trend lines  $\gamma_{c1}$  and  $\gamma_{c2}$  whose value is 31.80 GPa (the increment percentage is 14.80%).

The trend lines for concrete types C1 and C2 ( $\gamma_{c1}$  and  $\gamma_{c2}$ ) come very close to the axial stiffness of the bare bar with a value of  $E_s = 200 \text{ GPa}$ . (refer to the red line

in Fig. 7). This means that in the third stage, the overall response is almost parallel to the bare bar response. It is worth mentioning that the same experimental tensile response for the R-UHPFRC elements with the parallel curve response by the bare bar response has been observed in the experimental results of other authors [30, 38-42].

### 4.3. Tension stiffening effect and shrinkage influence

The cracked concrete elements can carry tension between cracks due to the reinforcing bar's bond behaviour. This ability is called the tension stiffening effect, which increases the element's stiffness before reinforcement yields [19]. Tension stiffening is important for studying the load-deformation characteristic of the reinforced concrete members within the post-cracking range and to calculate crack widths under service loads. In the R-UHPFRC specimens, fibres carry remarkable tensile forces at a crack and effectively increase tension stiffening. Thus, the tension stiffening effect is an essential parameter in structural elements designed under SLS conditions because it controls deflections, crack width and crack spacing.

Eurocode 2 [43] indicates that in order to verify the serviceability limit state, the shrinkage effect should be taken into account. Parameters like temperature, curing conditions, mixture properties, material properties and element geometry are involved in the shrinkage strain [44]. However, the high shrinkage strain of UHPFRC needs to be paid special attention for members under tensile stresses. Fig. 8.a and 8b are a qualitative representation of the mean stress-strain curve and tension stiffening response of a R-UHPFRC member, respectively. The shrinkage effects on the tensile response and tension stiffening response are shown. Fig. 8a depicts the stress-strain response in the rebar, while Fig. 8b illustrates the response of concrete.

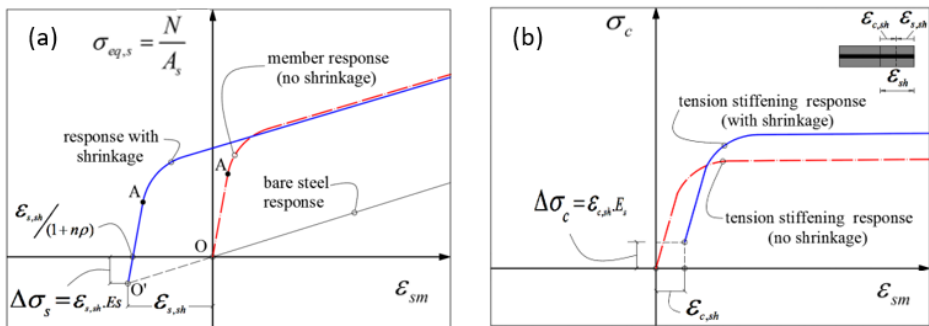


Figure 8: Shrinkage effect on the response of the R-UHPFRC tie: a) average stress-strain curve; b) tension stiffening response.

Creep is a time-dependent characteristic of concrete that causes strains under constant load or stress to increase with time. The effect of creep is usually considered using the concrete effective modulus ( $E_{c,eff}$ ):

$$E_{c,eff} = \frac{E_c(t_0)}{1 + \varphi(t, t_0)} \quad (2)$$

where  $\varphi(t, t_0)$  is the creep coefficient, which is used to measure the capacity of concrete to creep. The concrete effective modulus can be better evaluated with the modified creep coefficient by applying the relaxation factor [45] or ageing coefficient [46]  $\chi(t, t_0)$ . The coefficient  $\chi$  can be estimated at 0.80 for UHPFRC [47]. Hence, the above equation can be written as:

$$E_{c,eff} = \frac{E_c(t_0)}{[1 + \chi(t, t_0)\varphi(t, t_0)]} \quad (3)$$

Several design recommendations and guidelines for UHPFRC suggest values for the creep coefficient. The French code for UHPFRC [47] and Australian design guidelines [48] recommend a creep coefficient of 0.30 for specimens subjected to a standard thermal cure. The creep effect is always present when dealing with shrinkage. Severe creep strains can result in serviceability problems. Hence the equations for calculating the shrinkage effect should include the creep effect. Nevertheless, the creep effect is not considered within the scope of this paper. This effect should be studied in detail in future research by considering parameters such as cement type, water-cement ratio, concrete strength, relative humidity, temperature effect or size effect among others.

UHPFRC shrinkage would shorten the UHPFRC member without reinforcement, while the embedded reinforcement in the member would restrain shrinkage. It would also lead to a negative “pre-strain” ( $\varepsilon_{s,sh}$ ) with a compressive stress in the steel rebar ( $\Delta\sigma_{s,sh}$ ), and to an initial tensile strain in UHPFRC ( $\varepsilon_{c,sh}$ ) with a tensile stress ( $\Delta\sigma_{c,sh}$ ). Hence the real origin of the mean stress-strain relation would be point O', as shown in Fig. 8a. The matrix of UHPFRC would be already in tension, even without considering the effects of external actions. Thus, the microcracking load level (point A) lowered. The tension stiffening response curve should be modified due to the shrinkage effect by increasing the tension stress caused by shrinkage ( $\Delta\sigma_{c,sh}$ ) and by increasing the concrete tensile strain ( $\varepsilon_{c,sh}$ ).

In this study, we used the equation proposed by Swiss standard fprSIA 2052 code [9, 49] for calculating the free shrinkage ( $\varepsilon_{sh}$ ) magnitude for UHPFRC as follows:

$$\varepsilon_{sh}(t) = \varepsilon_{U_{300}} \cdot e^{\frac{c}{t+d}} \quad (4)$$



where the values of coefficients are  $c=-2.48$  and  $d=-0.86$ , and the age of concrete ( $t$ ) is expressed as days. The fprSIA 2052 [9] admits that the maximum value for free UHPFRC shrinkage is  $\varepsilon_{U_{frc}} = 0.6 - 0.8\text{‰}$ .

Intensive verification tests have been carried out to verify the validity of Eq. 4 at ICITECH facilities. The experimental programme for shrinkage evaluation consisted of three UHPFRC ties with an identical cross-section size ( $80 \times 80$  mm), whereas the steel reinforcement diameter was increased with diameters  $\text{Ø}10$  mm,  $\text{Ø}12$  mm and  $\text{Ø}16$  mm. Accordingly, the longitudinal reinforcement ratio increased by the values of 1.24%, 1.80% and 3.24%. Specimens were cast with UHPFRC with the  $160 \text{ kg/m}^3$  fibre content. Three strain gauges were attached to the steel reinforcement to measure the rebar compression strain at the middle and the one-third of each specimen extreme. The average recorded value was used as the compression strain caused by free UHPFRC shrinkage. The measurement process started immediately after casting specimens. Test specimens were cured at room temperature for the first 24 h prior to demoulding. After demoulding, all the specimens were cured at  $20 \pm 2^\circ\text{C}$  and 100% relative humidity for 28 days. It is also worth mentioning that during and after storing specimens in the chamber, the measurement process took place. The average experimental values of the rebar compression strain caused by shrinkage ( $\varepsilon_{s,sh}$ ) after 40 days were 0.341‰, 0.401‰, and 0.411‰ for the specimens with a reinforcement rebar of  $\text{Ø}16$  mm,  $\text{Ø}12$  mm, and  $\text{Ø}10$  mm, respectively. Note that these values are the rebar strain, and it is necessary to apply the uncracked section theory and compatibility conditions to obtain the free shrinkage strain ( $\varepsilon_{sh}$ ).

The free shrinkage strain ( $\varepsilon_{ch}$ ) can be derived as the sum of the steel reinforcement strain and concrete strain:

$$\varepsilon_{sh} = |\varepsilon_{s,sh}| + \varepsilon_{c,sh} \quad (5)$$

Consequently, the stresses in the steel rebar and concrete caused by free shrinkage are:

$$\Delta\sigma_{s,sh} = \frac{E_s \cdot \varepsilon_{s,sh}}{1 + n \cdot \rho} \quad (6)$$

$$\Delta\sigma_{c,sh} = \frac{n \cdot \rho}{1 + n \cdot \rho} \cdot E_c \cdot \varepsilon_{s,sh} \quad (7)$$

where ( $n$ ) is the modular ratio (equals  $E_s / E_c$ ) and ( $\rho$ ) is the reinforcing steel ratio (equals  $A_s / A_c$ ). Dividing two sides of Eq. 6 to ( $E_s$ ) and extract ( $\varepsilon_{sh}$ ) leads to:

$$\varepsilon_{sh} = \varepsilon_{s,sh} \cdot (1 + n \cdot \rho) \quad (8)$$

By employing Eq. 8, the rebar compression strain caused by shrinkage is converted into the free shrinkage strain. Thus, the experimental free shrinkage strains are 0.388‰, 0.422‰ and 0.443‰ for specimens with a reinforcement rebar of Ø16 mm, Ø12 mm and Ø10 mm, respectively. The difference between the obtained results allows the conclusion that UHPFRC shrinkage is affected by the reinforcement ratio and cover thickness. E Fehling [38] proposed an expression for ( $\varepsilon_{c,sh}$ ) by considering shrinkage and creep when they develop similarly to each other as follows:

$$\varepsilon_{c,sh} = \frac{\varepsilon_{sh}(1+n\rho)}{1+n\rho(1+\chi\psi)} \quad (9)$$

where ( $\chi$ ) is the relaxation factor, which can be estimated with ( $\chi = 0.8$ ), and ( $\psi$ ) is the creep of UHPFRC.

The free shrinkage strain ( $\varepsilon_{sh}$ ) was also calculated by Eq. 4 at the age of 40 days taking the value 0.8‰ for  $\varepsilon_{L_{5\infty}}$ . The ( $\varepsilon_{sh}$ ) calculated value was 0.538‰, which shows a good agreement between the experimental result obtained and the expression proposed by fprSIA 2052 [9]. The following expressions can be used to calculate the tensile stress caused by shrinkage ( $\Delta\sigma_{c,sh}$ ) and the corresponding strain ( $\varepsilon_{c,sh}$ )

$$\Delta\sigma_{c,sh} = E_c \cdot \varepsilon_{c,sh} ; \varepsilon_{c,sh} = \frac{\varepsilon_{sh} \cdot n \cdot \rho}{1+n\rho} \quad (10)$$

The average experimental value of UHPFRC Young's modulus ( $E_c = 47\text{ GPa}$ ), and ( $E_s = 200\text{ GPa}$ ) were used to calculate the initial tensile stress caused by shrinkage for both concrete types. The free shrinkage strain ( $\varepsilon_{sh}$ ) and the corresponding tensile stress and strain caused by shrinkage ( $\Delta\sigma_{c,sh}$ ,  $\varepsilon_{c,sh}$ ) calculated by Eq. 4 are provided in Table 5.

Table 5: Shrinkage effect on tension stiffening response (Eqs. 1 &amp; 2).

(Concrete age) t	$\mathcal{E}_{sh}$ (%)	Section size (mm)						
		60×60		80×80		100×100		
40 days	0.538	Reinforcement diameter (mm)						
		$\Delta\sigma_{c,sh}$ (MPa)	Ø 10	Ø 12	Ø 10	Ø 12	Ø 10	Ø 12
			2.19	3.07	1.27	1.80	0.82	1.17
		$\mathcal{E}_{c,sh}$ (%)	0.047	0.065	0.027	0.038	0.018	0.025
		$\Delta\sigma_{s,sh}$ (MPa)	98.31	94.58	102.23	99.98	104.13	102.64
		$\mathcal{E}_{s,sh}$ (%)	0.492	0.473	0.511	0.500	0.521	0.513

The tension stiffening response was obtained by subtracting the bare bar response from the average load carried by the cracked UHPFRC tensile element. The tension stiffening response was modified with the initial tensile strain in concrete ( $\mathcal{E}_{c,sh}$ ) and the initial tensile stress ( $\Delta\sigma_{c,sh}$ ) with the values presented in Table 5. The tension stiffening responses for UHPFRC with concrete types C1 and C2, including the shrinkage effect, are presented in Figs. 9a, and 9b. The reinforcement ratio increased from 0.79% to 3.13%. For the reinforcement ratio increment, the average tensile stress in UHPFRC increased from 7.5 to 9.5 MPa for concrete type C1 and from 6.0 to 8.2 MPa for concrete type C2. This increment in the tensile stress in UHPFRC can be related to the higher reinforcement ratio. Therefore, a slight increase of concrete's contribution with the higher reinforcement ratio was observed.

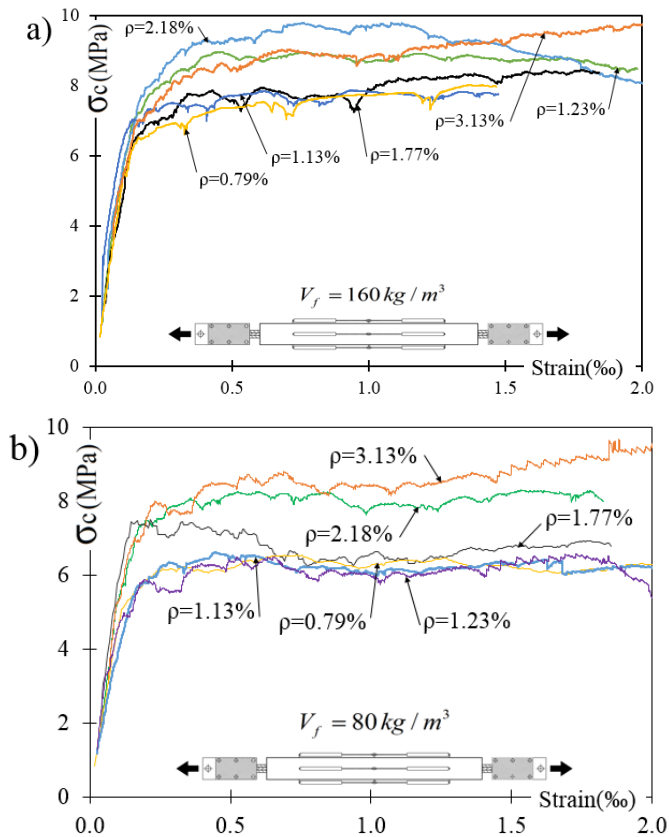


Figure 9: Concrete's contribution including the shrinkage effect, (a) concrete C1 and (b) concrete C2.

#### 4.4. Comparison between the constitutive model and the tension stiffening response

The tensile stress-strain response of UHPFRC is a fundamental constitutive property of this material, which is one of the most essential aspects of serviceability design and for predicting structural behaviour. Like the R-UHPFRC uniaxial tensile test, it is one of the most appropriate methods for determining the tensile properties of R-UHPFRC. Moreover, this method directly provides the tensile behaviour of reinforced UHPFRC members without having to resort to inverse analysis methodologies. However, the uniaxial tensile test for R-UHPFRC elements is challenging to perform and is very sensitive to several factors, such as boundary conditions, shrinkage effect, loading machine stiffness, specimen imperfection and eccentricity of reinforcement rebar, stress concentration and end effect [30, 50, 51]. On the contrary, determining the tensile properties of UHPFRC

can be easily done by running 4PBTs and using appropriate inverse analysis methods.

The tension stiffening response for all the specimens obtained from the R-UHPFRC ties was compared with the data of the 4PBT simplified inverse analysis results [27] by plotting both together in Figs. 10a, and 10b. The calculated parameters are presented in Table 2.

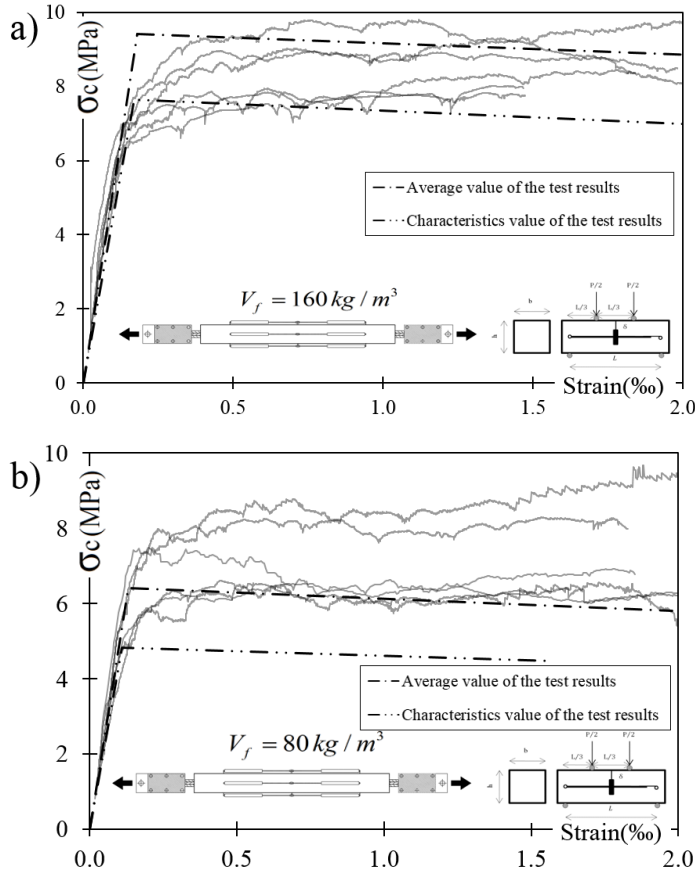


Figure 10: Comparison between the concrete's contribution and tensile properties from 4PBTs inverse analysis: a) concrete C1; b) concrete C2.

For the case of the R-UHPFRC specimens with  $160 \text{ kg/m}^3$  fibre content (Fig. 10a), a good match appears between the tension stiffening response obtained by the R-UHPFRC uniaxial tensile test and the results of the inverse analysis. Almost all the tension stiffening curves lie between the characteristic and average results of

the inverse analysis. The difference between the specimens' tension stiffening responses is due to the different cross-section sizes and rebar diameters, hence the reinforcement ratio effect. As a result, by using the obtained characteristic value, the proposed inverse analysis method exhibits a conservative response.

Based on the obtained experimental results, it was observed that the tensile contribution of the UHPFRC matrix for nearly all the 80 kg/m<sup>3</sup> specimens was located above the average tensile residual strength obtained by inverse analysis from bending tests (Fig. 10b). However, the tensile contribution of the UHPFRC matrix for the 160 kg/m<sup>3</sup> specimens was located between the characteristic and the average values (Fig. 10a). As a result, it can be stated that the fibres' efficiency in the specimens with 80 kg/m<sup>3</sup> is higher than in those with 160 kg/m<sup>3</sup>. However, future experimental work should be carried out to confirm the conclusion reached in these tests in a generalised way.

In any case, the UHPFRC concrete's contribution, for any reinforcement ratio and for both considered concrete types, is higher than the characteristic tensile properties derived from the 4PBT simplified inverse analysis.

It can also be seen in Fig. 10 that the scatter is lower for concrete C1. As a consequence of the stochastic nature of concrete cracking, there is often a significant scatter of experimental results. Therefore, the close-up comparison between the tensile properties obtained of 4PBTs and R-UHPFRC tensile elements may include some uncertainties regarding the test configuration, or the time-dependent properties of concrete such as shrinkage, creep or stress relaxation. Despite this, the dispersion obtained in the R-UHPFRC tensile elements is in a similar range to that obtained when deriving the tensile properties of 4PBT.

## **5. Conclusions**

The work herein presented provides a study on the behaviour of reinforced UHPFRC ties under serviceability conditions. To this end, the uniaxial tensile test programme, which consists of six series of tensile elements and two concrete types, was carried out. The studied parameters were the reinforcement ratio and fibre content. Tensile behaviour and the tension stiffening response were obtained and modified by considering the shrinkage effect. The tension stiffening response obtained from the tests was compared with the tensile properties obtained from the characterisation of the UHPFRC derived from 4PBT inverse analysis. The derived findings and conclusions are summarised as follows:

1. The overall response of the R-UHPFRC ties showed three well-defined stages for all the tested specimens: (1) elastic behaviour; (2) microcrack formation; (c) microcrack stabilisation. Moreover, no macrocrack formation was observed under the serviceability conditions.

2. The overall experimental response of the R-UHPFRC ties in the microcracking stabilisation stage was almost parallel to the bare bar response, with a nearly full tension stiffening response for both considered concrete types.
3. Increasing the fibre content in UHPFRC (80 kg/m<sup>3</sup> to 160 kg/m<sup>3</sup>) improved the energy absorption capacity of the cracked tensile element by approximately 21.4%. Thus, for UHPFRC structural applications, designers are recommended to evaluate whether the increase of the tensile response under service loads compensates using a larger fibre content.
4. Concrete's contribution has to be evaluated by taking into account the shrinkage effect. This effect significantly influences the internal stresses that both concrete and reinforcement exhibit, and has to be considered in the serviceability design.
5. A well-defined, but slight, increasing of the concrete's contribution with the increment in the reinforcement ratio was observed.
6. Concrete's contribution in the R-UHPFRC ties is higher than the characteristic tensile value derived from the inverse analysis in the 4PBTs.

**Acknowledgements.**

This study forms part of Project BIA2016-78460-C3-1-R, supported by the Ministry of Economy and Competitiveness of Spain.

**Funding** Project BIA2016-78460-C3-1-R, supported by the Ministry of Economy and Competitiveness of Spain.

**Code availability** Not applicable.

**Compliance with ethical standards**

**Conflicts of interest** Not applicable.

**Availability of data Material** Not applicable.

**References**

- [1] C. Burns, "Serviceability analysis of reinforced concrete based on the tension chord model," IBK Bericht, vol. 342, 2012.
- [2] D. Honfi, Design for Serviceability-A probabilistic approach. Lund

- University, 2013.
- [3] R. Sahamitmongkol and T. Kishi, "Tension stiffening effect and bonding characteristics of chemically prestressed concrete under tension," *Materials and structures*, vol. 44, no. 2, pp. 455-474, 2011.
  - [4] V. Gribniak, H. A. Mang, R. Kupliauskas, and G. Kaklauskas, "Stochastic tension-stiffening approach for the solution of serviceability problems in reinforced concrete: Constitutive modeling," *Computer-Aided Civil and Infrastructure Engineering*, vol. 30, no. 9, pp. 684-702, 2015.
  - [5] R. Muhamad, M. M. Ali, D. J. Oehlers, and M. Griffith, "The tension stiffening mechanism in reinforced concrete prisms," *Advances in Structural Engineering*, vol. 15, no. 12, pp. 2053-2069, 2012.
  - [6] J. C. Walraven, *Model Code 2010-Final draft: Volume 1*. fib Fédération internationale du béton, 2012.
  - [7] S. AFGC, "Bétons fibrés à ultra-hautes performances–Recommandations provisoires," AFGC, France, 2002.
  - [8] J. C. Committee, "Recommendations for design and construction of high performance fiber reinforced cement composites with multiple fine cracks," Japan Society of Civil Engineers, Tokyo, Japan, 2008.
  - [9] S. Cahier Technique, "Béton fibré ultra-performant (BFUP)-Matériaux, dimensionnement et exécution," *Projet*, 2014.
  - [10] A. Belarbi and T. T. Hsu, "Constitutive laws of concrete in tension and reinforcing bars stiffened by concrete," *Structural Journal*, vol. 91, no. 4, pp. 465-474, 1994.
  - [11] D. Z. Yankelevsky, M. Jabareen, and A. D. Abutbul, "One-dimensional analysis of tension stiffening in reinforced concrete with discrete cracks," *Engineering Structures*, vol. 30, no. 1, pp. 206-217, 2008.
  - [12] R. S. Stramandinoli and H. L. La Rovere, "An efficient tension-stiffening model for nonlinear analysis of reinforced concrete members," *Engineering Structures*, vol. 30, no. 7, pp. 2069-2080, 2008.
  - [13] M. P. Collins and D. Mitchell, *Prestressed concrete structures*. Prentice Hall Englewood Cliffs, NJ, 1991.
  - [14] G. Kaklauskas, "Integral constitutive model for deformational analysis of flexural reinforced concrete members," *Statyba*, vol. 7, no. 1, pp. 3-9, 2001.
  - [15] T. T. Hsu, *Unified theory of reinforced concrete*. Routledge, 2017.
  - [16] K. Fields and P. H. Bischoff, "Tension stiffening and cracking of high-strength reinforced concrete tension members," *Structural Journal*, vol. 101, no. 4, pp. 447-456, 2004.
  - [17] K. Patel, S. Chaudhary, and A. Nagpal, "A tension stiffening model for analysis of RC flexural members under service load," *Computers and Concrete*, vol. 17, no. 1, pp. 29-51, 2016.
  - [18] S.-C. Lee, J.-Y. Cho, and F. J. Vecchio, "Tension-Stiffening Model for Steel Fiber-Reinforced Concrete Containing Conventional Reinforcement," *ACI*



- Structural Journal, vol. 110, no. 4, 2013.
- [19] P. H. Bischoff, "Tension stiffening and cracking of steel fiber-reinforced concrete," *Journal of materials in civil engineering*, vol. 15, no. 2, pp. 174-182, 2003.
- [20] A. Amin, S. J. Foster, and M. Watts, "Modelling the tension stiffening effect in SFR-RC," *Magazine of Concrete Research*, vol. 68, no. 7, pp. 339-352, 2016.
- [21] J. R. Deluce and F. J. Vecchio, "Cracking Behavior of Steel Fiber-Reinforced Concrete Members Containing Conventional Reinforcement," *ACI Structural Journal*, vol. 110, no. 3, 2013.
- [22] P. Bernardi, E. Michellini, F. Minelli, and G. Tiberti, "Experimental and numerical study on cracking process in RC and R/FRC ties," *Materials and Structures*, vol. 49, no. 1-2, pp. 261-277, 2016.
- [23] F. Baby, B. Graybeal, P. Marchand, and F. Toutlemonde, "UHPFRC tensile behavior characterization: inverse analysis of four-point bending test results," *Materials and structures*, vol. 46, no. 8, pp. 1337-1354, 2013.
- [24] S.-C. Lee, H.-B. Kim, and C. Joh, "Inverse Analysis of UHPFRC Beams with a Notch to Evaluate Tensile Behavior," *Advances in Materials Science and Engineering*, vol. 2017, 2017.
- [25] F. Baby, B. A. Graybeal, P. Marchand, and F. Toutlemonde, "Identification of UHPFRC tensile behaviour: methodology based on bending tests," 2013.
- [26] F. Baby, B. Graybeal, P. Marchand, and F. Toutlemonde, "Proposed flexural test method and associated inverse analysis for ultra-high-performance fiber-reinforced concrete," *ACI Materials Journal*, vol. 109, no. 5, p. 545, 2012.
- [27] J. Á. López, P. Serna, J. Navarro-Gregori, and E. Camacho, "An inverse analysis method based on deflection to curvature transformation to determine the tensile properties of UHPFRC," *Materials and Structures*, vol. 48, no. 11, pp. 3703-3718, 2015.
- [28] J. A. López Martínez, "Characterisation of The Tensile Behaviour of UHPFRC by Means of Four-Point Bending Tests," 2017.
- [29] M. Khorami, J. Navarro-Gregori, P. Serna, and M. Navarro-Laguada, "A testing method for studying the serviceability behavior of reinforced UHPFRC tensile ties," in *IOP Conference Series: Materials Science and Engineering*, 2019, vol. 596, no. 1, p. 012022: IOP Publishing.
- [30] N. Lee and D. Chisholm, "Reactive Powder Concrete, Study Report SR 146," ed: Ltd. Judgeford, New Zealand, 2005.
- [31] M. H. Beigi, J. Berenjian, O. L. Omran, A. S. Nik, and I. M. Nikbin, "An experimental survey on combined effects of fibers and nanosilica on the mechanical, rheological, and durability properties of self-compacting concrete," *Materials & Design*, vol. 50, pp. 1019-1029, 2013.
- [32] V. C. Li, "Large volume, high-performance applications of fibers in civil

- engineering," *Journal of Applied Polymer Science*, vol. 83, no. 3, pp. 660-686, 2002.
- [33] J. Edgington, "Steel fibre reinforced concrete volume B," University of Surrey, 1973.
- [34] I. Löfgren, *Fibre-reinforced Concrete for Industrial Construction-a fracture mechanics approach to material testing and structural analysis*. Chalmers University of Technology, 2005.
- [35] V. Afroughsabet, L. Biolzi, and T. Ozbakkaloglu, "High-performance fiber-reinforced concrete: a review," *Journal of Materials Science*, vol. 51, no. 14, pp. 6517-6551, 2016.
- [36] T. E. T. Buttignol, J. Sousa, and T. Bittencourt, "Ultra High-Performance Fiber-Reinforced Concrete (UHPFRC): a review of material properties and design procedures," *Revista IBRACON de estruturas e materiais*, vol. 10, no. 4, pp. 957-971, 2017.
- [37] E. Fehling, M. Schmidt, J. Walraven, T. Leutbecher, and S. Fröhlich, *Ultra-high performance concrete UHPC: Fundamentals, design, examples*. John Wiley & Sons, 2014.
- [38] T. Makita and E. Brühwiler, "Tensile fatigue behaviour of Ultra-High Performance Fibre Reinforced Concrete combined with steel rebars (R-UHPFRC)," *International Journal of Fatigue*, vol. 59, pp. 145-152, 2014.
- [39] M. Rauch and V. Sigrist, "Dimensioning of Structures made of UHPFRC," in *IABSE Symposium Report, 2010*, vol. 97, no. 34, pp. 39-46: International Association for Bridge and Structural Engineering.
- [40] V. Sigrist and M. Rauch, "Deformation behavior of reinforced UHPFRC elements in tension," *Tailor Made Concrete Structures-Walraven & Stoelhorst* (eds), pp. 405-410, 2008.
- [41] D. Redaelli, "Testing of reinforced high performance fibre concrete members in tension," in *Proceedings of the 6th Int. Ph. D. Symposium in Civil Engineering, Zurich 2006*, 2006, no. CONF, p. 8: *Proceedings of the 6th Int. Ph. D. Symposium in Civil Engineering, Zurich 2006*.
- [42] B. S. Institution, *Eurocode 2: Design of concrete structures: Part 1-1: General rules and rules for buildings*. British Standards Institution, 2004.
- [43] V. Gribniak, G. Kaklauskas, and D. Bačinskas, "State-of-art review of shrinkage effect on cracking and deformations of concrete bridge elements," *Baltic Journal of Road & Bridge Engineering (Baltic Journal of Road & Bridge Engineering)*, vol. 2, no. 4, 2007.
- [44] E. Brühwiler, "Swiss Standard SIA 2052 UHPFRC: Materials, Design and Application," in *4th International Symposium on Ultra-High Performance Concrete and High Performance Materials*, 2016, no. POST\_TALK.
- [45] L. Ostergaard, R. Walter, and J. F. Olesen, "Method for determination of tensile properties of engineered cementitious composites (ECC)," *Proceedings of ConMat'05*, 2005.

- [46] T. Kanakubo, "Tensile characteristics evaluation method for ductile fiber-reinforced cementitious composites," *Journal of Advanced Concrete Technology*, vol. 4, no. 1, pp. 3-17, 2006.
- [47] J. López, P. Serna, J. Navarro-Gregori, and H. Coll, "Comparison between inverse analysis procedure results and experimental measurements obtained from UHPFRC Four-Point Bending Tests," in *Proceedings of the 7th RILEM Workshop on High Performance Fiber Reinforced Cement Composites (HPFRCC7)*, 2015, pp. 185-192.

**4<sup>th</sup> PAPER**

Details:

---

Type	Book chapter (BEFIB -RILEM Book series)
Title	<i>The Effect of Fiber Content on the Post-cracking Tensile Stiffness Capacity of R-UHPFRC</i>
Authors	<u>Majid Khorami</u> Juan Navarro-Gregori Pedro Serna Ros
Event	X RILEM-fib International Symposium on Fibre Reinforced Concrete (BEFIB) 2021
Publisher	Springer
ISSN	2211-0852 / 2211-0844
Quartiles	Q3, Civil and Structural Engineering, Building and Construction
Status	Published
Date	Accepted: 01 May 2020 Available online: 05 November 2020
Full reference	Khorami, M., et al. (2020). The Effect of Fiber Content on the Post-cracking Tensile Stiffness Capacity of R-UHPFRC. RILEM-fib International Symposium on Fibre Reinforced Concrete, Springer

---

**4<sup>th</sup> Paper. The Effect of Fiber Content on the Post-cracking Tensile Stiffness Capacity of R-UHPFRC**

M. Khorami<sup>1,2</sup>, J. Navarro-Gregori<sup>1</sup>, P. Serna<sup>1</sup>

<sup>1</sup>: Institute of Science and Concrete Technology, ICITECH, Universitat Politècnica de València, València, 46022, Spain.

<sup>2</sup>: Universidad UTE, Facultad de Arquitectura y Urbanismo, Calle Rumipamba s/n y Bourgeois, Quito, Ecuador

**Corresponding author:** J. Navarro-Gregori

Email: [juanagre@cst.upv.es](mailto:juanagre@cst.upv.es)

**Abstract**

Concrete cracking can be controlled by adding fibers to concrete, with the expected desirable behavior under serviceability conditions due to narrower close space cracks compared to similar concrete without fibers. Using fibers to produce Ultra-High Performance Fibre Reinforced Concrete (UHPFRC) has enhanced the post-cracking tensile capacity of composite material and increased the related energy absorption capacity for the cracked member. Accordingly, the amount and type of fiber in the matrix affect post-cracking behavior. In this experimental study, specimens reinforced by conventional steel rebars with a constant cross-sectional dimension and reinforced steel ratio were tested. The tested variables were: 1) type and length of fibers; 2) fiber content. The Direct Tensile Test was conducted, and the tensile behaviour of specimens was obtained. The results showed that the increment in fiber content (80 kg/m<sup>3</sup> to 160 kg/m<sup>3</sup> in this research) or the combination of micro- and macro-steel fibers with the same content (80 kg/m<sup>3</sup> for each fiber type) had no significant effect on the post-cracking stiffness capacity. Moreover, all the R-UHPFRC specimens provided the full tension stiffening with the quasi same post-cracking stiffness capacity close to the bare bar axial stiffness.

**Keywords:** tension stiffening, post-cracking tensile stiffness, serviceability, UHPFRC.

**1. Introduction**

In the structural concrete design, it is commonly assumed that reinforcement carries all tensile force at the crack face [1]. Away from the crack face, due to the bond between the steel rebar and the surrounding concrete, tensile stresses are

shared between the concrete and steel rebar. This contribution of concrete between cracks in tension is commonly termed tension stiffening. This phenomenon has an effect on member stiffness and is essential for determining serviceability deflection [2] and crack widths [3]. The tension stiffening response should be included in the analysis to predict member behaviour, under serviceability conditions.

The effects of cracking and reinforcement on member stiffness can be taken into account with effective axial member stiffness  $(EA)_{eff}$ . The effective modulus method is adopted by the fib Model Code 2010. It suggests an effective modulus for reinforcement  $(\bar{E}_b)$  and then the axial member response can be predicted using  $P = \bar{E}_b \cdot A_s \cdot \varepsilon_m$ . ( $A_s$  and  $\varepsilon_m$  are the reinforcing bar area and the average member strain, respectively). The load-strain relation and the effective modulus method to predict the member response are shown in Figure 1.

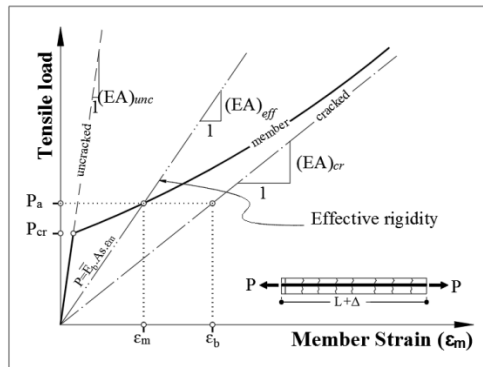


Figure 1: Load-strain relationship and effective modulus method (MC2010).

The presence of the fiber in the concrete leads to enhanced post-cracking behaviour and, as a result, improves the overall tensile response of the tensile elements. This improvement is due to the combination of tension stiffening and strain hardening mechanism. Strain hardening refers to the bridging effect and transmission of tensile stresses by fibers across crack faces, and tension stiffening refers to the bond behaviour of reinforcement and concrete [4].

Many theoretical and experimental studies have been performed to evaluate the fiber content effect on post-cracking behaviour at the material consideration level for FRC or UHPFRC [5-9], while real structural elements are combined by the reinforcement steel bar. Thus, studying post-cracking behaviour for these reinforcement elements is essential. In line with this, the present work focuses on the axial tensile stiffness of cracked tensile elements (herein called post-cracking tensile stiffness). The effect of fiber content was studied by employing three different doses and two types of fibers for UHPFRC and comparing to Ultra-High



Performance Concrete (UHPC). The average tension stress-strain of tensile elements was obtained. Post-cracking tensile stiffness was calculated by considering the tensile behaviour curve slope in the elastoplastic region of behavior. Finally based on the experimental results, the cracking behaviour and influence of fibers are also reported.

## 2. Experimental program

### 2.1. Materials

Four different types of UHPFRC were used in this study given the difference in fiber content and the type of steel fibers. Two types of steel fibers were considered in this study. The first type was high-strength micro-smooth steel fibers with a fine diameter ( $d_f = 0.2$  mm) and relatively short fiber length ( $L_f = 13 \pm 0.1$  mm). The second type was macrohooked end fibers (length  $L_f = 30 \pm 1$  mm and diameter  $d_f = 0.375$  mm). The geometry and parameters of the steel fibers are presented in Table 1.

Table 1: Properties of steel fibers

Fiber type	SF1=High-strength microsmooth steel fibers	SF2=Macrohooked end steel fibers
		
Fiber shape	straight	Hooked end
Length (mm)	13±1	30±1
Diameter (d)	0.2±0.04	0.375±0.04
Aspect ratio (L/d)	65	80
Tensile strength	>2000MPa	>2300MPa
Number of fibers per kg	77978	7801

The four types of UHPFRC were named as follows:

- (C160): the UHPFRC with fiber type (SF1) and fiber content of  $V_f = 2\%$  or  $160 \text{ kg/m}^3$ .
- (C80): the UHPFRC with fiber type (SF2) and fiber content of  $V_f = 1\%$  or  $160 \text{ kg/m}^3$ .
- (C8080): the UHPFRC with fiber type (SF1&SF2) and fiber content of  $V_f = 1\%$  for SF1, and  $V_f = 1\%$  for SF2.
- (C0): the UHPC without fibers.

The average compressive strength of UHPFRC and UHPC was determined at the tensile elements' testing age with four cube specimens ( $100 \times 100 \times 100$  mm). The resulting values are found in Table 2.

Table 2: UHPFRC and UHPC compressive strength.

Concrete type	$f_c$ (MPa)
C160	158.55
C80	151.42
C8080	142.59
C0	136.69

The matrix composition of UHPFRC herein used in all the concretes was based on our research group's previous experiences [10-14]. Table 3 provides the matrix composition of the employed UHPFRC and the UHPC matrix.

Table 3: Composition of the matrix mixture by the weight ratio for UHPFRC and UHPC

Cement (type I)	Medium Sand 0.6– 1.2 mm	Fine Sand 0.5 mm	Silica Flour U- S500	Silica fume (Elkem Microsilica, grade 940)	Superplasticizer	Water
1.00	0.70	0.37	0.28	0.22	0.037	0.20

## 2.2. Specimen geometry and test set-up

The uniaxial tensile tie test was carried out using prismatic concrete specimens with a 100x100 mm square cross-section and 1000±3 mm length. The tensile element was reinforced with a 12-mm central rebar ( $E_s = 200GPa$ ,  $f_y \approx 550MPa$ ). Ten specimens were cast for this study, six of them made with UHPFRC C160 and C80 (three for each type), and two specimens for each C8080 and C0. The uniaxial tensile test was conducted using a hydraulic jack machine with a loading capacity of 200 kN under displacement control at a loading rate of 0.5 mm/min. The complete details and testing procedure are available in M. Khorami et al. [15]. Figures. 2a and 2b show the test set-up and the R-UHPFRC tensile element.



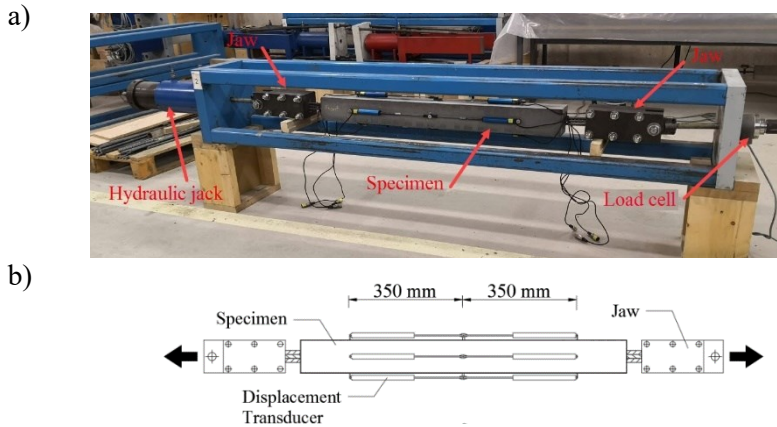


Figure 2: Uniaxial tensile test: (a) test set-up, (b) R-UHPFRC specimen

Eight displacement transducers (DTs) were installed on the surfaces of specimens (four of them on the right side and four on the left side of the specimen) to record element elongation during the test and to capture any undesired bending applied to the specimen due to unforeseen load eccentricities. Each DT measured the length variation between the fixing points placed with a 350 mm length from the center of specimens toward the ends (see Fig. 2b).

### 3. Test results and general discussion

#### 3.1. Tensile behavior

The average stress-strain curves obtained for each tensile element type are shown in Figures 3a to 3c. The tensile stress in reinforcement ( $\sigma_s$ ) was calculated by dividing the tensile load (N) by the reinforcement area ( $A_s$ ). The tensile elongation was measured when the test started and after curing and the storage time. The authors have studied the shrinkage effect on R-UHPFRC. UHPFRC shrinkage would shorten the member without reinforcement, while embedded reinforcement would restrain concrete shortening. This leads to a negative pre-strain ( $\epsilon_{s,sh}$ ) with compressive stress in the rebar, and initial tensile strain in the UHPFRC ( $\epsilon_{c,sh}$ ). Hence the real origin of the bare steel rebar response was modified by moving the compression strain value caused by shrinkage. The experimental value obtained for the reinforcement strain due to UHPFRC shrinkage was approximately ( $\epsilon_{s,sh} = 0.40\text{‰}$ ).

The cracking stress level at the interaction point between the fit line over the uncracked and cracked responses was defined. The slope of the elastoplastic region of the tensile behavior represents the post-cracking tensile stiffness for the R-UHPFRC tensile elements and was herein evaluated. The values calculated over

the average response of two or three specimens (red-colored curve) for each concrete are presented in Table 4 according to the criteria shown in Figure 4.

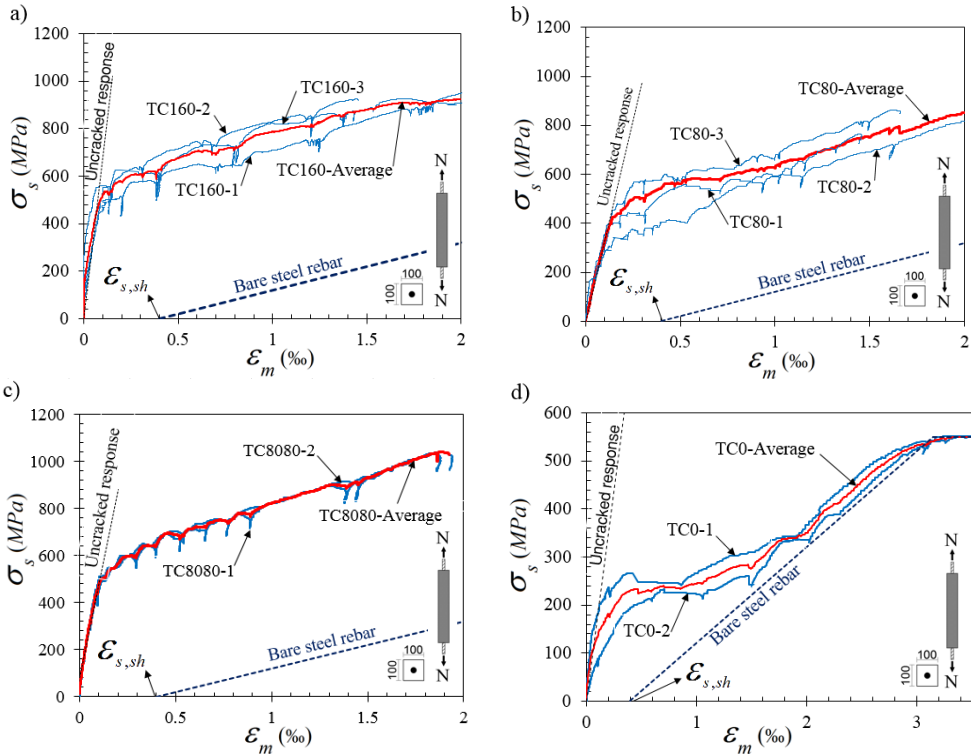


Figure 3: Average tensile response of tensile elements for four concrete types.

According to the obtained results (Table 4), the post-cracking tensile stiffness increased by a low value when increasing the fiber content when using the hybrid fibers for TC8080. Moreover, these values came very close to the axial stiffness of the bare bar with a value of  $E_s=200\text{GPa}$ . To better understand the influence of fiber content on post-cracking tensile stiffness and the difference between them, the stress-strain relations for four concrete types are presented together, as shown in Figure 5.

Table 4: Elastic tensile stiffness and post-cracking tensile stiffness.

Specimen ID	Stress in reinforcement at cracking $\sigma_{s,cr}(MPa)$	Stress in UHPFRC at cracking $\sigma_{c,cr}(MPa)$	Post-cracking tensile stiffness $\gamma(GPa)$
TC0	112.00	1.28	N.A
TC80	455.00	5.20	205.83
TC160	563.00	6.44	225.43
TC8080	591.00	6.76	237.59

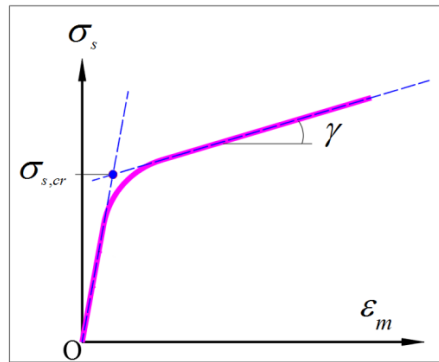


Figure 4: Criteria for calculating R-UHPFRC tensile response.

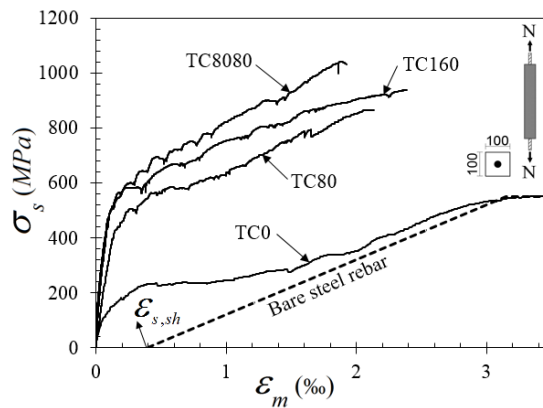


Figure 5: Tensile response of tensile elements with four concrete types.

As we can see, R-UHPFRC tensile elements TC160, and TC8080 almost have the same tensile cracking stress. Moreover, the post-cracking tensile stiffness for

all three types of R-UHPFRC tensile elements is in parallel to the bare bar response, while TC0 exhibits a very similar behavior to the tensile elements with conventional concrete (this finding is discussed in more detail in Section 4). By comparing the tensile response of TC80 with TC160, and TC8080, it can be concluded that if using a double fiber content is necessary (e.g. for the durability aspect of UHPFRC), employing the hybrid fiber for R-UHPFRC ( $80 \text{ kg/m}^3$  for the microsmooth steel fibers, plus  $80 \text{ kg/m}^3$  for the macrohooked end steel fibers) will present better tensile behavior on the one hand and, on the other hand, the employed steel fiber weight will be the same for both cases (TC8080 and TC160). The cracking behavior aspect and the influence of fiber on cracking propagation and crack width are discussed in Section 5.

#### **4. UHPFRC CONTRIBUTION IN TENSION**

The tension stiffening response refers to the tension carried by the concrete between cracks due to the reinforcing bar's bond behavior. This ability increases the element's stiffness before reinforcement yields and can be used to predict tensile behaviour, multiple crack spacing and crack widths.

Figure 6 is a qualitative representation of the tensile behavior of both R-UHPFRC and R-UHPC. The cracked R-UHPFRC tensile element exhibits constant contribution in tension, which refers to the parallel region of the behavior with the bare steel bar (called herein full tension stiffening), while the tension stiffening response for the UHPC tensile element after crack stabilization gradually decreases as the applied load increases, and the member response curve moves closer to the bare bar response. The bond factor parameter ( $\beta$ ) accounts for the variation in the concrete average tensile stress between cracks, and is generally expressed as an average tensile stress/cracking stress ratio. The bond factor value varies from zero to one for no bonded reinforcement and fully bonded, respectively ( $0 < \beta < 1$ ).

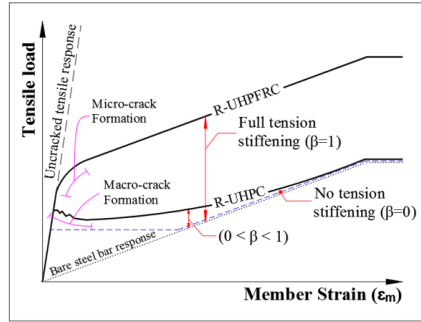


Figure 6: Qualitative representation of the tensile behavior of the R-UHPFRC and R-UHPC elements, full tension stiffening concept.

The R-UHPFRC tensile elements (TC80, TC160, and TC8080) exhibit the full tension stiffening with Beta values equalling one (see Fig. 5). This R-UHPFRC property is essential when the serviceability state is evaluated, especially for deflection control. Consequently, the high-tension stiffening capacity of R-UHPFRC leads to good performance under serviceability conditions and affirms the use of this material for special structures in which durability or permeability of concrete elements is essential.

For modeling the post-cracking tensile response of RC or FRC members, an empirical relation is needed to represent the gradual transition from the uncracked axial response to the fully cracked member (bare steel bar). An alternative approach to predict the post-cracking tensile response consists in using an effective axial stiffness  $(EA)_{eff}$  for the cracked member, which depends on the member's strain level. According to the fib Model Code 2010, the average strain of the RC or FRC member ( $\varepsilon_m$ ) is calculated by taking into account the tension stiffening effect, and can be calculated by the average reinforcement strain ( $\varepsilon_b$ ) minus the average concrete strain ( $\Delta\varepsilon_c$ ):

$$\varepsilon_m = \varepsilon_b - \Delta\varepsilon_c \quad (1)$$

As the  $(\Delta\varepsilon_c)$  is variable for the RC and FRC tensile members, the R-UHPFRC tensile elements provide a constant tension stiffening effect. Hence post-cracking tensile modeling and the deflection calculation may involve less complexity.

## 5. CRACKING BEHAVIOR

### 5.1. Fiber content effect

The crack distribution along the entire length element was determined to evaluate the crack behavior of the tensile elements. The number of cracks was obtained at

the end of the test when the average tensile strain reached 2‰. Water was used to wet the surface so that microcracks would be visible given the narrow width of cracks, which could not be seen by the naked eye, and the crack pattern was painted on the specimen surface. The number of cracks was recorded on each lateral surface at two surface edges over the red line (see Fig. 7) and the average number of cracks was calculated. The cracking measurement approach is shown in Figure 7.

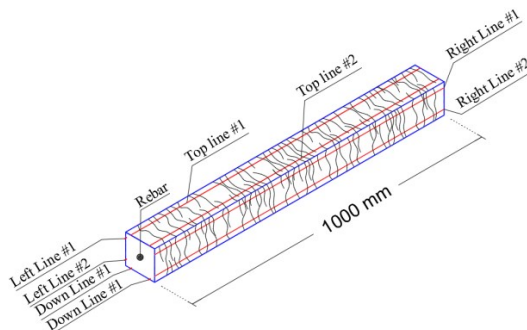


Figure 7: Cracking measurement approach of the R-UHPFRC ties elements.

It is worth mentioning that the R-UHPC tensile element exhibited a completely different cracking behavior with the localized macrocracks and wide crack spacing, while the R-UHPFRC ties provided a distributed crack propagation along the entire tie length.

The average crack width ( $w_m$ ) was calculated by dividing the total tension elongation ( $\varepsilon_t \times l$ ) to the total number of cracks ( $n$ ) as follows:

$$w_m = (\varepsilon_t \times l) / n \quad (2)$$

where ( $\varepsilon_t$ ) is the average tensile strain at the time the number of cracks was measured (2‰), and ( $l$ ) is tie length, which is 1000 mm. The parameter ( $n$ ) is the average number of the cracks. The obtained results are presented in Table 5.

Employing a high-dose fiber content for concrete causes higher bond strength and shorter transfer length [16]. Thus, crack spacing will narrow, and the number of cracks will increase. This phenomenon was observed when comparing the results for similar tensile elements with different UHPFRC types in fiber content terms.

In serviceability behavior terms, the multiple-cracking with the distributed crack propagation of R-UHPFRC led to very thin cracks (microcracks) at the high-tension strain ( $\varepsilon_m = 2‰$ ) in this study). The serviceability limit state can be controlled by applying limitations for the tensile stresses in reinforcement. These limitations are made to avoid inelastic strain, unacceptable cracking or deformation. Eurocode 2 indicates that the tensile stress in reinforcement cannot

exceed  $0.8f_{yk}$ , where  $f_{yk}$  is the characteristic yield strength of reinforcement.

Table 5: Average crack width at the tensile strain of 2‰.

Specimen ID	Total number of cracks	Average crack width Eq. (2) (mm)	Mean value (mm)
TC80-1	57	0.035	0.042
TC80-2	46	0.043	
TC80-3	43	0.047	
TC8080-1	63	0.032	0.028
TC8080-2	79	0.025	
TC160-1	137	0.015	0.014
TC160-2	113	0.018	
TC160-3	114	0.018	
TC0-1	9	0.220	0.200
TC0-2	11	0.181	

By comparing the mean crack width of TC160 to TC8080, it can be concluded that using microfibers led to a more efficient behavior compared to hybrid concrete (TC8080), and both cases were better than TC80. In addition, the microcracking process was better controlled in UHPFRC with  $160 \text{ kg/m}^3$  fiber content. From the serviceability perspective, the tensile elements with C160 exhibited better behavior than those with C8080 despite the steel fiber content being the same.

## 6. Conclusions

In the present study, the impact of fiber content on the axial post-cracking tensile stiffness capacity was studied by employing three UHPFRCs with fiber content and fiber type variation, and one type of non fiber UHPC. The uniaxial tensile test was conducted for tensile elements. Based on the experimental results, the following conclusive remarks are drawn:

- The reduction of the axial tensile stiffness for the R-UHPFRC specimens between the elastic region and microcrack stabilization region (the parallel zone of the behaviour with the bare bar response) rapidly happens. Moreover, during the applied tensile load, most microcracks appear at the same time in this region of behaviour.
- The tensile strength capacity in the cracking region depends on the fiber content of R-UHPFRC. However, the slope of the overall tensile behaviour of all the R-UHPFRC tensile elements (referring to the curve slope:  $\gamma$ ) almost parallels the bare bar response. Consequently, the R-UHPFRC tensile elements provide the full tension stiffening effect.
- Providing full tension stiffening for the R-UHPFRC members with a constant

value for concrete contribution for the cracked member leads to a facility of the computing deflection of reinforced members with UHPFRC, while for reinforced RC or FRC members an empirical model with descending branch after cracking is needed.

- Multiple cracking behaviour, and thus a large number of R-UHPFRC microcracks, emphasizes the high potential of UHPFRC composite material for structures in which durability and permeability aspects are essential. From the serviceability point of view, R-UHPFRC with a 2% microfibers content provides better behavior (crack width at a high rate of tensile strain) compared to the R-UHPFRC with hybrid fibers (1% of microfibers, plus 1% of macrofibers), while both contain the same fiber content.

## **ACKNOWLEDGMENTS**

This study forms a part of Project BIA2016-78460-C3-1-R supported by the State Research Agency of Spain.

## **REFERENCES**

- [1] P. H. Bischoff, "Reevaluation of deflection prediction for concrete beams reinforced with steel and fiber reinforced polymer bars," *Journal of structural engineering*, vol. 131, no. 5, pp. 752-767, 2005.
- [2] P. Visintin, D. Oehlers, R. Muhamad, and C. Wu, "Partial-interaction short term serviceability deflection of RC beams," *Engineering Structures*, vol. 56, pp. 993-1006, 2013.
- [3] P. H. Bischoff, "Tension stiffening and cracking of steel fiber-reinforced concrete," *Journal of materials in civil engineering*, vol. 15, no. 2, pp. 174-182, 2003.
- [4] P. Bernardi, R. Cerioni, and E. Michelini, "Analysis of post-cracking stage in SFRC elements through a non-linear numerical approach," *Engineering Fracture Mechanics*, vol. 108, pp. 238-250, 2013.
- [5] A. Kooiman and C. Walraven, "Modelling the post-cracking behaviour of steel fibre reinforced concrete for structural design purposes," *HERON*, vol. 45 (4), 2000, 2000.
- [6] N. Buratti, C. Mazzotti, and M. Savoia, "Post-cracking behaviour of steel and macro-synthetic fibre-reinforced concretes," *Construction and Building Materials*, vol. 25, no. 5, pp. 2713-2722, 2011.
- [7] A. Abrishambaf, J. A. Barros, and V. M. Cunha, "Relation between fibre distribution and post-cracking behaviour in steel fibre reinforced self-compacting concrete panels," *Cement and Concrete Research*, vol. 51, pp. 57-66, 2013.



- [8] E. Pereira, J. A. Barros, A. F. Ribeiro, and A. Camões, "Post-cracking behaviour of selfcompacting steel fibre reinforced concrete," 2004.
- [9] B. Zhou and Y. Uchida, "Relationship between fiber orientation/distribution and post-cracking behaviour in ultra-high-performance fiber-reinforced concrete (UHPFRC)," *Cement and Concrete Composites*, vol. 83, pp. 66-75, 2017.
- [10] J. López, P. Serna, J. Navarro-Gregori, and H. Coll, "Comparison between inverse analysis procedure results and experimental measurements obtained from UHPFRC Four-Point Bending Tests," in *Proceedings of the 7th RILEM Workshop on High Performance Fiber Reinforced Cement Composites (HPFRCC7)*, 2015, pp. 185-192.
- [11] J. Á. López, P. Serna, J. Navarro-Gregori, and E. Camacho, "An inverse analysis method based on deflection to curvature transformation to determine the tensile properties of UHPFRC," *Materials and Structures*, vol. 48, no. 11, pp. 3703-3718, 2015.
- [12] J. A. López Martínez, "Characterisation of The Tensile Behaviour of UHPFRC by Means ff Four-Point Bending Tests," 2017.
- [13] E. J. Mezquida-Alcaraz, J. Navarro-Gregori, J. A. Lopez, and P. Serna-Ros, "Validation of a non-linear hinge model for tensile behavior of UHPFRC using a Finite Element Model," *Computers and Concrete*, vol. 23, no. 1, pp. 11-23, 2019.
- [14] E. Mezquida-Alcaraz, J. Navarro-Gregori, and P. Serna-Ros, "Numerical validation of a simplified inverse analysis method to characterize the tensile properties in strain-softening UHPFRC," in *IOP Conference Series: Materials Science and Engineering*, 2019, vol. 596, no. 1, p. 012006: IOP Publishing.
- [15] M. Khorami, J. Navarro-Gregori, P. Serna, and M. Navarro-Laguarda, "A testing method for studying the serviceability behavior of reinforced UHPFRC tensile ties," in *IOP Conference Series: Materials Science and Engineering*, 2019, vol. 596, no. 1, p. 012022: IOP Publishing.
- [16] M. Harajli, B. Hamad, and K. Karam, "Bond-slip response of reinforcing bars embedded in plain and fiber concrete," *Journal of Materials in Civil Engineering*, vol. 14, no. 6, pp. 503-511, 2002.

**5<sup>th</sup> PAPER**

Details:

---

Type of paper	Conference paper
Title	<i>An Experimental Study on the Behavior of reinforced UHPFRC Ties Under Serviceability Conditions</i>
Authors	<u>Majid Khorami</u> Juan Navarro-Gregori Pedro Serna Ros
Congress	<i>VIII CONGRESO ACHE – SANTANDER 2022</i>
Date	20 <sup>th</sup> -22 <sup>th</sup> June, 2022
City	Santander (Spain)
Status	Accepted and presented
Full reference	M. Khorami, N.-G. Juan, and S. R. Pedro, "An Experimental Study on the Behavior of reinforced UHPFRC Ties Under Serviceability Conditions," vol. 73, pp. 1-9, 2022. Proceedings of the VIII Congress of ACHE - Santander

---

**5<sup>th</sup> Paper. An Experimental Study on the Behavior of Reinforced UHPFRC Ties Under Serviceability Conditions**

*Un Estudio Experimental Sobre el Comportamiento de Tirantes armados de HMAR bajo Condiciones de Servicio*

M. Khorami<sup>c,d</sup>, J. Navarro-Gregori<sup>a</sup>, P. Serna<sup>b</sup>

<sup>a</sup>: Associate Professor, Instituto de Ciencia y Tecnología del Hormigón (ICITECH), Universitat Politècnica de València

<sup>b</sup>: Professor, Instituto de Ciencia y Tecnología del Hormigón (ICITECH), Universitat Politècnica de València

<sup>c</sup>: Assistant Professor, Facultad de Arquitectura y Urbanismo, Universidad UTE, Quito, Ecuador

<sup>d</sup>: PhD candidate, Instituto de Ciencia y Tecnología del Hormigón (ICITECH), Universitat Politècnica de València

**Correspondence**

Majid Khorami

Email: [khoramimajid@gmail.com](mailto:khoramimajid@gmail.com)

**Abstract**

The study of tensile behaviour of Reinforced Ultra-High Performance Fibre-Reinforced Concrete elements (R-UHPFRC) is an essential aspect for the verification of Serviceability Limit State (SLS) crack and deflection control. This work presents the results of an experimental campaign of R- UHPFRC ties with different concrete matrices and reinforcement ratios. The tensile mechanical properties obtained in the reinforced elements are compared with those obtained from bending tests without reinforcement. The analysis of results reveals the importance of shrinkage in the response of the R-UHPFRC elements.

**Keywords:** bending test, serviceability, tie, UHPFRC.

**Resumen**

El estudio del comportamiento a tracción de los elementos armados de Hormigón de Muy Alto Rendimiento (R-HMAR) es un aspecto esencial para la verificación de los Estados Límite de Servicio (ELS) de fisuración y deformaciones. En este trabajo se presentan los resultados de una campaña experimental de tirantes R-HMAR con diferentes matrices de hormigón y cuantías de armado. Se comparan las propiedades

mecánicas a tracción obtenidas en los elementos armados con las obtenidas de probetas de flexo tracción sin armar. El análisis de resultados revela la importancia de la retracción en la respuesta de los elementos R-HMAR.

**Palabras Claves:** ensayo de flexión, servicio, tirante, R-HMAR.

## **1. Introduction**

The fundamental requirements associated with serviceability are functionality, user comfort, and appearance. However, these requirements cannot be verified directly; thus, performance criteria, such as deflection control, vibration control, and cracking control, are defined to meet these requirements [1]. In many structural design situations, practically in systems such as house and medium-sized commercial buildings, acceptable structure performance is seldom defined by ultimate limit states. Rather, it is controlled by serviceability requirements.

Serviceability calculation is complicated because of the cracking phenomenon, tension stiffening effect, shrinkage, and creep effects. Cracking control in reinforcement concrete structures is generally achieved by limiting the stress increment in steel reinforcement to an appropriately low value. Many concrete code designs specify maximum steel reinforcement stress after cracking and maximum crack width. The design serviceability aspects for Reinforced Ultra-High Performance Fiber-reinforced Concrete (R-UHPFRC) are not included in CEB-FIP Model Code 2010 (MC10) [2] and are poorly considered in UHPFRC codes or recommendations such as French standard and recommendations NF P18-470, AFGC [3] Japanese standard and guideline JSCE concrete Committee [4], and Switzerland technical notebook fprSIA 2052 [5]. Thus, research in this area is steadily growing.

To predict the structural behavior of UHPFRC concrete members, a simple model is required to represent the tensile behavior of the UHPFRC material. An inverse analysis method can be used to derive the tensile material properties from load-deflection response obtained from four-point bending tests (4PBTs) [6,7]. A new inverse analysis method based on deflection to curvature transformation to determine the tensile properties of UHPFRC was proposed in the previous research by authors [8,9]. In this research an uniaxial tensile R-UHPFRC tie test was conducted.

The experimental program included in this study consisted of nine series of prismatic tie elements with varying rebar diameters and cross-section dimensions and two different types of concrete in terms of fiber content. Finally, tension stiffening response under service loads was obtained, and compared with the tensile properties obtained from bending tests.

## 2. Experimental Program

### 2.1 Mixture proportion and mechanical properties of UHPFRC

Parameters related to fibers, such as type, content, and fiber length, affect the properties of UHPFRC. Therefore, the influence of each factor on the mix design of concrete must be considered. This study focuses on the influence of fiber content on the tensile behavior under SLS loads. However, the influences of reinforcement ratio and section dimensions are also presented to make a comprehensive conclusion.

The test program was conducted with two types of concrete mixtures that only vary in fiber content. Fiber dosages of 160 and 80 kg/m<sup>3</sup> were used in this study. The base of mixture proportion and aggregate characteristics were as previous research by authors [10]. The main components of the mixtures were cement, silica fume, silica flour, fine sand, and medium sand. The mix proportion is described in Table 1. The cement type was type I-sulfate resistant cement, and its compression strength was 42.5 MPa on the 28<sup>th</sup> day according to the supplier. The silica sand specific gravity was 2.61 g/cm<sup>3</sup>, and two size ranges were used. The fine and medium sand were 0.5 and 0.6–1.2 mm in size, respectively.

With its small grain size, silica fume fills the space in between cement grain and improves the density and reduces the porosity of UHPFRC [11]. Small steel fibers with a diameter length of 13 mm, and tensile strength beyond 2000 MPa were used in this study.

**Table 1.** Mix proportions of UHPFRC for concrete type C1 and C2-unit content (kg/m<sup>3</sup>)

Medium Sand 0.6–1.2 mm	Fine Sand 0.5 mm	Silica Flour U- S500	Silica fume (Elkem Microsilica, grade 940)	Cement	Superplasticizer	Water	Fiber	
565	302	225	175	800	30	160	Concrete type (C1)	160
							Concrete type (C2)	80

A standard horizontal pan mixer was used. First, the dry ingredients silica sand, cement, silica flour, and silica fume were mixed for approximately 1 min. Water and superplasticizer were then added, and the materials were further mixed for 10 min until a homogeneous mixture was obtained and the dry powder mix was transformed into a wet paste concrete. The small straight steel fibers were slowly spread by hand to the wet concrete paste in the mixer. The concrete was further mixed for 5 min to ensure the proper dispersion of fibers. Finally, the fresh UHPFRC material was cast into prismatic and cube standard specimen molds. Given that a superplasticizer was used, the concrete did not need to undergo vibration to remove entrapped air in the specimen molds. Specimens from both mixes were cured for 24 h at laboratory temperature (25 ± 2 °C) before demolding.

Thereafter, all of the specimens were placed in a high-humidity curing room at 95% relative humidity and temperature of  $T = 20 \pm 2$  °C until 2 or 3 days before testing.

Four cubic specimens ( $100 \text{ mm}^3$ ) were used to evaluate the average UHPFRC compression strength. The values were 152.97 and 142.95 MPa for concrete types C1 and C2, and the average Young's modulus values obtained by using two cylindrical specimens  $150 \times 300 \text{ mm}^2$  were 48.5 and 46.5 GPa. The nominal yield stress of steel rebars was  $f_y \approx 500$  MPa and the modulus of elasticity was  $E_s = 200$  GPa. The specimen description and concrete strength for each concrete type and concrete batch are presented in Table 2.

Table 2: Description of test specimens

Concrete Type and Fiber Content		Section Size	Rebar Size (mm)	$\rho$ (%)	Cover (mm)	Material Properties	
C1 ( $V_f = 160 \text{ kg/m}^3$ )	C2 ( $V_f = 80 \text{ kg/m}^3$ )					Compression Strength (MPa)	
Specimen Id	Specimen Id					$f'_c, C1$	$f'_c, C2$
d10F160S6-1-b3	d10F80S6-1-b3	60×60 mm <sup>2</sup>	Ø10	2.18	25	151.32	141.38
d10F160S6-2-b2	d10F80S6-2-b3					151.32	141.38
d10F160S6-3-b5	d10F80S6-3-b4 *					150.16	-
d12F160S6-1-b6	d12F80S6-1-b5		Ø12	3.13	24	154.41	147.12
d12F160S6-2-b6	d12F80S6-2-b5					154.41	147.12
d12F160S6-3-b2	d12F80S6-3-b6*					150.16	-
d16F160S6-1-b3*	d16F80S6-1-b6*		Ø16	5.58	22	-	-
d16F160S6-2-b3*	d16F80S6-2-b6*					-	-
d16F160S6-3-b4*	d16F80S6-3-b6*					-	-
d10F160S8-1-b6	d10F80S8-1-b6*	80×80 mm <sup>2</sup>	Ø10	1.23	35	150.16	-
d10F160S8-2-b3	d10F80S8-2-b6*					148.43	-
d10F160S8-3-b3	d10F80S8-3-b5*					148.43	-
d12F160S8-1-b2	d12F80S8-1-b4		Ø12	1.77	34	124.8	124.89
d12F160S8-2-b5	d12F80S8-2-b4					150.16	124.89
d12F160S8-3-b3	d12F80S8-3-b4					148.43	124.89
d16F160S8-1-b5	d16F80S8-1-b6*		Ø16	3.14	32	151.32	-
d16F160S8-2-b4	d16F80S8-2-b6*					149.39	-
d16F160S8-3-b4	d16F80S8-3-b5*					149.39	-
d10F160S10-1-b1	d10F80S10-1-b3	100×100 mm <sup>2</sup>	Ø10	0.79	45	166.67	148.25
d10F160S10-2-b2	d10F80S10-2-b5					150.16	148.25
d10F160S10-3-b1*	d10F80S10-3-b3					-	147.12
d12F160S10-1-b1	d12F80S10-1-b1		Ø12	1.13	44	151.32	148.25
d12F160S10-2-b2	d12F80S10-2-b1					166.67	148.25
d12F160S10-3-b1	d12F80S10-3-b2					166.67	166.67
d16F160S10-1-b1	d16F80S10-1-b1*		Ø16	2.01	42	151.32	-
d16F160S10-2-b2	d16F80S10-2-b1*					166.67	-
d16F160S10-3-b3	d16F80S10-3-b6*					166.67	-

\* These specimens are not yet tested.

The IDs of the specimens were as follows dxx Fxx Sxx-#-b#, where (dxx) is the rebar diameter in millimeters, (Fxx) is the fibre content in kg/m<sup>3</sup>, (Sxx) is the cross-section size in cm, (#) is the number of specimens of each group, and (b#) is the concrete batch number.

## 2.2 Specimen preparation and experimental test setup

The specimens were made in prismatic shape with square cross-section with a length of 1000 mm. In this experimental study, three different cross-section sizes (60, 80, and 100 mm) and three steel reinforcement rebar diameters (Ø10, Ø12, and Ø16) were used to consider the reinforcement ratio effect on the R-UHPFRC behavior. Three specimens were cast for every section and rebar size group.

Notably, not all of the specimens have been tested due to time limitations, large number of specimens, and challenges in direct tensile testing in the laboratory. Thus, this paper only discusses the test results obtained so far. Table 2 provides the main characteristics and details of R-UHPFRC ties.

### **2.3 Test procedure**

A novel test system for performing the tensile tie test has been proposed [10]. The proposed test system and method were suitable for the experimental test of R-UHPFRC ties under SLS loading. Two pieces of steel jaw were employed for applying the tension load to the 24 cm-length extended bars at each end of the specimen. The specimens were tested under manual displacement control at a rate of approximately 0.5 mm/min. Eight displacement transducers (DTs) were installed on the surfaces of the specimens to record element elongation during the test and capture any bending applied to the specimen due to unforeseen load eccentricities. The 35 cm-long DTs were used and attached from the center of specimens through at extremes. The average value of deformations recorded by DTs was used for rebar deformation by assuming that surface deformations of concrete with steel rebar reinforcement were equal. The main steel test frame, hydraulic jack, and installed specimen are shown in Fig. 1. A load cell was used to measure force values.

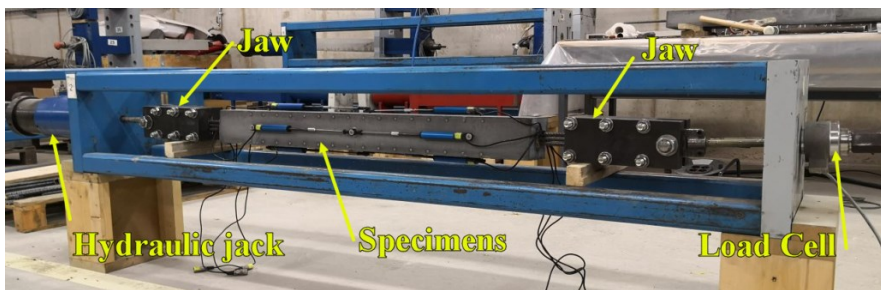


Figure 1: Test setup parts and installed specimen.

## **3. Tensile behavior of R-UHPFRC**

### **3.1 Tensile response**

The direct tensile behavior of all specimens with concrete types C1 and C2 is shown in Fig. 2a and 2.b. Each curve represents the average result (average of the tensile stress values) of three specimens tested with same cross-section size and rebar diameter under axial tensile load (the average values were calculated from three specimens with identical cross-section and rebar diameter). Stress is the



nominal stress obtained by uniaxial tensile force divided by concrete net-area. Note that these curves were labelled with reinforcement ratio ( $\rho=As/A_c$ ) and ( $\rho/D$ ), where ( $D$ ) is the rebar diameter.

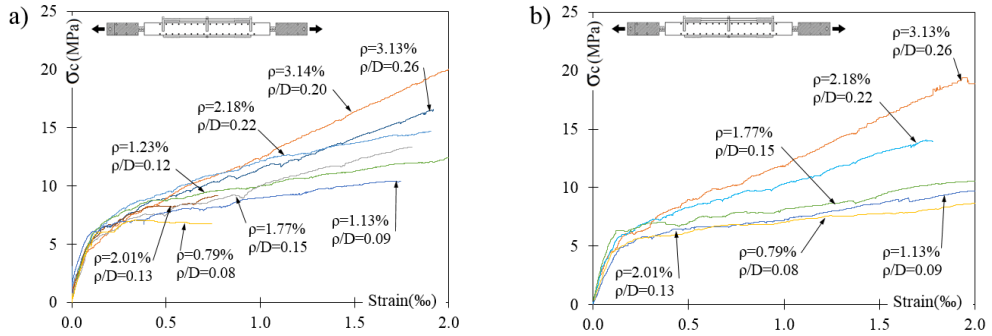


Figure 2: Tensile responses of reinforced UHPFRC: a) ties with concrete type C1 and b) ties with concrete type C2.

### 3.2 Tension stiffening response

The cracked concrete member can carry tension between cracks due to the bond behavior of the reinforcing bar. This ability is called tension stiffening effect, which increases member stiffness before reinforcement yields [11]. This change of stiffness affects deflection and crack widths under service loads. In UHPFRC members, fibers carry remarkable tensile forces at a crack and effectively increase tension stiffening. Thus, tension stiffening effect is an essential parameter in structural elements designed under SLS conditions because this effect controls deflections, crack width, and crack spacing. The tension stiffening response for the R-UHPFRC tensile ties of specimens is presented in Figs. 3a and 3b.

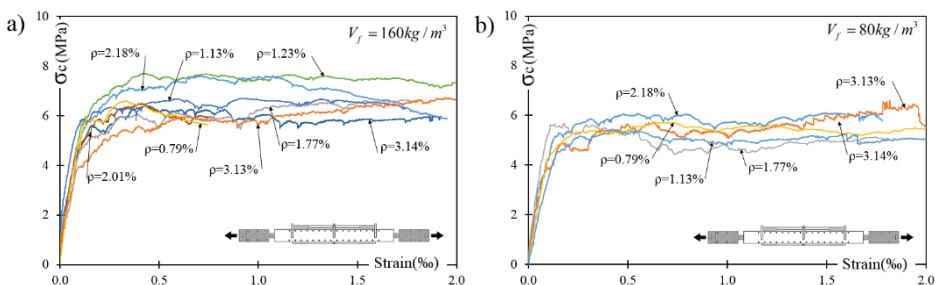


Figure 3: Tension stiffening response of a) ties with concrete type C1 and b) ties with concrete type C2.

The tension stiffening behavior for RC and FRC includes a descending branch

after first cracking. However, this phenomenon is not observed in the R-UHPFRC tensile members tested in this study, and the tension stiffening behavior remains near horizontal with a constant value. This result may be due to high bond-slip strength between the reinforcement and matrix of UHPFRC and the large number of microcracks along the entire length of the member, unlike localized cracks that typically occur in RC or FRC tie elements. Notably, microcracking was observed in all specimens during the test in the high rate of tensile strain before crack localization occurred.

#### 4. UHPFRC tensile behavior characterization

##### 4.1 Inverse analysis of four-point bending test results

The tensile stress-strain response of UHPFRC is a fundamental constitutive property of this material, which is one of the most essential aspects of serviceability design and prediction of the structural behavior. An inverse analysis method based on load–curvature method has been proposed and validated by the authors to determine the tensile properties of UHPFRC [8].

In order to validate and compare the tension contribution of UHPFRC (tension stiffening response) obtained by the R-UHPFRC tie test with inverse analysis method results, several four-point bending tests (4PBTs) were carried out. Two prismatic specimens ( $500 \times 100 \times 100 \text{ mm}^3$ ) were cast for each concrete batch and tested with flexural loading, and inverse analysis was applied to the results of each bending test. By inverse analysis method the parameters to define the constitutive UHPFRC behavior it can be obtained, which they are: cracking strength ( $f_i$ ), ultimate tensile strength ( $f_{t,u}$ ) and its corresponding strain ( $\epsilon_{t,u}$ ), the crack opening at the change of slope ( $w_d$ ), the crack opening at zero stress ( $w_c$ ), and the elastic modulus ( $E$ ). (see Fig. 4).

Table 3 present the parameters to define the ( $\sigma - \epsilon$ ) constitutive relationship according to the bending tests.

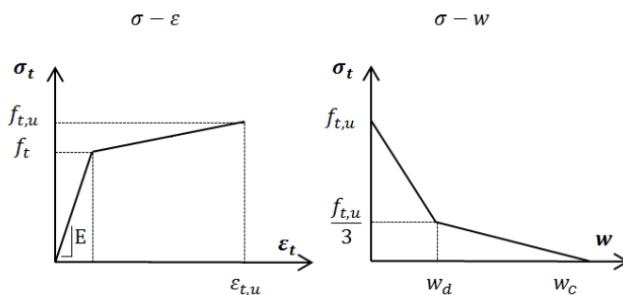


Figure 4: Assumed constitutive relationship for UHPFRC [12].

Table 3: Constitutive Relationship Parameters for each concrete batch

Concrete Type	Concrete batch number	Specimens	Constitutive Relationship Parameters				Modulus of elasticity of UHPFRC at 28 days (GPa)	
			$f_t$ (MPa)	$\varepsilon_{t,el}$ (‰)	$f_{t,u}$ (MPa)	$\varepsilon_{t,u}$ (‰)		
$C_1 (V_f = 160 \text{ kg/m}^3)$	1	A	11.66	0.22	11.12	5.79	48.4	
		B	8.94	0.18	8.03	4.40		
	2	A	8.05	0.16	6.77	2.09	48.1	
		B	7.77	0.14	6.27	2.14		
	3	A	10.43	0.19	8.90	4.49	48.1	
		B	9.49	0.17	8.40	4.43		
	4	A	8.89	0.17	7.91	4.47	48.9	
		B	8.79	0.17	7.97	1.54		
	5	B	10.42	0.20	9.95	3.57	49.2	
		C	10.45	0.22	10.42	4.71		
	Minimum result value			7.77	0.14	6.27	2.14	
	Average result value			9.49	0.17	8.40	4.43	
	Maximum result value			10.66	0.22	11.12	5.79	
	$C_2 (V_f = 80 \text{ kg/m}^3)$	1	A	6.10	0.10	4.37	3.32	46.3
			B	7.58	0.13	4.69	2.94	
2		A	7.44	0.12	4.27	2.9	46.5	
		B	7.35	0.13	4.13	2.81		
3		A	9.27	0.13	6.03	3.61	46.5	
		B	7.83	0.14	5.10	3.18		
4		A	8.06	0.15	7.22	2.60	46.6	
		B	9.15	0.16	9.05	2.83		
5		A	8.11	0.12	5.46	4.35	45.9	
		B	8.06	0.16	5.97	4.80		
6		A	8.54	0.18	4.61	2.24	45.9	
		B	8.72	0.15	4.44	1.24		
Minimum result value			6.10	0.10	4.37	3.32		
Average result value			8.11	0.12	5.46	4.35		
Maximum result value			9.27	0.13	6.03	3.61		

## 4.2 Comparison with experimental results

The tension stiffening response obtained from R-UHPFRC ties and the one obtained from the proposed constitutive inverse analysis are presented in Figs. 5a and 5b for two types of tensile ties. The average bending test results are greater

than the tension stiffening response obtained from the ties, even for the minimum obtained value. This discrepancy between the uniaxial tensile tie test results and the constitutive model can be due to several aspects such as fiber orientation, undesired internal bending rotations in the ties, or most probably due to the shrinkage effect.

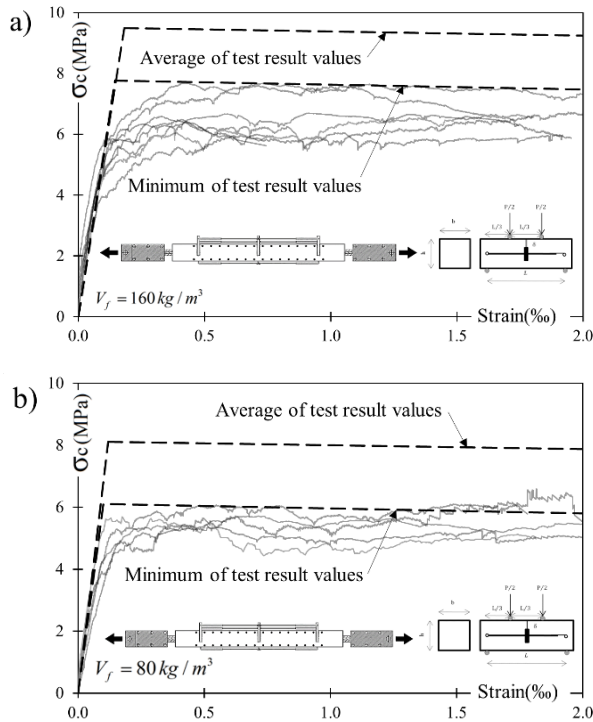


Figure 5: Comparison between tension stiffening response and proposed constitutive model a) ties with concrete type C1 and b) ties with concrete type C2.

Bischoff [13] reported that the member response of RC specimens drops as shrinkage increases and resulting a lower cracking load and less apparent tension stiffening. The same phenomenon can occur for R-UHPFRC tensile tie elements. Shrinkage of concrete leads to an initial shortening of the R-UHPFRC member as indicated in Fig. 6, and causes a reduction in the cracking load. Shrinkage effect is an important parameter of analysis of the member response and the neglect of this effect leads to a perceived reduction in the cracking strength of the concrete and increase the reinforcing ratio in the design process [13].

The shrinkage of UHPFRC induces a negative pre-strain in the steel reinforcement ( $\epsilon_{s,sh}$ ), which generates a negative stress (compression). Thus, the equivalent force

to modify the origin of the load-deformation curve can be calculated by  $E_s A_s \varepsilon_{s,sh}$ . The pre-strain caused by shrinkage might significantly affect on tension stiffening, where the free shrinkage value can be estimated for UHPFRC using the following equation proposed by fprSIA 2052[5]:

$$\varepsilon_{Us}(t) = \varepsilon_{Us\infty} e^{\frac{c}{\sqrt{t+d}}} \quad (1)$$

The coefficients (c) and (d) are coefficients for setting the shrinkage model of UHPFRC. The proposed values of the coefficients by fprSIA 2052 [5] are:  $c = -2.48$  and  $d = -0.86$ , and the age of concrete (t) is expressed in days. The fprSIA 2052[5] admits that the maximum value for shrinkage of UHPFRC is  $\varepsilon_{Us\infty} = 0.6 - 0.8\%$ . Due to a large number of specimens and the time required to complete the experimental program, the minimum and maximum age of specimens were 37 and 198 days, respectively. The shrinkage strain ( $\varepsilon_{Us}(t)$ ) and the corresponding concrete stress ( $\sigma_{c,sh}$ ) are provided in Table 4. The average Young's modulus values obtained by using  $150 \times 300 \text{ mm}^2$  cylindrical specimens were 48.53 and 46.49 GPa, respectively, and the value 47 GPa was used for calculating the shrinkage stress for both types of concrete.

**Table 4.** Tensile shrinkage strain and stress

t (Concrete age)	$\varepsilon_{Us}(t)$ ‰	$\sigma_{c,sh}$ (MPa)								
		Section 60x60 mm			Section 80x80 mm			Section 100x100 mm		
		Ø 10 (mm)	Ø 12 (mm)	Ø 16 (mm)	Ø 10 (mm)	Ø12 (mm)	Ø16 (mm)	Ø 10 (mm)	Ø12 (mm)	Ø 16 (mm)
Min = 37 days	0.53	2.16	3.02	-	1.25	1.77	3.02	1.01	1.43	2.46
Max = 198 days	0.67	2.73	3.82	-	1.58	2.24	3.82	1.28	1.81	3.12
Avg = 92 days	0.62	2.51	3.52	-	1.46	2.06	3.52	1.17	1.67	2.87

This result leads to modify the tension stiffening response diagram (see Fig. 6) and adjusting the origin with the approximate range value 1.01 to 3.82 MPa depending on the concrete age, section size, rebar diameter, and Young's modulus values for each specimen. Consequently, the existing discrepancy between the constitutive model and tension stiffening response will modify with the shrinkage effect.

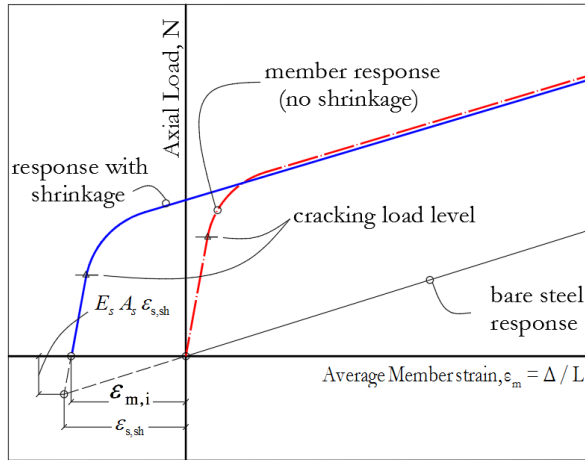


Figure 6: Typical tensile R-UHPFRC tie behavior and the effect of shrinkage on member response

## 5. Conclusions

The concrete tension contribution (tension stiffening response) obtained by the uniaxial R-UHPFRC tensile tie test was compared with the material characteristic properties of UHPFRC based on the proposed inverse analysis method. Nine series of ties and two types of concrete were developed to study the behavior of reinforced UHPFRC ties under serviceability conditions, and the shrinkage effect was evaluated theoretically. The shrinkage stresses were varied between 1.25 and 3.82 MPa depending on section size, rebar diameter, and age of concrete. This discrepancy between the uniaxial tensile tie test results and the characteristic properties obtained by the constitutive model indicates that it is necessary to incorporate the shrinkage effect in tension stiffening behavior of R-UHPFRC elements under serviceability conditions.

## Acknowledgments.

This study forms a part of the project BIA2016-78460-C3-1-R supported by the State Research Agency of Spain.

## References

- [1] D. Honfi, Design for Serviceability-A probabilistic approach, Lund University2013.
- [2] J.C. Walraven, Model Code 2010-Final draft: Volume 1, fib Fédération internationale du béton2012.

- [3] S. AFGC, Bétons fibrés à ultra-hautes performances–Recommandations provisoires, AFGC, France (2002).
- [4] J.C. Committee, Recommendations for design and construction of high performance fiber reinforced cement composites with multiple fine cracks, Japan Society of Civil Engineers, Tokyo, Japan (2008).
- [5] S. Cahier Technique, Béton fibré ultra-performant (BFUP)-Matériaux, dimensionnement et exécution, Projet (2014).
- [6] F. Baby, B. Graybeal, P. Marchand, F. Toutlemonde, UHPFRC tensile behavior characterization: inverse analysis of four-point bending test results, *Materials and structures* 46 (2013) 1337-1354.
- [7] S.-C. Lee, H.-B. Kim, C. Joh, Inverse Analysis of UHPFRC Beams with a Notch to Evaluate Tensile Behavior, *Advances in Materials Science and Engineering* 2017 (2017).
- [8] J.Á. López, P. Serna, J. Navarro-Gregori, E. Camacho, An inverse analysis method based on deflection to curvature transformation to determine the tensile properties of UHPFRC, *Materials and Structures* 48 (2015) 3703-3718.
- [9] J.A. López Martínez, Characterisation of The Tensile Behaviour of UHPFRC by Means ff Four-Point Bending Tests, 2017.
- [10] M. Khorami, J. Navarro-Gregori, P. Serna, M. Navarro-Laguarda, A testing method for studying the serviceability behavior of reinforced UHPFRC tensile ties, *IOP Conference Series: Materials Science and Engineering*, IOP Publishing, 2019, pp. 012022.
- [11] P.H. Bischoff, Tension stiffening and cracking of steel fiber-reinforced concrete, *Journal of materials in civil engineering* 15 (2003) 174-182.
- [12] J. López, P. Serna, J. Navarro-Gregori, H. Coll, Comparison between inverse analysis procedure results and experimental measurements obtained from UHPFRC Four-Point Bending Tests, *Proceedings of the 7th RILEM Workshop on High Performance Fiber Reinforced Cement Composites (HPFRCC7)*, 2015, pp. 185-192.
- [13] P.H. Bischoff, Effects of shrinkage on tension stiffening and cracking in reinforced concrete, *Canadian Journal of Civil Engineering* 28 (2001) 363-374.





## ***Chapter 5. Serviceability behaviour of reinforced UHPFRC tensile elements***

This chapter contains the 6<sup>th</sup> published paper, which presents an experimental study to evaluate the average and maximum crack width caused by tensile stresses in the R-UHPFRC tensile elements. The study present in this chapter includes a statistical analysis to develop the fragility curves based on obtained test data.

**6<sup>th</sup> PAPER**

Details:

---

Type of paper	Journal article
Title	<i>Serviceability behaviour of reinforced UHPFRC tensile elements: Assessment of the ratio between maximum and average crack widths</i>
Authors	<u>Majid Khorami</u> Juan Navarro-Gregori Pedro Serna Ros
Journal	Construction and Building Materials
Publisher	Elsevier
ISSN	0950-0618
JIF	6.142 (2020)
Quartiles	Q1, Civil and Structural Engineering, Material Science
Status	Published
Date	Accepted: 08 August 2021 Available online: 11 October 2021
Full reference	M. Khorami, J. Navarro-Gregori, P. J. C. Serna, Construction and Building Materials, "Serviceability behaviour of reinforced UHPFRC tensile elements: Assessment of the ratio between maximum and average crack widths," vol. 303, No. 124513, 2021

---

**6<sup>th</sup> Paper. Serviceability behaviour of reinforced UHPFRC tensile elements: Assessment of the ratio between maximum and average crack widths**

M. Khorami<sup>a,b,1</sup>, J. Navarro-Gregori<sup>a,\*2</sup>, P. Serna<sup>a,3</sup>

<sup>a</sup>: Institute of Science and Concrete Technology, ICITECH, Universitat Politècnica de València, València, 46022, Spain.

<sup>b</sup>: Universidad UTE, Facultad de Arquitectura y Urbanismo, Calle Rumipamba s/n y Bourgeois, Quito, Ecuador

\* **Corresponding Author:** Universitat Politècnica de València, Spain.

E-mail address: [juanagre@cts.upv.es](mailto:juanagre@cts.upv.es) (J. Navarro-Gregori).

<sup>1</sup> Orcid: 0000-0003-4592-0233

<sup>2</sup> Orcid: 0000-0002-6319-7029

<sup>3</sup> Orcid: 0000-0001-8754-1165

## **Abstract**

This study aimed to evaluate the maximum crack width formed under tensile stresses for two reinforced ultra-high performance fibre-reinforced concrete (UHPFRC) types with different steel fibre volume contents, and to compare them to average values. The maximum crack width values can more than double the average ones based on the applied tensile strain. The difference between maximum and average crack widths should be considered for examining UHPFRC structures for the serviceability and durability design. This paper also introduces appropriate statistical procedures for developing fragility curves based on cracking data by assuming that they can be represented by Rice distribution functions.

**Keywords:** Serviceability behaviour; tensile elements; UHPFRC; cracking behaviour; durability, fragility curve.

## **1. Introduction**

The durability of reinforced concrete structures to environmental actions is essentially related to controlling crack width under specific environmental

conditions, while preventing steel corrosion caused by increasing chloride ions and carbon dioxide.

Concrete cracking degrades required performance, such as safety and serviceability, due to steel corrosion during the design working life. Cracking examinations can be done by controlling the crack width of concrete structure elements to meet the crack width limitations to avoid steel corrosion as determined under specific environmental conditions. Another parameter to examine cracking is predicting the chloride ion concentration upon steel reinforcement under specified environmental conditions, while limiting it to the permissible concentration for steel corrosion onset during working life. Both concrete cover and concrete quality are other parameters applied to verify if steel is protected from corrosion due to chloride ion ingress. Water tightness and structure appearance are important factors for examining cracking and permissible crack width, and should be specified for such cases. Controlling crack width in UHPFRC is essential for resisting environmental actions, serviceability behaviour and safety, and for avoiding steel corrosion and aesthetics during UHPFRC structures' working life. To design UHPFRC structural elements, resistance to environmental actions should be examined by controlling crack width, while cracks should be tested (due to stresses) to control impaired structures' serviceability and safety [1, 2]. The capability of controlling crack width is the major characteristic of UHPFRC structural members [3-6]. The characteristic crack width (considered as a cautious estimate of the true value of crack width such that there is a probability of 95% the mean value is lower than the calculated) should be calculated by applying an appropriate combination of actions [7-10]. On predicting crack width in the literature, Borosnyói and Balász [11] summarized different approaches as four categories:

- (a) An analytical approach for calculating crack width by solving the differential equation of bond-slip.
- (b) A semi-analytical approach for calculating the average crack width ( $w_m$ ) as the product of the mean crack spacing ( $s_{rm}$ ), and the difference between the mean strain in the reinforcement ( $\epsilon_{sm}$ ) and the mean strain in the concrete between cracks ( $\epsilon_{cm}$ ).

In this case, the characteristic crack width ( $w_k$ ) value can be calculated by the following relation:

$$w_k = \beta \cdot w_m = \beta \cdot s_{rm} \cdot (\epsilon_{sm} - \epsilon_{cm}) \quad (1)$$

where ( $\beta$ ) is a factor that relates the average crack width to the characteristic value.

According to different authors and design codes,  $\beta$  factor is supposed to lie between 1.3 and 2 [12-16] For example, the Spanish design code for concrete

structures (EHE-08) [15] recommends  $\beta$  equalling 1.3 if cracking is caused by indirect actions only, and 1.7 otherwise. It should be noted that current concrete design codes, such as CEB-FIP Model code 2010 [7], Eurocode 2 [8], and French code NF P 18-710 for UHPFRC structures [17], do not explicitly use  $\beta$  for calculating crack widths, but the characteristic crack width is calculated directly by multiplying the crack spacing  $s_{r,max}$  by the difference in the longitudinal reinforcement and concrete mean strains ( $\varepsilon_{sm} - \varepsilon_{cm}$ ):

$$w_k = s_{r,max} \cdot (\varepsilon_{sm} - \varepsilon_{cm}) \quad (2)$$

Borosnyói and Balász [11] calculated the characteristic average crack width ratio ( $\beta = w_k / w_m$ ) by using the formula recommended by MC90 [18] for a rectangular concrete cross-section with a reinforcement ratio of 0.5% to 2.5%, and a concrete compressive strength from 30 to 50 N/mm<sup>2</sup>. They demonstrated that  $\beta = 1.5$  and is independent of both the reinforcement ratio and concrete strength.

- (c) An empirical relation based on fitting a large number of experimental data.
- (d) A numerical model, such as FEM models, fracture mechanics models or damage models.

If steel fibres are used in concrete, such as fibre-reinforced concrete (FRC), the crack width calculation is similar to that of normal reinforcement concrete, and the general equation for determining the characteristic crack width value can be used (Eq. 2), while the tensile stress in FRC not equalling zero after cracking should also be considered [7]. According to RILEM TC 162-TDF 2003 [19], crack width is calculated by Eq. 1 when considering factor  $\beta$  to be 1.7 for load-induced cracking and 1.3 for restrained cracking in those sections with a minimum depth of 300 mm or less. With UHPFRC elements, E. Fehling et al [20] indicated that the characteristic crack width value can be determined by the general equation for crack width calculations (Eq. 2), and proposed an expression for calculating the mean strain difference between bar reinforcement and the concrete between cracks [21-25].

In order to investigate reinforced concrete's cracking behaviour, the uniaxial tensile test is normally performed and prismatic concrete specimens are used with steel reinforcement in the central section. Following the literature [26-30], the average measured crack width on the surface can be obtained by dividing the total tensile elongation by the number of cracks. An experimental study was carried out that involved testing a dog bone-shaped UHPFRC tie element to find the relation between the maximum experimental measured crack width with the average crack width.

## **2. Research significance**

Controlling crack width is a fundamental parameter to design reinforced UHPFRC (R-UHPFRC) structures under serviceability conditions. As tensile microcracks occur along specimen length, and obtaining the crack width for each crack in each force stage is often complicated, the average crack width is considered to be an empirical output and the solution is computed as follows:

$$\text{Average crack width} = \frac{\text{Extended recorded length during test}}{\text{Number of cracks}}$$

The existing difference between the maximum measured crack width and the average value should be considered for examining R-UHPFRC structures for the serviceability limit state (SLS), and for their durability. Test results provide valuable information about the SLS for developing further design recommendations for R-UHPFRC members.

## **3. Serviceability design and conditions**

The SLS requirements are applied to concrete reinforcement structures to guarantee their functionality and structure integrity under service conditions. To verify the SLS and to define the serviceability requirements for concrete structures, the SLS is normally considered by restraining stresses in material, crack width and spacing restriction, structure element vibration, and long- or short-term deflections. The stress level (tension and compression) should be controlled under service loads in both concrete and steel reinforcement. Under SLS loads, compression stresses are normally limited by design codes to avoid excessive compression stresses, longitudinal cracks and excessive creep deformations. The French code NF P 18-710 [17] requirements for UHPFRC elements resemble the RC and FRC elements provided by Eurocode 2 [7], and limit compressive stress with a value of  $0.6f_{ck}$  (compressive concrete strength). Japanese UHPFRC design recommendations [31] limit compressive stresses to  $0.4f_{ck}$  under permanent loads. If tensile stresses are limited in reinforcement, an appropriate safety margin needs to be set below the yielding strength to prevent uncontrolled cracking [7]. Under serviceability conditions, inelastic reinforcement deformation should be avoided to prevent large and permanently open cracks. For RC and FRC structural elements, Model Code 2010 [7] indicates that tensile rebar stress does not exceed  $0.8f_{ck}$  (the characteristic tensile yield stress value of reinforcement) and French code NF P 18-710 [17] applies the same tensile stress limitation requirement for UHPFRC elements. Japanese UHPFRC design

recommendations [31] indicate that steel reinforcement behaviour should be elastic under compression and perfectly elastoplastic under tension. Steel tensile stress is also limited to the characteristic steel tensile strength value ( $f_{yk}$ ).

Concrete stress verification in the SLS for UHPFRC depends on the post-cracking behaviour under uniaxial tensile stresses (strain-hardening or strain-softening behaviour). French code NF P 18-710 [17] categorizes tensile UHPFRC behaviour as three classes: T1 (tension-softening), T2 (slight strain-hardening) and T3 (considerable strain-hardening). According to this code, cracking control is not necessary for UHPFRC class T3, but for classes T1 and T2 provide a crack opening expression. It is worth mentioning that Swiss standard fprSIA 2052 [27] verifies SLS requirements by limiting the maximum tensile concrete stress up to 90% of the characteristic elastic tensile strength value for UHPFRC with strain-hardening tensile behaviour, and up to 70% for UHPFRC with tension-softening behaviour. As a plural and identical agreement for serviceability requirement and an SLS design is lacking for R-UHPFRC, further research is necessary.

## **4. Experimental Program**

In this study, an experimental test was run to specify and evaluate the maximum and average crack widths for R-UHPFRC tensile elements. Eight dog bone-shaped concrete specimens with two different UHPFRCs in distinct fibre content terms were manufactured. Four specimens with UHPFRC by a 2 vol.% fibre content, and four specimens with UHPFRC by 1 vol.%, were cast.

All eight series of dog bone-shaped elements were produced, and their size and reinforcement rebar diameter were the same to ensure identical geometrical conditions. In this circumstance, the presence of two different fibre volume contents for specimens is capable of evaluating the fibre content influence on cracking behaviour and crack width values under tensile force.

### **4.1. Test setup**

The equipment to be used to carry out tests was designed to perform the direct tensile test using R-UHPFRC specimens with the dog bone-shaped geometry. The main test setup part included a steel frame with four longitudinal steel tube sections ( $60 \times 60 \times 6$  mm) and two steel plates ( $320 \times 320 \times 50$  mm) at both ends. A hydraulic jack was installed at one end of the steel frame to apply tensile force to the reinforcement placed into the concrete specimen. Two measurement systems were employed for measuring the applied force: the first for measuring the pressure of oil in the hydraulic jack, and another used the cell-force measurement equipment. This cell-force equipment was installed alongside the endplate on the other steel frame side (see Fig. 5). The connection between the R-UHPFRC specimen and the transformer force system included two steel (2 mm-

high) jaw-indented corrugations assembled by six bolts. The main steel test frame, the hydraulic jack, the installed specimen, and the jaw details are shown in Figure 1.

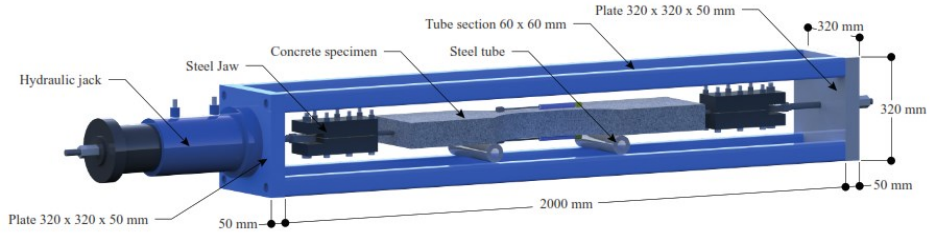


Figure 1: Test setup detail.

Tensile force was transferred to the concrete specimen by the friction between jaws and reinforcements. The authors have published the complete details of the test setup system, and the process of performing direct tensile tests, to study R-UHPFRC prismatic tensile elements under serviceability loads [28].

## **4.2. Specimens and material**

### **4.2.1. Preparing dog bone-shaped specimens**

All the dog bone-shaped UHPFRC ties were reinforced with a steel rebar ( $\text{Ø}12$  mm) in such a way that the rebar passed from the central cross-section of the tie and lay along it. According to the jaw geometry, to connect the specimen to transfer force system, and to avoid yielding rebar failure outside the specimen at two ends, it was necessary to attach two additional rebars at the two main rebar ends. These rebars were welded on its end to the main rebar by 5-cm welding. The general geometry of the dog bone-shaped specimens, the reinforcement details and the wooden mould geometry are shown in Figure 2.





Figure2: Dog bone-shaped specimen and reinforcement detail.

The dog bone shape was used for tensile elements to prevent cracking at the specimen end zone (end-effect), specifically where there is a stiffness difference between the section with the three steel rebars and the section with one steel rebar (see Fig. 2: Sections 1 and 2). Based on the experience acquired by the authors in previous works and from running lots of direct tensile tests of prismatic R-UHPFRC tensile elements [28,29], the dog bone-shaped specimen was herein suggested to increase the stiffness of the ties in the end zones to prevent any undesired crack occurring beyond the studied zone. Another reason for using the dog bone shape was to obtain a small limited zone over the specimen to measure crack widths by a microscope camera. This small zone is essential because detecting all the cracks along the entire tie element length is time-consuming. Dog bone specimens are generally used for specifying the mechanical tensile properties of small-sized fibre-reinforced concretes with no reinforcement bars. Some codes and recommendations provide standard dimensions for performing direct tensile tests for dog bone-shaped concrete or mortar specimens, such as the Japanese

recommendation [26], the Swiss standard [27], ASTM C190-85 [32] and JSCE [33]. In this study, the dog bone-shaped specimens were designed as so: 1050 mm long, 240 mm wide, and 80 mm at both ends and at the middle of elements, respectively. Thickness was 80 mm and remained constant along the specimen (Fig. 3).

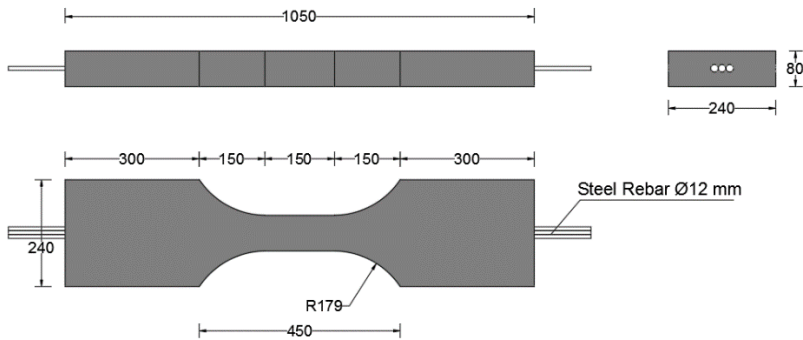


Figure 3: Specimen geometry and dimensions (units: mm).

The central specimen zone (length  $L=150$  mm) had a constant width, and the cross-section at the centre of the tie was  $80 \times 80$  mm<sup>2</sup> with a reinforcement ratio of  $\rho = 1.76\%$ . During the test, almost all the tensile cracks took place in this zone, and no crack occurred at the section from the changing stiffness. To facilitate the microscope camera's movements over lateral specimen surfaces, a semihard plastic laminate was glued to the mould surface at the specimen mid-part to create a smooth surface on the lateral UHPFRC surfaces. This created smooth surface helped to improve image resolution, and to better visualize the crack width on the UHPFRC specimen surface.

#### 4.2.2 Mix design

UHPFRC is composed of cement, water, aggregates, additives, admixtures and fibres. The difference between UHPFRC and conventional concrete mix designs lies in the amount of binder, aggregate sizes and the presence of fibres. To accomplish acceptable UHPFRC workability, it is necessary to use superplasticizers (SP). UHPFRC is generally much denser and it is important to achieve the maximum possible packing density to improve mechanical and durability properties. The mix design herein employed aligns with previous works performed by the authors [28,29,34]. Two UHPFRC types were developed with different fibre contents for this experimental study. The UHPFRC-type one (U1) included 2 vol.% of steel fibres, which is the equivalent to 160 kg/m<sup>3</sup> of steel fibre

content. The second UHPFRC type (U2) contained 1 vol.% (80 kg/m<sup>3</sup>). Small-sized steel fibres were used in UHPFRC as so: 13 mm long, a diameter of 0.2 mm and tensile strength beyond 2000 MPa. The nominal yield stress of rebars was 500 MPa. The composition of the UHPFRC mixtures is given in Figure 4.

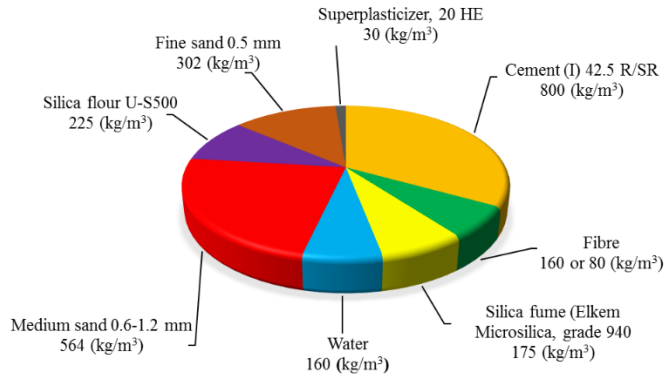


Figure 4: The proportion of UHPFRC components [28,34].

The UHPFRC mixture must achieve good workability, particle distribution and packing density by the end of the mixing process. As it contained constituents and fine particles, and given its tendency to agglomerate, breaking these chunks would be easier if particles were dry. Hence mixing all the fine dry particles before adding water is recommended [35,36]. The mix procedure started by placing all the dry aggregates and mixing them for 1 minute. Then water and the additive were gradually added. Mixing continued for 5 minutes to make it completely workable. Small steel fibres were gradually added to the flowable mixture. UHPFRC was mixed for another 5 min. to avoid the chunks formation of fibres in concrete. The complete mixing time was 16 min., which was done in a standard horizontal 100-liter mixture machine. As the tensile response of the UHPFRC is affected by fibre distribution and orientation, a specific casting and specimen production process was followed to ensure the same fibre distribution and orientation in all specimens. The UHPFRC was always placed slowly into the moulds from one end and allowed to flow through the entire tensile element. The influence of other pouring procedure or specimen's geometry on the crack pattern is out of the scope of this work. In this study, four specimens were cast per concrete type and one UHPFRC batch was prepared for every two specimens. Compressive UHPFRC strength was measured on four cube samples (100 mm in size). The average compressive strength for each batch and the corresponding specimen code are found in Table 1.

Table 1: The average compressive strength value of each UHPFRC batch and the specimen nomenclature.

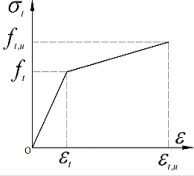
<b>Batch number /UHPFRC type</b>	<b>Specimen code</b>	<b>Compressive strength of each cube sample (MPa)</b>	<b>Average value (MPa)</b>
Batch #1/ U1-160	DB #U1-1 & DB #U1-2	171.7	161.8 (CV=7.0%)
		158.3	
		147.3	
		169.8	
Batch #2/ U1-160	DB #U1-3 & DB #U1-4	163.5	158.4 (CV=6.6%)
		145.0	
		169.3	
		155.9	
Batch #1/ U2-80	DB #U2-1 & DB #U2-2	157.1	157.6 (CV=3.5%)
		164.6	
		157.3	
		151.2	
Batch #2/ U2-80	DB #U2-3 & DB #U2-4	148.0	156.0 (CV=1.7%)
		153.4	
		158.7	
		155.8	

The average compressive strength values for both UHPFRC types (4 batches) were similar. The coefficient of variation (CV) values was low, which means that the UHPFRC matrix for all the batches was almost the same (with 5% CV for all the compressive results for both UHPFRC types) and fibre content did no significantly influence UHPFRC compressive strength.

Other important mechanical UHPFRC properties are tensile strength and post-cracking behaviour. These tensile properties can be obtained from the load-deflection curve following an inverse analysis method. Although ideal UHPFRC is deemed to show strain hardening behaviour in tension, some standards such as NF P 18-710 [17] accept UHPFRC with low strain softening behaviour. In this paper an inverse analysis method proposed in [37,38], adapted to UHPFRC with strain-softening behaviour [39] was applied to characterize the tensile properties ( $\sigma - \epsilon$  constitutive law) of the UHPFRCs used (see Table 2) [34]. This behaviour is related with the low dose of steel fibres used to produce economically competitive UHPFRCs [40].

Table 2: Tensile properties of concrete types U1 and U2 [34].

Constitutive Relation Model Parameters (average result value)	$f_t$ (MPa)	$\varepsilon_{t,el}$ (%)	$f_{t,u}$ (MPa)	$\varepsilon_{t,u}$ (%)
U1 ( $V_f=160 \text{ kg/m}^3$ )	9.41	0.18	8.49	6.56
U2 ( $V_f=80 \text{ kg/m}^3$ )	6.41	0.13	5.81	1.98



The purpose of using UHPFRC with a low dose of microsteel fibres was to gain economical concrete that acceptably performs in the SLS.

### 4.3. Test procedure

The dog bone-shaped R-UHPFRC specimens were horizontally placed inside the test frame machine. The R-UHPFRC specimen was connected to the force transfer system by two steel jaws at each end by placing it inside the jaw and fixing it by tightening six bolts. The horizontal specimen position in the test frame system conferred good access and facilitated the microscope camera's movements over the lateral specimen surfaces during the direct tensile test. To reduce the specimen's self-weight effect and the resulting bending in the middle of the specimen, two steel tubes were placed under the specimen on each one-third of the length from the ends as roller supports (see Fig. 5).

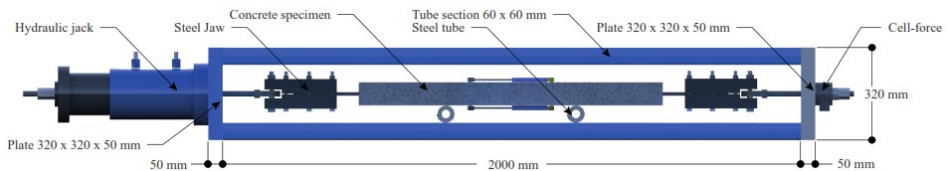


Figure 5: Placing the specimen inside the steel frame and roller support.

In order to measure R-UHPFRC specimen elongation, particularly in the study area (central testing zone), two displacement transducers (DTs) were installed on the up and bottom specimen surfaces (300 mm length). Before the main tests were run, one specimen was tested as a prototype sample to evaluate both the accuracy and efficiency of the measurement process. As some cracks occurred outside the test zone, a decision was made for measurements to be taken on a longer length. The DT length of 300 mm was chosen for this purpose. A simple linear finite element model of the dog-bone specimen was made to evaluate the difference between the deformation measured in the central testing zone and the DT length of 300 mm. The deformation measured over the central testing zone was about 8%

greater than the DT length zone, which would not significantly affect the results. The applied force was measured by the load cell equipment. The load-displacement behaviour curve of the R-UHPFRC specimens was also recorded by considering the data obtained from both DTs and the load cell. Crack monitoring and detecting crack widths during the test were performed on the lateral R-UHPFRC surface on the specimen's mid-part where the tensile element had a square section ( $80 \times 80 \text{ mm}^2$ ). Cracks were detected by a microscope camera at three specimen thickness levels: bottom, middle and top. The first line passed the specimen's longitudinal axial elevation, which corresponded exactly to the rebar axis. The second and third lines were located at a 10-mm distance from the top and bottom lateral surface edges (Fig. 6). These lines were marked on the surface with a pen to move the microscope camera on the direct line over these lines, which were divided into three different colours to denote millimetre divisions. The central testing zone and the guiding lines on the specimen's lateral surface are shown in Figure 6.

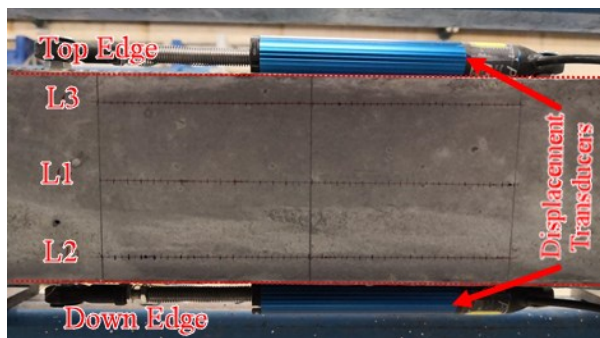


Figure 6: The three guiding lines for detecting cracks on the lateral surface

The intention of measuring crack width at the three different elevation levels (bottom, middle, top) was to better observe the formed inhomogeneous crack propagation. Moreover, given the possibility of the width of the tensile cracks along the length (perpendicular to the longitudinal applied force) not being constant, the width of the formed cracks could be wider on the edges or in the middle over the reinforcement axis. Figure 7 illustrates the cracking possibilities of the tie element and the different crack forms. This could be due to the existing bending caused by either the specimen's self-weight or improper reinforcement rebar placing. One suggestion was to take crack width measurements over the three lines located on the bottom, middle, top elevations of specimen thickness to obtain clear crack properties. Section 5.1 describes the crack width calculation.

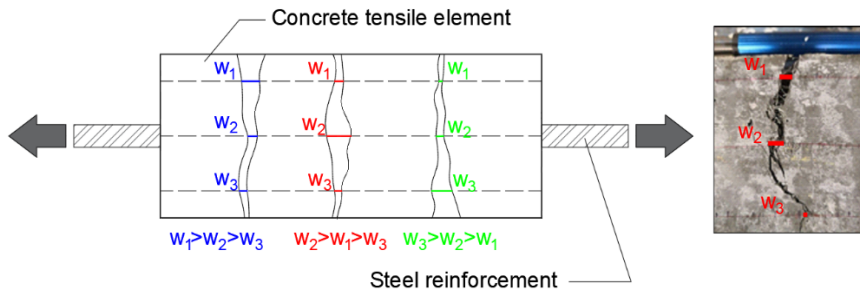


Figure 7: The crack formation and crack width variation possibilities along its length.

The tensile test began by applying tensile elongation to the R-UHPFRC specimen. The video recording of the specimen's surface was done at the different applied tensile elongation levels (almost by increasing 0.5‰ for each level) and the force value was recorded at these levels.

#### 4.4. Crack width measurement

When the video recording of the surface over each line began, the concrete crack width ruler card was placed on the specimen surface and acted as a base for the measurement taken to calculate crack width. Then the recorded video was analysed and reviewed on the desktop monitor. By making a linear proportional calculation between the marked line on the crack width ruler card and the crack mouth opening on the monitor, the real crack width was calculated. As the video recording over lines was time-consuming, both the applied force value and tensile elongation could slightly change. When video recording started and ended (with an average duration of 3 minutes for each strain level and each line), the applied force value and tensile elongation were noted, and the average mean value was used for the subsequent analysis. In this experimental work, an attempt was made to detect the first formed crack. To this end, the first microscope camera video recording of the surface was taken at very low tensile strains (0.03 ‰ to 0.05 ‰). As previously mentioned, the average crack width can be obtained by dividing tensile elongation by the number of cracks. To do so, the number of cracks that formed on each line was counted in each stage. The crack width measurement was taken for a minimum of 10 tensile strain levels. With the obtained experimental data, it was possible to draw both the force-elongation and crack width-elongation at the same time and on the same graph. These obtained results and diagrams are herein found in Section 5. The objective of this study was to evaluate both the cracking and tensile behaviours of the R-UHPFRC tie up to the 2.0 ‰ tensile strain level. However, the tensile test was performed for a higher tensile strain and, therefore, two additional crack width recordings were taken at the 2.5 ‰ and 3.0 ‰ strain levels.

## **5. Test results and discussion**

### **5.1. Average crack width**

Attempts were made to measure the crack width for all the specimens at the same tensile strain level. Due to cracking, the applied elongation sometimes increased suddenly and could not be controlled. As incremented elongation was not generally marked, it had no significant effect on the presented results and diagrams. By way of example, the detailed test data and results obtained from specimen DB #U1-1 are explained below. To present the behaviour of the R-UHPFRC specimen under the applied average tensile strain, a diagram was used so that the top side of this diagram would show the force-strain relation and the downside would depict the crack width-strain. The first video recording was done at a very low tensile strain (0.03‰) to detect the possible pre-created cracks due to shrinkage. The video recording process started on the specimen surface from the centre line (L1). Table 3 provides the average tensile strain and tensile force at the start and end of the video recording on every line and for each average strain level for specimen DB #U1-1.

For this specific specimen (DB #U1-1), no cracks were observed up to the tensile strain of 0.10 ‰, and the first cracks were detected at the fifth level of the applied average tensile strain with a value of 0.291 ‰ at the level force value of 42.8 kN (see Table 3). The number of cracks increased clearly with rising the applied average tensile strain (see the number of cracks column in Table 3). The force-strain relation and the average crack width-strain relation of specimen DB #U1-1 are presented in Fig. 8. The presented average crack width is based on the number of cracks detected on the central line (L2) exactly over the rebar axis.



Table 3: The experimental data from the tensile test of specimen DB#U1-1

# Strain level	# Line on the surface	Initial Force (kN)	Initial Avg. Strain (‰)	Number of cracks	Final Force Value (kN)	Final Avg. Strain (‰)
N1	L3	18.1	0.0296	0	17.3	0.0296
	L2	18.1	0.0296	0	17.7	0.0311
	L1	18.0	0.0311	0	17.6	0.0311
N2	L3	25.2	0.0552	0	24.4	0.0566
	L2	25.0	0.0566	0	23.9	0.0551
	L1	25.8	0.0581	0	24.5	0.0581
N3	L3	33.3	0.0808	0	31.8	0.0793
	L2	31.8	0.0808	0	30.5	0.0808
	L1	31.7	0.0808	0	30.4	0.0808
N4	L3	37.0	0.1390	0	35.4	0.1390
	L2	35.6	0.1420	0	35.5	0.1420
	L1	36.4	0.1420	0	35.0	0.1420
N5	L3	45.1	0.2140	0	42.7	0.2930
	L2	42.8	0.2910	4	40.2	0.2910
	L1	43.2	0.2940	4	40.6	0.2960
N6	L3	51.2	0.5170	0	47.6	0.6500
	L2	47.0	0.6510	6	46.9	0.6510
	L1	47.6	0.6510	9	44.0	0.6480
N7	L3	56.1	0.8140	1	52.5	0.8410
	L2	55.2	0.8510	8	51.7	0.8680
	L1	54.8	0.8800	11	51.8	0.8790
N8	L3	61.2	1.1600	2	58.1	1.1500
	L2	62.1	1.1100	10	58.5	1.1200
	L1	61.1	1.1300	13	58.0	1.1400
N9	L3	68.9	1.4200	3	64.7	1.4300
	L2	64.2	1.4300	13	63.7	1.4300
	L1	65.2	1.4400	15	62.5	1.4300
N10	L3	81.4	2.0200	11	76.9	2.0200
	L2	80.8	2.0400	19	76.8	2.0300
	L1	80.1	2.0300	18	76.4	2.0300
N11	L3	92.2	2.5200	14	87.0	2.5300
	L2	90.2	2.5500	21	85.6	2.5300
	L1	90.3	2.5400	17	85.9	2.5400
N12	L3	99.8	3.1000	17	93.8	3.0700
	L2	93.0	3.1000	23	93.4	3.0700
	L1	92.2	3.1000	19	92.8	3.0700
N13	L3	-	-	-	-	-
	L2	10.1	4.6000	25	93.1	4.5200
	L1	-	-	-	-	-

In Figure 8, we see that the slope of tension behaviour curve changed when the average tensile strain was approximately 0.15‰. Crack width was almost the same ( $w=0.04$  mm) within the strain range between 0.50‰ and 2.0‰, which led to the stabilized cracking stage happening within this strain range.

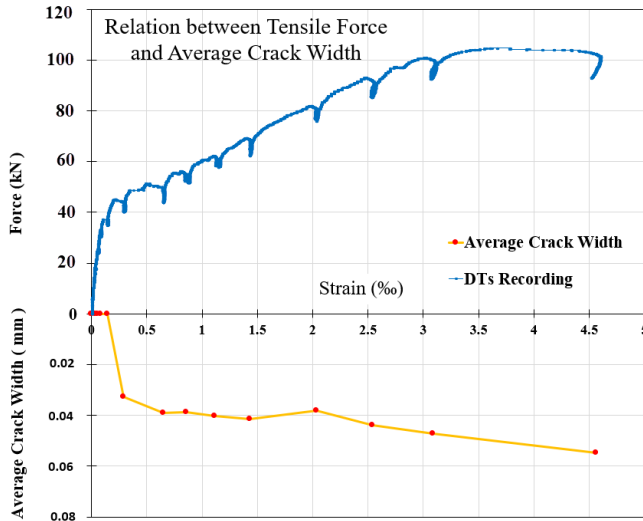


Figure 8: The force-strain and crack width-strain relations of specimen DB #U1-1.

Figures 9a and 9b illustrate the results obtained for all the specimens from the two employed UHPFRC types. It is important to mention that specimen DB #U2-4, with concrete type U2 ( $V_f=80 \text{ kg/m}^3$ ), failed due to an improper friction between the jaw dents and the rebar surface. According to these figures, the first cracks happened before the 0.5 ‰ average tensile strain for both UHPFRC types (U1 and U2). The crack width value for specimens with UHPFRC type U1 at a strain level above 0.5 ‰ was almost constant (0.040 mm), while for the specimens with UHPFRC type U2, the crack width at the strain level between 0.5 and 1.0 ‰ was almost 0.070 mm and almost 0.055 mm for the strain level higher than 1.0 ‰. By considering the same mixture composition for UHPFRC types U1 and U2, the difference between crack width could be caused by the difference in the fibre volume contents for each UHPFRC type. Regarding the SLS requirements (crack width controlling) for UHPFRC and durability issues, the R-UHPFRC tensile elements with the 2. vol% fibre content behaved better than the tensile R-UHPFRC elements with the 1. vol% fibre content. For the UHPFRC U1 type, crack width was narrower than type U2 and its value remained approximately constant up to the high tensile strain rate.

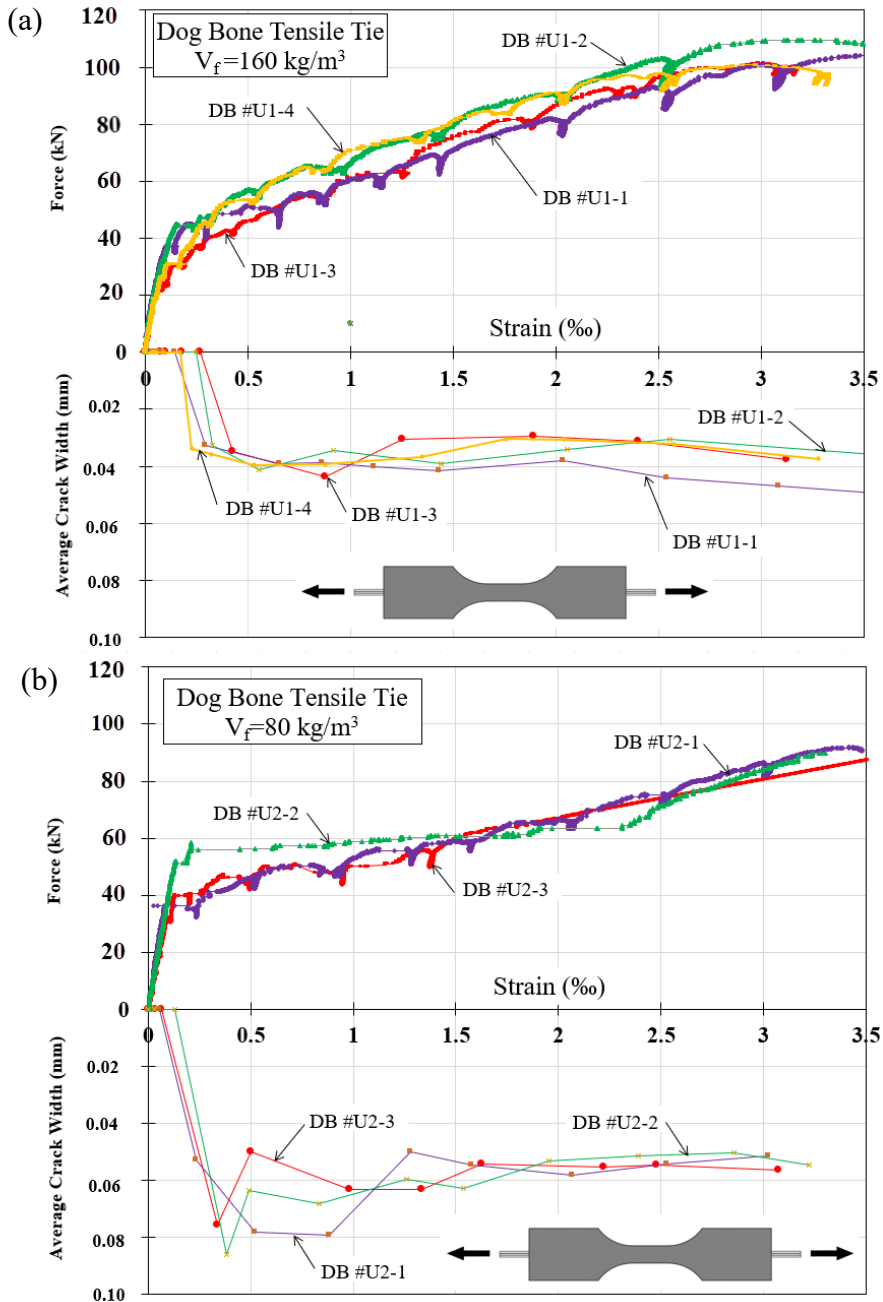


Figure 9: Force-strain and crack width-strain curves of the dog bone-shaped R-UHPFRC ties (a)  $V_f = 160 \text{ kg/m}^3$ , (b)  $V_f = 80 \text{ kg/m}^3$ .

Shrinkage is an essential effect to be considered in R-UHPFRC, inducing significant tensile strains in the concrete matrix, and therefore, modifying the general tensile behaviour of the R-UHPFRC tie elements. French code NF P 18-710 [17] provides an indicative value of 550  $\mu\text{m}/\text{m}$  for UHPFRC shrinkage. A primary study about this effect on the behaviour of R-UHPFRC ties with the same UHPFRC employed herein has been performed by the authors [34], but an in-depth study is needed to consider all the effective UHPFRC shrinkage factors.

## **5.2. Maximum crack width**

The maximum crack width was obtained by reviewing the recorded video and monitoring all cracks. Table 4 provides a series of formed crack images on the central axial line ( $L_1$ ) of specimen DB #U1-1 as a sample (in this study) to understand the maximum crack width calculation, as well as the crack formation process. Table 4 indicates the average tensile applied force value ( $F_{\text{avg}}$ ) of the initial and final recording processes, where ( $w_{\text{max}}$ ) is the maximum value of the detected crack width on line  $L_1$ , ( $n$ ) is the number of cracks on line  $L_1$ , ( $w_{\text{avg}}$ ) is the average crack width calculated by dividing the tensile elongation by the number of cracks and ( $\epsilon_i$ ) is the average tensile strain value of the initial and final recording video process.

According to the images obtained from specimen DB #U1-1 test, i.e. for force stage N10, the cracks that formed along the specimen had different width values. Therefore, due to crack width variation, the difference between the average crack width value ( $w_{\text{avg}} = 0.0321 \text{ mm}$ ) and the maximum value ( $w_{\text{max}} = 0.1000 \text{ mm}$ ) was significant. The diagrams presented in Fig. 10 provide the calculated average and maximum crack width values for the 10 load stages analysed.

Table 4.a: Cracks captured during the tensile test of specimen DB #U1-1 on the central axial line (L1).

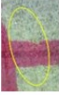

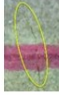


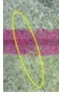
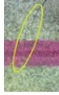

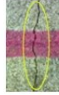

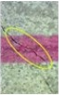
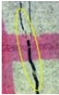
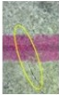

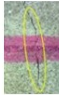
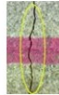

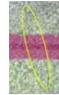

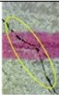
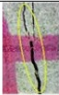

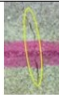
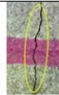
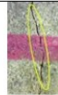

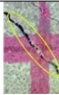
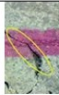
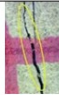
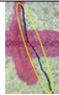
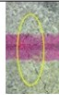
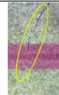
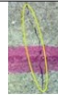
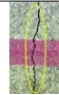

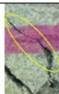

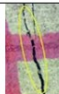

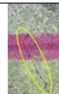

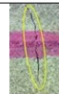

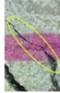
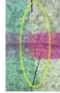
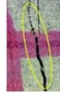
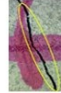
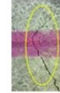

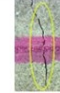

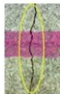


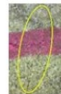


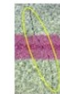


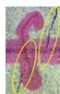


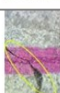
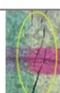

































































Test data	Captured images of the cracks							
<p><b>N5</b></p> <p>n = 4</p> <p><math>F_{avg} = 41.5 \text{ kN}</math></p> <p><math>W_{max} = 0.0440</math></p> <p>mm</p> <p><math>W_{avg} = 0.0218</math></p> <p>mm</p> <p><math>\epsilon_t = 0.291\%</math></p>					-	-	-	-
<p><b>N6</b></p> <p>n = 6</p> <p><math>F_{avg} = 46.9 \text{ kN}</math></p> <p><math>W_{max} = 0.0500</math></p> <p>mm</p> <p><math>W_{avg} = 0.0326</math></p> <p>mm</p> <p><math>\epsilon_t = 0.651\%</math></p>							-	-
<p><b>N7</b></p> <p>n = 8</p> <p><math>F_{avg} = 53.4 \text{ kN}</math></p> <p><math>W_{max} = 0.0750</math></p> <p>mm</p> <p><math>W_{avg} = 0.0322</math></p> <p>mm</p> <p><math>\epsilon_t = 0.859\%</math></p>								
<p><b>N8</b></p> <p>n = 10</p> <p><math>F_{avg} = 60.3 \text{ kN}</math></p> <p><math>W_{max} = 0.0750</math></p> <p>mm</p> <p><math>W_{avg} = 0.0335</math></p> <p>mm</p> <p><math>\epsilon_t = 1.115\%</math></p>								
<p><b>N9</b></p> <p>n = 13</p> <p><math>F_{avg} = 63.9 \text{ kN}</math></p> <p><math>W_{max} = 0.0620</math></p> <p>mm</p> <p><math>W_{avg} = 0.0330</math></p> <p>mm</p> <p><math>\epsilon_t = 1.43\%</math></p>								
<p><b>N10</b></p> <p>n = 19</p> <p><math>F_{avg} = 78.8 \text{ kN}</math></p> <p><math>W_{max} = 0.1000</math></p> <p>mm</p> <p><math>W_{avg} = 0.0321</math></p> <p>mm</p> <p><math>\epsilon_t = 2.035\%</math></p>								

Table 4.a: Continue of Table 4.a, Cracks captured during the tensile test of specimen DB #U1-1 on the central axial line (L1).

<b>N11</b>									
	$n = 21$								
	$F_{avg} = 87.9 \text{ kN}$					-	-	-	-
	$w_{max} = 0.1870 \text{ mm}$					-	-	-	-
$w_{avg} = 0.0363 \text{ mm}$									
$\epsilon_t = 2.540\%$									
<b>N12</b>									
$n = 23$									
$F_{avg} = 93.2 \text{ kN}$									
$w_{max} = 0.3120 \text{ mm}$									
$w_{avg} = 0.0402 \text{ mm}$									
$\epsilon_t = 3.085\%$									

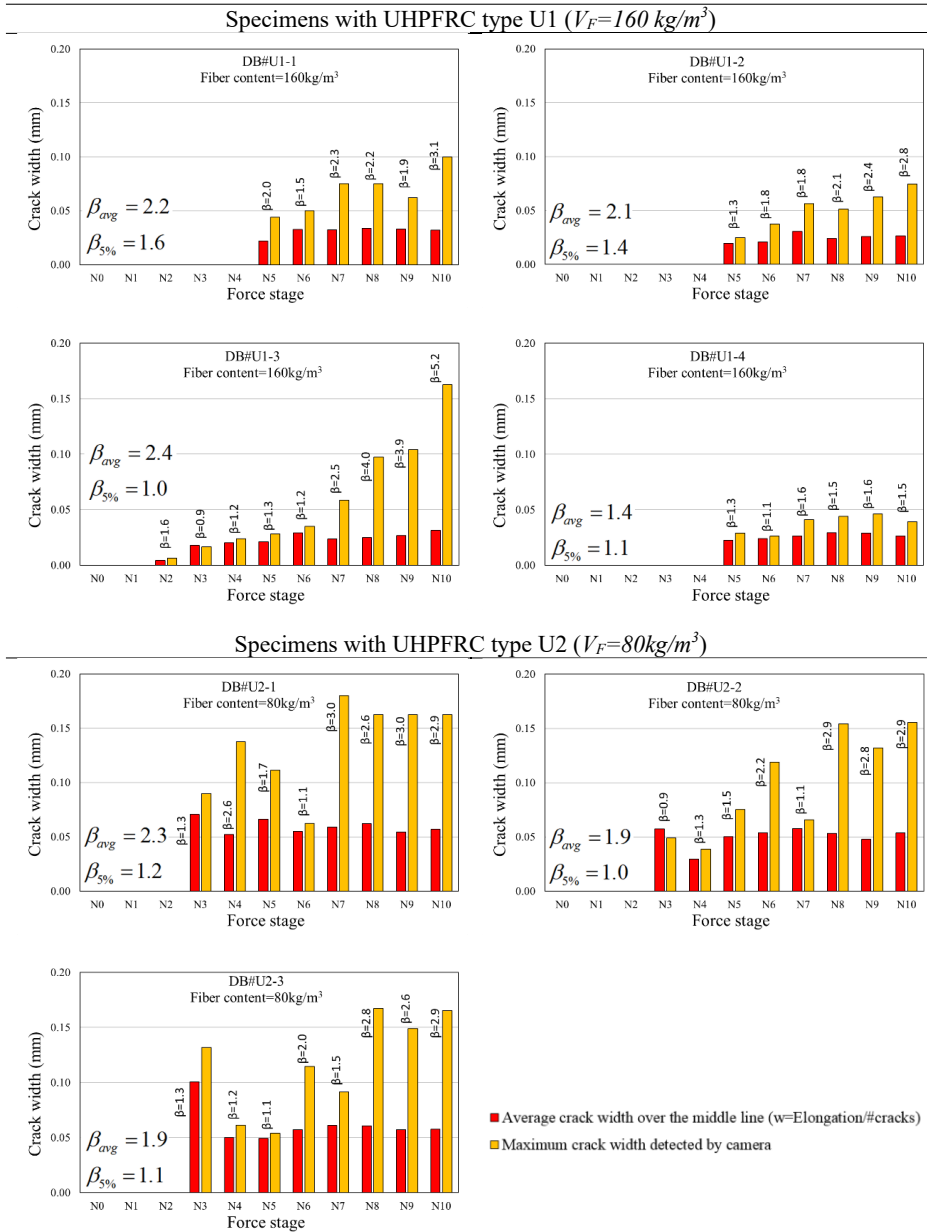


Figure 10: Comparing the maximum crack width to the average crack width values for the R-UHPFRC elements with UHPFRC types U1 and U2.

As previously explained in Section 1, under service loads  $\beta$  is defined as the factor that relates the ratio between the characteristic crack width (or the maximum crack width) and the average crack width values ( $\beta = w_k / w_m$ ). This  $\beta$  factor was calculated for each applied force stage, along with its value for each stage (Fig. 10). Obviously, the maximum crack width values at high applied tensile force values (Stages N9 and N10) and at the high tensile strain rate (between 2.0‰ and 3.5‰) could be more than 2.8-fold the average crack width values (the average value  $\beta$  for two last force stages for all specimens) for both UHPFRC types U1 and U2. The mean  $\beta_{avg}$  values for the tensile elements were 2.02 and 2.03 for UHPFRC type U1 and type U2, respectively. In experimental terms, it can be assumed that the maximum crack width ( $w_k$ ) can be calculated by multiplying the average crack width ( $w_m = \text{elongation}/\text{number of cracks}$ ) by  $\beta$  (approximately ( $\beta = 2.0$ ) for both UHPFRC types. It should be noted that the  $\beta$  value was obtained as the average of the values from the low to high tensile strain rates (up to 3.5‰ in some cases). In the SLS design of the concrete elements, the characteristic crack width should be calculated under service loads so that tensile strain would be far less under SLS conditions. French code NF P 18-710 [17] provides the maximum crack width limitations for the SLS design of the UHPFRC structure elements under service conditions. To meet the serviceability requirement, the crack widths of the elements under service loads should go below these values. By comparing the obtained experimental maximum crack width values (see the diagrams in Fig. 10) to the limit values of NF P 18-710 in Table 7.201 [17], almost all the experimental maximum crack widths of R-UHPFRC type U1 (fibre content=160 kg/m<sup>3</sup>) were less than 0.10 mm. This means that the R-UHPFRC type U1 met the crack width limitation for all the exposure classes. However, the maximum experimental crack width for UHPFRC type U2 (fibre content=80 kg/m<sup>3</sup>) obtained values that came close to 0.15 mm, which does not meet the SLS requirement for exposure classes XD1, XD2, XD3, XS1, XS2, and XS3 (corrosion induced by chlorides and seawater).

### **5.3. Crack number**

Cracking behaviour can be evaluated by the number of cracks at a given average tensile strain. The cracking data were obtained by counting the number of cracks at three tensile strain levels to evaluate and compare the cracking phenomenon for the two used UHPFRC types. The measured number of cracks for the tensile strain values of 1.0‰, 2.0‰ and 3.0‰ are found in Figure 11.



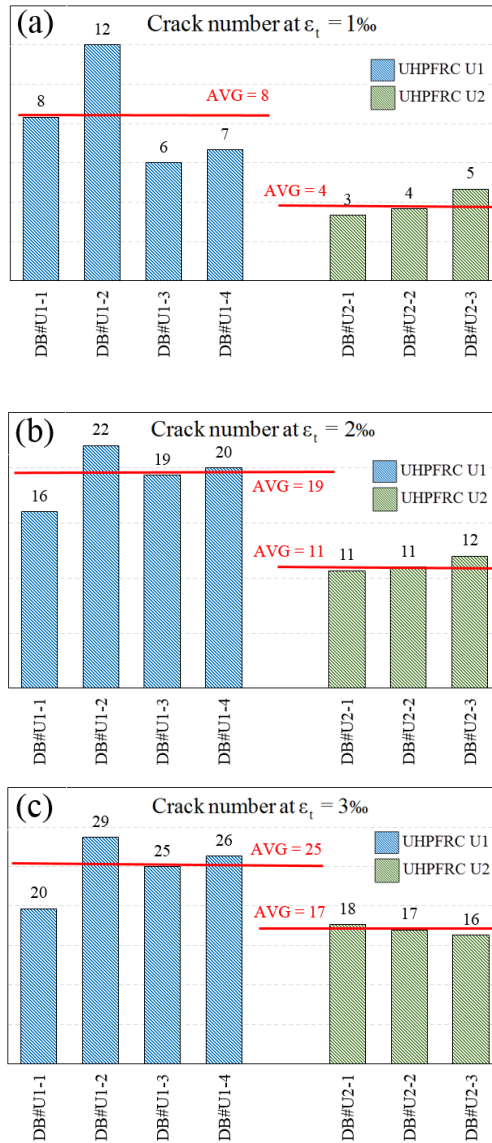
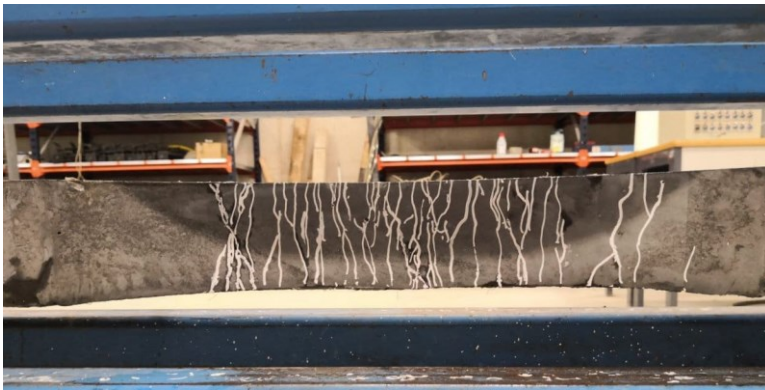


Figure 11: Comparing the crack number values for tensile strain values: (a) 1.0%, (b) 2.0% and (c) 3.0%.

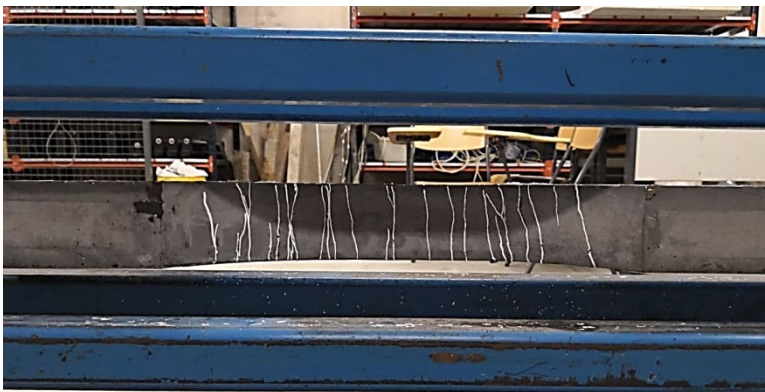
Fibre content very clear influenced the specimens with two different fibre volume contents (U1 with  $V_f = 160 \text{ kg/m}^3$  and U2 with  $V_f = 80 \text{ kg/m}^3$ ), especially considering that all the specimens had an identical UHPFRC matrix, rebar

diameter and cross-section dimensions. The average value of the number of cracks obtained for the specimens with UHPFRC type U1 increased from 8 to 25 (almost 3-fold) simply by increasing tensile strain from 1.0‰ to 3.0‰. For the specimens with UHPFRC type U2, the number of the cracks rose from 3 to 17 (almost 6-fold). Hence crack spacing decreased with increasingly applied tensile strain. From the photographs in Figure 12, the crack spacing for the specimens with UHPFRC type U1 is narrower than it is for UHPFRC type U2, and it displays better microcrack propagation behaviour.

(a)



(b)



**Figure 12.** The crack pattern obtained at the 3.5‰ tensile strain level,

a) specimen DB #U1-1 with  $V_f = 160 \text{ kg/m}^3$ , b) specimen DB #U2-1 with  $V_f = 80 \text{ kg/m}^3$ .

From these observations, we note that the number of cracks and the average crack spacing of the UHPFRC tensile elements were influenced by fibre content.

#### 5.4. Developing a fragility curve for the cracking data

A probability distribution is a statistical function that describes all the possible values and likelihoods that a random variable can take within a given range [41]. An alternative description of distribution is given by the cumulative distribution function (CDF), which is the probability of the value of the variable being less than or equalling  $x$  [42].

$$F(x) = P[X \leq x] = \alpha \quad (3)$$

The CDF is the area according to the probability density function from  $-\infty$  to  $x$ . For continuous distribution, it can be expressed mathematically as Eq. 4:

$$F(x) = P[-\infty < X \leq x] = \int_{-\infty}^x f(x) dx \quad (4)$$

For discrete distribution, the CDF can be expressed as Eq.5:

$$F(x) = P[X \leq x] = \sum_{i=0}^x f(i) \quad (5)$$

On probability curves, the horizontal axis is the allowable domain for the given probability function. As the vertical axis is a probability, it must fall between zero and one.

In the present research, we used the Rice probability density function (Eq. 6) and the corresponding CDF (Eq. 7).

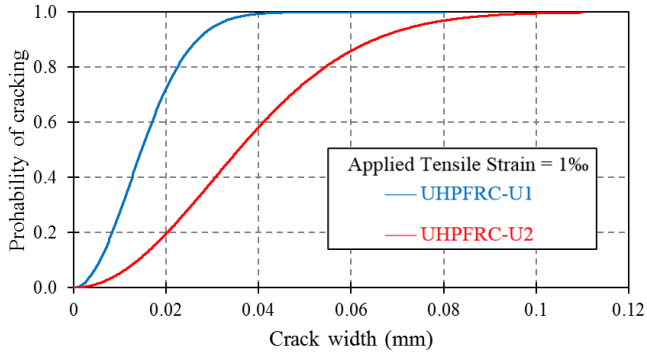
$$f(x) = \frac{x}{\sigma^2} \exp\left(-\frac{(x^2 + \nu^2)}{2\sigma^2}\right) I_0\left(\frac{x\nu}{\sigma^2}\right) \quad (6)$$

$$f(x) = 1 - Q_1\left(\frac{\nu}{\sigma}, \frac{x}{\sigma}\right) \quad (7)$$

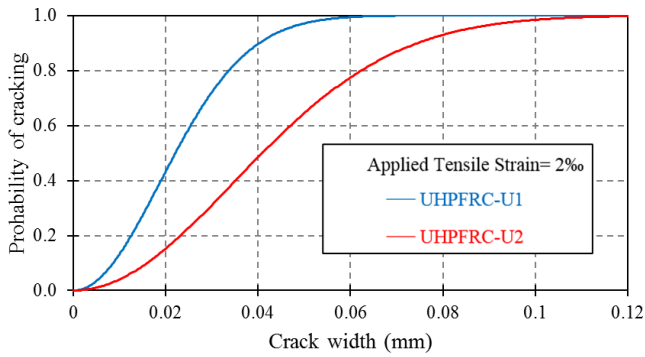
where  $\sigma$  and  $\nu$  are continuous parameters,  $I_0$  is the modified Bessel function of the first kind with order zero, and  $Q_1$  is the Marcum Q-function.

A fragility function (or a fragility curve) represents the CDF of an asset's capacity to resist an undesirable limit state [43]. We applied this analysis method to present the probability of exceeding crack width with a specific tensile strain for UHPFRC types U1 and U2. Fragility curves were calculated based on all the crack widths detected for all the specimens at the applied tensile strains of 1.0‰, 2.0‰ and 3.0‰ (see Fig. 13).

(a)



(b)



(c)

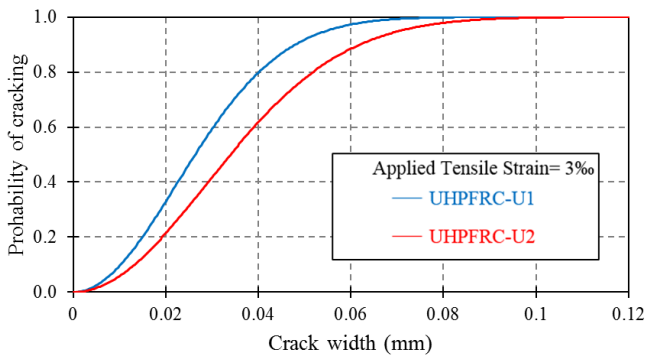


Figure 13: Fragility curves based on the cracking data obtained for the specimens with UHPFRC U1 and U2: tensile strain level (a) 1.0‰; (b) 2.0‰; (c) 3.0‰.

At all different applied tensile strain levels, the probability curve of UHPFRC type U1 was placed on top of the UHPFRC type U2 probability curve. This means that for the specific probability level, the UHPFRC type U2 had a wider crack width. For a high tensile strain rate (see Fig. 13.c), the probability curve of the two UHPFRC came closer to one another and the difference between them was smaller. This behaviour can be explained by the fibre pull-out mechanism that happens at the high tensile strain rate. At these rates of tensile strains, almost all the fibres were pulled out from the concrete matrix and, therefore, tensile stresses were mostly carried out by steel rebars. As the steel rebar diameter was the same for the two considered UHPFRC concretes, both curves were close together. Hence, for the UHPFRC elements with a high steel reinforcement rate, the steel fibre efficiency in the ultimate limit state was poor.

In order to better understand the difference between the fragility curve behaviour of UHPFRC types U1 and U2, the crack widths corresponding to the 5%, 50%, and 95% probability levels are presented in Table 5. These values represent the lower and higher characteristic values of the results.

Table 5: Crack width corresponding to the probability 0.05, 0.50 and 0.95 values for UHPFRC U1 and U2 (units: in mm).

UHPFRC type	Lower characteristic value (5% of the results)	Mean value (50% of the results)	Higher characteristic value (95% of the results)	$\left( \beta = \frac{w_{95\%}}{w_{50\%}} \right)$
1 ‰				
U1	0.004	0.015	0.031	2.07
U2	0.010	0.036	0.074	2.08
2 ‰				
U1	0.006	0.022	0.046	2.08
U2	0.011	0.041	0.085	2.09
3 ‰				
U1	0.007	0.026	0.055	2.09
U2	0.009	0.034	0.071	2.08

By increasing the tensile strain rate, the crack width values rose. For all cases, UHPFRC type U2 obtained higher crack width values. In serviceability behaviour terms, at the probability level of 0.95 (see Table 5), crack width was narrower than the limit crack width limitation value defined by French code NF P 18-710 [17] for UHPFRC elements (0.1 mm, the lowest value for R-UHPFRC members). Neither UHPFRC type exceeded this crack width limitation despite the fact that the average strains surpassed the level of the reinforcement yielding. The  $\beta$  value was calculated by dividing the maximum value ( $w_{95\%}$ ) by the mean value ( $w_{50\%}$ ). The  $\beta$  values obtained by this method can be considered reliable and accurate

enough to relate the maximum to the average crack width values.

## **6. Conclusions**

An experimental program based on direct tensile tests was performed to study the cracking behaviour of R-UHPFRC by also comparing the maximum crack widths to average values. In this study, two UHPFRC types with different fibre volume contents were used and the main following conclusions were drawn:

- For both the R-UHPFRC tensile elements with UHPFRC types U1 ( $V_f = 2\%$ ) and U2 ( $V_f = 1\%$ ), the first detected crack occurred at a lower tensile strain level than 0.5%. Average crack width after the first cracking for the R-UHPFRC ties with UHPFRC type U1 was almost constant with a value of about 0.04 mm, and one of about 0.07 mm for type U2.
- The maximum crack width (obtained by a microscope camera that detected all cracks) can be more than double the average crack width, and the  $\beta$  factor can be accepted as two.
- As expected, R-UHPFRC type U1 generally demonstrated better cracking behaviour than R-UHPFRC type U2. At the high applied tensile strain level (up to 3.5% in this study), the maximum crack width obtained values up to 0.1 mm, which means that this UHPFRC type can meet the crack width limitation for all exposure classes.
- The characteristic crack width value obtained from the fragility curves corresponding to the probability level of 0.95 under SLS conditions was narrower than the crack width limitation by French code NF P 18-710 (0.1 mm, the lowest value for R-UHPFRC members). This result leads to the conclusion that both reinforced UHPFRC types can meet the serviceability crack width limitation, thanks to the rebars and fibres synergy.

## **Acknowledgments**

This study forms part of Project BIA2016-78460-C3-1-R, supported by the Ministry of Economy and Competitiveness of Spain.

## **References**

- [1] C. Burns, "Serviceability analysis of reinforced concrete based on the tension chord model," IBK Bericht, vol. 342, 2012.
- [2] D. Honfi, Design for Serviceability-A probabilistic approach. Lund University, 2013.
- [3] R. Sahamitmongkol and T. Kishi, "Tension stiffening effect and bonding characteristics of chemically prestressed concrete under tension," Materials

- and structures, vol. 44, no. 2, pp. 455-474, 2011.
- [4] V. Gribniak, H. A. Mang, R. Kupliauskas, and G. Kaklauskas, "Stochastic tension-stiffening approach for the solution of serviceability problems in reinforced concrete: Constitutive modeling," *Computer-Aided Civil and Infrastructure Engineering*, vol. 30, no. 9, pp. 684-702, 2015.
- [5] R. Muhamad, M. M. Ali, D. J. Oehlers, and M. Griffith, "The tension stiffening mechanism in reinforced concrete prisms," *Advances in Structural Engineering*, vol. 15, no. 12, pp. 2053-2069, 2012.
- [6] J. C. Walraven, *Model Code 2010-Final draft: Volume 1*. fib Fédération internationale du béton, 2012.
- [7] S. AFGC, "Bétons fibrés à ultra-hautes performances–Recommandations provisoires," AFGC, France, 2002.
- [8] J. C. Committee, "Recommendations for design and construction of high performance fiber reinforced cement composites with multiple fine cracks," Japan Society of Civil Engineers, Tokyo, Japan, 2008.
- [9] S. Cahier Technique, "Béton fibré ultra-performant (BFUP)-Matériaux, dimensionnement et exécution," *Projet*, 2014.
- [10] A. Belarbi and T. T. Hsu, "Constitutive laws of concrete in tension and reinforcing bars stiffened by concrete," *Structural Journal*, vol. 91, no. 4, pp. 465-474, 1994.
- [11] D. Z. Yankelevsky, M. Jabareen, and A. D. Abutbul, "One-dimensional analysis of tension stiffening in reinforced concrete with discrete cracks," *Engineering Structures*, vol. 30, no. 1, pp. 206-217, 2008.
- [12] R. S. Stramandinoli and H. L. La Rovere, "An efficient tension-stiffening model for nonlinear analysis of reinforced concrete members," *Engineering Structures*, vol. 30, no. 7, pp. 2069-2080, 2008.
- [13] M. P. Collins and D. Mitchell, *Prestressed concrete structures*. Prentice Hall Englewood Cliffs, NJ, 1991.
- [14] G. Kaklauskas, "Integral constitutive model for deformational analysis of flexural reinforced concrete members," *Statyba*, vol. 7, no. 1, pp. 3-9, 2001.
- [15] T. T. Hsu, *Unified theory of reinforced concrete*. Routledge, 2017.
- [16] K. Fields and P. H. Bischoff, "Tension stiffening and cracking of high-strength reinforced concrete tension members," *Structural Journal*, vol. 101, no. 4, pp. 447-456, 2004.
- [17] K. Patel, S. Chaudhary, and A. Nagpal, "A tension stiffening model for analysis of RC flexural members under service load," *Computers and Concrete*, vol. 17, no. 1, pp. 29-51, 2016.
- [18] S.-C. Lee, J.-Y. Cho, and F. J. Vecchio, "Tension-Stiffening Model for Steel Fiber-Reinforced Concrete Containing Conventional Reinforcement," *ACI Structural Journal*, vol. 110, no. 4, 2013.
- [19] P. H. Bischoff, "Tension stiffening and cracking of steel fiber-reinforced concrete," *Journal of materials in civil engineering*, vol. 15, no. 2, pp. 174-

- 182, 2003.
- [20] A. Amin, S. J. Foster, and M. Watts, "Modelling the tension stiffening effect in SFR-RC," *Magazine of Concrete Research*, vol. 68, no. 7, pp. 339-352, 2016.
  - [21] J. R. Deluce and F. J. Vecchio, "Cracking Behavior of Steel Fiber-Reinforced Concrete Members Containing Conventional Reinforcement," *ACI Structural Journal*, vol. 110, no. 3, 2013.
  - [22] P. Bernardi, E. Michelini, F. Minelli, and G. Tiberti, "Experimental and numerical study on cracking process in RC and R/FRC ties," *Materials and Structures*, vol. 49, no. 1-2, pp. 261-277, 2016.
  - [23] F. Baby, B. Graybeal, P. Marchand, and F. Toutlemonde, "UHPFRC tensile behavior characterization: inverse analysis of four-point bending test results," *Materials and structures*, vol. 46, no. 8, pp. 1337-1354, 2013.
  - [24] S.-C. Lee, H.-B. Kim, and C. Joh, "Inverse Analysis of UHPFRC Beams with a Notch to Evaluate Tensile Behavior," *Advances in Materials Science and Engineering*, vol. 2017, 2017.
  - [25] F. Baby, B. A. Graybeal, P. Marchand, and F. Toutlemonde, "Identification of UHPFRC tensile behaviour: methodology based on bending tests," 2013.
  - [26] F. Baby, B. Graybeal, P. Marchand, and F. Toutlemonde, "Proposed flexural test method and associated inverse analysis for ultra-high-performance fiber-reinforced concrete," *ACI Materials Journal*, vol. 109, no. 5, p. 545, 2012.
  - [27] J. Á. López, P. Serna, J. Navarro-Gregori, and E. Camacho, "An inverse analysis method based on deflection to curvature transformation to determine the tensile properties of UHPFRC," *Materials and Structures*, vol. 48, no. 11, pp. 3703-3718, 2015.
  - [28] J. A. López Martínez, "Characterisation of The Tensile Behaviour of UHPFRC by Means of Four-Point Bending Tests," 2017.
  - [29] M. Khorami, J. Navarro-Gregori, P. Serna, and M. Navarro-Laguarda, "A testing method for studying the serviceability behavior of reinforced UHPFRC tensile ties," in *IOP Conference Series: Materials Science and Engineering*, 2019, vol. 596, no. 1, p. 012022: IOP Publishing.
  - [30] N. Lee and D. Chisholm, "Reactive Powder Concrete, Study Report SR 146," ed: Ltd. Judgeford, New Zealand, 2005.
  - [31] M. H. Beigi, J. Berenjian, O. L. Omran, A. S. Nik, and I. M. Nikbin, "An experimental survey on combined effects of fibers and nanosilica on the mechanical, rheological, and durability properties of self-compacting concrete," *Materials & Design*, vol. 50, pp. 1019-1029, 2013.
  - [32] V. C. Li, "Large volume, high-performance applications of fibers in civil engineering," *Journal of Applied Polymer Science*, vol. 83, no. 3, pp. 660-686, 2002.
  - [33] J. Edgington, "Steel fibre reinforced concrete volume B," University of



- Surrey, 1973.
- [34] I. Löfgren, *Fibre-reinforced Concrete for Industrial Construction-a fracture mechanics approach to material testing and structural analysis*. Chalmers University of Technology, 2005.
  - [35] V. Afroughsabet, L. Biolzi, and T. Ozbakkaloglu, "High-performance fiber-reinforced concrete: a review," *Journal of Materials Science*, vol. 51, no. 14, pp. 6517-6551, 2016.
  - [36] T. E. T. Buttignol, J. Sousa, and T. Bittencourt, "Ultra High-Performance Fiber-Reinforced Concrete (UHPFRC): a review of material properties and design procedures," *Revista IBRACON de estruturas e materiais*, vol. 10, no. 4, pp. 957-971, 2017.
  - [37] E. Fehling, M. Schmidt, J. Walraven, T. Leutbecher, and S. Fröhlich, *Ultra-high performance concrete UHPC: Fundamentals, design, examples*. John Wiley & Sons, 2014.
  - [38] T. Makita and E. Brühwiler, "Tensile fatigue behaviour of Ultra-High Performance Fibre Reinforced Concrete combined with steel rebars (R-UHPFRC)," *International Journal of Fatigue*, vol. 59, pp. 145-152, 2014.
  - [39] M. Rauch and V. Sigrist, "Dimensioning of Structures made of UHPFRC," in *IABSE Symposium Report*, 2010, vol. 97, no. 34, pp. 39-46: International Association for Bridge and Structural Engineering.
  - [40] V. Sigrist and M. Rauch, "Deformation behavior of reinforced UHPFRC elements in tension," *Tailor Made Concrete Structures-Walraven & Stoelhorst* (eds), pp. 405-410, 2008.
  - [41] D. Redaelli, "Testing of reinforced high performance fibre concrete members in tension," in *Proceedings of the 6th Int. Ph. D. Symposium in Civil Engineering, Zurich 2006*, 2006, no. CONF, p. 8: *Proceedings of the 6th Int. Ph. D. Symposium in Civil Engineering, Zurich 2006*.
  - [42] B. S. Institution, *Eurocode 2: Design of concrete structures: Part 1-1: General rules and rules for buildings*. British Standards Institution, 2004.
  - [43] V. Gribniak, G. Kaklauskas, and D. Bačinskas, "State-of-art review of shrinkage effect on cracking and deformations of concrete bridge elements," *Baltic Journal of Road & Bridge Engineering (Baltic Journal of Road & Bridge Engineering)*, vol. 2, no. 4, 2007.
  - [44] E. Brühwiler, "Swiss Standard SIA 2052 UHPFRC: Materials, Design and Application," in *4th International Symposium on Ultra-High Performance Concrete and High Performance Materials*, 2016, no. POST\_TALK.
  - [45] L. Ostergaard, R. Walter, and J. F. Olesen, "Method for determination of tensile properties of engineered cementitious composites (ECC)," *Proceedings of ConMat'05*, 2005.
  - [46] T. Kanakubo, "Tensile characteristics evaluation method for ductile fiber-reinforced cementitious composites," *Journal of Advanced Concrete Technology*, vol. 4, no. 1, pp. 3-17, 2006.

- [47] J. López, P. Serna, J. Navarro-Gregori, and H. Coll, "Comparison between inverse analysis procedure results and experimental measurements obtained from UHPFRC Four-Point Bending Tests," in Proceedings of the 7th RILEM Workshop on High Performance Fiber Reinforced Cement Composites (HPFRCC7), 2015, pp. 185-192.

## ***Chapter 6. Resume and general discussion of the results***

This chapter gives an overview of the previous chapters of the thesis. All the works carried out in this thesis are briefly presented and the main results are provided. In this way, the reader can read this chapter together with Chapter 1. “Introduction” and get an overview of the work done in this thesis.

Some examples of the most important results are given in this chapter. However, further details can be found in the respective papers of the thesis.

The discussion is divided into four parts: Proposed test method, Tensile behaviour, and tension stiffening of R-UHPFRC tie elements, Shrinkage behaviour of UHPFRC and Cracking and serviceability behaviour.

## **6.1. Proposed test method**

### **6.1.1. Description and justification of the proposed test setup**

The first phase of this PhD project was designing and evaluating a novel test methodology to conduct the uniaxial tensile test for studying the tensile and cracking behaviour of R-UHPFRC tie elements (Chapter 3 in this thesis).

The uniaxial tensile test is the most appropriate test method for examining the UHPFRC behavior under SLS circumstances. To have a convenient and efficient test method, the most essential parameters involved in the tensile behaviour of R-UHPFRC such as material properties, reinforcement ratio, section size, the cover of the concrete, and fibre amount should be considered for design of the test method. There are other involved parameters in designing the test machine, such as easy to perform and economical features, ease and convenience for preparing specimens in the lab, available technologies and measurement devices, machine size and required space in the laboratory, the safety of operation, ease of installing the specimens in the test machine and simplicity of analysing results. Based on available facilities, an attempt was made to meet all mentioned parameters for designing the proposed test method.

In order to study the UHPFRC design requirement under SLS, an appropriate testing method was needed to perform experimental studies for the present PhD thesis. A test method was proposed to able to examine the behaviour of R-UHPFRC tensile elements under serviceability loads. For evaluating the proposed test method, two experimental campaigns were programmed with UHPFRC materials with two different fibre volume content. By conducting the uniaxial test and employing the proposed test method, some parameters were obtained, such as the stiffness of the elastic region, the average tensile stress-strain relationship of the element, the tension stiffening behaviour, and the average crack width, number of cracks and the average spacing between cracks. In the final loading stage, after reaching the strain of 2‰ recorded by the displacement transducers, the cracking pattern along the specimen was captured.

Details of the proposed test methodology and the preliminary experimental results and analysis of the obtained data were described by means of one conference paper and one journal paper:

- 1<sup>st</sup> paper: Khorami, M., et al. (2019). A testing method for studying the serviceability behavior of reinforced UHPFRC tensile ties. IOP Conference Series: Materials Science and Engineering, IOP Publishing.
- 2<sup>nd</sup> paper: Khorami, M., et al. "Experimental methodology on the serviceability behaviour of reinforced ultra-high performance fibre reinforced concrete tensile elements." *Strain*: e12361.

The following important criteria were taken into account when designing the main frame:

- Easy access to the specimen and suitable height for the machine to facilitate the operator's work: for visual observations during the performing test, the specimen should be located in an adequate position and the operator should have good access to carry out any manual measurement.
- Easy installation and the possibility to use the tower crane in the lab to carry the heavy concrete specimens and put them into the machine from the topside.
- The available space in the laboratory and portability of the machine: an attempt was made that the test machine be portable and do not need to support or be fixed to the floor or walls of the laboratory.
- Possibility to perform the test by one person.
- Easy installation of the measurement instruments after placing the specimen in the machine and performing the measurements.

The design of the main frame should be done in such a way that it can carry and support the applied tensile force to the RC specimen while also the deformation in its components being in the allowable range. The horizontal mode would be the best location for the test machine based on the criteria listed above. The proposed main frame of the test machine consists of two vertical plates placed at both ends of the main frame and they were connected by four steel rectangle tube sections. The main steel frame was designed under an axial load of 200 kN which was applied at the center of the lateral plates. Figure 7.1 illustrates the components of the main frame of the proposed test machine.

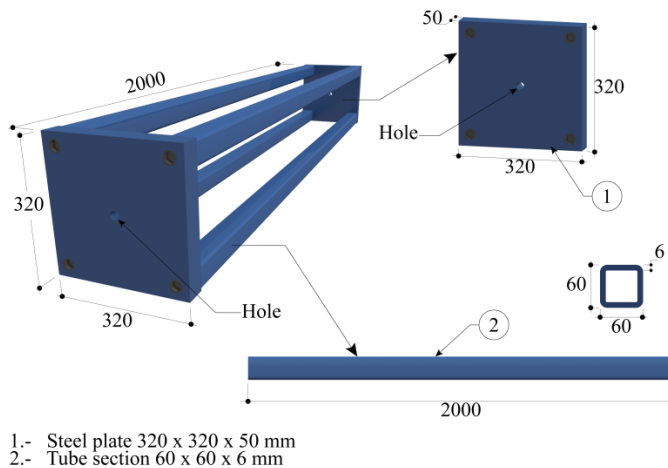


Figure 6- 1: Main steel frame and its components.

Both end plates were designed by a dimension of 320×320 mm with a thickness

of 50 mm. The horizontal tube bars between two end plates have 2000 mm lengths with a rectangle section of 60×60 mm and 6 mm-thick.

A hydraulic jack was designed to create a tensile load. The designed hydraulic jack had two outside and inside cylindrical segments and by increasing the oil pressure into the outside cylindrical segment, the inside cylindrical segment goes out and generate an outward displacement. The hydraulic jack was designed as a circular tube with a longitudinal hole to able passing a steel rod through the longitudinal axis of the cylindric segments to convert the generated displacement to tensile load. Figure 6.2 illustrate the designed hydraulic jack and its functionality. The hydraulic jack was placed at the left side of the main frame, and it was attached to the end plate by a flange connection.

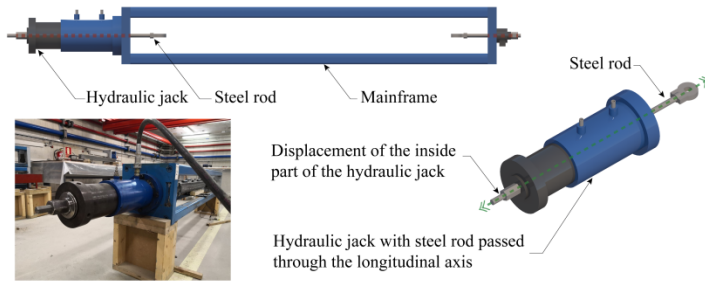


Figure 6- 2: Hydraulic jack functionality for generating the tensile load.

The hydraulic jack was controlled by an electric oil pump and the oil pressure was controlled manually. The connection between the oil pump and hydraulic jack was made by a high-pressure hose and intel nozzle.

The connection mechanism for fastening the reinforced concrete element to the transfer force device was a primary challenge in conducting the direct tensile test. A novel connection system was designed which included two-piece steel jaws with 2 mm-high indented corrugations. Each segment was symmetric with the other segment and assembled by using six bolts in three axes (see Figure 6-3) with a diameter of 13 mm. Dimensions of the steel-jaw were 250 mm length, 100 mm width and 40 mm of thickness. The steel jaw was designed with two separate components to make specimen assembly simple. It was proposed to install two additional reinforcements at both ends of the specimens (detail of specimen and rebars are provided in the next section) to increase the frictional force between the rebar and the indented corrugations over the jaw surface, hence the width of the indented corrugations zone was chosen by 50 mm. This width size for the corrugation zone allows connecting specimens with different rebar diameters. For instance, for specimens reinforced by rebars with  $\text{Ø}=10$  mm, the occupied width inside the steel jaw would be 30 mm.

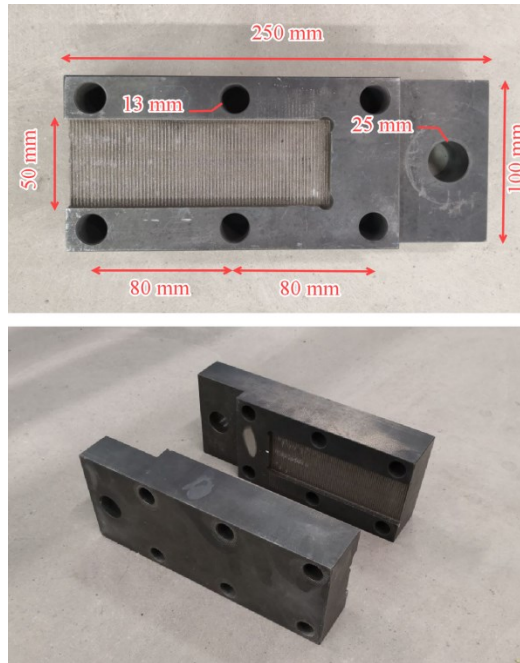


Figure 6- 3: Details of the proposed steel jaw.

By tightening the bolts of the steel jaw, the indented corrugations of the steel jaw go into the rebar body and produce sufficient friction to transfer the tensile load to the specimen.

The generated tensile load in the steel rod by the hydraulic jack should be transferred to the steel jaw. For that, at the end part of the steel jaw, a hole was placed to able passing a bolt with  $\text{Ø}=25$  mm and connect the steel jaw to the steel rod. The connection of the steel rod to the bolt was done by a bearing system placed at the end part of the rod (see Figure 6-4).

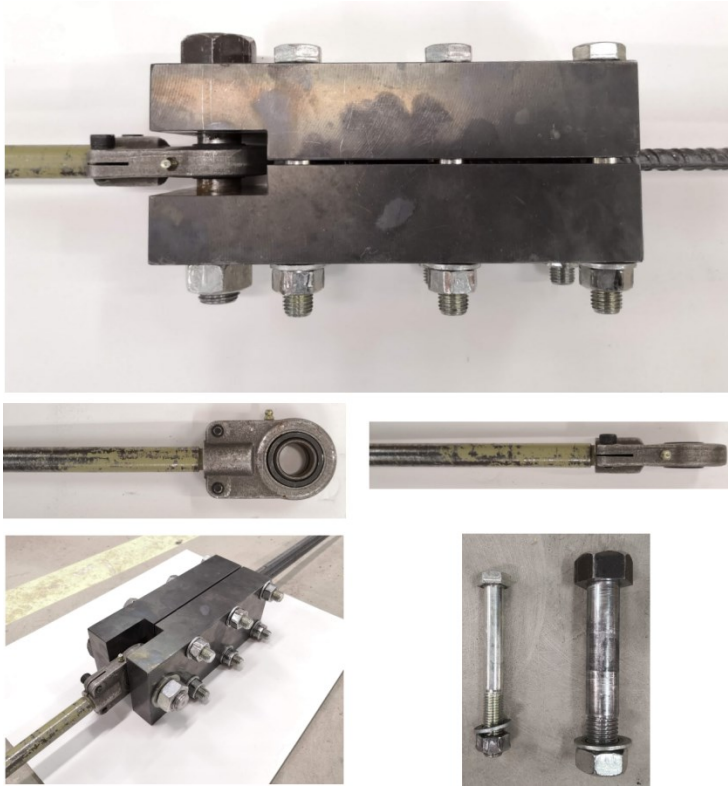


Figure 6- 4: Bearing connection and connecting system steel rod to steel jaw.

The steel rod was designed by using a high-strength steel material with  $f_y=1000$  MPa to carry the 200 kN tensile force. The diameter of the designed steel rod was  $\varnothing=20$  mm and it was placed on both sides of the main frame. The left steel rod had 800 mm-length and the right side one had 600 mm-length. To fix the steel rod at the back side of the right plate and end border of the hydraulic jack and for tightening the specimen in the test machine, a screw thread was designed on both extremes of the steel rods. A steel anchorage with 50 mm length and a steel washer was placed at each side. The bearing connection system provides a hinge connection at the ends of the specimen and prevents to cause any bending due to any global rotations of the specimen. Figures 6-5 (a) and (b) illustrate the complete view of the designed test machine from two different viewpoints.



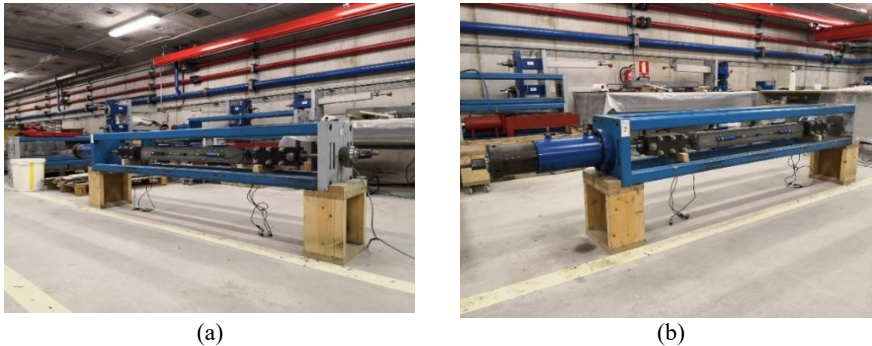


Figure 6- 5: Complete view of the designed test machine

### 6.1.2. Specimens preparation

Two different types of specimens were used in this PhD project. The main work presented in this thesis is based on test results obtained from the uniaxial tensile test with prismatic specimens. Furthermore, a special tensile test with specimens with Dog bone-shaped was performed to investigate the serviceability behaviour of reinforced UHPFRC tensile elements and their cracking behaviour. Complete detail of Dog-bone specimens and the test method are presented in section 6.4. in this chapter.

The prismatic reinforced specimens were made with a square cross-section and central rebar. The specimen length was  $1000 \pm 2$  mm and metallic molds were used to casting them. Three different cross-section sizes and three different steel reinforcement rebar diameters were used in this PhD project. Using different section sizes and rebar diameters helps to have different reinforcement ratios to study the reinforcement ration effect and also the size effect.

The dimensions of the specimens' cross-section and reinforcement rebar were selected in such a way that to achieve the tensile deformation of 2.5%, the applied tensile load would be not beyond 160 kN, because the test machine was designed for an applied tensile load of 200 kN. Furthermore, it is also possible that at high levels of the applied tensile load, rebar slip occurs inside the steel jaw.

The geometry of the specimens used in this PhD thesis is reported in Table 6.1. It should be mentioned that in this PhD project, two types of UHPFRC with a difference of the fibre volume content were used and for each specimen category, 3 samples were prepared. Hence, 54 specimens were made for two types of UHPFRC and three different section sizes with three different rebar diameters were employed. Although, for studies presented in chapter 3 (paper 4<sup>th</sup>), some specimens were made without fibre and with hybrid fibre content.

Table 6- 1: General geometry details of the specimens.

#	Cross-section dimension (mm <sup>2</sup> )	Number of the specimens	Reinforcement diameter (mm)	Reinf. Ratio (%)	Cover (mm)
1	100×100	3	16	2.01	42
2	100×100	3	12	1.13	44
3	100×100	3	10	0.79	45
4	80×80	3	16	3.14	32
5	80×80	3	12	1.77	34
6	80×80	3	10	1.23	35
7	60×60	3	16	5.58	22
8	60×60	3	12	3.14	24
9	60×60	3	10	2.18	25

The realized studies in paper 1<sup>st</sup> and paper 2<sup>nd</sup> were preliminary studies for evaluating the proposed test method, and for that, a small experimental campaign was conducted for that purpose. In paper 1<sup>st</sup>, one type of UHPFRC with a fibre content volume of 160 kg/m<sup>3</sup> equivalent to 2% by volume of concrete was used, while in paper 2<sup>nd</sup>, two concrete mixture types that only vary in fibre content terms were employed. So that, the fibre dosage was 160 kg/m<sup>3</sup> (concrete C1) and 80 kg/m<sup>3</sup> (concrete C2), 2 vol% and 1 vol% fibre content, respectively.

The specimen's geometry details used in paper 1<sup>st</sup> and paper 2<sup>nd</sup> are shown in Table 6-2. In paper 1<sup>st</sup>, all the specimens were with cross-sections 80×80 mm<sup>2</sup> and rebar diameters with 10 mm, 12mm, and 16mm. For each test category (based on section size and rebar diameter), three specimens were cast. In paper 2<sup>nd</sup>, for each UHPFRC type, the same cross-section size (100×100 mm<sup>2</sup>) and rebar diameter of 12 mm were used. For each test category, three specimens were also cast.

Table 6- 2: The specimen's geometry details used in papers 1<sup>st</sup> and Paper 2<sup>nd</sup>

Paper number	Material Code	Fibre dosage	Specimen ID	Section size (mm <sup>2</sup> )	Rebar diameter (mm)
Paper Ia	C1	160 kg/m <sup>3</sup> (Vol. 2%)	T-10-1	80×80	10
			T-10-2	80×80	10
			T-10-3	80×80	10
			T-12-1	80×80	12
			T-12-2	80×80	12
			T-12-3	80×80	12
			T-16-1	80×80	16
			T-16-2	80×80	16
			T-16-3	80×80	16
Paper Ib	C1	160 kg/m <sup>3</sup> (Vol. 2%)	T-10-12-C1-1	100×100	12
			T-10-12-C1-2	100×100	12
			T-10-12-C1-3	100×100	12
	C2	80 kg/m <sup>3</sup> (Vol. 1%)	T-10-12-C2-1	100×100	12
			T-10-12-C2-2	100×100	12
			T-10-12-C2-3	100×100	12

The main problem in running the uniaxial tensile experiment of reinforced concrete ties is yielding the outer part of the rebar (without concrete) of the specimen. In order to prevent the main bar from yielding and failing on both ends without concrete, two 45-cm long rebars were attached in the external region of the specimen, and penetrated 22.5 cm into the concrete specimen (see Fig. 6-6). These two complementary rebars were welded at a length of 5 cm to the main bar to ensure that no pull-out would occur.

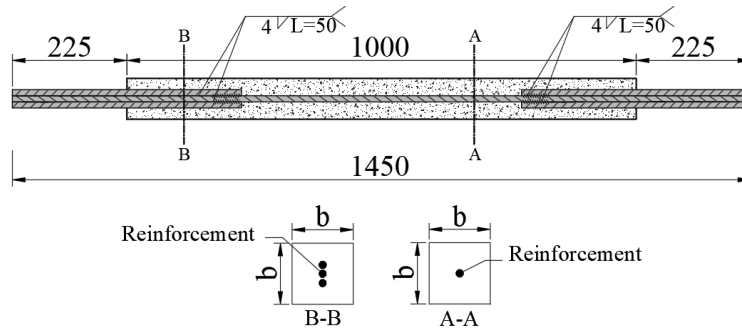


Figure 6- 6: Specimen reinforcement details (units in mm), prismatic reinforcement specimen with main and complimentary rebars.

The main steel reinforcement rebar had 1450 mm-long and during the manufacturing procedure, an attempt was made to locate it exactly on the centre section to avoid eccentricity and bending effects.

### 6.1.3. Material


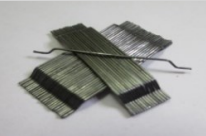
#### *Steel fibres*

The considered experimental programs for all individual papers contain the same material composition. Two types of UHPFRC material were used by the difference of fibre dosage. The dosage of steel fibres for the first (C1) and second (C2) mix designs were 160 and 80 kg/m<sup>3</sup>, respectively. These dosages correspond to 1% and 2% of the concrete volume. The steel fibres type for two UHPFRC types were same. The length and diameter of applied steel fibres were 13 and 0.2 mm, respectively and their tensile strength was more than 2000 MPa.

It should be mentioned that for the study presented in chapter 4 which is about the cracking behaviour and the effect of fibre content on the post-cracking tensile stiffness capacity of R-UHPFRC, four different fibre dosages with the same composition of the matrix mixture were employed. In this specific study, two of the UHPFRC mixtures had same fibre dosage value as UHPFRC type C1 and C2,

and one mixture without fibre (C0). The fourth UHPFRC type (C3) was made with a hybrid combination of short and long fibres. The long fibres were the hooked end type with a length of 30 mm and diameter of 0.375 mm and the short fibres were identical fibres used for C1 and C2. Table 6-3 provides a summary of the properties of steel fibres that were used in this present PhD study.

Table 6- 3: Properties details of steel fibres.

Steel Fibre type (SF)	SF1=High-strength microsmooth steel fibres	SF2=Macrohooked end steel fibres
		
fibre shape	straight	Hooked end
Length (mm)	13±1	30±1
Diameter (d)	0.2±0.04	0.375±0.04
Aspect ratio (L/d)	65	80
Tensile strength	>2000MPa	>2300MPa
Number of fibres per kg	77978	7801

The Hybrid combination for UHPFRC type (C3) was called (C8080) with fibre type SF1 and SF2 (see Table 6-3) and fibre content of  $V_f=1\%$  for SF1, and  $V_f=1\%$  for SF2. The hybrid combination fibre dosage was used in the work presented in paper 4<sup>th</sup>.

### ***Reinforcement steel rebars***

The main steel rebar had 1450 mm length and three different diameters ( $\text{Ø}10$ ,  $\text{Ø}12$ , and  $\text{Ø}16$  mm) were used for each cross-section group. The complementary rebars had the same diameter as the main steel rebar with 450 mm length. The variation of rebars ratios was from 0.79% to 5.5% (see table 6-1) and it was for considering the reinforcement ratio effect on R-UHPFRC tensile behaviour. The nominal yield stress of rebars was 500 MPa and a 200 GPa modulus of elasticity was assumed for steel reinforcements.

### ***UHPFRC Mixture Design***

The mixing properties used in the present PhD project are given in Table 6-4. This mixture design was used in all experimental programs presented in this PhD study. The water/binder (W/B) ratio of the UHPFRC mixture was 0.16. Cement and silica fume were used as cementitious materials. The cement type was CEM I 42.5 R-SR5, with properties according to specification EN 197-1:2011, produced by LafargeHolsim Cement Co., Ltd (Spain); the silica fume was supplied by Elkem

Co., Ltd. The Elkem Microsilica® 940 D with a density of  $500 \text{ kg/m}^3$  was used to improve the properties and performances of high-performance concrete. To achieve denser packing, silica sand with two size ranges were used. The fine sand and the medium sand were 0.5 and 0.6–1.2 mm in size and their specific gravity was  $2610 \text{ kg/m}^3$ , and silica flour with an average diameter of  $2 \mu\text{m}$  and containing over 98%  $\text{SiO}_2$  was used as the filler. Superplasticizers were used to achieve the expected fluidity and improve compatibility. As mentioned above, two types of steel fibres with a dosage of 1% and 2% of the concrete volume were used for the whole experimental program proposed in this PhD thesis.

Table 6- 4: Mix proportions of UHPFRC

Component	Content ( $\text{kg/m}^3$ )
Cement I 42.5 R/RS	800
Silica Fume 940 D Elkem UD	175
Silica Flour U-S500	225
Fine Sand 0.5 mm	302
Medium Sand 0.6-1.2 mm	565
Water	160
Superplasticizer, Viscocrete 20 HE	30
Fibre	160 or 80

#### 6.1.4. Measurement devices

For studying the serviceability behaviour of R-UHPFRC tensile elements, relevant data from the experimental test should be obtained. These data would be used to evaluate the SLS requirements proposed by existing UHPFRC design codes or for recommending adequate design requirements. Therefore, the test method should be capable to detect the necessary information such as average stress-strain relationship, average tensile stress in the concrete matrix and reinforcement, and the cracking behaviour including the crack width and crack spacing information. The most common and appropriate approach for monitoring the deformation of the RC elements is to use devices that measure the displacement between two points over the concrete surface and Displacement Transducers (DTs) can be a suitable choice. Hence, eight DTs with 350 mm lengths were attached over the specimen by one screw at both ends of the DTs. Four of them were installed on the left side of the specimen (herein called DT-L) and the other four were installed on the right side (herein called DT-R). The position of the eight DTs is shown in Figures 6-7 (a) and (b). Installing the DTs over each face of the specimen, makes it possible to detect any bending or curvature of the specimen during the test.

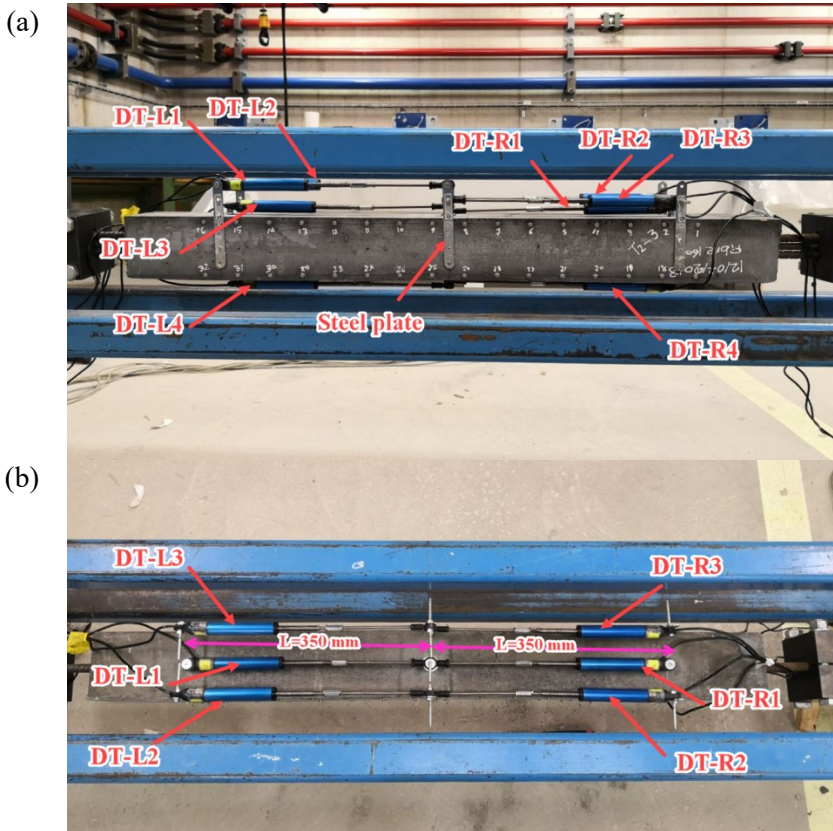


Figure 6- 7: Displacement Transducers position, (a) lateral view, (b) top view.

The average tensile deformation (tensile strain) of the R-UHPFRC element was obtained by dividing the average elongation recorded by eight DTs to 350 mm.

### 6.1.5. Test procedure

The test procedure included two main stages. The first stage was to obtain the average stress-strain relationship of the R-UHPFRC tensile elements, and the second stage was to obtain the cracking behaviour (average crack width, crack spacing and cracking pattern) of the R-UHPFRC tensile elements. The average tensile strain and stress carried by reinforcement and UHPFRC were obtained by assuming that the surface deformations of concrete with steel rebar deformation were equal. The average tensile strain was calculated by the average elongation recorded by eight DTs installed on the left and right sides dividing to the DTs length ( $L=350$  mm).

The first stage of the test was completed when the average element tensile strain

reached to 2‰. At this time, the experiment was stopped, and the crack propagation scheme was drawn (using a correction liquid pen with a steelhead) on the specimen's surfaces without unloading to keep the cracks open. Finally, the number of cracks on two edges of the front, top, and back faces (six edges) was recorded.

#### **6.1.6. Data analysis and interpretation of the results**

The first step for tests data analysis to obtain the average stress-strain relationship of the specimens was evaluating the elongations recorded by DTs in the right and left sides of the specimen and obtaining the average behaviour.

A summary of the average tensile behaviour of the specimens employed in the experimental campaign for paper 1<sup>st</sup> and paper 2<sup>nd</sup> are illustrated in Figures 6-8 and 6-9.

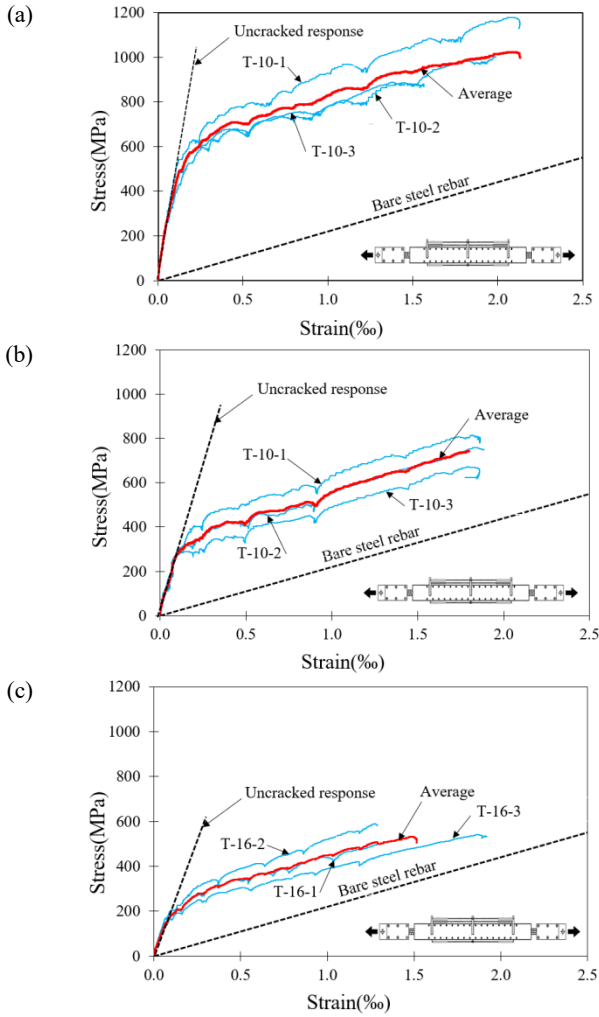


Figure 6- 8: Average tensile behaviour for specimens employed in paper 1<sup>st</sup>, (a) Specimens with rebar  $\varnothing=10$  mm, (b) Specimens with rebar  $\varnothing=12$  mm, (c) Specimens with rebar  $\varnothing=16$  mm.



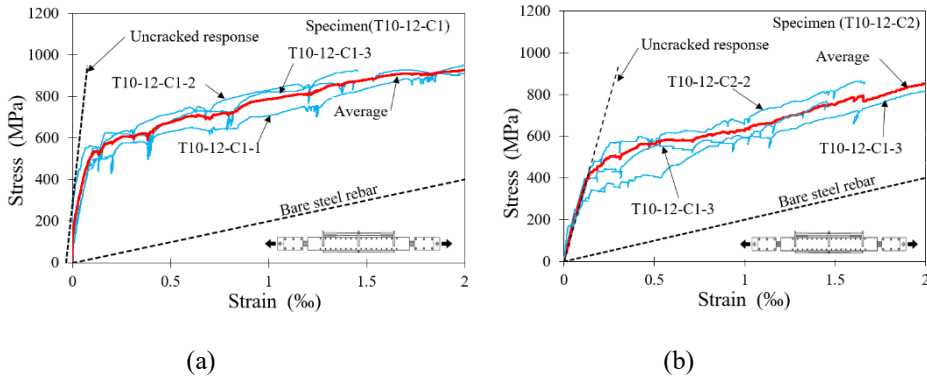


Figure 6- 9: Average tensile behaviour for specimens employed in paper 2<sup>st</sup>, (a) Specimens with UHPFRC type C1 T10-12-C1, (b) Specimens with UHPFRC type C2.

It should be mentioned that the bare steel response was added to the average tensile behaviour diagram to demonstrate the contribution in tension (tension stiffening behaviour: the ability of the concrete to carry the tension between cracks) of the UHPFRC elements. By assuming the simultaneous participation of concrete and steel in tension and with the same strain, it was possible to obtain tensile stresses in concrete by subtracting the strain-stress curve of the bare steel rebar from the total stress-strain curve.

For all of the stress-strain relationship behaviour (hereinafter called average tensile behaviour) of the specimens reported in this PhD thesis, the described approach was used.

Regarding the results obtained from the experimental program for paper 1<sup>st</sup>, the elastic stiffness in the linear region varied from 39 to 42 GPa for the specimens with the Ø10-mm bar, from 19 to 25 GPa for the ties with the Ø12-mm bar, and from 15 to 18 GPa for the ties with the Ø16-mm bar. Based on results obtained from the experimental program for paper 2<sup>nd</sup>, a significant difference was observed for the first cracking strength by increasing the fibre content in the concrete matrix. A significant difference was observed for the first cracking strength by increasing the fibre content in the concrete matrix. The first cracking strength for tie types C1 and C2 was 533 and 426 MPa, respectively, and the average elastic stiffness for UHPFRC types C1 and C2 were 68 and 31 GPa, respectively.

A significant difference was observed for the first cracking strength by increasing the fibre content in the concrete matrix. The first cracking strength for tie type C1 and C2 was 533 and 426 MPa, respectively.

The average tension stiffening diagram of the R-UHPFRC specimens employed in the experimental campaign of paper 1<sup>st</sup> and paper 2<sup>nd</sup> are illustrated in Figures 6-10 and 6-11. It can be observed that no significant strain-hardening behaviour was observed for UHPFRC with  $V_f=160 \text{ kg/m}^3$ . In the other words, the R-UHPFRC specimens exhibit a quasi-constant tension stiffening effect (refer to the

horizontal branch of the curve), even at high-tension strain rates closed to 2‰. Moreover, the increment of the UHPFRC concrete contribution due to the increasing fibre content can be seen.

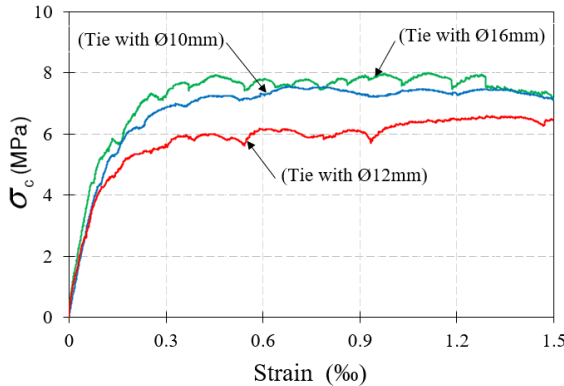


Figure 6- 10: Average tension stiffening diagram of the R-UHPFRC for specimens employed in paper 1<sup>st</sup>.

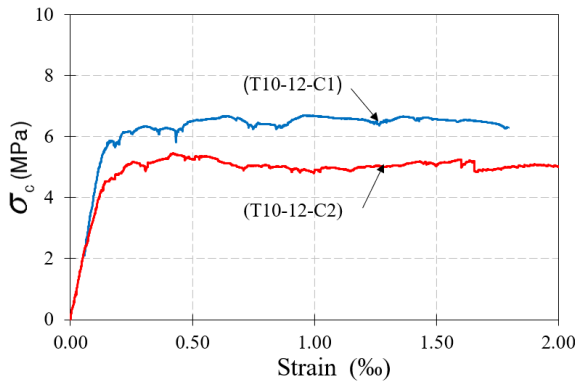


Figure 6- 11: Average tension stiffening diagram of the R-UHPFRC for specimens employed in paper 2<sup>nd</sup>.

In order to study the cracking behaviour and evaluate crack width and propagation of the cracks, the number of the cracks were recorded and the average crack width was calculated by dividing the total elongation at the end of the test procedure by the number of cracks. The crack width measurement was done over two edges of three faces (front, back and top face) of the specimen. The number of cracks in each edge was slightly different due to the inhomogeneous cracking manner.

This measurement method was used for specimens of the experimental campaign in paper 2<sup>nd</sup> to evaluate the proposed test method for studying the fibre content effect on the width of the cracks. As an instance, the obtained results for R-UHPFRC tensile elements with concrete types C1 and C2 for specimens T10-12-

C1-1 and T10-12-C2-1 are presented in Table 6-5.

Table 6- 5: Total number of the cracks and average crack with calculated over six edges for specimen T-12-2.

		T10-12-C1-1 (Force level value = 122.82 kN)			T10-12-C2-1 (Force level value = 110.72 kN)		
Measurement Surface Side	Edges	Total Number of Cracks	Achieved Elongation (mm)	Average Crack Width (mm)	Total Number of Cracks	Achieved Elongation (mm)	Average Crack Width (mm)
Top side	Edge1	78	1.890	0.0242	39	2.299	0.0589
	Edge2	78	1.890	0.0242	39	2.299	0.0589
Front Side	Edge1	77	1.890	0.0245	50	2.299	0.0459
	Edge2	64	1.890	0.0295	47	2.299	0.0489
Back Side	Edge1	87	1.890	0.0217	45	2.299	0.0510
	Edge2	59	1.890	0.0320	38	2.299	0.0605
			Average	0.026		Average	0.054

In this preliminary study that was performed to validate the proposed test method, it was found that the medium crack width for R-UHPFRC tensile elements with fibre volume content of 80 and 160 kg/m<sup>3</sup> were 0.054 and 0.026 mm, respectively. With the proposed test method, the main crack spacing can be obtained by dividing the entire length of the measurement zone by average number of cracks in six edges. The achieved main crack spacing for UHPFRC type C1 and C2 was 10.16 and 17.44 mm, respectively.

Due to the significant importance of the crack width value on the serviceability behaviour, a specific study was performed to evaluate the maximum crack width formed under SLS tensile loads for UHPFRC types C1 and C2, and it was compared with the average values. This research is described in chapter 6 and briefly in section 6.4, which is related to paper 6<sup>th</sup>.

The crack pattern obtained for the two types of UHPFRC showed that substantial microcracks occurred in the specimens with high fibre content and the high fibre content caused the cracking process by minor distance between them. Figures 6-12 (a) and (b) illustrate the crack propagation for UHPFRC types C1 and C2. Considering the difference in cracks amounts and crack distance for two UHPFRC types, the microcracking effect can be taken into account for tension stiffening analysis and serviceability behaviour study.



Figure 6- 12: Crack pattern of specimens (a) UHPFRC type C1 (b) UHPFRC type C2

Regarding to the test parameters, the following conclusions were drawn: The study presented in paper 2<sup>nd</sup> with UHPFRC with fibre content 80 and 160 kg/m<sup>3</sup>, showed that the increase in fibre volume content of concrete has a significant influence on first cracking strength. Hence, the fibre volume content had an important influence on the cracking and serviceability behaviour of R-UHPFRC. The obtained results of the two experimental campaigns (presented in paper 1<sup>st</sup> and 2<sup>nd</sup>) demonstrated the suitability of the proposed test method and pertinent employed measurement devices. Consequently, the proposed test method was appropriate for future studies on serviceability behaviour of R-UHPFRC tensile elements and the proposed testing method and the obtained results are suitable to studies required in the present PhD thesis.

## **6.2. Tensile behaviour and tension stiffening of R-UHPFRC tie elements**

### **6.2.1. Experimental studies**

Two test programs were conducted to study the tensile behaviour and the tension stiffening behaviour of R-UHPFRC tie elements. The first one was an extensive experimental program in which 36 R-UHPFRC tie elements were tested under uniaxial force by employing the proposed tensile test methodology. The reinforcement ratio and steel fibre volume content were two main parameters studied in this work. The average overall tensile behaviour of R-UHPFRC tie elements was obtained experimentally and the contribution of the concrete was compared to tensile properties derived from 4PBT using our research group's proposed inverse analysis method.

In the second test programme, the effect of using micro and macro fibres on the post-cracking behaviour was studied. Results of these two experimental studies were published in a peer-review paper and book chapter:

- Paper 3<sup>th</sup>: Tensile behaviour of reinforced UHPFRC elements under serviceability conditions

*Khorami, M., et al. (2021). "Tensile behaviour of reinforced UHPFRC elements under serviceability conditions." Materials and structures 54(1): 43.*

- 4<sup>th</sup>: Book chapter (BEFIB -RILEM Book series): The Effect of Fiber Content on the Post-cracking Tensile Stiffness Capacity of R-UHPFRC

*Khorami, M., et al. (2020). The Effect of Fiber Content on the Post-cracking Tensile Stiffness Capacity of R-UHPFRC. RILEM-fib International Symposium on Fibre Reinforced Concrete, Springer*

## 6.2.2. Materials, specimens, test setup and procedure

As stated in section 6.1.3, the material used in all papers presented in this Ph.D study is the same. Therefore, the test program in this study was carried out with concrete types C1 ( $V_f = 160 \text{ kg/m}^3$ ) and C2 ( $V_f = 80 \text{ kg/m}^3$ ). The mechanical properties of steel fibres, steel reinforcements rebars, and the UHPFRC mixture proportion are the same as the papers 1<sup>st</sup> and 2<sup>nd</sup>, which are explained in section 6.1.3.

The curing process was the same as the previous experimental work, and all specimens were placed in a high-humidity curing room at 95% relative humidity and temperature of  $T = 20 \pm 2 \text{ }^\circ\text{C}$  for 28 days. For casting the 36 R-UHPFRC specimens, six batches were prepared for each concrete type. The average compression strength values were 154.0 MPa (CV=4.3%) and 139.2 MPa (CV=7.0%) for UHPFRC type C1 and C2, and the average Young's modulus were 48.4 (CV=1.1%) GPa and 46.5 GPa (CV=1.1%).

The tensile properties of both types of UHPFRC were determined (see Table 6-6) by conducting 4PBT and using the inverse analysis method proposed by López, J.A et al. [1, 2], as explained in section 2.4.3. The inverse analysis calculation was done using the average and characteristic curve data that can be seen in Figure 6-13. In these diagrams, the parameter ( $\sigma_{fl}$ ) is the equivalent bending stress.

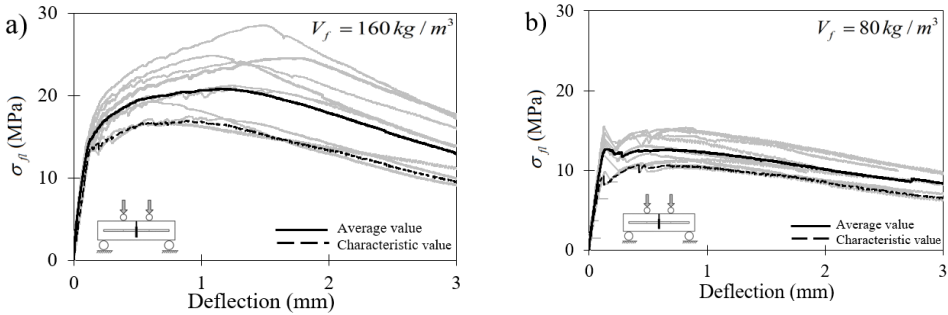


Figure 6- 13: 4PBTs test results; (a) UHPFRC type C1, (b) UHPFRC type C2

Table 6- 6: Tensile properties of UHPFRC type C1 and C2.

Constitutive Relation Model Parameters	$f_t$ (MPa)	$\epsilon_{t,el}$ (‰)	$f_{t,u}$ (MPa)	$\epsilon_{t,u}$ (‰)
<b>C1 (<math>V_f=160 \text{ kg/m}^3</math>)</b>				
Values of characteristic results	7.65	0.17	6.79	4.95
Average result value	9.41	0.18	8.49	6.56
<b>C2 (<math>V_f=80 \text{ kg/m}^3</math>)</b>				
Values of characteristic results	4.82	0.11	4.48	1.57
Average result value	6.41	0.13	5.81	1.98

The geometry of the R-UHPFRC tensile specimens is the same as specimens employed in paper 1<sup>st</sup> and 2<sup>nd</sup>, with the difference that for the present study, specimens with a cross-section size of  $60 \times 60 \text{ mm}^2$  were added to the experimental campaign. Therefore, three different cross-section sizes were used in this study (60, 80, and 100 mm). The diameter of the employed steel reinforcement was  $\varnothing 10$  and  $\varnothing 12 \text{ mm}$ . The variation of the cross-section sizes and steel reinforcement diameters lead to having a wide range of the reinforcement ratio ( $\rho$ ) between 0.79% to 3.13% and cover variation size between 25 to 45 mm, as can be observed in specimen description in Table 6-7.

Table 6- 6: Specimen's description detail

Section Size	Concrete type and fibre content				Rebar diameter	$\rho$ (%)	Cover (mm)
	C1 ( $V_f = 160\text{kg} / \text{m}^3$ )		C2 ( $V_f = 80\text{kg} / \text{m}^3$ )				
	Concrete batch number	Specimen ID	Concrete batch number	Specimen ID			
60×60 mm <sup>2</sup>	3	Ø10F160S60-1	3	Ø10F80S60-1	Ø10	2.18	25
	2	Ø10F160S60-2	3	Ø10F80S60-2			
	5	Ø10F160S60-3	4	Ø10F80S60-3			
	6	Ø12F160S60-1	5	Ø12F80S60-1	Ø12	3.13	24
	6	Ø12F160S60-2	5	Ø12F80S60-2			
	2	Ø12F160S60-3	6	Ø12F80S60-3			
80×80 mm <sup>2</sup>	6	Ø10F160S80-1	6	Ø10F80S80-1	Ø10	1.23	35
	3	Ø10F160S80-2	6	Ø10F80S80-2			
	3	Ø10F160S80-3	5	Ø10F80S80-3			
	2	Ø12F160S80-1	4	Ø12F80S80-1	Ø12	1.77	34
	5	Ø12F160S80-2	4	Ø12F80S80-2			
	3	Ø12F160S80-3	4	Ø12F80S80-3			
100×100 mm <sup>2</sup>	1	Ø10F160S100-1	3	Ø10F80S100-1	Ø10	0.79	45
	2	Ø10F160S100-2	5	Ø10F80S100-2			
	1	Ø10F160S100-3	3	Ø10F80S100-3			
	1	Ø12F160S100-1	1	Ø12F80S100-1	Ø12	1.13	44
	2	Ø12F160S100-2	1	Ø12F80S100-2			
	1	Ø12F160S100-3	2	Ø12F80S100-3			

### 6.2.3. Uniaxial tensile test results and analysis

The average tensile strain and stress of the R-UHPFRC tie elements were obtained by employing the proposed test method and procedure. Because this PhD thesis aims to study the behaviour of the R-UHPFRC tensile elements under service loads, the applied tensile strain was 2.0‰-2.5‰ as a maximum, which was considered the end of the test.

The obtain stress-strain curves for all specimens with UHPFRC type C1 and C2. are presented in Figures 6-14 (a) and (b).

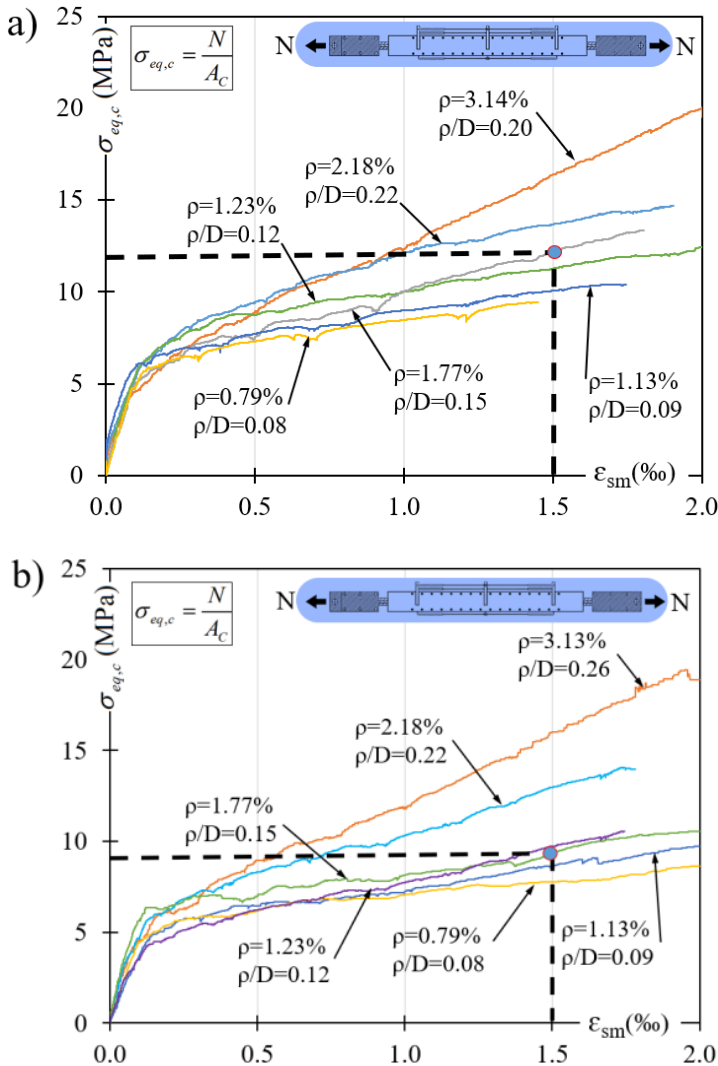


Figure 6-14: Tensile response of the R-UHPFRC ties; (a) ties with UHPFRC type C1, (b) ties with UHPFRC type C2.

As shown in Table 6-7, three specimens were cast for each specimen category (in terms of section size and reinforcement diameter). Therefore, each curve in Figure 6-14 represents the average result of the three specimens of each category. The values ( $\rho$ ) and ( $\rho/D$ ) were placed over each specimen curve result to evaluate the influence of the diameter and reinforcement ratio on the general tensile behaviour of the elements.

The tensile properties of the R-HPFRC (such as overall tensile strength and



toughness) are affected by the fibre content in the matrix, and they will increase as the amount of fibres increases. It can be seen in Figure 6-14 that the tensile strength of the two identical R-UHPFRC elements with different UHPFRC types, e. g., tie elements with ( $\rho=1.77\%$ ) at the given tensile strain (1.5‰), present tensile strength values of 12.14 and 9 MPa, respectively. Furthermore, the R-UHPFRC elements with UHPFRC type C1 demonstrate a higher slope in the inelastic region of its behaviour.

It can be observed that the first cracking strength for R-UHPFRC with concrete type C1 ( $V_f=160\text{kg}/\text{m}^3$ ) varies more slightly compared with type C2 ( $V_f=80\text{kg}/\text{m}^3$ ), which is suitable for serviceability performance or ductility capacity. The ductility capacity of the R-UHPFRC is mainly governed by parameters such as strain at first cracking, UHPFRC strain capacity, and steel bar yielding strain [3].

### ***Effect of the steel fibre content***

The toughness of the material is an inherent property that describes the nature of the material to break. It can be evaluated by energy absorption by the material by measuring the area under the tensile stress-strain curve. This concept was employed in the present work to define the amount of Increase of Energy Absorption (IEA) of the R-UHPFRC tensile elements due to fibre content difference. IEA was defined as the area between both curves specimens with identical section size and reinforcement ratio terms for both UHPFRC types as shown in Figures 6-15 (a) to (f).

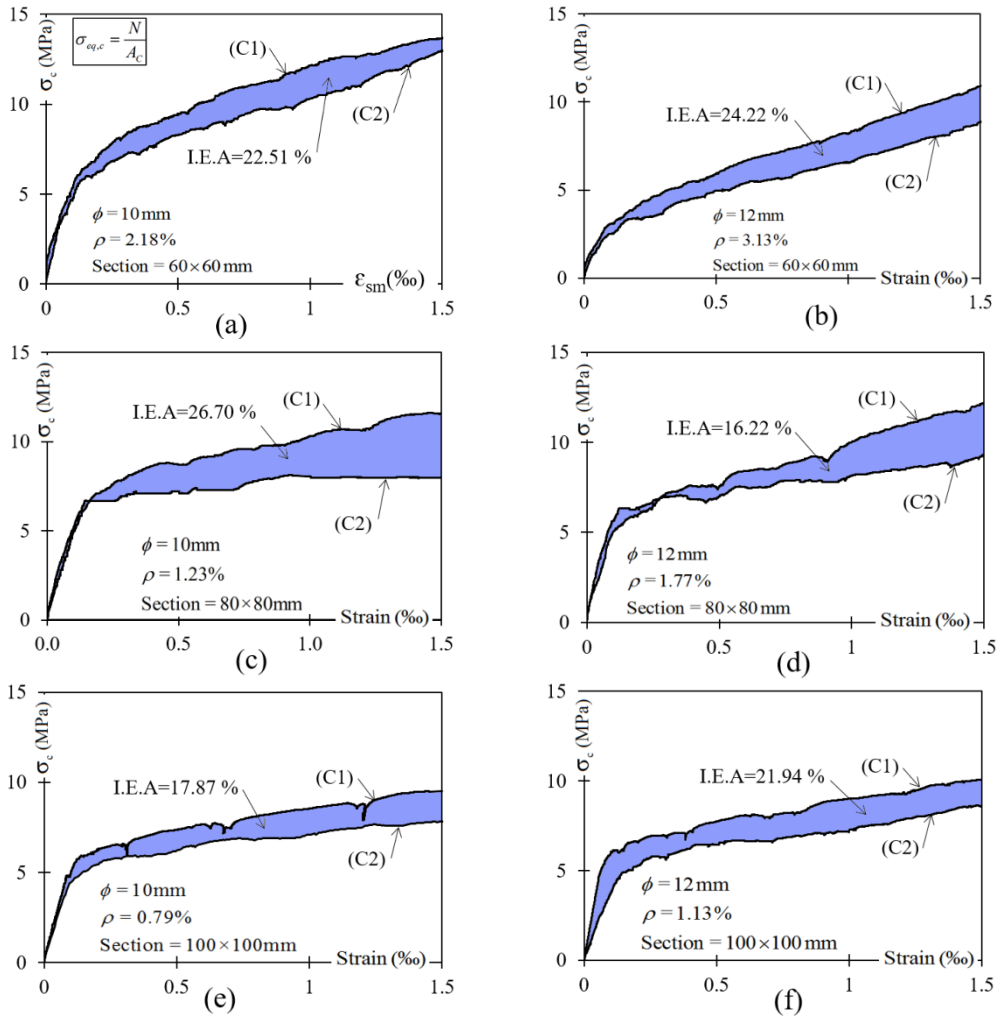


Figure 6-15: Increasing the IEA value due to increment of the fibre content (80 to 160 kg/m<sup>3</sup>)

It can be observed that the average value of IEA for all cases came close to 21.4%. This increase in energy absorption is due to a greater number of fibres bridging over the cracks faces, which improves the element's post-cracking behaviour. This result shows that using a high-fibre dose had no significant effect on the cracked specimen's energy absorption capacity. So, from an economic point of view, using the double fibre dose in R-UHPFRC ( $V_f = 160 \text{ kg/m}^3$  and  $V_f = 80 \text{ kg/m}^3$  in this case study) only improved tensile capacity by 21.4% on average. However, the tensile elements' cracking behaviour (crack opening and spacing) and durability performance under SLS load could lead to a more significant

improvement.

### ***Effect of the reinforcement ratio and rebar diameter***

A bilinear curve with a parabolic part in the interaction zone was proposed to define the typical load-strain response of a R-UHPFRC tensile element, as shown in Figure 6-16. The full tension stiffening effect ( $\beta = 1$ ) was considered in this definition, and the response curve is parallel to the bare bar response.

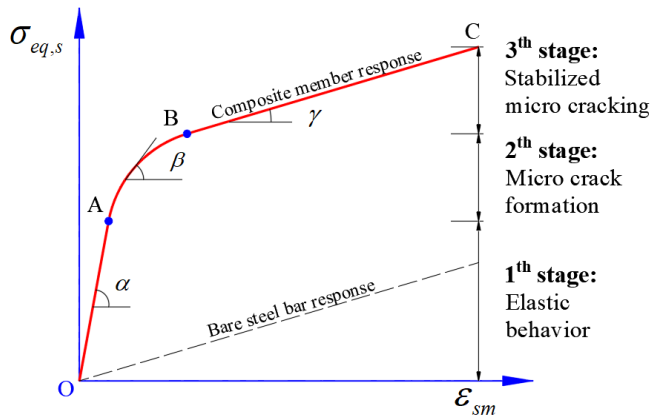


Figure 6- 16: Typical load-deformation response of R-UHPFRC tensile element

By evaluating the values of parameters ( $\rho$ ) and ( $\rho/D$ ) indicated in Figure 6-14 (a) and (b), it can be concluded that the aforementioned parameters have a significant influence on the cracked specimen's stiffness. We defined the slope of the overall tensile response in the stabilised microcracking stage ( $\gamma$  value) between points B and C.

The average proportion of ( $\alpha$ ) value for UHPFRC type C1 and C2 ( $\alpha_{c1} / \alpha_{c2}$ ) was calculated for identical specimens. It had a value of 1.13, indicating that increasing the fibre volume content (from 80 to 160 kg/m<sup>3</sup> in this study) has no significant effect on the elastic tensile stiffness of reinforced UHPFRC tensile elements. In general, introducing the steel fibres into the concrete matrix (compared to conventional concrete) improves bond-slip behaviour and, consequently, the elastic stiffness increases [4-6].

For the cracked R-UHPFRC tensile elements (region BC of the load-deformation response), the stiffness of the element ( $\gamma$ ) is related to the bridging effect provided by steel reinforcement and steel fibres. Figure 6-17 depicts the variation of the ( $\gamma$ ) value as a function of the reinforcement ratio ( $\rho$ ).

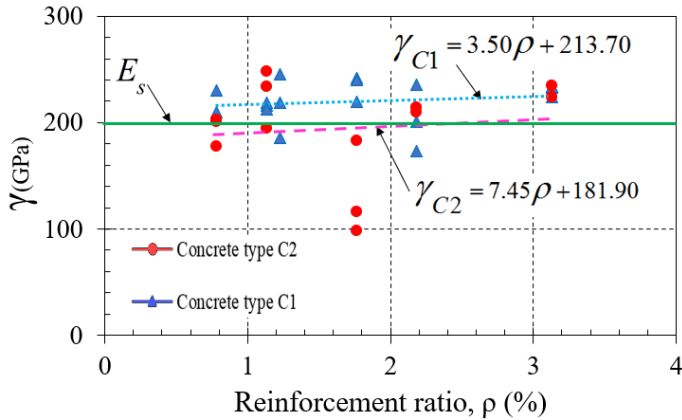


Figure 6- 17: Influence of the ( $\rho$ ) on the post-cracking stiffness of the R-UHPFRC tensile elements.

As can be seen, for UHPFRCs C1 and C2, two trend lines for all specimens are nearly parallel and the axial tensile stiffness is higher for specimens with higher fibre content. This increment (the offset distance between two trend lines) is about 31.80 GPa, which indicates a 14.80% increment of the stiffness. On the other hand, the trend lines for two groups of the specimens with UHPFRC type C1 and C2 come very close to the axial stiffness of the bare bar (see the green line in Figure 6-17,  $E_s = 200\text{GPa}$ ). This means that the overall response of the tensile element at the third stage is nearly parallel to the bare bar response, and it confirms the occurrence of the full-tension stiffening effect ( $\beta = 1$ ) in this stage of the behaviour.

### ***Shrinkage influence and tension stiffening effect***

Bischoff [7] reported that the member response of RC specimens drops as shrinkage increases and results in a lower cracking load and less apparent tension stiffening. The same phenomenon can occur for R-UHPFRC tensile tie elements. Shrinkage of concrete leads to an initial shortening of the R-UHPFRC member and causes a reduction in the cracking load and effects on the tensile response and tension stiffening response as indicated in Figure 6-18 (a) and (b). However, the high shrinkage strain of UHPFRC needs to be paid special attention for elements under tensile stresses.

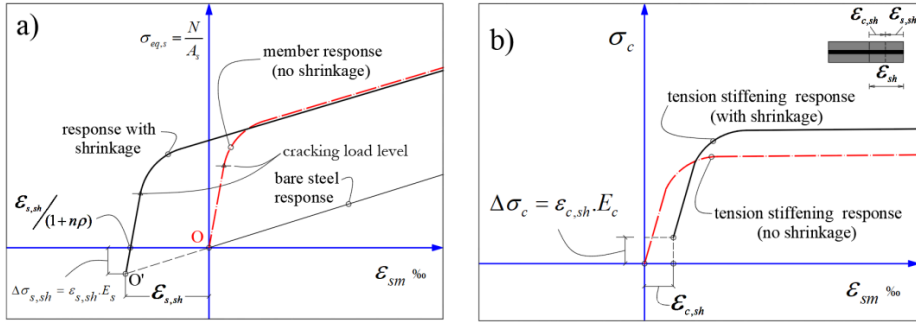


Figure 6- 18: Effect of the shrinkage on the tensile response of R-UHPFRC; (a) average stress-strain response, (b) UHPFRC's contribution in tension.

The shrinkage of UHPFRC induces a negative pre-strain in the steel reinforcement ( $\epsilon_{s,sh}$ ), which generates a compression stress in the steel rebar ( $\Delta\sigma_{s,sh}$ ). Thus, the equivalent stress to modify the origin of the stress-deformation tensile curve response can be calculated by ( $\Delta\sigma_{s,sh} = \epsilon_{s,sh} \cdot E_s$ ). Also, for modifying the tension response curve of the UHPFRC (Figure 6-18 (b)), the following expressions can be used to calculate the tensile stress caused by shrinkage ( $\Delta\sigma_{c,sh}$ ) and the corresponding strain ( $\epsilon_{c,sh}$ ).

$$\Delta\sigma_{c,sh} = E_c \cdot \epsilon_{c,sh} \rightarrow \epsilon_{c,sh} = \frac{\epsilon_{s,sh} \cdot n \cdot \rho}{1 + n \cdot \rho} \quad (6-1)$$

The tension stiffening response of the R-UHPFRC tensile elements was obtained by subtracting the bare bar response from the overall average stress-strain response of the element. To modify this response due to the shrinkage effect, the following equation was used to calculate the free shrinkage ( $\epsilon_{sh}$ ) magnitude using the Swiss standard fprSIA 2052 code [8]:

$$\epsilon_{sh}(t) = \epsilon_{U_{500}} \cdot e^{\frac{c}{\sqrt{t+d}}} \quad (6-2)$$

According to fprSIA 2052 code [8], the values of parameters in this Equation are: ( $C = -0.48$ ), ( $d = -0.86$ ) and ( $\epsilon_{U_{500}} = 0.6 - 0.86\text{‰}$ ).

The value of the free shrinkage calculated by Equation 6-2 and corresponding caused tensile stress and strain ( $\Delta\sigma_{c,sh}$  &  $\epsilon_{c,sh}$ ) were calculated by Equation 6-1, and they are provided in Table 6-8. Modified UHPFRC's contribution in tension (tension stiffening response) for both concrete types are depicted in Figures 6-19 (a) and (b).

Table 6- 8: Stress and strain values for modification of the tension stiffening response

$\epsilon_{sh}$ (‰)	Section size (mm)					
	60×60		80×80		100×100	
0.538	Reinforcement diameter (mm)					
	Ø 10	Ø 12	Ø 10	Ø12	Ø 10	Ø12
	$\Delta\sigma_{c,sh}$ (MPa)					
	2.19	3.07	1.27	1.80	0.82	1.17
$\epsilon_{c,sh}$ (‰)						
0.047	0.065	0.027	0.038	0.018	0.025	

It is important to mention that an intensive experimental programme was carried out to evaluate the used free shrinkage value. A brief description of the employed test method is presented in section 7.3.

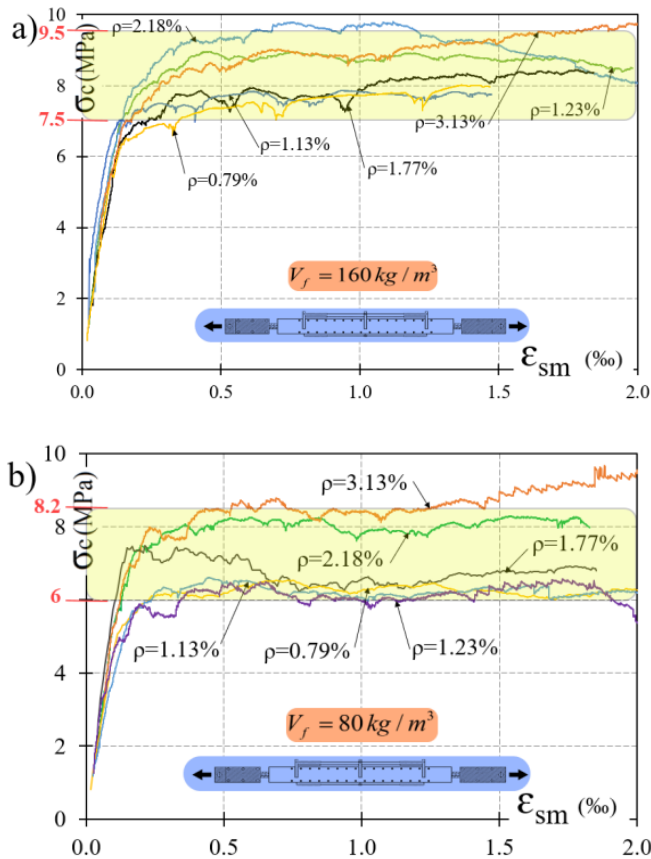


Figure 6- 19: Tension stiffening response including the shrinkage effect; (a) UHPFRC type C1, (b) UHPFRC type C2.

As can be observed in Figure 6-19, due to the increment of the reinforcement ratio, the tension stiffening value increased from 7.5 MPa to 9.5 MPa for UHPFRC type C1 and from 6.0 to 8.2 MPa for UHPFRC type C2 (see the highlighted area range in Figure 6-19).

### ***Comparison between the inverse analysis results and the tension stiffening response***

The tensile properties of the UHPFRC employed in this study were obtained by running 4PBTs and using the constitutive model described in section 2.4.3. The obtained test results are shown in Table 6.6, and they were compared with modified tension stiffening responses in Figure 6-20 by plotting both together.

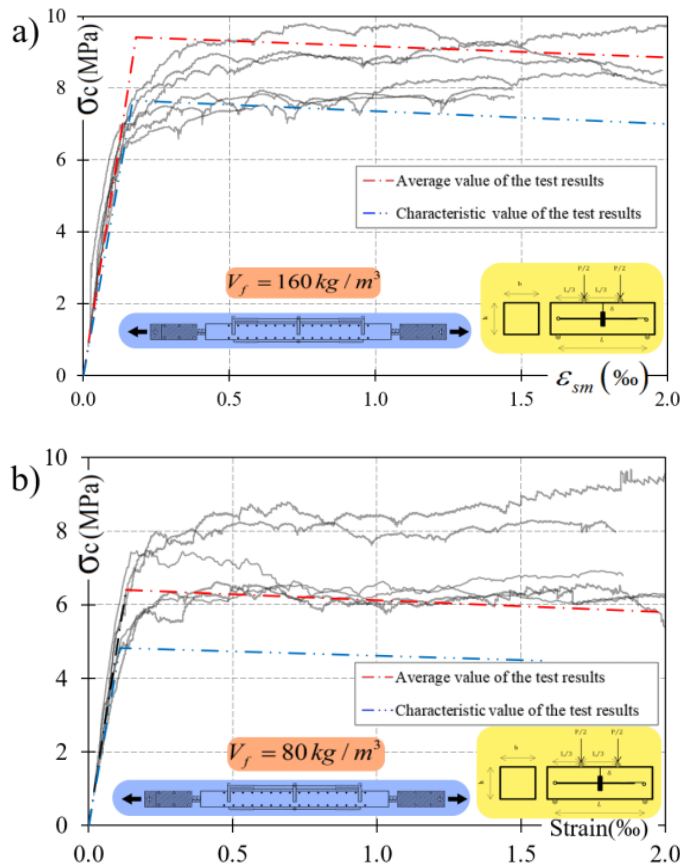


Figure 6-20: Comparison between the tension stiffening response and constitutive model results; (a) UHPFRC type C1, (b) UHPFRC type C2.

As can be observed, there is a good matching between the inverse analysis result and the experimental tension stiffening response for specimens with ( $V_f = 160 \text{ kg/m}^3$ ) obtained by the R-UHPFRC uniaxial tensile test. The average and characteristic values are defined in this diagram and as can be seen, almost all tensile contribution curves responses lie between these two values. The difference between the contribution curves responses is due to reinforcement ratio effect (section sizes and reinforcement diameters). As a consequence, a conservative response can be achieved by using the obtained characteristic value of the proposed inverse analysis method.

For the case of the R-UHPFRC elements with ( $V_f = 80 \text{ kg/m}^3$ ), nearly all tensile contribution curves response were above the average tensile strength obtained by the inverse analysis method (see Figure 6-20(b)). It could be because specimens with UHPFRC type C2 have higher fibre efficiency than type C1. However, more research should be done in the future to confirm the findings of these tests in a more generalized way. In both cases and for any reinforcement ratio, the UHPFRC contribution in tension is higher than the characteristic tensile strength obtained by the inverse analysis result.

In the other experimental work (4<sup>th</sup>: related to the published book chapter), the effect of the combination of micro and macro steel fibres was studied. In this study, four types of UHPFRC were used: UHPFR type C1 and C2 (called here C160 and C80, respectively) as used in the previous works, UHPFRC with micro and macro steel fibres with the same content ( $80 \text{ kg/m}^3$  for each fibre type) which called C8080, and UHPFRC without fibres (C0). The properties details of steel fibres are provided in Table 6-3.

For each UHPFRC group, three specimens with a cross-section of  $100 \times 100 \text{ mm}$  and reinforcement with a diameter of 12-mm were cast. The result of the uniaxial test and the average tensile response for these four groups of the specimens is illustrated in Figure 6-21. It should be mentioned that the negative shrinkage strain was considered to modify the tensile response of the tensile element by an approximate value of ( $\varepsilon_{s,sh} = 0.40\%$ ), which was obtained experimentally (see section 6.3).



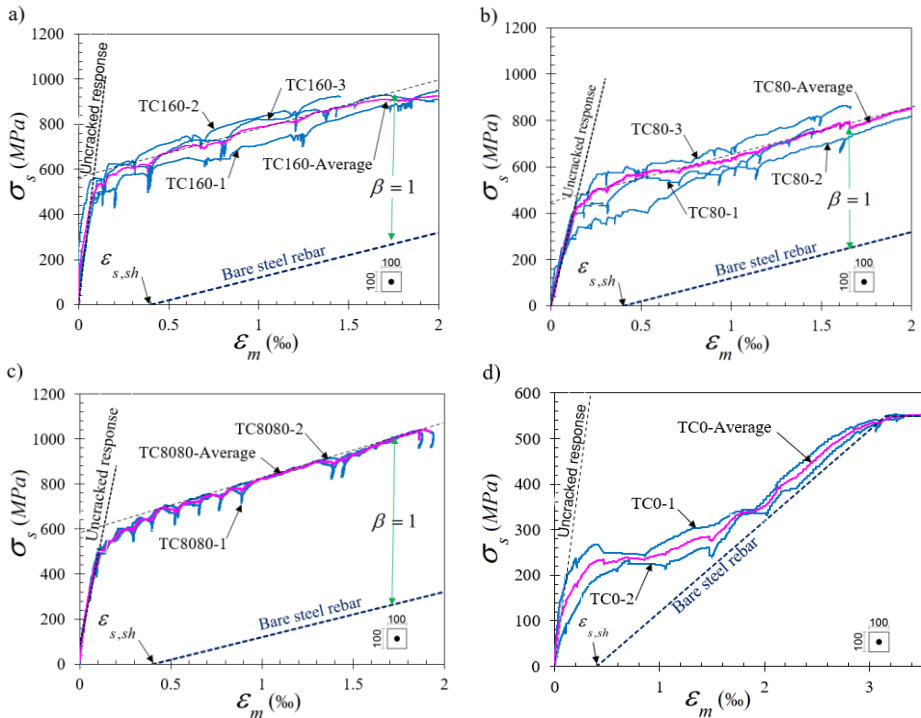


Figure 6- 21: Uniaxial tensile response for four UHPFRC types

In this study, the stress in the reinforcement at first cracking level was defined as presented in Figure 6-22, and these values are provided in Table 6-9. These values were calculated over the average curve response.

Table 6- 7: Cracking stress sans post-cracking tensile stiffness for tensile elements

Specimen ID	Stress in reinforcement at cracking $\sigma_{s,cr}$ (MPa)	Stress in UHPFRC at cracking $\sigma_{c,cr}$ (MPa)	Post-cracking tensile stiffness $\gamma$ (GPa)
TC0	112.00	1.28	N.A
TC80	455.00	5.20	205.83
TC160	563.00	6.44	225.43
TC8080	591.00	6.76	237.59

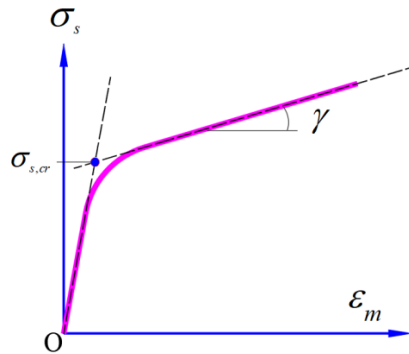


Figure 6- 22: Criteria for obtaining the cracking stress strength and post-cracking stiffness.

According to the obtained results, the post-cracking tensile stiffness ( $\gamma$ ) increased for the hybrid mixture (C8080). To better understand the effect of fibre content on overall tensile behaviour and pos-cracking tensile stiffness, the average stress-strain response of each of four groups of specimens is illustrated in Figure 7-23.

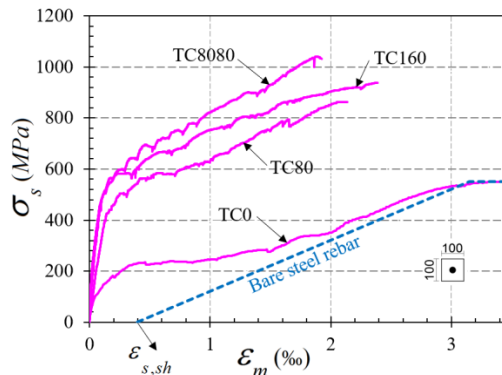


Figure 6- 23: Average tensile response of tie elements with four different UHPFRC types.

As can be observed, specimens with UHPFRC type C2 (C160) and C8080 almost have the same tensile cracking stress strength. All three types of UHPFRC with different fibre volume contents were presented full-tension stiffening behaviour for its post-cracking response ( $\beta=1$ ). By comparing the tensile response of specimens with 80 and 160 fibre content (T80 and T160) by specimens with hybrid fibre content (T8080), it can be concluded that employing the hybrid fibre content presents better tensile behaviour since the employed steel fibre weight is the same as the UHPFRC type C160.

The derived findings and conclusions are summarised as follows:

- a) For all R-UHPFRC tensile specimens, the overall tensile behaviour (average

stress-stress relationship) revealed three well-defined stages: (stage 1) lineal elastic behaviour; (stage 2) microcrack formation with a sharp reduction of the tensile stiffness; (stage 3) microcrack stabilization. Furthermore, under serviceability conditions, no macrocrack formation was observed.

- b) In the microcracking stabilisation stage, the overall experimental response of the R-UHPFRC tensile elements was parallel to that of the bare bar, and both UHPFRC types show nearly full-tension stiffening ( $\beta = 1$ ).
- c) The energy absorption capacity of the cracked tensile element was increased by approximately 21.4 percent by increasing the amount of fibre in UHPFRC from 80 to 160 kilogrammes per meter cubic. Consequently, from an economic perspective, using the double fibre dose in real applications should be evaluated carefully by designers. However, the tensile elements' cracking behaviour (crack opening and spacing) and durability performance under SLS load could lead to a more significant improvement.
- d) The preliminary evaluation of the shrinkage effect on tension stiffening shows that this effect significantly influences the internal stresses that both UHPFRC and reinforcement exhibit. Thus, the shrinkage effect should be considered in the serviceability design of the R-UHPFRC structural elements.
- e) With the increase in the reinforcement ratio, a slight increase in the concrete's contribution was noted.
- f) The contribution of UHPFRC in tension is higher than the characteristic tensile value derived from the employed inverse analysis result obtained from 4PBTs.
- g) Tensile tie elements with hybrid fibre content (80 kg/m<sup>3</sup> for the micro smooth steel fibres, plus 80 kg/m<sup>3</sup> for the micro hooked end steel fibres) present the same tensile cracking stress strength as tie elements with a fibre content of 160 kg/m<sup>3</sup>.

### **6.3. Shrinkage behaviour of UHPFRC**

UHPFRC has a high shrinkage value due to the low water-to-binder ratio and high binder content. This effect depends on the mixture property of the concrete (cement and water content), properties of the materials (aggregates and cement properties and chemical composition of the cement), curing process and method, temperature and humidity conditions of the ambient, geometrical conditions of the structure element, and amount of fibres.

The effect of shrinkage on the cracking behaviour of the UHPFRC elements provides a major concern to the structural designer because of inaccuracies and unknowns that surround them. This effect should be taken into account for long-term deformation, short-term loading and cracking resistance of R-UHPFRC elements. High early-age shrinkage of UHPFRC can lead to early-age cracking and hence potentially affect the serviceability, durability, as well as aesthetics of

UHPFRC structures. Thus, some recommendations, such as the Japanese recommendation [9], require obtaining an accurate shrinkage value by experimental results.

Two intensive experimental program tests were conducted to obtain the shrinkage value of the UHPFRC used in this PhD study. Results of this study were used in the following paper:

- Paper 5<sup>th</sup>: (An Experimental Study on the Behavior of reinforced UHPFRC Ties Under Serviceability Conditions).

*M. Khorami, N.-G. Juan, and S. R. Pedro, "An Experimental Study on the Behavior of reinforced UHPFRC Ties Under Serviceability Conditions," vol. 73, pp. 1-9, 2022. Proceedings of the VIII Congress of ACHE - Santander*

### **6.3.1. Experimental shrinkage test**

Two different tests programs were conducted in this work. The purpose of these two shrinkage test was to address the experimental results of two different test methods to obtain the free shrinkage value of UHPFRC and using that to modify the tension stiffening diagrams. Shrinkage of the concrete caused an initial shortening in the member and leads to a reduction in tension stiffening, which becomes more predominant as increasing the percentage of reinforcement [10] and this initial shortening of the member must be taken into account in order to evaluate tension stiffening effects. The shrinkage effect can be measured directly by measuring member shortening. Bischoff (2001) [11] proposed a test method to obtain the shrinkage strains directly from the uniaxial test for Reinforced plain Concrete (RC) by using the tie element with unbonded steel rebar. In this method, the tensile behaviour of tie with unbonded steel rebar under tensile force follows the bare steel response after cracking, and the initial shortening can be measured by the offset between bare steel response and the origin point of member response (see Figure 4-10 (a)). In the case of the presence of fibres in the concrete, the member response does not follow the unbonded bare steel after the specimen has cracks. Thus this test method was adapted for Fibre Reinforced Concrete (FRC) [12] by matching the yield point of the member response with the yield point of the bare steel to obtain the member offset (see Figure 4-10 (b)) when the crack localization occurs.

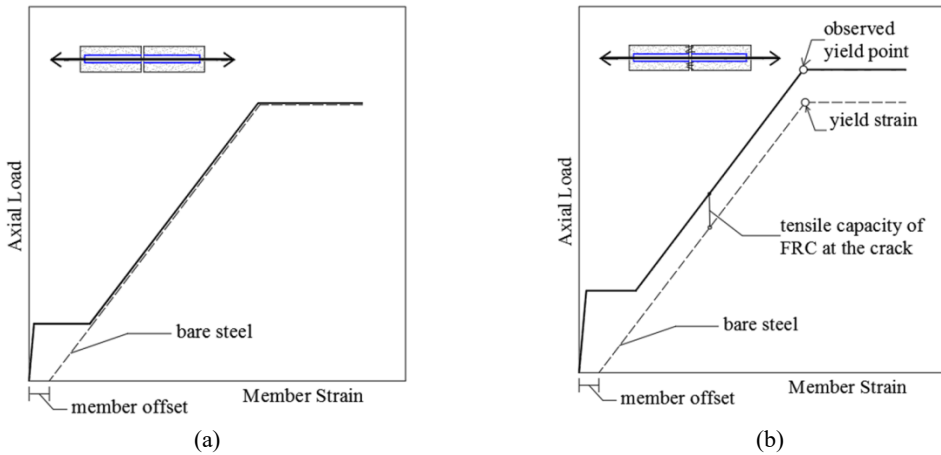


Figure 6- 24: Initial shortening of tie element due to shrinkage using unbonded steel rebar [12], (a) RC tie element, (b) FRC tie element.

The mix proportion used in this experimental study is the same as the previous works described in the previous chapters. Due to the limitation of laboratory equipment and time, just one type of UHPFRC was tested. Therefore, specimens were cast with UHPFRC type C1, which has a fibre volume content of  $160 \text{ kg/m}^3$  ( $V_f=2\%$ ).

### 6.3.2. Laboratory tests

The present experimental program includes two different laboratory test methods that were employed to obtain the shrinkage strain of UHPFRC by the presence of steel reinforcement rebar. The first test program was adapted to Bischoff's method (described above) to obtain the shrinkage value from uniaxial tensile test, and by the second test program, the shrinkage strain was measured and calculated directly by measuring the reinforcement strain by using strain gauges and calculating the concrete shrinkage.

For both test programs, specimens have a normal square cross-section size of  $80 \times 80 \text{ mm}^2$  and the reinforcement was located in the centre of the cross-section. For each test program, specimens were cast by one batch. Description of each test program and test procedure are given following:

#### *Test program 1*

The test method used in this program is similar to the approach proposed by Bischoff [11, 12] which in that the reinforcement in the specimen is unbonded by using a plastic tube covering the reinforcement rebar and isolating the rebar from the concrete. The plastic tube covered 98% of the length of steel reinforcement.

For this test program, two specimens were cast (one bonded and the other unbonded) with the same reinforcement diameter ( $\text{Ø}12\text{ mm}$ ,  $\rho=1.76\%$ ). Specimens were cured after demolding in the chamber at  $20\pm 2^\circ\text{C}$  and 100% relative humidity for 28 days and then air-dried and left to shrink for another 60 days before being tested. Details of specimens are shown in Figure 6-25. The unbonded specimen was used to determine the initial shortening of the R-UHPFRC element by measuring the offset of the bare steel response.

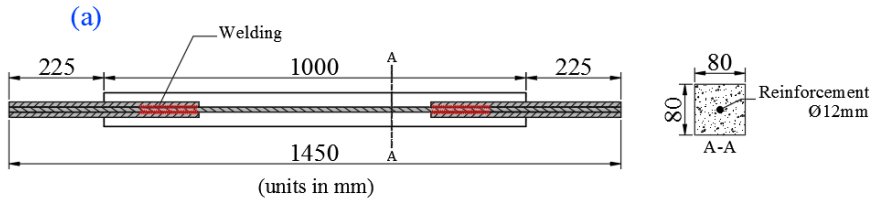


Figure 6- 25: Specimens details for test program 1, (a) general geometry of specimens(b) specimen without plastic tube [bonded], (c) specimen with plastic tube [unbonded].

### ***Test program 2***

The geometry of the specimens for this program test is the same as test program 1 by the difference that the steel rebar is bonded and the UHPFRC shrinkage was calculated by measuring the rebar deformation with strain gauges. Specimens had prismatic shape with two identical square cross-sections size of  $80\times 80\text{mm}^2$  in the ends, as shown in Figure 6-26. The specimen's length was  $1000\pm 2\text{ mm}$  and they were reinforced by a steel rebar located in the centre of the cross-section. The proposed program test included three specimens with different rebar sizes ( $\text{Ø}16$ ,  $\text{Ø}12$  and  $\text{Ø}10\text{ mm}$ ).

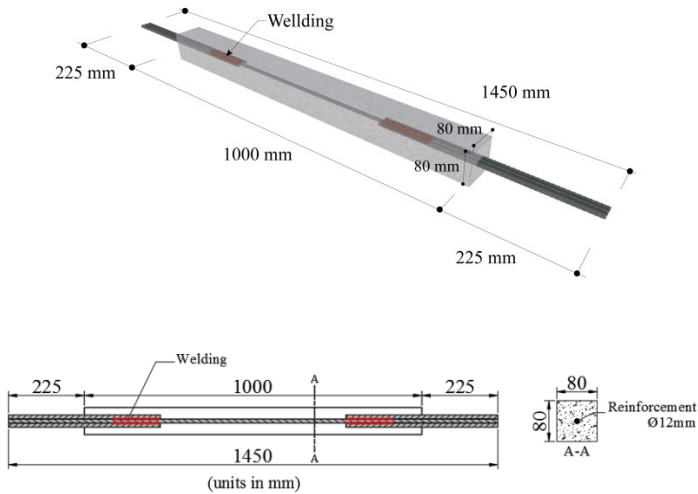


Figure 6- 26: Specimen geometry and details for test program 2.

For the proposed test program 2, the rebar deformation was measured by strain gauges immediately after casting the specimen and also during the storage in the chamber and out of the chamber for 60 days. A special wooden mold was designed to protect the cables connected to the strain gauges from possible movements and damages caused by the transport of the specimen and also prevent the creation of unwanted deformations in the steel rebar due to the stripping process or bending caused by the specimen's weight. The stripping of the specimen was done just by opening the front and backside of the wooden mold. Figures 6-27 (a) and (b) show the mold details.

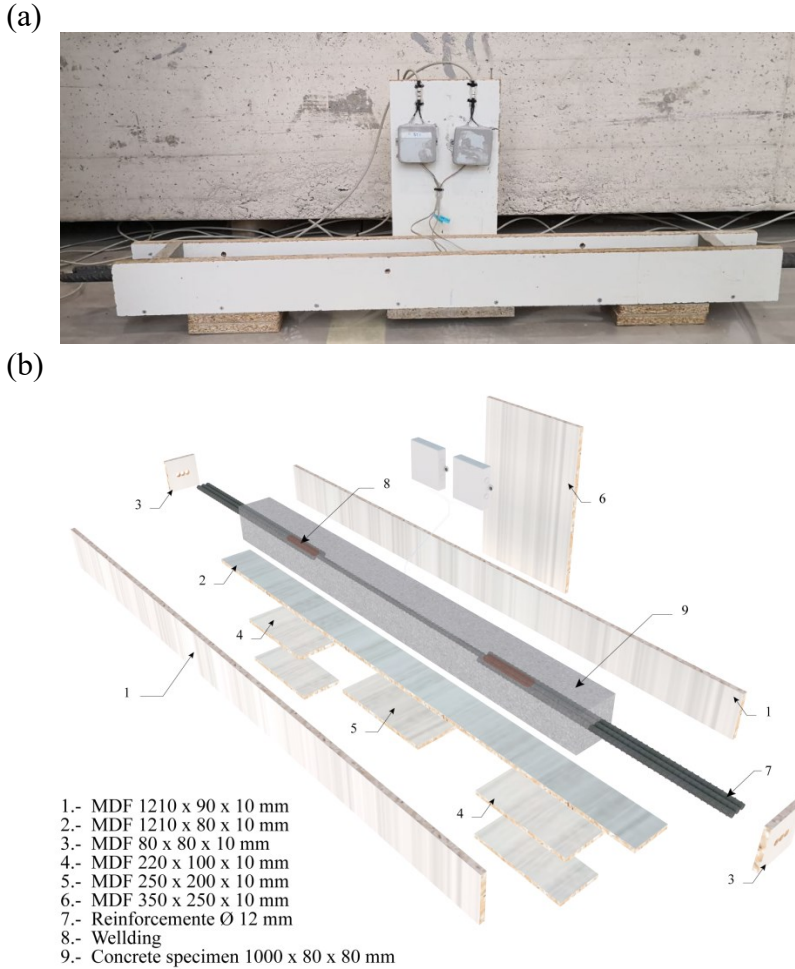


Figure 6- 27: wooden mold detail, (a) general view of the mold (b) assembly parts of the mold.

### **6.3.3. Instrumentation and test procedure**

#### ***Test program 1***

The proposed uniaxial tensile test (described in section 7.1) was used to carry out the test program 1. By employing the displacement transducers and cell-force measurement, the average tensile strain-stress of the tie elements were obtained.

#### ***Test program 2***

For detecting the deformation of the steel rebar caused by the UHPFRC shrinkage



effect, three strain gauges were attached to the reinforcement surface in three different positions to monitor the average rebar deformation during the test. Figures 6-28 (a) and (b) show the strain gauges locations before casting and the specimen after stripping the lateral wooden panels.

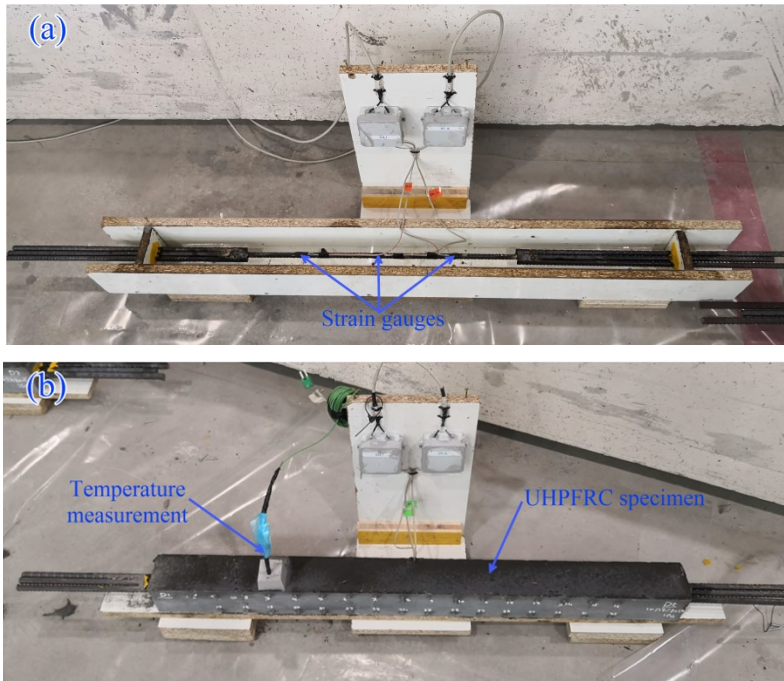


Figure 6- 28: UHPFRC specimens for test, (a) position of the strain gauges and cable connection details, (b) concrete specimen with the wood base after stripping of lateral wooden panels.

After stripping of the specimens, they were cured in the chamber at  $20\pm 2^{\circ}\text{C}$  and 100% relative humidity for 28 days and then air-dried and left to shrink for another 32 days. The deformation and temperature were recorded immediately after casting and also during the storage of the specimens in the chamber and out of the chamber during the mentioned 60 days. The temperature inside the UHPFRC matrix and also the outside (laboratory or chamber temperature) were recorded by using two concrete thermometers.

### 6.3.4. Shrinkage test and discussion

#### *Test program 1*

This section includes the obtained results for two explained program tests. Based

on the Bischoff method (test program 1), to obtain the pre-deformation caused by shrinkage, it is necessary to carry out the tensile uniaxial test for two cases (specimens with bonded and unbonded steel rebar). The strain-stress behaviour of tie elements is presented in Figure 6-29.

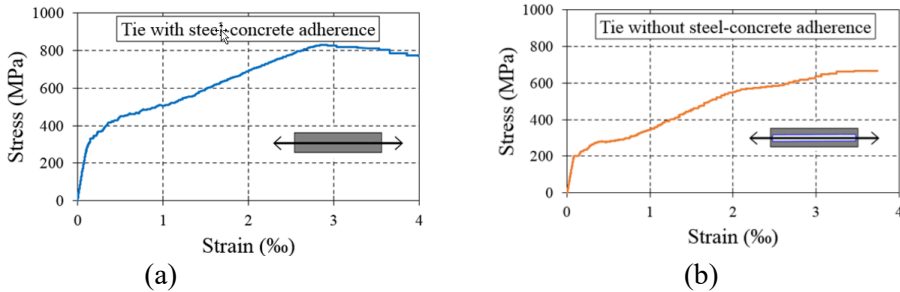


Figure 6- 29: Stress-Strain relationship of UHPFRC tie elements for test program 2, (a) With adherence between steel rebar and UHPFRC, (b) Without adherence between steel rebar and UHPFRC.

Due to the occurrence of crack localization in UHPFRC ties beyond the yield point of steel rebar, the offset between two tensile behaviour curves can be obtained just by matching together the yield points of tensile curves. Figure 7-30 (a) presents the yield point values of the UHPFRC tie elements for two cases of bonded and unbonded steel rebar, and in Figure 7-31(b), it can be observed the offset value between two cases which presents the shrinkage value of UHPFRC which is 620 (0.62%).

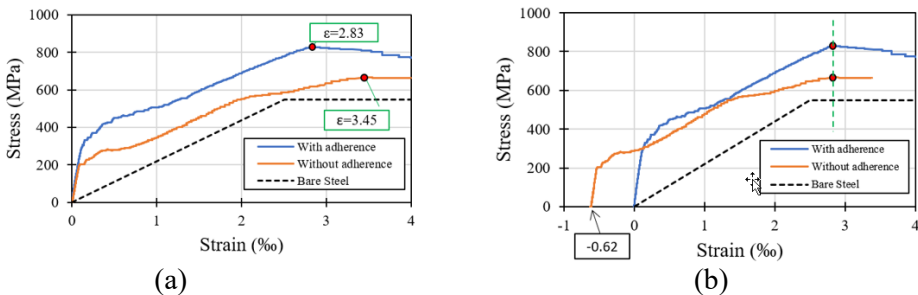


Figure 6- 30: Shrinkage calculation by Bischoff method, (a) yield point values of two UHPFRC tie elements, (b) matching yield points to obtain the offset and shrinkage value.

Based on shrinkage values from literature with different test methods presented in Table 2-3 and proposed shrinkage values by codes (see section 2.5.1), a good agreement can be observed between experimental results and value recommendation by codes and similar studies.

## Test program 2

The rebar compression strain caused by UHPFRC shrinkage was measured immediately after casting of specimens, as well as during and after storage of the specimens in the chamber for 60 days, to calculate the shrinkage of UHPFRC using the second method. The average values of compression strain of steel reinforcement were monitored. The free shrinkage strain ( $\varepsilon_{sh}$ ) was calculated by employing Equation (2-87). The rebar deformation ( $\varepsilon_{s,sh}$ ) and corresponding free shrinkage ( $\varepsilon_{sh}$ ) for three different periods (20, 40 and 60 days) are provided in Table 6-10. It can be observed that after 40 days the average compressive strain in the rebar and consequently the free shrinkage in the UHPFRC matrix takes an almost constant value.

Table 6- 8: Free shrinkage calculated with Eq. 2-116 based on experimental data for 20, 40, and 60 days

Specimen ID	$A_s$ (mm <sup>2</sup> )	$A_c$ (mm <sup>2</sup> )	$\rho = (A_s / A_c)$	$n = (E_s / E_c)$	Time (day)	$\varepsilon_{s,sh}$ ( $\mu m / m$ )	$\varepsilon_{sh}$ ( $\mu m / m$ )
Specimen 1 (Ø16 mm)	78.54	6321.46	0.0124	4.26	20d	270	285
					40d	341	341
					60d	344	344
Specimen 2 (Ø12 mm)	113.10	6286.90	0.0180	4.26	20d	334	359
					40d	402	402
					60d	405	405
Specimen 3 (Ø10 mm)	201.06	6198.94	0.0324	4.26	20d	336	382
					40d	413	413
					60d	420	420

In this section, the procedure of two intensive experimental tests was explained, which were conducted to obtain the free shrinkage value of the UHPFRC employed in this Ph.D work. The free shrinkage value obtained by the first test method was  $620 \mu m / m$  and by the second method was  $420 \mu m / m$ . According to obtained results, it can be concluded that the shrinkage strain values proposed by codes ( $550-800 \mu m / m$ ) are suitable for carrying out the structure calculation at the preliminary design or project stages in case of inability to do an experimental shrinkage test.

Considering the serviceability criteria, the shrinkage effect (initial member shortening caused by shrinkage) should be taken into account by increasing the tensile stress inside the matrix. Ignorance of the shrinkage effect could result in significant errors in the serviceability design. This effect must also be considered in the constitutive modelling.

## **6.4. Cracking and serviceability behaviour**

In the work related to the paper 6<sup>th</sup>, the significance of the serviceability design for concrete structures was explained. Mortherfore, the basic serviceability requirement for designing the R-UHPFRC structures in serviceability limit states provided by some international recommendations and codes for UHPFRC structures were discussed.

An experimental program based on direct tensile test with dog bone-shaped specimens was performed to study de cracking behaviour of R-UHPFRC tie elements. This study aimed to compare the maximum crack width to average values and obtain the ( $\beta$ ) value experimentally for R-UHPFRC tensile elements.

For that, a particular test procedure by using a microscope camera was performed, and the real opening dimension of all formed cracks under low to high tensile strain rates was measured.

Mortherfore, a statistical procedure for developing fragility curves based on cracking data by employing the Rice distribution functions were developed. The fragility curves were calculated based on all crack widths recorded at tensile strains of 1.0‰, 2.0‰ and 3.0‰ for all specimens in each group of specimens.

### **6.4.1. Experimental study to obtain the factor $\beta$**

Microcracks form along the specimen length under tensile loads and measuring the width dimension for each crack is extremely difficult, especially for R-UHPFRC due to the large number of microcracks and their finesse. Figure 6-31 shows the crack pattern of the tensile R-UHPFRC tie element which affirms this fact. Due to this measuring difficulty, the average crack with calculation is recommended by researchers by dividing the total tensile elongation by the number of cracks as an empirical output.

$$\text{Average crack width} = \frac{\text{Tensile elongation recorded under the load}}{\text{Number of cracks}}$$



Figure 6- 31: A large number of the microcracks along the tensile R-UHPFRC element length.

The main aim of presented experimental study in this work was to specify and evaluate the maximum captured crack width and average crack width (obtained by the above definition) for R-UHPFRC tensile elements from the experimental observations and also obtain the coefficient of ( $\beta$ ) to know that how many times

the real maximum crack width is bigger than the average value. The existing difference between the maximum measured crack width and the average value should be considered for examining R-UHPFRC structures for the serviceability limit state (SLS), and for their durability.

Same as the previous works presented in the other papers, in this experimental program, two UHPFRC types (C1 and C2) were used with 1% and 2 % fibre content per volume, respectively. In this circumstance, the difference of the fibre volume content helps to evaluate the fibre content influence on cracking behaviour and crack width values under tensile load. For each UHPFRC type, four specimens were made. All specimens had the same geometrical properties with the same steel reinforcement in the center of the cross-section.

#### 6.4.2. test setup, specimen and material preparation

The equipment that was used to conduct the uniaxial tensile test for this experimental program was the same as the test setup employed in the previous works by this different that specimens were designed with dog bone-shaped and a microscope camera were used to monitoring the crack widths.

All the dog bone-shaped specimens were reinforced with central steel rebar with a diameter of  $\text{\O}12\text{mm}$ . The same connection details were used by using the steel jaw and two additional welded rebars in both ends to avoid yielding rebar failure. Figure 6-32 (a) and (b) shows the specimen's geometry and reinforcement details.



Figure 6- 32: Reinforcement and mold details of dog bone-shaped specimens.

The reason for designing the specimens with dog bone form was to prevent the occurrence of the cracks in the end zone of the specimens (end-effect), particularly where there is a stiffness difference between sections one and two (see Figure 6-32 (b)) due to the difference of the number of the reinforcement rebars. This suggested specimen geometry for tensile specimens was based on the experience acquired in previous works and from running lots of uniaxial tensile tests of prismatic R-UHPFRC ties. In some cases, it was observed that the main crack in the crack stabilization phase occurs in the end part of the three welded rebars (the three rebars section to one rebar section). Dog bone-shaped helps to increase the stiffness of the reinforced tensile element in the end zones to prevent the occurrence of the undesired cracks out of the studied zone. Also, the dog bone-

shaped provides a limited zone over where the microscope camera was used to measure crack widths (the straight central part of the specimen). In this study, the reinforced dog bone-shaped specimens were 1050 mm long, 240 mm wide and both ends and 80 mm in the middle. The thickness was constant (80 mm) along the whole length of the specimen, as illustrated in Figure 6-33.

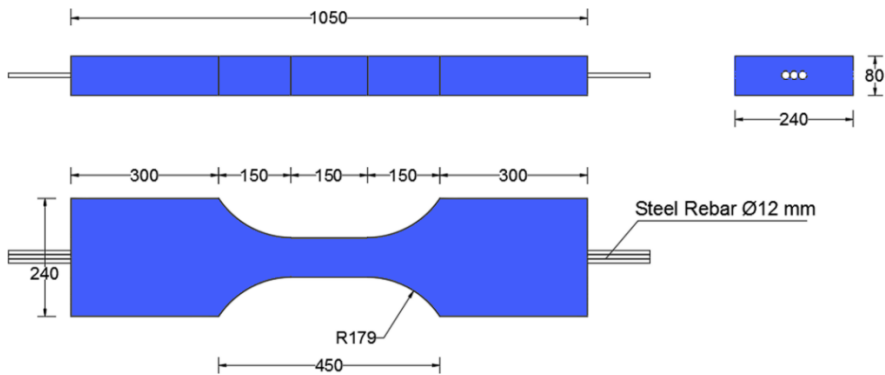


Figure 6- 33: Dog bone-shape specimen's geometry and dimension (units: mm).

For each type of UHPFRC (C1 and C2 which are here in this work called U1 and U2), four specimens were cast, and one batch was made for every two specimens. Table 6-11 provide the compressive strength and specimen IDs.

Table 6- 9: Specimens identification and compressive strength value of UHPFRC type C1 and C2 for each batch.

Batch number /UHPFRC type	Specimen IDs	Compressive strength of each cube sample (MPa)	Average value (MPa)
Batch #1/ U1-160	DB #U1-1 & DB #U1-2	171.7	161.8 (CV=7.0%)
		158.3	
		147.3	
		169.8	
Batch #2/ U1-160	DB #U1-3 & DB #U1-4	163.5	158.4 (CV=6.6%)
		145.0	
		169.3	
		155.9	
Batch #1/ U2-80	DB #U2-1 & DB #U2-2	157.1	157.6 (CV=3.5%)
		164.6	
		157.3	
		151.2	
Batch #2/ U2-80	DB #U2-3 & DB #U2-4	148,0	156.0 (CV=1.7%)
		153.4	
		158.7	
		155.8	

### 6.4.3. Test procedure

Specimens were located horizontally in the uniaxial tensile test machine, and they were connected to the force transfer system by steel jaws. The specimen's elongation was measured using two 300 mm-DTs attached to up and bottom of the specimen in the middle of the specimens and over the testing zone. Crack monitoring and detecting crack widths were performed at three specimen thicknesses levels (bottom, middle and top) by passing the microscope camera over the specified lines levels. Figure 6-34 shows the mentioned guidelines over the lateral surface. The first line (L1) passed over the longitudinal axial of the specimen corresponded to the rebar axis, while the second and third lines (L2 and L3) were located at a 10-mm distance from the bottom and top edges of the specimen.

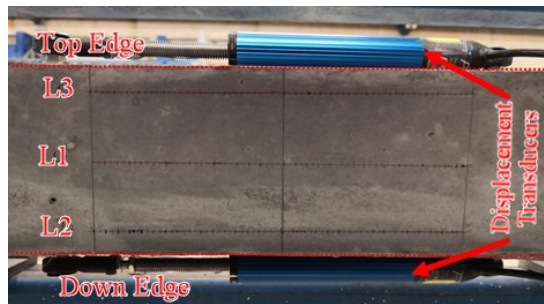


Figure 6- 34: The three guidelines over the lateral surface of the dog bone-shape specimen.

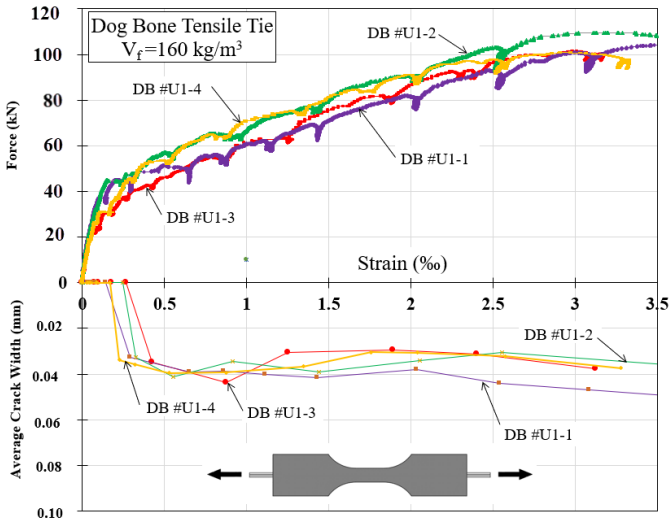
Capturing the cracks over the three guidelines were done by recording a video passing the microscope camera over the guidelines for each tensile elongation level. Then the recorded video was analysed and reviewed on the desktop monitor to obtain the number of the cracks and calculate the width of each crack. The first video recording was taken at very low tensile strain (0.03‰~0.05‰) and the applied tensile elongation increased 0.5‰ for each level. The test was conducted for at least ten tensile strain levels and for each level, the maximum crack width detected and the average value was recorded. The objective of this experimental study was to evaluate the cracking and deformation behaviour of the R-UHPFRC tensile elements up to the 2.0‰ tensile strain level. However, the test was continued for higher strain (2.5‰~3.0‰).

### 6.4.4. Test results

It was tried to measure the crack width for all specimens at the same tensile strain level. The main obtained results from this test program were the force-strain relationship and the crack width for specific strain values. Hence, a diagram was

proposed with the force-strain relationship on the top side and the crack width-strain on the bottom side. Based on the recorded crack number and recorded force and elongation by cell load and DTs measure equipment, both force-strain and average crack width-strain relationship can be illustrated in the one diagram. The obtained specimens behaviour are illustrated in Figures 6-35 (a) and (b).

(a)



(b)

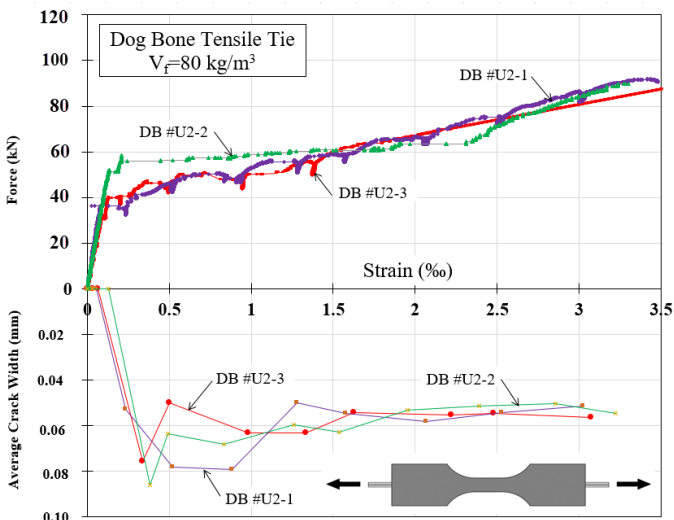


Figure 6- 35: Dog bone-shaped R-UHPFRC test results, Upside: Force-strain and bottom side: crack width-strain curves, (a) UHPFRC type U1:  $V_f = 160 \text{ kg/m}^3$ , (b) UHPFRC type U2:  $V_f = 80 \text{ kg/m}^3$



As can be seen in Figures 6-35 (a) and (b), the first cracks happen before the tensile strain of 0.50‰ for both types of the UHPFRCs. The crack width value for specimens with UHPFRC type U1 at a strain level above 0.5‰ was almost constant (0.040 mm), while for the specimens with UHPFRC type U2, the crack width at the strain level between 0.5 and 1.0‰ was almost 0.070 mm and almost 0.055 mm for the strain level higher than 1.0‰.

The variance in crack width between UHPFRC types U1 and U2 might be caused by the difference in fibre volume contents for each UHPFRC type while using the same mixture composition. Regarding the SLS requirements (crack width controlling) for UHPFRC and durability issues, specimens with UHPFRC type U1 (2. vol% fibre content) behaved better than the specimens with UHPFRC type U2 (1. vol% fibre content). For the UHPFRC U1 type, crack width was narrower than type U2 and its value remained approximately constant up to the high tensile strain rate.

#### **6.4.5. Maximum crack width**

The maximum crack width for each tensile load level and over each guideline was determined by reviewing the recorded video and monitoring all cracks.

The diagram presented in Figure 6-36 provides the maximum crack width values and the average calculated crack width, as well as the ( $\beta = w_{\max}/w_{\text{avg}}$ ) value for 10 load stages.

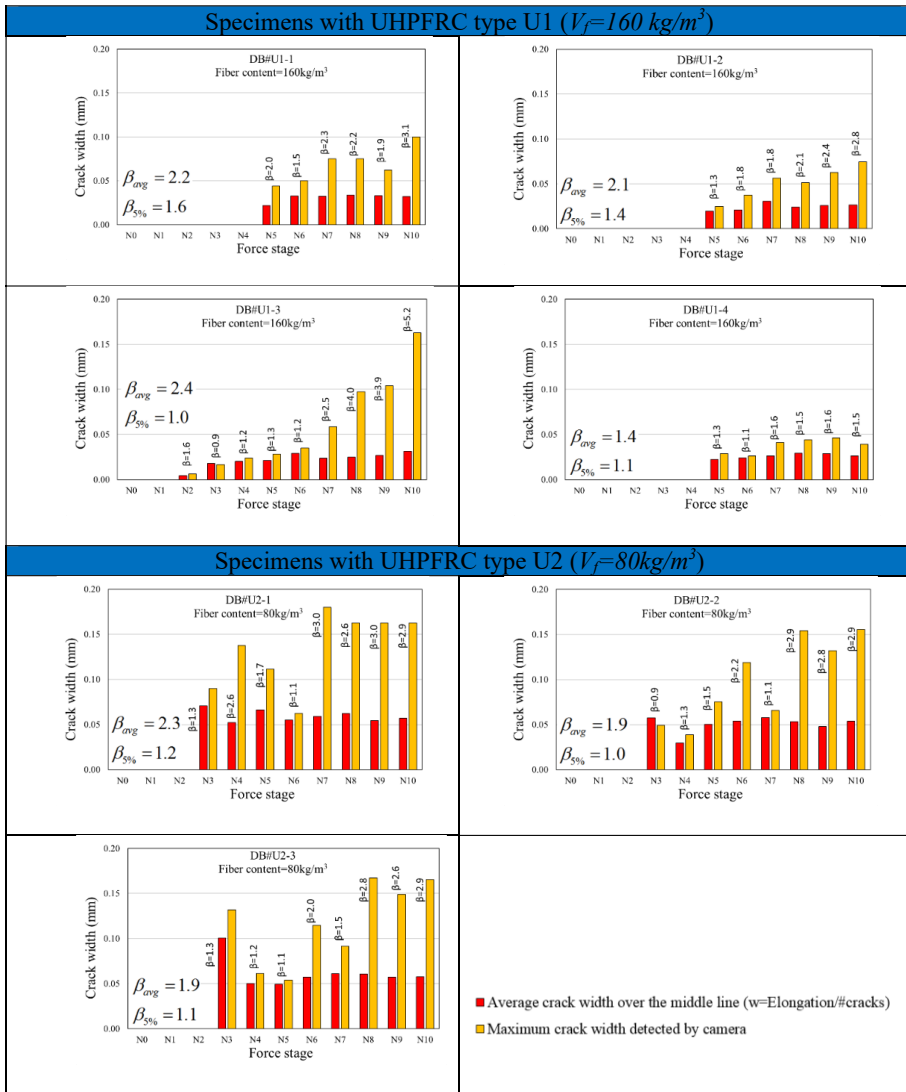


Figure 6- 36: Experimental maximum crack width values, average calculated crack width values and ( $\beta$ ) values for dog bone-shaped specimens with concrete type U1 and U2.

The average value of ( $\beta$ ) for the two last force stages (N9 and N10) for all specimens, where the tensile strain rate was between 2.0‰ and 3.5‰ was more than 2.8. In other words, the maximum crack width can be 2.8 times the average calculated crack width for both UHPFRC types. However, its main value ( $\beta_{avg}$ ) for specimens with UHPFRC type U1 and U2 was 2.02 and 2.03, respectively.

Consequently, in experimental terms, the maximum crack width maybe be estimated by multiplying the average crack width ( $w_m = \text{elongation/number of cracks}$ ) by  $\beta$  (approximately  $\beta=2.0$ ) for both UHPFRC types. It should be emphasized that the  $\beta=2.0$  value was calculated by averaging results from low to high tensile strain rates (up to 3.5‰ in some situations). In contrast, in the SLS design for UHPFRC elements, the average tensile strain is lower than 3.5‰.

As can be observed in Figure 6-36, almost the majority of the experimental maximum crack width values for specimens with UHPFRC type U1 (fibre content = 160 kg/m<sup>3</sup>) were less than 0.10 mm. Comparing these values with crack width limitation under service conditions provided by French code NF P 18-710 for R-UHPFRC structures [13] (see Table 2-4), it can be concluded that the UHPFRC type U1 meet the crack width limitation for all exposures classes. While the maximum experimental crack width for UHPFRS type U2 (fibre content = 80 kg/m<sup>3</sup>) was 0.15 mm, which does not meet the SLS requirement for exposure classes XD1, XD2, XD3, XS1, XS2, and XS3 (corrosion induced by chlorides and seawater).

#### 6.4.6. Fragility curve from cracking data

A probability distribution is a statistical function that describes all the possible values and likelihoods that a random variable can take within a given range [14]. An alternative description of distribution is given by the cumulative distribution function (CDF), which is the probability of the value of the variable being less than or equalling  $x$  [15] (see expression 6-3).

$$F(x) = P[X \leq x] = \alpha \quad (6-3)$$

In probability theory and statistics, the CDF of a real-valued random variable  $x$ , evaluated at  $x$ , is the probability function that  $X$  will take a value less than or equal to  $x$ . CDF finds the cumulative probability for given value and is the area determined by the probability density function from  $-\infty$  to  $x$ . It can be represented mathematically for continuous distribution as Equation (6-4).

$$F(x) = P[-\infty < X \leq x] = \int_{-\infty}^x f(x) dx \quad (6-4)$$

The CDF for a discrete distribution may be stated as Equation (6-5):

$$F(x) = P[X \leq x] = \sum_{i=0}^x f(i) \quad (6-5)$$

The probability curve that is used here identify by two axes; the horizontal axis is the allowable domain for the given probability function, and the vertical axis is a

probability; it must fall between zero and one. We used the Rice probability density function with expression (6-6) and the corresponding CDF defined by Expression (6-7).

$$f(x) = \frac{x}{\sigma^2} \exp\left(\frac{-(x^2 + v^2)}{2\sigma^2}\right) I_0\left(\frac{xv}{\sigma^2}\right) \quad (6-6)$$

$$f(x) = 1 - Q_1\left(\frac{v}{\sigma}, \frac{x}{\sigma}\right) \quad (6-7)$$

where  $(\sigma)$  and  $(v)$  are continuous parameters,  $(I_0)$  is the modified Bessel function of the first kind with order zero, and  $(Q_1)$  is the Marcum Q- function.

A fragility function (or a fragility curve) represents the CDF of an asset's capacity to resist an undesirable limit state [16]. For the present study, it was applied this analysis approach to present the probability of exceeding crack width with a specific tensile strain. For that, all crack widths recorded at tensile strains of 1.0‰, 2.0‰ and 3.0‰ for all specimens in each group (classified according to UHPFRC type) were used to generate the fragility curves, as shown in Figures 6-37 (a), (b) and (c).

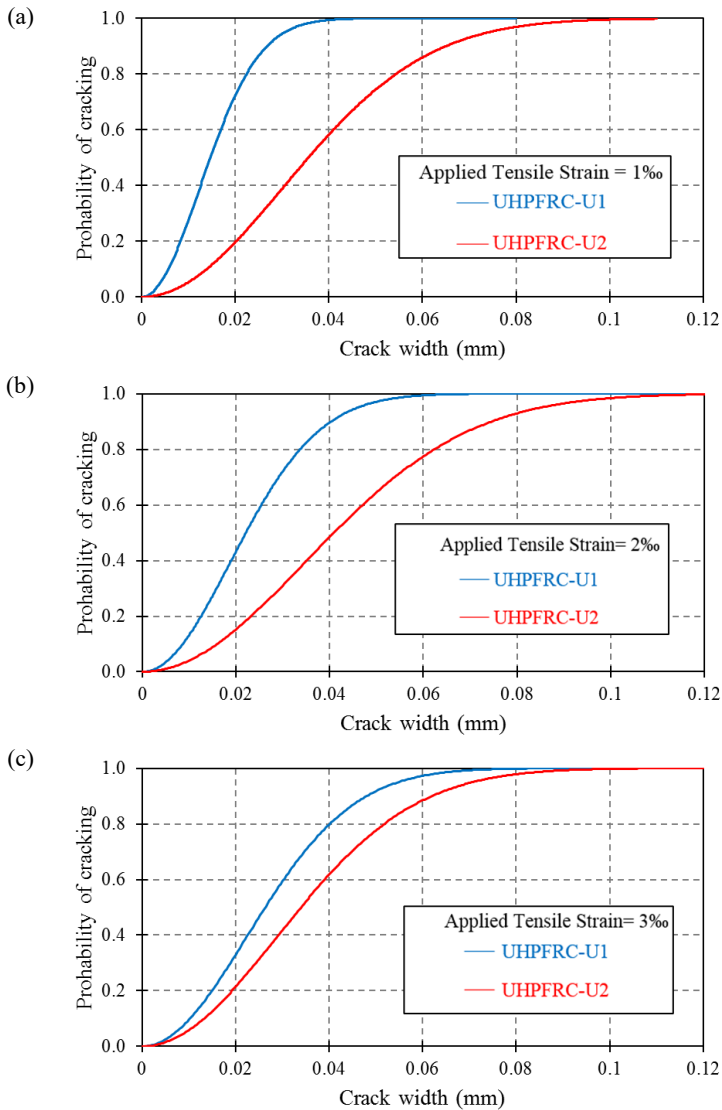


Figure 6- 37: Fragility curves for R-UHPFRC tensile elements with UHPFRC U1 and U2: tensile strain level (a) 1.0‰; (b) 2.0‰; (c) 3.0‰.

It can be seen that for all tensile strain levels, the probability curve related to specimens with UHPFRC type U1 was placed on top of curves of UHPFRC type U2. It leads to conclude that for the specific probability level, specimens with UHPFRC type U2 present a wider crack width. At a high tensile strain rate (in this study 3.0‰), the probability curves of UHPFRC type U1 and U2 came closer to one another and the difference between them was smaller. The fibre pull-out

process that occurs at high tensile strain rates can explain this behaviour. At these tensile strain rates, practically all of the fibres were pull-out of the concrete matrix, and thus, the tensile stresses were mostly carried out by steel rebars. Because the reinforcement diameter was the same for both types of UHPFRC specimens, both curves were close together.

Table 6-12 shows the crack widths corresponding to the 5%, 50%, and 95% probability levels in order to better understand the difference between the fragility curve behaviour of R-UHPFRC tensile elements types U1 and U2. The ( $\beta$ ) value was calculated by dividing the higher characteristic value ( $w_{95\%}$ ) divided by the mean value ( $w_{50\%}$ ).

Table 6- 10: Crack width corresponding to the probability values of 5%, 50% and 95% for UHPFRC type U1 and U2 (units: in mm).

UHPFRC type	Lower characteristic value (5% of the results)	Mean value (50% of the results)	Higher characteristic value (95% of the results)	$\left( \beta = \frac{w_{95\%}}{w_{50\%}} \right)$
<b>1 ‰</b>				
U1	0.004	0.015	0.031	2.07
U2	0.010	0.036	0.074	2.08
<b>2 ‰</b>				
U1	0.006	0.022	0.046	2.08
U2	0.011	0.041	0.085	2.09
<b>3 ‰</b>				
U1	0.007	0.026	0.055	2.09
U2	0.009	0.034	0.071	2.08

It is apparent that the crack width rose by increasing the tensile strain rate. In all cases, specimens with UHPFRC type U2 provided higher crack width values. Furthermore, at the probability level of 95%, all crack width values for both UHPFRC types were less than 0.1 mm, which is the crack width limitation recommended by French code, NF P 18-710 for R-UHPFRC structures [13] for all exposure classes as a serviceability design requirement (see Table 2-4). The ( $\beta$ ) value obtained by this approach is about equal to 2.0 (provided in table 6-12), which is the same as the experimental value, and it may be deemed trustworthy and accurate enough to relate the maximum to the average crack width values. The derived findings and conclusions are summarised as follows:

- (a) The first detected crack under tensile load for both dog bone-shaped specimens with UHPFRC type U1 ( $V_f = 1\%$ ) and U2 ( $V_f = 2\%$ ) occurred at a lower tensile strain level than 0.5‰.
- (b) The R-UHPFRC tensile elements with UHPFRC type U1 had an average crack width of around 0.04 mm after the first cracking, while type 2 had an average crack width of about 0.07 mm.

- (c) Maximum crack width (as detected by microscope camera) can be greater than twice the average crack width, and the ( $\beta$ ) factor for R-UHPFRC tensile elements can be accepted as two.
- (d) R-UHPFRC cracking behaviour for elements with UHPFRC type U1 was typically better than R-UHPFRC type U2, as predicted. The detected maximum crack widths value for R-UHPFRC tensile elements with UHPFRC type U1 were lower than 0.1 mm under high tensile strain level (3.5‰ in this study), indicating that this UHPFRC type may fulfil the crack width limits for all exposure classes.
- (e) The characteristic crack width value derived from the fragility curves at a probability level of 0.95 under SLS conditions was shorter than the crack width limitation imposed by French code NF P 18–710 (0.1 mm, the lowest value for R-UHPFRC elements). This finding leads to the conclusion that both UHPFRC types (U1 and U2) can meet the serviceability crack width limitation, thanks to the rebars and fibres synergy.

## References

- [1] J. Á. López, P. Serna, J. Navarro-Gregori, and E. Camacho, "An inverse analysis method based on deflection to curvature transformation to determine the tensile properties of UHPFRC," *Materials and Structures*, vol. 48, no. 11, pp. 3703-3718, 2015.
- [2] J. A. López Martínez, "Characterisation of The Tensile Behaviour of UHPFRC by Means ff Four-Point Bending Tests," 2017.
- [3] Z. Zhang, X.-D. Shao, P. J. C. Zhu, and B. Materials, "Direct tensile behaviors of steel-bar reinforced ultra-high performance fiber reinforced concrete: Effects of steel fibers and steel rebars," vol. 243, p. 118054, 2020.
- [4] E. Fehling, M. Schmidt, J. Walraven, T. Leutbecher, and S. Fröhlich, *Ultra-high performance concrete UHPC: Fundamentals, design, examples*. John Wiley & Sons, 2015.
- [5] T. E. T. Buttignol, J. Sousa, and T. N. J. R. I. d. e. e. m. Bittencourt, "Ultra High-Performance Fiber-Reinforced Concrete (UHPFRC): a review of material properties and design procedures," vol. 10, pp. 957-971, 2017.
- [6] J. Edgington, "Steel fibre reinforced concrete volume B," University of Surrey, 1973.
- [7] P. H. J. C. J. o. C. E. Bischoff, "Effects of shrinkage on tension stiffening and cracking in reinforced concrete," vol. 28, no. 3, pp. 363-374, 2001.
- [8] SIA 2052, "Béton fibré ultra-performant (BFUP)-Matériaux, dimensionnement et exécution. Draft," 2016.
- [9] J. C. Committee, "Recommendations for design and construction of high performance fiber reinforced cement composites with multiple fine cracks,"

- Japan Society of Civil Engineers, Tokyo, Japan, 2008.
- [10] G. Kaklauskas, V. Gribniak, D. Bacinskas, and P. Vainiunas, "Shrinkage influence on tension stiffening in concrete members," *Engineering Structures*, vol. 31, no. 6, pp. 1305-1312, 2009.
  - [11] P. H. Bischoff, "Effects of shrinkage on tension stiffening and cracking in reinforced concrete," *Canadian Journal of Civil Engineering*, vol. 28, no. 3, pp. 363-374, 2001.
  - [12] P. H. Bischoff, "Tension stiffening and cracking of steel fiber-reinforced concrete," *Journal of materials in civil engineering*, vol. 15, no. 2, pp. 174-182, 2003.
  - [13] P. J. A. NF, Paris, "NF P 18-710, Complément national à l'Eurocode 2 — Calcul des structures en béton : règles spécifiques pour les Bétons Fibrés à Ultra-Hautes Performances (BFUP)."
  - [14] R. B. Ash, *Basic probability theory*. Courier Corporation, 2008.
  - [15] F. M. Dekking, C. Kraaikamp, H. P. Lopuhaä, and L. E. Meester, *A Modern Introduction to Probability and Statistics: Understanding why and how*. Springer Science & Business Media, 2005.
  - [16] K. Porter, "A beginner's guide to fragility, vulnerability, and risk," *Encyclopedia of earthquake engineering*, vol. 2015, pp. 235-260, 2015.



## ***Chapter 7. Conclusions and future research lines***

The main conclusions drawn from this PhD thesis are listed in this chapter. In addition, recommendations for future research based on the limitations found during this research are provided.

## **7.1. Summary and main conclusions**

This PhD thesis presents several experimental programmes, undertaken to study the serviceability behaviour of Reinforced Ultra-High Performance Fibre-Reinforced Concrete (R-UHPFRC). The main purpose of this research is to evaluate the tensile deformation and cracking behaviour of R-UHPFRC elements under service conditions. With this objective, two main items were addressed and adequately met. The first one was to design an innovative and upgraded test methodology to carry out the experiments required for this PhD project. The second involved evaluating the tension stiffening response and cracking behaviour of R-UHPFRC, which are fundamental parameters for serviceability design. To study these two parameters, some important parameters, such as fibre content volume effect, fibre type, size effect, reinforcement ratio effect and shrinkage effect, were considered.

This section presents the main conclusions drawn from the present PhD document. This thesis is written based on six academic research papers, and one book chapter appended at the end of this document. The document is structured following a logical sequence because research was conducted, and each chapter relates to the corresponding published paper/s.

First of all, a review of the most commonly used uniaxial tensile test methods for RC elements, as well as their advantages and disadvantages, was performed. Then a proposed tensile test methodology was explained by demonstrating the preliminary test results. The innovative proposed test method was used to carry out the experiments required for this PhD project after assessing and validating the acquired data.

After establishing and controlling the test procedure, comprehensive experimental programmes were undertaken with two different steel fibre types and fibre contents. Different cross-section and reinforcement ratios were used to evaluate the size effect and fibre content effect, respectively. All the experimental studies were done by casting specimens with two UHPFRC types with the same mix design, but with different fibre volume contents. The fibre content (steel microfiber types) for UHPFRC type C1 was  $160 \text{ kg/m}^3$  ( $V_f = 2.0\%$ ) and was  $80 \text{ kg/m}^3$  ( $V_f = 1.0\%$ ) for type C2. The effect of a combination of micro- and macrosteel fibres (called UHPFRC type C8080) on the deformation and cracking behaviour of tensile R-UHPFRC elements was investigated in a specific experimental study.

A review of the tensile behaviour and tension stiffening effect of conventional RC, fibre (FRC), and current research into this effect for Ultra-High Performance Fibre Concrete (UHPFRC) is presented. Moreover, the tension stiffening factor (or bond factor:  $\beta$ ) concept was explained, which is considered in the concrete structures codes for SLS design. The effect of using fibres in concrete and their influence on tension stiffening behaviour and bond factor were explained by comparing the

tensile post-cracking behaviour of RC and R-FRC tensile elements. The tensile response and classification of the UHPFRC material based on its tensile and flexure behaviour were explained to understand important aspects, such as the hardening and softening behaviour of the UHPFRC material. Furthermore, the full-tension stiffening aspect for R-UHPFRC was described, and experimental evidence was provided to confirm this phenomenon for tensile R-UHPFRC elements. The theoretical definition of the inverse analysis method to obtain the characteristic parameters to define UHPFRC tensile behaviour by employing the four-point bending test (4PBT) was provided. In this part of the study, two test programmes were designed. In the first test programme, the average overall tensile behaviour of R-UHPFRC tie elements was experimentally obtained and concrete's contribution was compared to the tensile properties that derived from the 4PBT using our research group's proposed inverse analysis method. In the second test programme, the effect of using micro- and macrofibres on post-cracking behaviour was studied.

It was observed that the shrinkage effect on UHPFRC elements' cracking behaviour posed a major concern about their serviceability design. This effect should be taken into account for the long-term deformation, short-term loading and cracking resistance of R-UHPFRC elements. Therefore, two intensive shrinkage experimental studies were conducted to obtain the shrinkage value of the UHPFRC used in this PhD study.

Finally, test procedures were improved by modifying specimen geometry and using dog bone-shaped specimens to prevent the end effect during the uniaxial test. A new test measurement procedure was employed to evaluate the average and maximum crack widths (real detected value) caused by tensile stresses in R-UHPFRC tensile elements. The difference between the maximum and average crack widths was evaluated. It is important to consider this for examining R-UHPFRC structures design under serviceability conditions or for the durability performance of R-UHPFRC. Moreover, a statistical analysis was conducted to develop the fragility curves based on the obtained test data.

Therefore, the main conclusions drawn from all the research work herein performed are presented below.

## **7.2. Partial conclusions**

### ***On the upgraded proposed test method***

The results obtained from the preliminary experimental programme demonstrated the suitability of the proposed test method and usefulness of the employed measurement devices. Consequently, the proposed test method proved appropriate for future studies on the serviceability behaviour of R-UHPFRC tensile elements, and the proposed testing method and the obtained results were suitable for the

studies required in the present PhD thesis. Moreover, when analysing the results obtained from this preliminary test programme, the increase in fibre volume content of concrete was seen to have a significant influence on the first cracking strength. Hence the fibre volume content strongly influenced the cracking and serviceability behaviour of R-UHPFRC, and this could be the main variable for further studies.

***On the tension behaviour and tension stiffening response of R-UHPFRC tensile elements***

- (a) Overall tensile behaviour (the average stress-strain relation) for all the R-UHPFRC tensile specimens revealed three well-defined stages: (stage 1) linear elastic behaviour; (stage 2) microcrack formation with a sharp drop in tensile stiffness; (stage 3) microcrack stabilisation. Additionally, no macrocrack formation was observed under serviceability conditions.
- (b) The overall experimental response of the R-UHPFRC tensile elements in the microcracking stabilisation stage was similar to that of the bare bar, and both UHPFRC types (C1 & C2) exhibited almost full-tension stiffening ( $\beta = 1$ ).
- (c) By increasing the amount of fibre in UHPFRC from 80 to 160 kg/m<sup>3</sup>, the cracked tensile element's energy absorption capacity was raised by roughly 21.4%. As a result, designers should carefully consider the economics of using the double fibre dose in real-world applications. The cracking behaviour (crack opening and spacing) and durability performance of the tensile elements under SLS loads could lead to a more remarkable improvement.
- (d) The shrinkage effect on tension stiffening was preliminarily evaluated, and it would appear that this effect has a considerable impact on the internal stresses that both UHPFRC and reinforcement exhibit. As a result, the shrinkage effect should be considered in the serviceability design of R-UHPFRC structural elements.
- (e) A slight increase in concrete's contribution was observed as the reinforcement ratio was increased.
- (f) The contribution of UHPFRC to tension is more than the characteristic tensile value calculated from the 4PBTs' inverse analysis result.
- (g) R-UHPFRC tensile elements with hybrid fibre content (80 kg/m<sup>3</sup> for micro smooth steel fibres and 80 kg/m<sup>3</sup> for macro hooked end steel fibres) have a similar tensile cracking stress strength to the R-UHPFRC tensile elements with a fibre content of 160 kg/m<sup>3</sup>.

***On the shrinkage behaviour of UHPFRC***

From the first test method, the obtained free shrinkage value was 620  $\mu\text{m} / \text{m}$ , while it was 422  $\mu\text{m} / \text{m}$  by the second method. Based on these experimental

results, it can be concluded that the shrinkage strain values proposed by codes (550-800) are suitable for doing structure calculations during the preliminary design or project stages if an experimental shrinkage test is not possible.

When considering the serviceability criterion, the shrinkage effect should be considered by increasing the tensile stress inside the matrix. Not knowing the shrinkage effect might mean making substantial mistakes in the serviceability design. This impact must also be included in constitutive modelling.

### ***On the serviceability behaviour of R-UHPFRC tensile elements***

- (a) The first detectable crack under tensile stress for both dog bone-shaped specimens with UHPFRC types U1 and U2 occurred at a tensile strain level below 0.5‰.
- (b) After the first cracking stage, the R-UHPFRC tensile elements with UHPFRC type U1 had an average crack width of around 0.04 mm, whereas type U2 had an average crack width of 0.07 mm.
- (c) The maximum crack width (measured by the microscope camera) can be more than twice the average crack width, and the ( $\beta$ ) factor for R-UHPFRC tensile elements can be taken as 2.
- (d) The R-UHPFRC cracking behaviour for elements with UHPFRC type U1 was typically better than R-UHPFRC type U2, as predicted. The detected maximum crack widths value for the R-UHPFRC tensile elements with UHPFRC type U1 were lower than 0.1 mm at a high tensile strain level (3.5‰ in this study), which indicates that this UHPFRC type may fulfil the crack width limits for all the exposure classes.
- (e) Under SLS conditions, the characteristic crack width value calculated from the fragility curves at a probability level of 0.95 was lower than the crack width limits set by French code NF P 18-710. (0.1 mm, the lowest value for R-UHPFRC elements for all the exposure classes). This observation led to the conclusion that, owing to the rebars and fibres synergy, both UHPFRC types (U1 and U2) can fulfil the serviceability crack width constraint.

### **7.3. Global conclusions**

Generally, for designing structural concrete elements under SLS conditions, three fundamental requirements should be met: tension stress limitation in rebars and concrete; deflection and cracking control; vibration control. In this PhD thesis, the first and second parameters were investigated by studying the uniaxial tensile behaviour of R-UHPFRC tie elements. These elements' global tensile behaviour is generally different from RC or FRC tensile elements. Both R-UHPFRC tensile elements types (C1,  $V_f=160 \text{ kg/m}^3$  and C2,  $V_f=80 \text{ kg/m}^3$ ) presented full tension stiffening behaviour (ascending behaviour) after the first tensile cracking, while

tensile elements RC and FRC displayed descending behaviour.

As the UHPFRC (without reinforcement) with fibre content of  $80 \text{ kg/m}^3$  in the direct tensile test displays no strain hardening behaviour, many researchers do not consider that this concrete is a high-performance concrete type. Based on the experimentally obtained results by considering parameters, such as different sizes and with a statistical probability analysis, the general tensile behaviour of the reinforced UHPFRC elements with a low fibre content presented strain hardening behaviour when working in synergy with adequate reinforcement with traditional rebars. This was because the full tension stiffening effect existed (with ascending tension-deformation behaviour after the first cracking). Therefore, the R-UHPFRC with  $80 \text{ kg/m}^3$  of fibre content well performed under SLS conditions and the crack width value was under the code limitations. This means that we can decrease the fibre content for R-UHPFRC elements and meet the SLS limitation. However, future studies are necessary to obtain the optimal fibre content for reinforced UHPFRC elements to meet SLS requirements.

For the practical approach to design UHPFRC structural elements, it is possible to ignore the cracking calculation to check if crack width requirements are met. This is because, based on the statistical studies done in this PhD project, the characteristic crack width was lower than  $0.1 \text{ mm}$  at high tensile strain levels, even for the UHPFRC with low fibre content (UHPFRC type C2,  $V_f=80 \text{ kg/m}^3$ ). This indicates that this UHPFRC type can fulfil the crack width limits for all the exposure classes, and that the stress control of the steel rebar and concrete is enough to meet the SLS.

Finally, to consider the SLS in the structural models for R-UHPFRC structure elements, both the shrinkage and tension stiffening effect should be taken into account by considering the full tension stiffening effect for these elements.

#### **7.4. Future research lines**

Several ideas for future research lines may be derived from the research undertaken in this PhD project:

- (a) The interrelation between the instantaneous and sustained tensile loading conditions for the serviceability of UHPFRC elements is poorly understood. Thus, it is crucial to analyse the tension stiffening mechanism and the post-cracking behaviour of R-UHPFRC elements under long-term serviceability conditions. The shrinkage effect (autogenous and drying shrinkages) must be considered in this type of study, and a specific shrinkage experimental study is needed to obtain their values. Perhaps a novel testing method needs to be designed to be able to apply the sustained tensile load at different sustained levels.

- (b) The probabilistic study and the fragility function data can be improved by using other probability density functions. The accuracy of this method can be improved by using more experimental data from conducting more experiments.
- (c) The study of the fibre content effect on the tension stiffening response could be improved by using a wider range of fibre content volumes. This study can also help to obtain the optimal fibre content ( $V_f < 80 \text{ kg/m}^3$ ) for R-UHPFRC elements to ensure meeting the SLS requirements for UHPFRCs with low fibre content.
- (d) The present study is only limited to tensile UHPFRC elements reinforced with conventional reinforcement. The influence of high-strength steel rebars used for reinforcing these elements must be investigated.





***Annex I. Justification of the  
impact index of the  
publications included in the  
thesis***

<b>Title:</b> Experimental methodology on the serviceability behaviour of reinforced ultra-high performance fibre reinforced concrete tensile elements		
<b>Author(s):</b> Khorami, M (Khorami, Majid); Navarro-Gregori, J (Navarro-Gregori, Juan); Serna, P (Serna, Pedro)		
<b>Source:</b> STRAIN <b>Volume:</b> 56 <b>Issue:</b> 5 <b>Article Number:</b> e12361 <b>DOI:</b> 10.1111/str.12361 <b>Early Access Date:</b> JUN 2020 <b>Published:</b> OCT 2020		
<b>Accession Number:</b> WOS:000537403400001		
<b>Author Identifiers:</b>		
<b>Author</b>	<b>Web of Science Researcher ID</b>	<b>ORCID Number</b>
Khorami, Majid	AAN-1515-2021	0000-0003-4592-0233
Serna, Pedro	DXR-8749-2022	0000-0001-8754-1165
Navarro-Gregori, Juan	H-7116-2015	0000-0002-6319-7029
<b>ISSN:</b> 0039-2103		
<b>eISSN:</b> 1475-1305		

## STRAIN

### Journal Impact Factor™

2021

Five Year

2.578

2.435

JCR Category	Category Rank	Category Quartile
MATERIALS SCIENCE, CHARACTERIZATION & TESTING <i>in SCIE edition</i>	13/32	Q2

Source: Journal Citation Reports 2021. [Learn more](#)

<b>Title:</b> Tensile behaviour of reinforced UHPFRC elements under serviceability conditions		
<b>Author(s):</b> Khorami, M (Khorami, M.); Navarro-Gregori, J (Navarro-Gregori, Juan); Serna, P (Serna, P.)		
<b>Source:</b> MATERIALS <span style="float: right;">AND</span> STRUCTURES <b>Volume:</b> 54 <b>Issue:</b> 1 <b>Article</b> <b>Number:</b> 43 <b>DOI:</b> 10.1617/s11527-021-01630-z <b>Published:</b> FEB 10 2021		
<b>Accession Number:</b> WOS:000619166300002		
<b>Author Identifiers:</b>		
<b>Author</b>	<b>Web of Science Researcher ID</b>	<b>ORCID Number</b>
Khorami, Majid	AAN-1515-2021	0000-0003- 4592-0233
Serna, Pedro	DXR-8749-2022	0000-0001- 8754-1165
Navarro- Gregori, Juan	H-7116-2015	0000-0002- 6319-7029
<b>ISSN:</b> 1359-5997		
<b>eISSN:</b> 1871-6873		

**MATERIALS AND STRUCTURES**

## Journal Impact Factor™

2021	Five Year
<b>4.285</b>	<b>4.795</b>

JCR Category	Category Rank	Category Quartile
CONSTRUCTION & BUILDING TECHNOLOGY <i>in SCIE edition</i>	21/68	Q2
ENGINEERING, CIVIL <i>in SCIE edition</i>	37/138	Q2
MATERIALS SCIENCE, MULTIDISCIPLINARY <i>in SCIE edition</i>	139/345	Q2

<b>Title:</b> Serviceability behaviour of reinforced UHPFRC tensile elements: Assessment of the ratio between maximum and average crack widths		
<b>Author(s):</b> Khorami, M (Khorami, M.); Navarro-Gregori, J (Navarro-Gregori, Juan); Serna, P (Serna, P.)		
<b>Source:</b> CONSTRUCTION AND BUILDING MATERIALS <b>Volume:</b> 303 <b>Article Number:</b> 124513 <b>DOI:</b> 10.1016/j.conbuildmat.2021.124513 <b>Early Access Date:</b> AUG 2021 <b>Published:</b> OCT 11 2021		
<b>Accession Number:</b> WOS:000696981300003		
<b>Author Identifiers:</b>		
<b>Author</b>	<b>Web of Science Researcher ID</b>	<b>ORCID Number</b>
Khorami, Majid	AAN-1515-2021	0000-0003-4592-0233
Serna, Pedro	DXR-8749-2022	0000-0001-8754-1165
Navarro-Gregori, Juan	H-7116-2015	0000-0002-6319-7029
<b>ISSN:</b> 0950-0618		
<b>eISSN:</b> 1879-0526		

## CONSTRUCTION AND BUILDING MATERIALS

### Journal Impact Factor™

2021	Five Year
<b>7.693</b>	<b>8.194</b>

JCR Category	Category Rank	Category Quartile
CONSTRUCTION & BUILDING TECHNOLOGY <i>in SCIE edition</i>	6/68	Q1
ENGINEERING, CIVIL <i>in SCIE edition</i>	5/138	Q1
MATERIALS SCIENCE, MULTIDISCIPLINARY <i>in SCIE edition</i>	76/345	Q1